# DETERMINATION OF SOIL PROPERTIES FOR SANDY SOILS AND ROAD BASE AT RIVERSIDE CAMPUS USING LABORATORY TESTING AND NUMERICAL SIMULATION

A Thesis

by

DEEYVID OSCAR SAEZ BARRIOS

Submitted to the Office of Graduate Studies of
Texas A&M University
in partial fulfillment of the requirements for the degree of

MASTER OF SCIENCE

May 2010

Major Subject: Civil Engineering

# DETERMINATION OF SOIL PROPERTIES FOR SANDY SOILS AND ROAD BASE AT RIVERSIDE CAMPUS USING LABORATORY TESTING AND NUMERICAL SIMULATION

A Thesis

by

DEEYVID OSCAR SAEZ BARRIOS

Submitted to the Office of Graduate Studies of
Texas A&M University
in partial fulfillment of the requirements for the degree of

MASTER OF SCIENCE

Approved by:

| | |
|---|---|
| Chair of Committee, | Jean-Louis Briaud |
| Committee Members, | Charles Aubeny |
| | Julian Kang |
| Head of Department, | John Niedzwecki |

Major Subject: Civil Engineering

# ABSTRACT

Determination of Soil Properties of Sandy Soils and Road Base at Riverside Campus Using Laboratory Testing and Numerical Simulation.

(May 2010)

Deeyvid Oscar Saez Barrios, B.En., Technological University of Panama

Chair of Advisory Committee: Jean-Louis Briaud

This study evaluated the soil properties of clean sand, a silty sand, and a road base that are extensively used as a backfill for full-scale testing at Riverside Campus at Texas A&M University. The three soils were collected at the Riverside Campus and the testing schedule included grain size analysis, hydrometer test, specific gravity, maximum dry density, Atterberg limit, stiffness, direct shear test, triaxial test, and a simple procedure to estimate the maximum and minimum void ratio of the clean sand. Relation between strength/deformation, vertical displacement/shear displacement, and physical properties were evaluated to estimate the frictional resistance and angle of dilation of the clean sand and the silty sand.

Numerical simulations of the Direct Shear Test (DST) were conducted on the clean sand using Finite Element Model in the computer program LS-DYNA. The simulations were intended to reproduce the Direct Shear Test (DST) to estimate the frictional resistance and dilatancy effects of the clean sand under different compressive stresses.

Field tests were also conducted on the clean sand and the road base. These tests included the in-situ density determination, in-situ water content, and the soil modulus using the Briaud Compaction Device (BCD).

# DEDICATION

To my parents:

Eyda Raquel Barrios Rivera and Oscar Alberto Saez Barrios,

My sister;

Yessica Lisbeth Saez Barrios,

And my girlfriend:

Librada Maria Velazquez Mudarra

# ACKNOWLEDGEMENTS

I would first like to thank you, Dr. Jean- Louis Briaud, for supporting, advising and guiding me on this project and on my graduate school career. I would also like to thank Dr. Charles Aubeny for aiding in my understanding of frictional resistance of sands. I am indebted to Mr. Mike Linger for his assistance and technical support in all my laboratory endeavors.

I also acknowledge the help of Mr. Gustavus Lee, Mr. Gary Gerke, Seok-Gyo Lim, Hrishikesh Sharma, and Michelle Lee Bernhardt for their assistance in collecting samples, laboratory testing and Numerical Simulation.

My sincere gratitude goes out to my entire family, and specifically to my parents, who encouraged me to go to college and then on to graduate school. I would like to thank all my friends in the geotechnical group for their support and enjoyment in work and life.

# TABLE OF CONTENTS

Page

Page

Page

# LIST OF FIGURES

Page

Page

Page

Page

Page

Page

Page

Page

# LIST OF TABLES

Page

Page

# 1. INTRODUCTION

## 1.1 General Concepts

Granular materials, such as clean sand and road base, are preferred for structural fill because they are strong, drain water rapidly, and settle little under compressive load conditions. Considering these reasons, one of the most important engineering applications of these materials is to serve as a backfill for mechanically stabilized walls (MSE) and reinforced soil (RS) slopes. For these engineering applications, the friction angle ($\Phi$) and the dilation angle ($\psi$) of the sand are the most important engineering parameters.

The clean sand and the road base material are extensively used at The Riverside Campus (a research facility for the Texas Transportation Institute at Texas A&M University) for full scale testing. Nearly 100 full-scale crash tests are conducted every year on a variety of safety devices using different types of vehicles. This allows researchers to model real conditions that will validate advanced computer simulation that have been developed previous to the tests.

The requirement of the backfill (in term of soil properties and compactness) will depend on the requirements imposed by the sponsor or regulatory agency. Several soil conditions are simulated in advanced; then, they are reproduced in full-scale tests.

---

This thesis follows the style of the *Journal of Geotechnical and Environmental Engineering.*

Therefore, knowing the physical and mechanical properties of the soils represent an important feature on the validation of the numerical simulation.

Considering that, a set of field and laboratory tests were conducted on the three soils (clean sand, silty sand, and road base) in order to document the physical and mechanical properties of these materials. The field tests include: in-situ density, water content, and determination of the soil modulus using the Briaud Compaction Device (BCD test). The laboratory tests include: wet sieve analysis, hydrometer analysis, and specific gravity for the clean sand, estimation of the maximum and minimum void ratio, modified proctor compaction test for the clean sand and the road base, laboratory BCD test, direct shear test (DST), and triaxial compression test (TC). From the results of the Direct Shear Test (DST), the frictional resistance ($\Phi$) and dilation angle ($\psi$) of the clean sand and the silty sand were computed. These soils were testing under different states conditions (loose, dense, and compacted at different water content).

In addition to the laboratory tests conducted on the clean sand, a set numerical simulation using Finite Element Method (FEM) in the computer program LS-DYNA was also performed. The main purpose of conducting a numerical simulation was to reproduce the results of the Laboratory Direct Shear Test (DST) in order to have a better estimation of the frictional resistance ($\Phi$) and the dilation angle ($\psi$) of the clean sand under different states condition (loose and compacted states).

## 1.2 Finding

This paper titled “Determination of Soil Properties of Sandy Soil and Road Base at Riverside Campus Using Laboratory Testing and Numerical Simulation”, discusses the physical properties of the silty sand, the clean sand, and the road base used at Riverside Campus for full scale tests. It also discusses the shear strength, the frictional resistance and the dilatancy effects of sands under different state conditions based on the results of the laboratory tests and the numerical simulations (in the case of the clean sand).

In the research program described in this paper, the primarily objective was to document the physical and engineering properties of these soils. A series of laboratory tests and field tests were conducted to accomplish this goal, following the criterion established by the American Society of Testing and Materials (ASTM).

A second objective was to develop a direct shear test (DST) procedure capable of providing repeatable and reliable estimate of the dilation angle ($\psi$) of the clean sands subjected to different stress-state conditions. The dilation angle estimated from the results of the direct shear test (DST) was compare with the results of the numerical simulation in LS-DYNA. This frictional resistance, the most important parameter for being responsible of the strength of cohesionless material, was computed from the direct shear test (DST) in a small box of 62-mm diameter in accordance with the designation ASTM D-3080 (Standard Method for Direct Shear Test Under Consolidated Drained Condition). The tested sands presented high shear resistance, even for the loosest state,

due to different physical properties such as lower roundness, low fine content, and broader particle size distribution, as well as the application of low normal stresses, which increase the dilation effect of the compacted states.

The last objective was to conduct triaxial compression tests on the clean sand (in the loose state) and in the road base material (compacted at about 95% of the Maximum Dry Unit Weight from the Modified Proctor Compaction Test). Sample specimens of 8.5 inches height by 6 inches diameter were tested on a big triaxial cell. The tests were conducted to estimate the frictional resistance of both soils. The results of the clean sand were compared with the result obtained from the DST. Considering the limitation of the sample size of the DST and the triaxial cell for the case of the road base and the crushed rock, a propose FULL-SCALE DST is recommended to test the road base and the crushed rock use at Riverside Campus for FULL-SCALE Impact Test.

Appendix A, “Result of the Direct Shear Test for the Clean Sand” complements the information of the direct shear results conducted on the clean sand.

# 2. EXCECUTIVE SUMMARY

The use of sandy soil and road base in the design of mechanically stabilized earth wall (MSE), embankment, or reinforced soil for full scale tests, conducted at the research facility of Riverside Campus, normally follows criterion establish by the sponsor agency or a specific case of study. The friction angle, which represents the main parameter that provides the frictional resistance of coarse soil, is normally assumed for these soils. Assumptions are made base on the physical properties of the cited soil (gradation, particle shape, grain size, etc.) and engineering judgments.

Several field and laboratory tests were conducted on all three different soils to determine their physical and mechanical properties. The soils were classified as a Poorly-Graded Silty Sand (SP-SM), a Clean Sand (SP), and Silty Gravel (GM). The field tests consisted on in-situ density determination using the sand cone method according to the designation ASTM D 1556 (Standard Test Method for Density and Unit Weight of Soils in Place by Sand-Cone Method), in-place water content, and soil modulus determination using the Briaud Compaction Device (BCD) following the procedure described by Briaud et al. (2009).

The laboratory tests for the soil sample includes: a grain size analysis using a wet procedure specified by the designation ASTM D 2217-85 (Standard Practice for Wet Preparation of Soil Samples for Particle-Size Analysis and Determination of Soil Constants), a hydrometer analysis conducted in accordance to the specification ASTM D 422 (Standard Method for Particle Size Analysis of Soils), a laboratory procedure using

a vibratory motor to estimate the maximum and minimum void ratio of the clean sand, a modified proctor compaction test following the criterion established by the designation ASTM D 1557-07 (Standard Method for Laboratory Compaction Characteristics of Soil Using Modified Effort -56,000 ft-lbf/ft$^3$), a direct shear test (DST) specified by ASTM D 3080 (Standard Test for Direct Shear Test Under Consolidated Drained Condition), and a triaxial compression test TC (The specimen used for the triaxial test did not meet the scale criterion of height to diameter of 2:1). In addition, Atterberg limits for the silty sand and the road base were conducted on the portion passing sieve #40 in accordance to the designation ASTM D 4318-00 (Standard Tests Methods for Liquid Limit, Plastic Limit, and Plasticity Index of Soils). Also, a BCD modulus versus water content curve was developed and compare to the maximum dry density curve in order to show the susceptibility of these two parameters to the water content.

The main purpose of this research report is to estimate the frictional resistance of the sandy soil performing a direct shear test (DST). In addition to the friction angle of the sands ($\Phi$), a dilation enveloped of the soil and an estimation of the dilation angle ($\psi$) is also is presented. The dilation angle was computed from the measurement of the vertical displacement and the shear displacement of the soil specimen, as described in chapter 3, and compare with the results of the numerical simulation using FEM in the computer program LS-DYNA.

In the case of the road base, the gradation of the road base goes beyond the particle size criterion require to conduct the direct shear test (DST); therefore, it was

estimated from the triaxial compression test (TC) using soil specimen of 8.5 inches height and 6 inches diameters.

The lack of laboratory equipment to test large aggregates prevented the application of any test to the crushed rock (another material used for backfill in Riverside Campus); therefore, a recommendation procedure is presented to conduct a full-scale direct shear test (FS-DST). This will allow the estimation of the friction angle and the dilatancy effect of those materials whose particles size exceeds the limit of the standard laboratory equipment.

# 3. BACKGROUND

## 3.1 Shear Strength of Granular Soils

The shear strength of a soil mass is defined as the internal resistance per unit area that the soil mass can offer to resist failure and sliding along any plane inside it. It depends on the frictional resistance between the particles at the point of contact, cohesion between particles (if any exists), and the interlocking of particles within the soil skeleton (Dass 2006).

The linear relation between normal and shear stress was first proposed by Coulomb (1776) and then it was theorized by Otto Mohr in 1900 (Dass 2006). The final equation is called the Mohr-Coulomb failure criterion and it is written as fallow:

$$\tau = c + \sigma' \tan \phi \quad (1)$$

Where: c= cohesion; φ= angle of internal friction; σ’ =normal effective stress in the plane of failure; $\tau_f$ = shear strength of soils.

## 3.2 Mechanism Contributing to Shear Strength of Granular Soils

The internal angle of friction (Φ’) account for three different contribution of energy expanded during shearing (Bareither et al. 2008b):

- Sliding frictional resistance between grains.
- Rearrangement and dilation, associates with interlocking and rotation of grains, and;

- Particle breakage.

Other factors and phenomena such as mineralogy, grain size, grain shape, grain size distribution, relative density, and stress state, type of tests and stress path, and drainage also contribute to the shearing resistance of granular soils (Mitchell & Soga 2005).

## 3.3 Particle Shape

Particles shape has been shown that affect the packing of sands in that an increase in roundness decreases that maximum void ratio ($e_{max}$), minimum void ratio ($e_{min}$), and void ratio spread ($e_{max} - e_{min}$). However, as particles become more angular, greater interlocking occurs, which increases the energy necessary to cause particles displacement and increases the shear strength.

## 3.4 Particle Size and Gradation

Bareither et al. (2008b) cited several discussion of the influence of particles size and gradation on the shear strength of granular material. Some of these studies have reported an increase on the frictional resistance (Φ) of uniformly graded specimen of rounded gravel and crushed rock with increasing grain size. Other studies conducted on granular materials on a triaxial compression tests reported an increase on the friction angle with a decrease in the mean particle size (of soil having the same mineralogy and gradation, but different mean particle size). On the other hands, other authors reported no influence of particle size and gradation on the frictional resistance. They attribute

these variations to mineralogy, roughness, and surface texture (Fakhimi & Hosseinpour, 2008).

Cerato & Luteneger (2006) conducted Direct Shear Test (DST) using three different sizes of boxes (60 x 60 mm; 101.6 x 101.6 mm, and; 304.8 x 304.8 mm). Following the ASTM D 3080, bigger shear boxes can hold bigger soil particles. In their study, they reported decreases in the friction angles with an increase of the shear box. Also, they studied the scale ratio of the specimen (height to diameter (H/D) and width to maximum particle size ($W/D_{max}$). They reported an increase of the friction angle with a decrease of the H/D ratio; in addition, they founded that the scale ratio of H/D does not influence the frictional resistance when the ratio of $W/D_{max}$ is between 50 and 300.

### 3.5 Effect of Confining Pressure on the Shear Strength

The correct interpretation of the frictional resistance of granular materials require the understanding of the real Mohr Coulomb Enveloped as well as the stress level at which the soil sample is being tested. Figure 1 presents a schematic representation of the real Mohr Coulomb Envelop of granular soils.

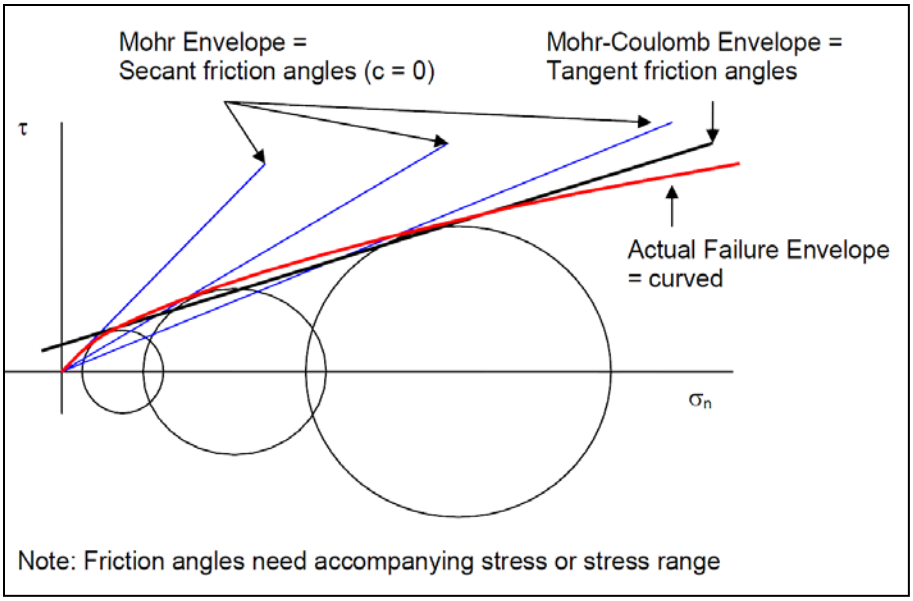


Figure 1. Interpretation of the Mohr-Coulomb Enveloped of Granular Materials (Unknown source: www.google.com)

The Mohr Coulomb Enveloped of granular materials is not a straight line that goes to the origin of the shear stress vs. normal stress plot. On a direct shear test, three specimens are tested at different confining pressure that represents the stress level that the soil sample is undertaken at the field. For low confining pressure, the friction angle tends to be higher than for high confining pressure. The reason of this phenomenon is the curvature that the Mohr Coulomb Envelop presents at low confining pressures. Considering that, when a friction angle is reported, it is also important to report the normal stresses used for the computation of the frictional resistance. The results presents in section 5.7 (Direct Shear Test for clean sand) show a decrease on the friction angle with an increase on the normal stresses.

## 3.6 Soil Modulus of Granular Materials

Soils range often in a high variability because of their complex composition; therefore, they are heterogeneous rather than homogeneous and their stress-strain behavior is not linear (Holtz & Kovacs 1981). Consequently, this no-linear behavior brings a natural dependence of the soil modulus on different soil parameters and loading condition.

Briaud (2002) discussed some of the soil parameters and loading parameters that can affect the modulus of soils. The soil parameter includes porosity, dry density, water content and cementation. The first two parameters, the porosity and the water content, can lead to a better packing of the soil particles leading to an increase in the soil modulus; low water content generate suction, which also lead to a high soil modulus. The cementitious property of a soil mass can also increase the soil modulus. It can be the result of two effects: the chemical bounding developed at the contact area of the soil grains or the effect of having a low water content which also increases the bounding effect.

The loading factors that affect the soil modulus are summarized as the mean stress level applied to the soil, the strain level in the soil, the strain rate in the soil, and the number of cycles experienced by the soil. An increase in the mean stress level or the strain rate in the soil will increase the soil modulus while an increase in strain level or number of cycles will decrease the modulus of a soil mass.

It has also been reported that the modulus of the soil can also be affected by the soil structure and the fabric of the soil as well as the over consolidation ratio (OCR), which lead to an increase on the stiffness of the soil (Mitchell & Soga 2005); Holtz & Kovacs 1981).

## 3.7 Frictional Resistance, Critical State, and Dilatancy Effect of Sands

### 3.7.1 Angle of Internal Friction

The angle of friction represents the basic parameter that account for the frictional resistance of a mass of granular soil. Its value depends on the nature of the mineral, the properties of its surface, the roughness, and the size of the load per particle (Craig 2004). Table 1 summarizes other factors that affect the angle of internal friction of soils.

Table 1. Summary of Factors Affecting the Angle of Internal Friction (φ) (Holtz & Kovacs 1981)

| **Factor** | **Effect** |
|---|---|
| Void Ratio (e) | e↑, φ↓ |
| Angularity (A) | A↑, φ↑ |
| Grain Size Distribution | $C_u$↑, φ↑ |
| Surface Roughness (R) | R↑, φ↑ |
| Water (W) | W↑, φ↓ slightly |
| Particle Size (S) | No effect with constant e |
| Intermediate Principal Stress | $^{1,2}\varphi_{ps} \geq {}^{3}\varphi_{tx}$ |
| Overconsolidation or Prestress | Little effect |

$^{1}\varphi_{ps}$ = angle of internal friction at plane strain; $^{2}\varphi_{ps} = 1.5\varphi_{ts}-17$ for $\varphi_{ts}>34$ otherwise $\varphi_{ps} = \varphi_{ts}$; $^{3}\varphi_{ts}$=angle of internal friction from the triaxial test.

### 3.7.2 The Critical State Concept

When granular materials are being subjected to shearing, a random movement of solid soil particles of diverse sizes scratch, rub, chip, and even bounce against each other in the process of continuous deformation. If this process were viewed at the microscopic level, it will be noticed that a small shearing fringe exists where stochastic process of random movement of soil particles is taken place. At a very close range, it will found many causes of power dissipation and some damage to particles (especially if the soil sample is being subjected to large confining stresses); however, from a macroscopic point of view, the whole process is described as “friction”, neglecting the possibilities of degradation or of orientation of particles (Wood 1990).

When drained tests are conducted in granular materials at a given effective stress level, loose sands will contracts while dense sands will expands. The behavior of loose sands is similar to that of normally consolidated clays (it will contract); while the behavior of dense sands is similar to that of overconsolidated clays (it will expand). The reason loose sands and normally consolidated clays contracts while shearing is because they have an initially high specific volume that allows the packing and rearrangement of the soil particles during shearing. On the other hand, dense sands and overconsolidated clays have an initially low specific volume; therefore, there is not too much space among the soil specimen to accommodate soil particles during shearing leading to a volume expansion (Wood 1990). Figure 2 shows the behavior loose and dense sands under a given confining pressure.

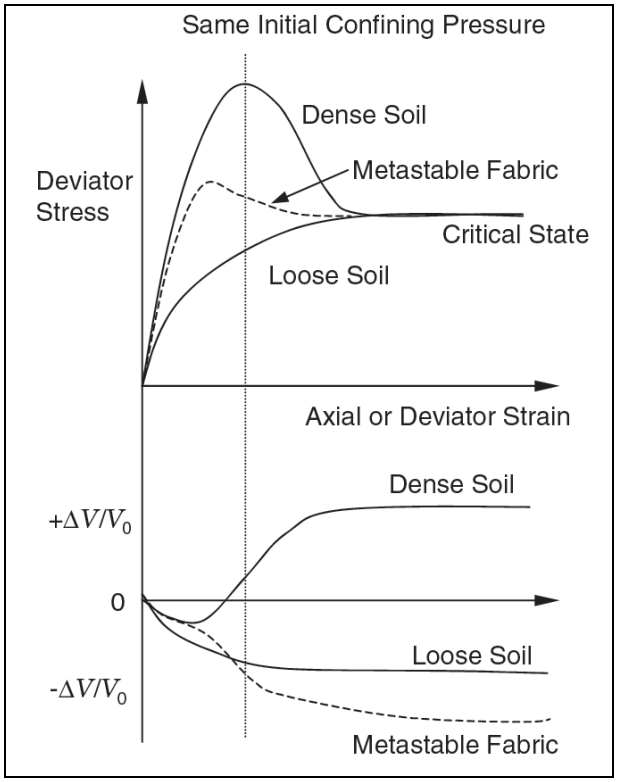


Figure 2. Volume Change of Sands during Shearing (Mitchell & Soga 2005)

After large shear-induce volume change, the soil will arrive to a point called critical state, which has specific water content and void ratio and it is independent of the initial state. At this point, shearing will continue without changes in volume (dilation angle correspond to zero after the soil has reached the critical state).

3.7.3 The Dilatancy Effect of Granular Materials

Several definitions have been proposed to explain the concept of dilatancy of particles during shearing. Rowe (1962) cited that dense sand expands during shearing at failure, whereas loose sand contracts. This proved that particles movement during

deformation and failure are not necessarily in the direction of the applied shear stress. Craig (2004) explains that during shearing of dense sand, the macroscopic shear plane is horizontal, but sliding between individual particles take place on numerous macroscopic planes inclined at various angles above the horizontal, as the particles move up and over their neighboring particles (figure 3). He defines the term dilatancy as the increase in volume of the dense sand during shearing and represented the rate of dilation as the gradient of the volumetric strain to shear strain $d\varepsilon_v/d\gamma$ (the maximum rate corresponding to the peak stress).

Figure 3 represents a sketch of the sliding movement of the soil particles located above the horizontal shear plane. As explained before, the particles will move and rotate in different directions. It also shows that angular materials provide more contact area between particles, providing more shearing resistance (high friction angle).

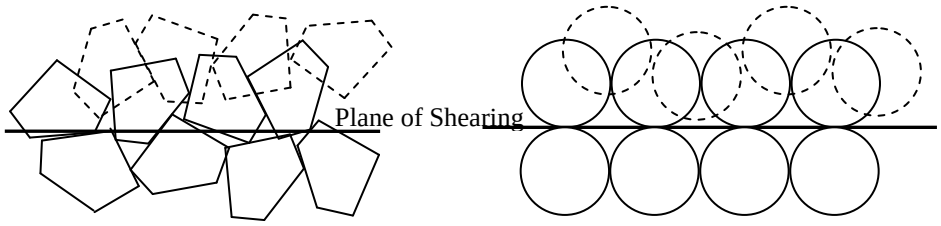


Figure 3. Sketch of Particles Movement during Shearing

Figure 4 sketches a dilating granular soil as it is subjected to a shearing force. Because the soil is expanding as it is being sheared, it is supposed that the sliding within the soil take place, not on horizontal planes, but on planes inclined at an angle of dilation

($\psi$) with respect to the horizontal plane (sliding between adjacent soil particles occurs on the inclined planes) (Wood 1990).

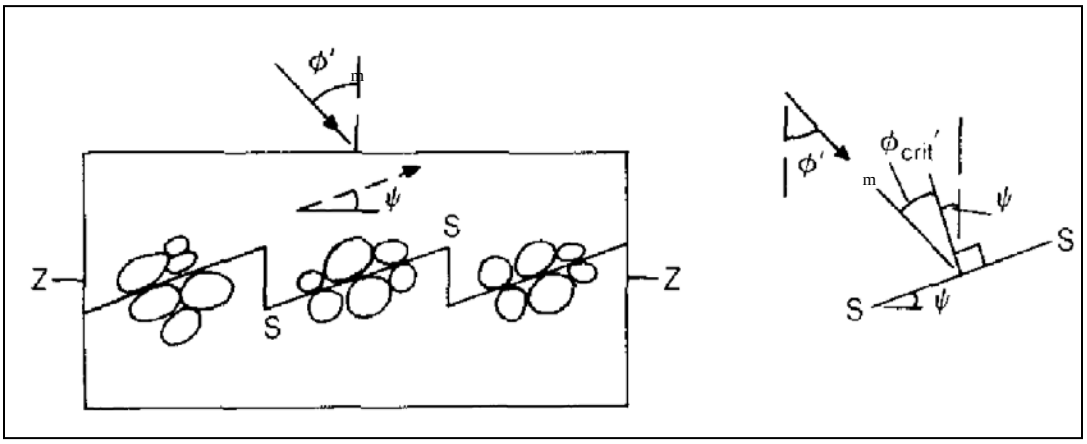


Figure 4. Sliding or Interlocking Saw Blades on Inclined Rough Surface (Bolton 1986)

Rowe (1962) also recognized that the mobilized friction angle $\Phi'_m$ must take into account particle rearrangements as well as sliding resistance at contacts and dilation. Particles crushing, which increases in importance as confining pressure increases and void ratio decreases, should also be added to the components (Mitchell & Soga 2005). Figure 5 shows the relationship of the strength contributing factors and porosity.

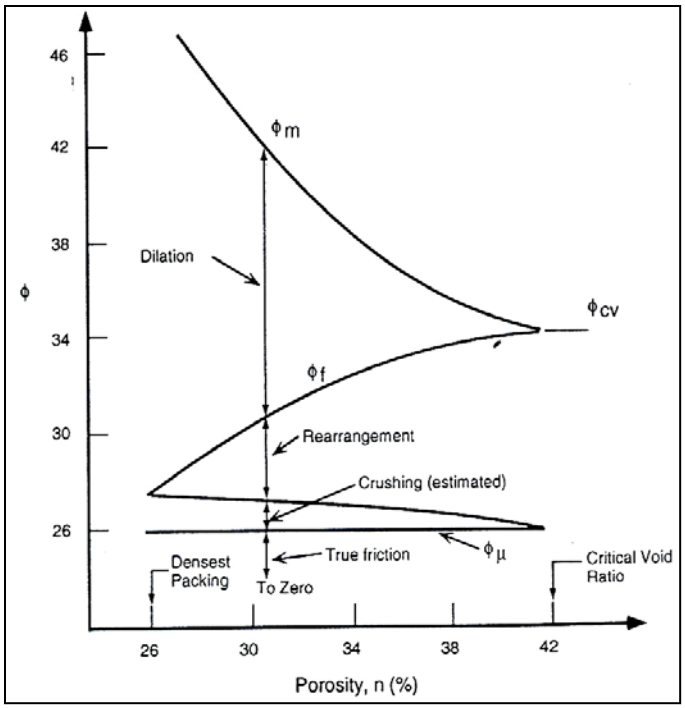


Figure 5. Contribution of Soil Strength of Granular Soils (Mitchell & Soga 2005)

The phenomenon of dilatancy in soils was first formulated by Taylor (1948), who calculated the work at peak shear-stress state and showed that the energy input is dissipated by friction using the following stress-dilatancy equation (Mitchell & Soga 2005):

$$\tau_{peak} dx - \sigma'_n \, dy = \mu \sigma'_n \, dx \tag{2}$$

Then, equation 2 results in:

$$\frac{\tau_{peak}}{\sigma'_n} = \tan\left(\phi'_m\right) = \mu + \left(\frac{dy}{dx}\right) \tag{3}$$

Where: $\tau_{peak}$= peak shear stress; $\sigma'_n$= normal effective stress; *dx*= incremental horizontal displacement; *dy*= incremental vertical displacement; μ=friction coefficient, $\Phi'_m$= mobilized friction angle; $\varphi_{crit}$=critical angle of friction, and; ψ=angle of dilation.

The first term of equation 2 ($\tau_{peak}d_x$) represents the work done by the shearing force. Because of the interlocking, not all the shearing work is dissipated by the soil. Some of it is required to lift the normal load and overcome the interlocking of the soil particles and it is represented by the second term of equation 2 ($\sigma'_n d_y$). The right side term represents the net work that goes into the sample, indicating that some of the work may be stored in elastic deformation of the soil, but must is dissipated as a frictional resistance between the grains (Wood 1990).

In general sense, equation 3 points out that the mobilized friction angle ($\varphi'_m$) of a mass of granular soil will accounts for sliding friction between grain particles (μ), and interlocking between grains (*dy/dx*). Then, equation 3 and 4 can be writing as:

$$\phi'_m = \phi_{crit} + \psi \tag{4}$$

It is supposed that the angle of friction resisting motion between layers of soil particles is always $\varphi_{crit.}$ This angle can be seemed as a soil constant, and become a stress dilatancy relation linking the mobilized friction angle ($\varphi_m$) with the angle of dilation ψ.

The mechanical significance of the angle of dilation in a plane strain deformation can be also applied to the case of the direct shear test, as shown in figure 6. If rigid

blocks of non-failing soil are assumed to bound the thin uniformly straining rupture zone AA, this must mean that for compatibility AA must be a zero extension line; therefore, $d\varepsilon_x = 0$ within the rupture zone (Bolton 1986).

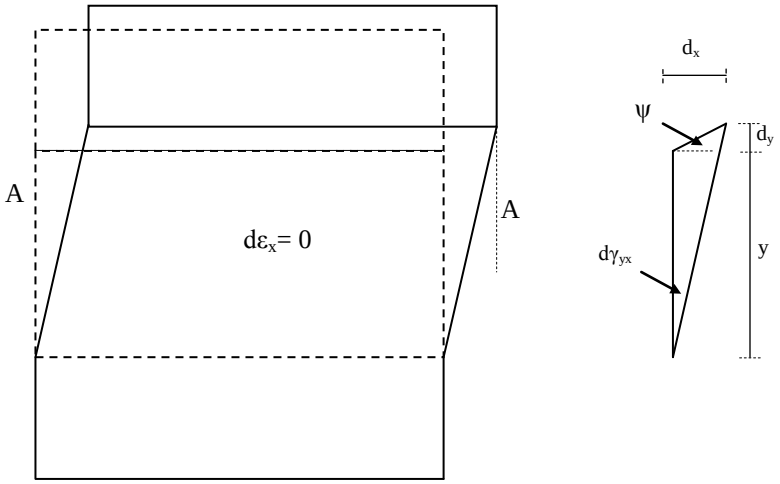


Figure 6. Representation of the Angle of Dilation on the Plane Shear (After Bolton 1986)

Considering that, the dilation angle of a soil can be computed using the following relation:

$$d\gamma_{yx} = \frac{dx}{y} \tag{5}$$

$$d\varepsilon y = -\frac{dy}{y} \tag{6}$$

$$\tan(\psi) = \frac{d\varepsilon v}{d\ \gamma_{xy}} = \frac{dy}{dx} \tag{7}$$

Where: $\gamma_{yx}$= shear strain; $\varepsilon_{y=}$ vertical strain, *dy* = change in thickness in mm; *dx* = change in relative horizontal displacement in mm, and ψ = dilation angle define as the slope of the curve *dy vs dx*.

Bolton (1986) states that the angle of dilation can be considered to be equal to the instantaneous angle of motion of the sliding blocks relative to the rupture surface (figure 7). In other words, dilation or contraction is assumed to occur only in a small shear band of thickness "y" (along the shearing plane).

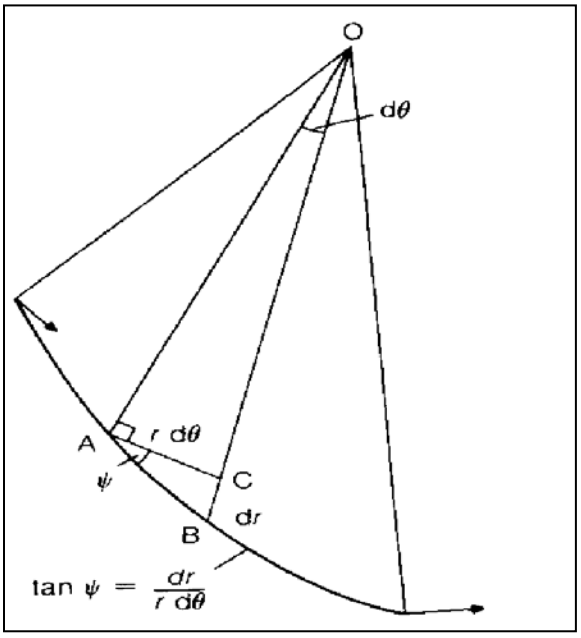


Figure 7. Schematic Representation of the Instantaneous Angle of Dilation (Bolton 1986)

# 4. TEST PROCEDURES

## 4.1 Density and Water Content

A field density and water content determination of soil compaction was done to the clean sand and the road base. The density tests were conducted using the sand cone method in accordance with ASTM D 1556 (Standard Test Method for Density and Unit Weight of Soils in Place by Sand-Cone Method). They were performed in two mechanically stabilized earth wall (MSEW) located at the facility research area of Riverside Campus. Three tests were conducted on the first embankment (figure 8) while one test was performed on the second embankment. The first embankment was built with a backfill of 10-ft of clean sand and 3-ft of road base at the top. The second wall was built with a backfill of 10-ft of crash rock with 3-ft of road base at the top.


Figure 8. Field Area Tested on MSE -Wall (Riverside Campus, Texas A&M University)

4.1.1 Summary of the Test Procedure for the Sand Cone Method

Prior to the in-situ density determination, two important procedures should be performed: 1) determination of the bulk density of the sand used for the test, and 2) determination of the weight of sand required filling the large cone of the apparatus (figure 9). The bulk density can be calculated using a container of known volume; knowing the weight of the sand and volume of the container, the bulk density is determined at its loosest state.

The procedure to determine the weight of sand retained in the cone can be described as follow:

1) Fill the apparatus with the calibration sand and record the weight to the nearest 0.01 lb
2) Place the base plate of the apparatus on a clean and level surface.
3) Invert the apparatus onto the base plate and open the valve to allow the cone and the base plate to fill with sand.
4) When the sand stops flowing into the cone, shut the valve and weigh the apparatus to the nearest 0.01 lb.
5) The difference between the full weight of the apparatus and the final weight after filling the cone is referred to as the Cone Correction.


a) Sand Calibration b) Cone Calibration

Figure 9. Calibration of the Unit Weight of the Sand and the Weight of Sand Retained in the Large Cone Apparatus

Once the unit weight of the sand and the weight of sand retained in the cone are known, the in-place density can be determined. This procedure is detailed in ASTM D 1556 and can be summarized as follow :

1) Fill the apparatus with calibration sand and record the weight.
2) Record the weight of a pan or an empty plastic bag to collect the soil.
3) Locate a representative area to conduct the test.
4) Remove any loose or uncompacted soil from the test site and level the area from the base plate to be seated.
5) Dig a hole into the soil through the hole in the base plate for the full depth of the layer being tested.

6) Place the soil in the pan, or plastic bag, and record the weight of the soil plus the container. It is important to have a portable scale to weight the soil in order to minimize the loose of water content.
7) Reset the base plate over the test hole and invert the apparatus onto the base plate and open the valve to allow sand to flow into the test hole. When the sand flow stops, shut off the valve and remove and weight the apparatus. Do not vibrate the apparatus during this process. These procedures can be seen in figure 10.

a) Determination of the Weight of the Sand Cone. b) Hole in the Road Base and Sample Collection.

c) Determination of the Unit Weight in the Road Base. d) Determination of Unit Weight in the Clean Sand.

Figure 10. Field Sand Cone Test Procedure for Density Determination

The water content of the soil was also determined at the site. A considerable amount of soil was collected to minimize error due to loss of water content and scale precision.

## 4.2 Grain Size Analysis

Particles size analyses were conducted on the three soil samples (silty sand, the clean sand, and the road base). The tests were performed in accordance to the designation ASTM D 2217-85 (Standard Practice for Wet Preparation of Soil Samples for Particle-Size Analysis and Determination of Soil Constants). This procedure is explained in detailed in the cited designation and it can be summarized as follow;

1) Take a portion of about 500 grams of air-dry material, if the soil is sand, or about 4000 grams of air dry materials, if the soil is gravel. In the case of the tested sands, the soil sample were between 500 g and 700 g and for the road base the sample was 4500 g .The amount of soil taken from each soil followed the criterion established in ASTM D 2217-85, in reference to the maximum particle size.
2) The soil sample should be first air- dry and then sieved. The fraction passing sieve #10 is collected and washed through sieve #200. A portion of 10 grams of calgon solution, to reduce the presence of lumps in the soil specimen, were used in all the wet sieve analysis performed on the samples. Figure 11 shows the sand portion of the silty sand retained in sieve # 200 after washing.

3) Collect the soil retains in the sieve #200 (sand portion) and oven dry for 24 hr at a temperature of about 110 $^{o}$C (230 F).
4) Weigh the sand portion of the soil specimen and perform a dry sieve analysis on that portion of the soil sample. The results of the dry sieve analysis for the clean sand, the silty sand, and the road base are presented in section 5.2, 6.1 and 7.2 respectively.

Figure 11. Sand Portion of the Silty Sand Retained in Sieve #200 after Washing

## 4.3 Hydrometer Analysis

Hydrometer analysis is used to determine the grain size distribution of fine grain soil having particles sizes smaller than 75 microns. The principle of the hydrometer

analysis is based on Stokes' Law. It assumes that disperse soil particles of various shapes and grain sizes fall in water under their own weight as non-interacting spheres (Bardet 1997). The distribution of particles sizes in computed as:

$$D = \sqrt{\frac{30\eta Hr}{981(Gs-1)\rho_w t}} \tag{8}$$

Where: D = particle diameter in mm; η = viscosity of the water in g/(cm.s); Hr = corrected depth of fall in cm; Gs = specific gravity of the soil particles; ρ = density of the water in g/cm$^3$, and; t = elapsed time in minutes.

Basically, two corrections are done in the computation of the particles size distribution: composite correction and temperature correction. The first account for the addition of dispersing agent added to the soil specimen, which increases the liquid density; the second account for the influences of the temperature on the density of the solution.

The test procedure for the hydrometer test is explained in the designation ASTM D 422 (Standard Method for Particle Size Analysis of Soil) and it is summarized as follows:

1) Prepare a dispersing agent solution (40g of calgon per litter) and determine the dispersing agent correction (composite correction).

2) Measure the specific gravity of the soil sample. In the case of the clean sand, a psycrometer test was conducted to determine the specific gravity of the clean sand. In the case of the silty sand and the road base, the specific gravity was assumed.

3) Take a soil sample between 75 grams to 100 grams, if the soil is sand or about 50 grams if the soil is clay. In the case of the soils tested, a sample size of about 80 grams for the sandy soil and 60 grams for the road base were collected from the particles passing sieve #200. The sample size follows the recommendation established by the ASTM D 422 in reference to specimen size base on the type of soil.

4) Pour the soil specimen on a container (Specified by ASTM D 422) with a 125 ml of the dispersing solution. Let the soil-water slurry stand up for about 16 hours. Then, add distilled water to the solution and mixed in a dispersing machine for 1 minute.

5) Transfer the solution to a 1000-ml sedimentation cylinder and add enough distilled water to fill the 1000 mL cylinder.

6) Mix the soil-water slurry in the graduate cylinder for 1 minute. Then, immersed the hydrometer slowly in the liquid. This last step should be done about 20 to 25 second before each reading.

7) Take the readings were at 5, 15, 30, 60, 90, and 120 second during the first two minutes. Because of the difficulty of these readings, this procedure was repeated and the averages of two readings were computed for all tests. After the two minutes, removed the hydrometer from the cylinder to avoid that the material will settle or adhere to hydrometer bulb.

8) The designation ASTM D 422 specifies that reading should be taken at 0.5, 1.0, 4.0, and 19 hrs. However, in the hydrometer analysis performed to the soil samples, reading were taking every five minutes during the first half hour and then continue to 0.5, 1.0, 1.5, 2.0, 3.0, 4.0, and 19.0 hours. After removing the hydrometer from each reading, the temperature of the water was also determined. Figure 12 shows the hydrometer reading of the silty sand.

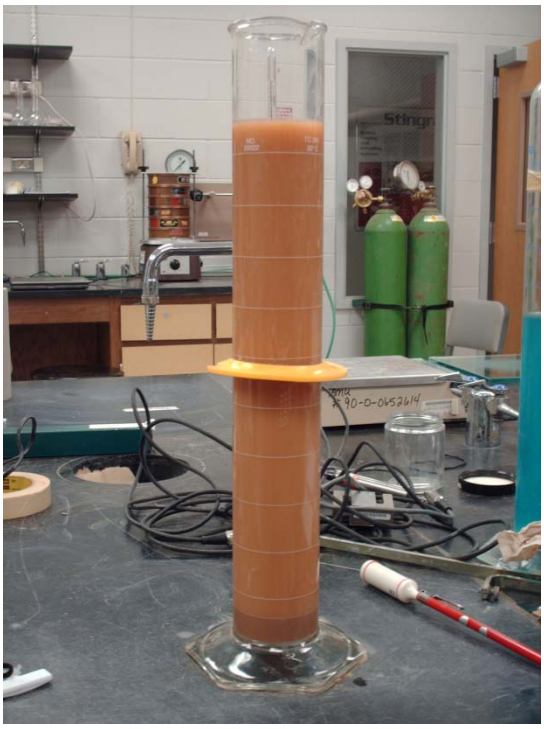

Figure 12. Hydrometer Analysis for the Silty Sand

## 4.4 Atterberg Limits

The Swedish soil scientist Albert Atterberg originally defined seven “limits of consistency” to classified fine grained soils, but in current engineering practice only two of the limits, the liquid limit and the plastic limit, are used. The Atterberg limits are based on the moisture content of the soil. The plastic limit ($w_p$) is the moisture content that defines where the soil changes from a semi-solid to a plastic (flexible) state. The liquid limit ($w_L$) is the moisture content that defines where the soil changes from a plastic to a viscous fluid state. From these limits of consistency, the Plasticity Index of

fine grained soils is defined as the difference between the Liquid Limit and the Plastic Limit.

The Atterberg Limits were conducted on those soils whose fine content exceed 10% (the silty sand and the road base). The tests were performed on the portion of soil passing sieve #40. The procedure of the test is detailed in the specification ASTM D 4318-00 (Standard Tests Methods for Liquid Limit, Plastic Limit, and Plasticity Index of Soils) and is summarized as follow:

1) Take a soil sample of about 200 grams of soil passing sieve #40. These samples were only taken from the silty sand and the road base due to its high fine content.
2) The soil must be thoroughly mixed with distilled water to reach a consistency of about 25 to 35 blows, in the liquid limit device, to close the groove.
3) Transfer the wet soil to the cup using a spatula. At this point, the cup must be resting in the base and the soil should be squeezed down until it forms a horizontal surface.
4) Form a groove at the center of the soil sample using suitable tools. Then, lift and drop the cup by turning the crank at a rate of approximately 2 drops per second until the two halves of the soil pat come in contact at the bottom of the groove along a distance of 13mm ( 1/2 in).
5) After the groove close at the specified distance, the numbers of blows have to be recorded. In addition, a soil portion from the center of the groove has to be taking to determine the water content.

6) Remove the entire soil specimen from the liquid limit device and repeat steps 2 to 5 by adding more water to the soil sample in order to ensure a consistency between 20 and 30 blows and 15 to 25 blows.
7) Plot the water content versus the number of blows in a semi log scale and determine the water content corresponding to 25 blows. This water content is defined as the liquid limit ($w_L$) of the soil sample.
8) The soil preparation for the plastic limit ($w_P$) is similar to the procedure followed for the liquid limit ($w_L$). In that case, the plastic limit is defined as the water content necessary to roll a soil specimen to a diameter of 3.2 mm before it breaks. During the Atterberg Limits Tests, two plastic limits ($w_p$) tests were performed and the plastic limit was taken as the average of the two (making sure that the difference between both tests does not exceed 1.4 %).

4.5 Specific Gravity (Gs)

The specific gravity of the solid particles is defined as the ratio of mass of a given volume of solids to the mass of an equal volume of water at $4^oC$ ($G_s=\rho_{s/}\rho_w$). The specific gravity test was performed to the clean sand in accordance with ASTM D 854-00 (Standard Test Method for Specific Gravity of Soils Solids by Water Psycrometer). The procedure can be summarized as follow:

1) Calibrate the weight of the psycrometer by weighting the artifact 5 times and determine the average of the weight and its standard deviation.

2) The volume psycrometer is calibrated by adding deaired water 5 times to the mark on the flask and recording the weight (psycrometer and water) and temperature.
3) Calculate the volume of the psycrometer by subtracting step 2 from step 1 and multiply the result for the correction factor (k).
4) Take a sample of about 50+/15 grams of air-dry sand.
5) Mix the soil with about 200 mL of deaired water for about 5 to 10 minutes.
6) Transfer the soil-water mixture to the flask and add deaired water to about 2/3 to 3/4 of the volume of the flask.
7) Attach the flack to a vacuum line and agitate while applying vacuum for about 2 hr.
8) When the vacuum process is completed, add enough deaired water to the mark of the flask, weigh, and located the psycrometer in a water bath for 24 hr.
9) After that period, weight the psycrometer and the water and take the temperature. Empty the flask and its content and oven-dry the soil. Then, record the weight of dry soil.
10) The specific gravity is calculated using the following formula:

$$G_s = \frac{W_s}{W_S + W_{fw} - W_{fs}} \tag{9}$$

Where: $W_s$= weight of the dry soil; $W_{fs}$ = weight of the flask filled with soil; $W_{fs}$ = weight of the flask filled with deaired water.

Figure 13 shows the psycrometer analysis conducted of the clean sand. Two tests were performed simultaneously in order to reduce uncertainties on the test. The results presented a difference of less than 2%.

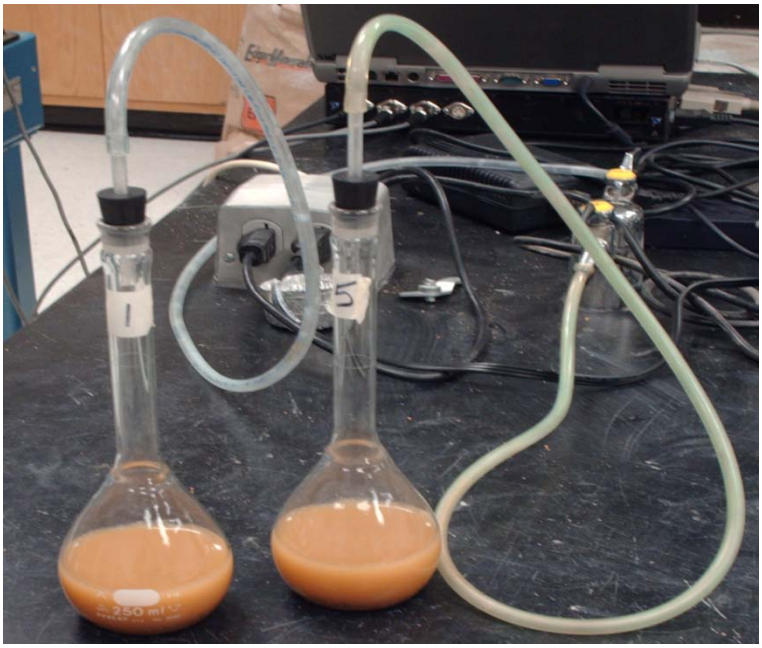

Figure 13. Specific Gravity Test by Water Psycrometer Conducted on the Clean Sand

4.6 Estimation of the Maximum and Minimum Void Ratio

The greatest possible void ratio or loosest possible condition of a soil is defined as the maximum void ratio ($e_{max}$). Similarly, the minimum void ratio ($e_{min}$) is the densest possible condition that a given soil can attain. Because of the importance of these parameters on studying the behavior of sandy soils, a laboratory procedure was set up to estimate the maximum void ratio ($e_{max}$) and the minimum void ratio ($e_{min}$) of the clean sand. The procedure is explained in the following paragraph.

In the case of the maximum void ratio ($e_{max}$), a calibrated cylinder of known volume was used to reproduce the loosest state of the clean sand. About 300 grams of clean sand sieved #4 was carefully poured on the contained avoiding any sort of particles arrangement. The sand was almost dry (w ≈0.3%) and the maximum void ($e_{max}$) was calculated using the following formula:

$$\frac{\gamma_d}{\gamma_w} = \frac{G_s(1+w)}{1+e_{max}} \tag{10}$$

Where: $\gamma_d$= dry unit weight on kN/m$^3$; $\gamma_w$= unit weight of the water in kN/m$^3$; $G_s$= specific gravity of the sand; *w*= water content in %, and; $e_{max}$= maximum void ratio.

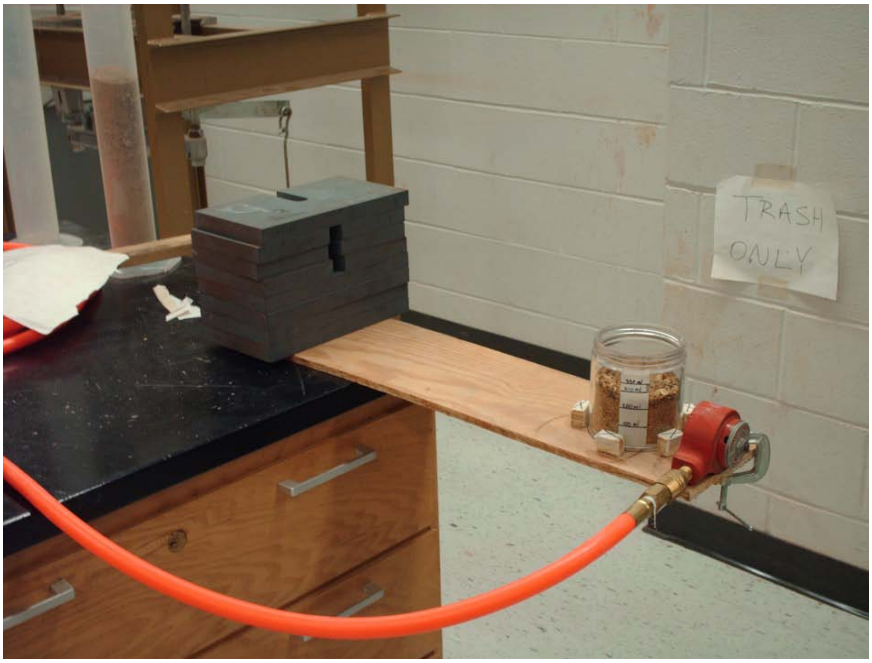


Figure 14. Experiment Set Up for Estimation of the Minimum and Maximum Void Ratio

In the case of the minimum void ratio ($e_{min}$), a calibrated container with 350 grams of sand, and a surcharge of 271.4 Pa at the top of the soil, was located at the end of a rectangular piece of wood. The sand was vibrated for a period of 20 minutes using a vibratory motor located at the end of the table, close to the container (figure 14). Finally, the minimum void ratio was calculated using equation 10.

## 4.7 Direct Shear Test (DST)

In the DST, a soil specimen is confined in a metal box of square or circular cross-section split horizontally at mid-height. If the specimen is saturated, a porous stones are placed below and above the soil specimen to allow free drainage; if the specimen is dry, a metal plates may be used in the same position. Suitable equipments are used to record the change in thickness, the horizontal displacement and the shear force. The shear strain ($\gamma$) is calculated as the change in shear deformation ($\Delta x$) divided by the original height of the of the specimen ($h_o$) and the volumetric strain ($\varepsilon_v$) by $\Delta h/h_o$.

A set of Direct Shear Tests (DST) were conducted on the clean sand following the criterion established by the designation ASTM D 3080 (Standard Methods for Direct Shear Test of Soils under Consolidated Drained Condition). The Direct Shear Tests were conducted on a circular shear box of 62-mm diameter containing a soil specimen of approximately 27-mm height. The tests were reproduced in the three different states: loose, dense and compacted states, this last using three different water content (2%, 4% and 6%). The procedure used to perform the DST is summarized as follow:

1) Determine the dimensions of the direct shear box use for the test as well as the weight of the empty box and the cap.
2) Take about 500 grams of sand sieved-#4 in order to avoid the presence of particles sizes larger than 4.75 mm. The procedure was performed in accordance to the ASTM D 3080 that specified a ratio of width/$D_{max}$ larger than 10.
3) The amount of soil necessary to achieve the loosest and the densest state was calculated based on the specific gravity of the soil, and the minimum and maximum void ratio estimated from the lab procedure. This procedure can only be done if the $G_s$ of the soil is known. Otherwise, an estimation of the value can be done by using engineering judgment.
4) Assembly the shear box and adjust the gap between the two halves by turning the set-screws. This procedure is very important to minimize the friction between the two parts of the shear box.
5) While the two pins hold the two parts of the shear box together, pour the sand carefully to obtain the loose specimen. In the case of the dense state, the sand can be poured and vibrated in three different layers in order to achieve the desire void ratio.
6) After pouring the soil, weigh the shear box and the soil sample in order to determine the exact amount of soil used for the test. From that information, the void ratio and unit weight of the specimen can be calculated.

7) As it is recommended for dry sands, two steel discs (one at the top and one at the bottom), were used in assembling the shear box with the soil specimen for the DST performed.
8) Level the soil surface at the shear box before the test started. Also, record the height of the soil specimen.
9) Assembly the shear box in the DS device. Add the dead weight to the frame in order to achieve the desire normal stresses.
10) For the case of the clean and the silty sand, the DST tests were conducted using a shear rate of 0.5 mm/min. Two linear strain conversion transducers were used to record the vertical and the horizontal displacement of the soil specimen. The shear force was recorded using a force transducer. Detail of the Direct Shear Device and the location of these displacement and force transducer are presented in figure 15 and 16.

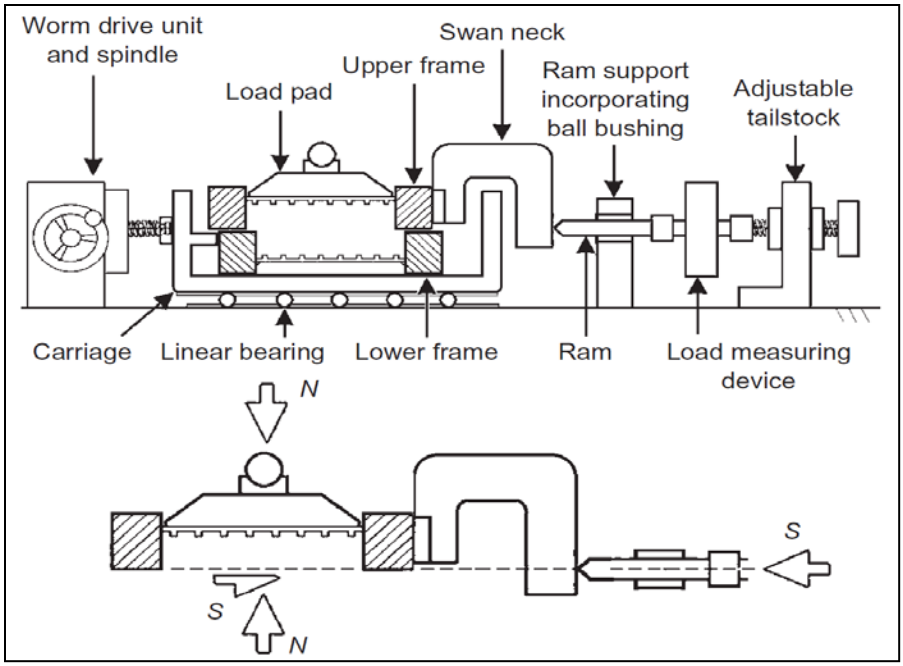


Figure 15. Sketch of the Direct Shear Apparatus (DSA). (Lings &Dietz 2004)

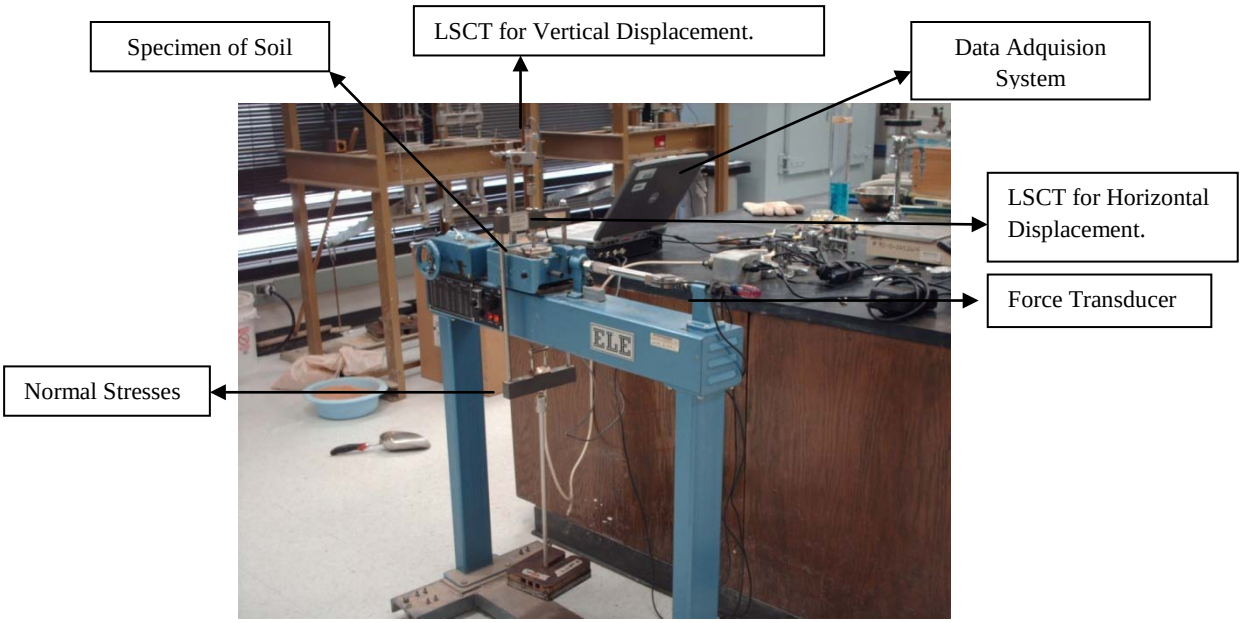


Figure 16. Assembly of the Direct Shear Device

4.7.1 Area Correction of the Soil Specimen

Area corrections were applied to the shear stresses calculations for the results of the Direct Shear Tests (DST). The corrected area of the specimen ($A_{cs}$) in the shear plane of the shear circular box test can be calculated as follow:

$$A_c = \frac{D^2}{2}\left(\theta - \frac{\delta}{D}\sin\theta\right) \quad (11)$$

$$\theta = \cos^{-1}\left(\frac{\delta}{D}\right) \quad (12)$$

Where: $A_c$= corrected area in $m^2$; D = diameter of the shear box in m; θ= deformation angle in radians, and; δ= relative horizontal displacement of the soil specimen in m.

According to Bardet (1997), for a typical sample diameter of D = 6.3 cm, the error on shear and normal stresses may reach 20% when δ=1 cm.

4.7.2 Checking the Frictional Resistance of the Direct Shear Apparatus (DSA)

An experiment to determine the frictional resistance of the Direct Shear Apparatus (DSA) was conducted. Five different normal forces were applied to the shear box (8.51 N, 18.3 N, 37.91 N, 67.23 N, and 106.42 N) without having any soil specimen inside it. The purpose of the test was to determine the coefficient of friction of the DSA, if any exists. Figure 17 shows the relationship between the normal and the shear force. From figure17, it is estimate that the friction coefficient μ of the device is 0.2086.

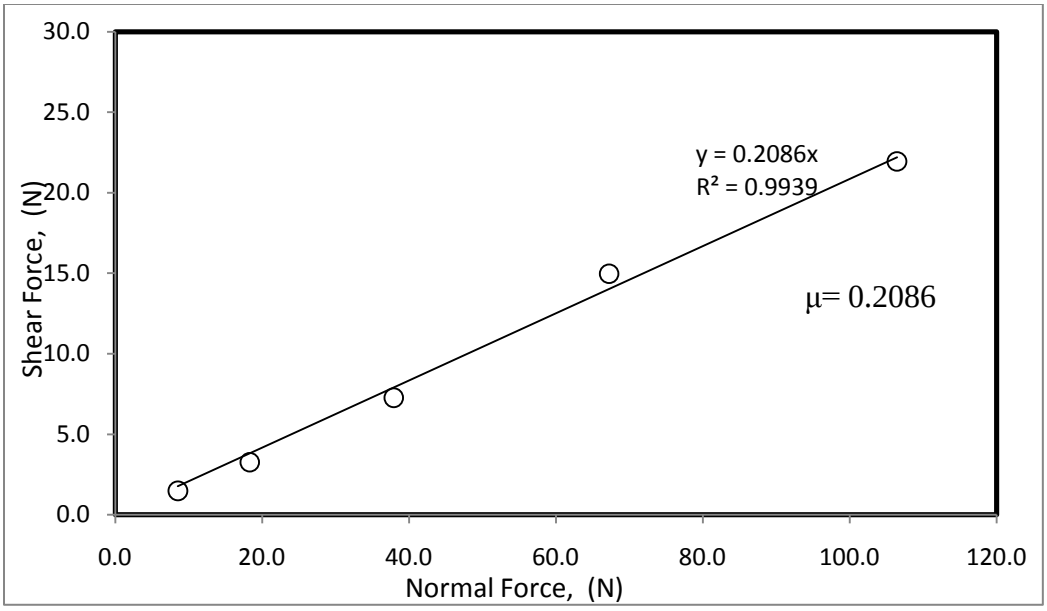


Figure 17. Estimation of the Coefficient of Friction of the Direct Shear Apparatus (DSA)

Equation 1 was the proposed formula to calculate the frictional resistance of the system.

$$\tau_B = \frac{F_N + W'_B}{A_{CB}} \times \mu_B \tag{13}$$

Where: $F_N$= applied normal force (N); $W'_B$= effective weight of the upper box; $A_{CB}$= contact area of the shear box interface ($m^2$), and; $\mu_B$=coefficient of friction of the shear box interface.

The friction correction of the shear box was calculated using the upper weight of the shear box (W=0.867 kg) resulting on a shear stress correction of 0.61 kPa, practically negligible. Therefore, frictional correction was not accounted on the shear stress calculation.

## 4.8 Triaxial Compression Test (TC)

A Triaxial Compression Tests were conducted on the clean sand and the road base using a specimen of 8.5 inches height and 6 inches diameter. The maximum particle size of the clean sand was 5 mm while the maximum particle size used for the road base was 25 mm. These conditions do not follow the requirement of the American Standard Testing of Materials (ASTM) that required a ratio of height- diameter of 2:1. Also, the standard requires that the maximum particle size of one tenth of diameter, which correspond to 15.24 mm for the road base.

For the clean sand, the soil was air-dried in the same manner as those for the DST. The sand was poured carefully in a mold of 8.5 in height by 6 in diameter covered with a rubber membrane of unknown correction factor. One pore stone was located at the base of the mold and two at the top. Two samples were tested at confining pressure of 7 psi and 12 psi respectively (48.12 and 82.76 kPa). The rate of loading was specified as 0.15 in/min (3.81 mm/min).

For the road base, compaction of the specimen was achieved using the modified proctor test with 7 layer and 56 blows per layer. The number of layers was adjusted accordingly in order to achieve a maximum dry unit weight of approximately 90% to 95 % of the maximum dry unit weight obtained from the modified compaction curve. The specimens were assembled in the mold with one pore stone at the bottom and two at the top. The confining pressures used for the road base were 7 psi and 10 psi (48.12 and 82.76 kPa). Figure 18 shows the triaxial compression test conducted in a big triaxial cell

at the Material Lab. of the Zachry Department of Civil Engineering at Texas A&M University.


Figure 18. Triaxial Compression Test Conducted on the Clean Sand and the Road Base

4.9 Soil Modulus Test (Briaud Compaction Device, BCD)

Nowadays, there is a trend towards the use of a soil modulus as an alternative parameter to the dry density for the compaction process (Briaud, et al. 2009). This trend is based on two motivating factors:

1. Avoiding nuclear devices, such as the nuclear density gage, and;

2. Using a parameter more directly related to limiting deformations, which is the design criterion.

The Briaud Compaction Device (BCD) is a rapid Modulus Device use for determination of soil modulus. The potential of the BCD is in the field of soil compaction. This includes compaction of soil layers for highway and airport pavements, compaction of soil layers for embankments, compaction of backfills for retaining walls. It has two main advantages compared to other soil modulus devices: 1) it is a much faster test (approximately 5 seconds), and; 2) it can be used both in the laboratory to obtain the target modulus and in the field to verify that the target modulus has been achieved (Briaud et al. 2009).

The BCD test was conducted on both, in field and in the laboratory. The procedure followed to perform both tests is explained in detailed by Briaud et al. (2009), and summarized as follow:

- Field Test Procedure for the BCD :

1) Prepare a sand cushion using fine sand with a water of approximately 10%. The sand cushion should be located in the target area with a thickness of about 4-5 mm. This will ensure about 90% contact between the BCD plate and the soil.
2) Place the BCD as perpendicular as possible to the prepared sand cushion. Then, set up the device for the field test.

3) Once the BCD is set up, load the device by leaning on it until a beep is heard. This beep represents the first loading test which is not used. The beep also indicates that the correct load of 223 N (50 lb) has been reached.
4) The application of the load should be done slowly, within a period of about 5 second, as recommend by Briaud et al. (2009).
5) Unload the device until another beep is herd. Then, the BCD was loaded again by leaning on it for a second time. At this point, the BCD displays the Reload Modulus.
6) A number of 4 tests should be conducted on each point. The field BCD Modulus is reported as the average of the four measurements.

The laboratory BCD test was performed on top of a modified proctor mold of 6 inches diameter (150 mm) and 4.58 inches height (116.33 mm). The specimen was compacted in accordance to the designation ASTM D 1557-07 (Standard Method for Laboratory Compaction Characteristics of Soil Using Modified Effort -56,000 ft-lbf/ft$^3$). The test procedure is detailed by Briaud et al. (2009), and is summarized in the following steps:

- Laboratory BCD Test:
  1) Place the BCD plate of the top of the modified proctor mold. Keep the BCD as perpendicular as possible to soil specimen throughout the test.
  2) Ensure that the edge of the BCD plate does not touch the wall of the mold. Check all around the BCD plate and set up the BCD to be ready to test.

3) If the soil surface of the specimen is very irregular, use a sand cushion with the same specification as describe in the field test procedure.
4) Follow the same procedure as for the field BCD test to obtain the laboratory BCD modulus.

Figure 19 presents a the conduction of a laboratory and field BCD test.

(a) Laboratory BCD Test. (b) Field BCD Test.

Figure 19. Laboratory and Field BCD Test

## 4.10 Modified Proctor Compaction Test

Laboratory compaction tests are used to determine the relation between the water content and the dry unit weight of soils as well as to find the maximum dry unit weight and optimum water content of a soil specimen. The modified compaction test was conducted on the clean sand and the road base in accordance to the designation ASTM D

1557-07 (Standard Method for Laboratory Compaction Characteristics of Soil Using Modified Effort -56,000 ft-lbf/ft$^3$). A mold of 4.58 inches height (116.33 mm) and 6 inches diameter (150 mm) was used to prepare the specimen. The soil was compacted in five layers using a hammer with a weight of 44.5 kN and a dropping distance of 18 inches (457 mm). The procedure for the test is detailed in ASTM D 1557-07 and summarized as follow:

1) Weight about 5000 grams of air dry soil. The weight of this sample can vary depending of the particles size of the tested soil.
2) Add suitable amount of water to the soil specimen and mix thoroughly. The weight of the water to be added can be determined prior to the specimen preparation.
3) Place the mold assembly on a solid base such as a concrete base. Then, place the soil into the mold and compact the soil by applying 56 blows of the hammer dropped from the controlled height of 18 inches (457 mm).
4) Ensure an evenly distribution of the compaction energy by moving the hammer around the mold in all positions.
5) Place another layer and repeat step 3 and four until you reach the number of desire layers (5).
6) Remove the extension collar and cut away all the remaining soil on the top of the mold. Then, weigh the mold and the soil and extrude the sample on the extractor device.

7) Take a representative sample of the material to compute the water content.
8) Repeat steps 2 to 7 at different water content and plot in arithmetic scale the dry unit weight versus water content. Then estimate the maximum the dry density and optimum water content from the curve.

   Figure 20 shows the conduction of a Modified Proctor Compaction Test in the Geotechnical Graduate Lab. of the Zachry Department of Civil Engineering at Texas A&M University.


Figure 20. Modified Proctor Compaction Test

# 5. TESTS RESULTS FOR THE CLEAN SAND

Sandy soils, such as the clean sand, are extensively used as a backfill for full-scale tests at the research facility of the Texas Transportation Institute (Riverside Campus at Texas A&M University). A set of laboratory and in-situ tests were conducted to the clean sand in order to compute their physical and mechanical properties such as its frictional resistance (φ) and its dilation angle (ψ). The sand is classified as poorly-graded sand SP (according to the Unified Soil Classification System) and the samples for the tests were collected from a pile of loose sand at Riverside Campus at Texas A&M University (figure 21). The original source of the clean sand is a local pit called Scamardo Pit. The reports of these properties are presented on the following sections.

Figure 21. Pile of Loose Clean Sand Used to Collect the Samples for the Laboratory Tests

## 5.1 Field Test Results for the Clean Sand (Density, Soil Modulus and Water Content).

In place-density, BCD modulus and field water content were conducted to the clean sand at the field. The in-situ density was determined using the Sand Cone Method in accordance to the designation ASTM D 1557-07 (Standard Test Method for Density and Unit Weight of Soils in Place by the Sand Cone Method). The BCD Modulus Test was performed following the procedure described in section 4.9 for the field BCD test. In this particular case, a sand cushion of approximated 5 mm thick was placed in the target area in order to ensure a good contact between the BCD plate and the soil surface (approximately 90% of contact). The water content of the sand cushion was estimated to be between 4 to 5%. The results of the tests are presented on table 2.

Table 2. Field Test Results for the Clean Sand

| IN PLACE DENSITY DETERMINATION- SAND CONE METHOD | | | |
|---|---|---|---|
| Project Name: MSE Wall Project | | Tested By: Deeyvid SAEZ | |
| Soil Type: Clean Sand (SP) | | Date: 07/22/2009 | |
| Test site: Riverside Campus | | Section: Area 3 | |
| **CALIBRATION OF THE SAND (STANDARD MATERIAL)** | | | |
| Weight of the mould (g) | 4591.66 | 4591.53 | 4591.48 |
| Weight of the mould + sand (g) | 6062.30 | 6060.87 | 6058.59 |
| Weight of material (g) | 1470.64 | 1469.34 | 1467.11 |
| Volume of the mould, ($m^3$) | 0.0009408211 | 0.0009408211 | 0.0009408211 |
| Density of the material ($kg/m^3$) | 1.563 | 1.562 | 1.559 |
| Average density of the material ($kN/m^3$) | 1.561 | | |
| Average unit weight of the material ($kN/m^3$) | 15.318 | | |
| **CALIBRATION OF THE CONE** | | | |
| Initial weight of the cone +sand (g) | 6974.15 | 6090.67 | 6085.18 |
| Final weight of the cone + sand (g) | 5326.79 | 4428.28 | 4436.08 |
| Weight of the sand retained in the cone (g) | 1647.36 | 1662.39 | 1649.1 |
| Average weight of the sand retained in the cone (g) | 1652.95 | | |
| **VOLUME OF THE HOLE** | | | |
| Initial weight of the cone + sand (g) | 6800 | | |
| Final weight of the cone + sand (g) | 3100 | | |
| Weight of the sand release (g) | 3700 | | |
| Weight of sand release in the hole (g) | 2047.05 | | |
| Volume of the hole ($m^3$) | 0.001311006 | | |
| **WATER CONTENT DETERMINATION** | | | |
| Weight of the bowl (g) | 357.60 | | |
| Weight of the wet soil + bowl (g) | 3623.80 | | |
| Weight of the dry soil + bowl (g) | 3417.50 | | |
| Weight of water (g) | 206.30 | | |
| Water Content (%) | **6.04** | | |
| **UNIT WEIGHT DETERMINATION** | | | |
| Weight of plastic bag (g) | 12.1 | | |
| Weight of wet soil + plastic bag (g) | 2460.9 | | |
| Weight of wet soil (g) | 2448.8 | | |
| Unit weight of the soil ($kN/m^3$) | **18.32** | | |
| Dry Unit Weight of the soil ($kN/m^3$) | **17.28** | | |
| BCD Modulus (MPa) | **15.14** | | |

The Sand Cone test was conducted using Ottawa Sand as a reference material. Prior to the test, the unit weight of the Ottawa Sand, in its loosest state, was calibrated. The results showed that the field total unit weight of the clean sand was 18.32 $kN/m^3$ with an in-situ water content of 6.04 % and a dry unit weight of 17.28 $kN/m^3$. For this condition, the field BCD modulus was 15.14 MPa.

## 5.2 Index Properties

A set of three particles size analyses were conducted on the clean sand by performing a wet sieve analysis in accordance with the designation ASTM D 2217-85 (Standard Practice for Wet Preparation of Soil Samples for Particle-Size Analysis and Determination of Soil Constants). Figure 22 shows the gradation curve of the three wet sieve analyses performed on the clean sand. The fine content of the sand vary from 2.8% to 3.4 % with an average of 3.1%. The soil presents a coefficient of uniformity ($C_u$) of 3.85 and a coefficient of curvature ($C_c$) of 0.84, which provides a fairly good gradation.

The sand was classified as poorly graded sand (SP) according to the Unified Soil Classification System (USCS). Despite the fact the sand presents a well distribution of their particles sizes (figure 22), it did not meet the requirement of the coefficient of uniformity and the coefficient of curvature of a well graded sand ($1.0 < C_c < 3.0$ and $C_u > 6.0$).

A specific gravity test was conducted on the clean sand by performing a psycrometer analysis, in accordance with the designation ASTM D 854-00. The tests were performed on the portion of soil passing the sieve #4. The result shows that the clean sand has an average specific gravity ($G_s$) of 2.64. This specific gravity is within the reasonable value for poorly graded soils as it is presented by the result of the tests conducted by Bareither (2006).

Atterberg limits were not tested on the clean sand (SP) because the sand presents a fine content less than 5%. The index properties of the clean sand are summarized in table 3 and particles size distributions are presented on figure 22.

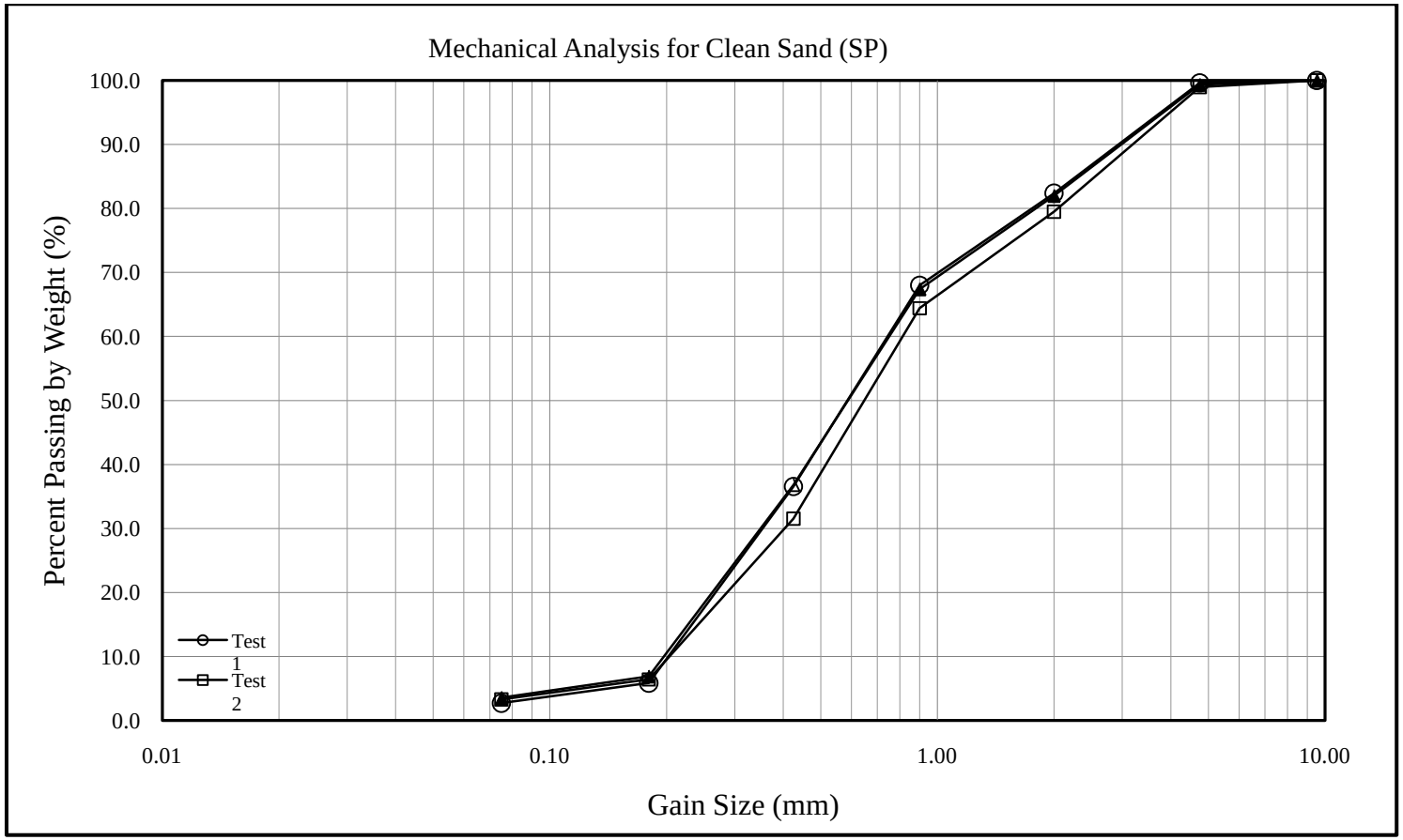


Figure 22. Particles Size Distribution Curves for Clean Sand

Table 3. Select Index Properties of the Clean Sand

| Sample | $D_{10}$[1] | $D_{30}$[2] | $D_{50}$[3] | $D_{60}$[4] | Perc. Fines | $C_c$[5] | $C_u$[6] | $w_L$ | $w_P$ | $w_{PI}$ | Perc. Grav. | Gs | USCS[5] |
|---|---|---|---|---|---|---|---|---|---|---|---|---|---|
| Clean Sand | 0.20 | 0.36 | 0.51 | 0.77 | 3.1 | 0.84 | 3.85 | - | - | - | 0.7 | 2.64 | SP |

[1]$D_{10}$= particle diameter at 10% finer; [2]$D_{30}$= particle diameter at 30% finer; [3]$D_{50}$=particle diameter at 50% finer; [4]$D_{60}$= particle diameter at 60% finer; $C_c$ = coefficient of curvature; $C_u$= coefficient of uniformity; USCS[7]= Unified Soil Classification System.

Note: the index properties presented on table 1 represents the average of three tests.

## 5.3 Estimation of the Minimum and Maximum Void Ratio

A simple procedure was set up to estimate the maximum void ratio ($e_{max}$) and the minimum void ratio ($e_{min}$) of the clean sand. A total of 5 tests were performed following the procedure explained in section 4.6 in order to ensure repeatability of the tests. Figure 23 shows the results of the 5 tests conducted to the loose and the dense states of the clean sand. The average maximum void ratio ($e_{max}$) was approximately 0.598 with a standard deviation (STDEV) of 0.005 and a coefficient of variance COV = 0.81%. In the case of the dense state, the average minimum void ratio ($e_{min}$) resulted on 0.430 with a standard deviation (STDEV) of 0.007 and a coefficient of variance on the tests of COV=1.56%. Table 4 presents all the results and calculations for the minimum and the maximum void ratio of the clean sand.

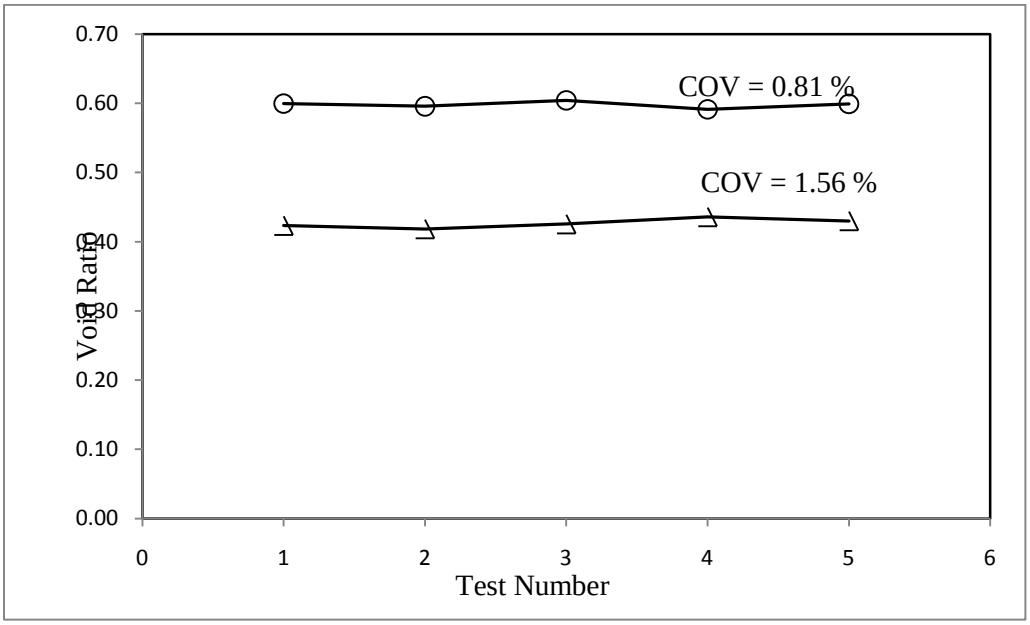


Figure 23. Estimation of Maximum and Minimum Void Ratio for the Clean Sand

Table 4. Estimation of the Maximum and Minimum Void Ratio for the Clean Sand

| **ESTIMATION OF MAXIMUM AND MINIMUM VOID RATIO FOR THE WASH SAND** | | | | | | |
|---|---|---|---|---|---|---|
| Description of the sample: Poor graded sand (SP) | | | Location: Riverside Campus - Texas A&M University | | | |
| Date: 07/21/2009 | | | Tested by: Deeyvid Saez Barrios | | | |
| Vibration time (min) | | 20 | Specific Gravity of the Sand, Gs | | | 2.64 |
| Applied Surcharge (Pa) | | 271.4 | Unit Weight of the Water, ($kN/m^3$) | | | 9.810 |
| **ESTIMATION OF THE MAXIMUN VOID RATIO ($e_{max}$)** | | | | | | |
| Determination No. | T-1 | T-2 | T-3 | T-4 | T-5 | STDEV |
| Mass of container (g) | 136.45 | 136.44 | 136.45 | 136.45 | 136.46 | 0.007 |
| Volume of the sand (cc) | 400.00 | 400.00 | 400.00 | 400.00 | 400.00 | 0.000 |
| Container + soil (g) | 799.37 | 801.02 | 797.49 | 802.84 | 799.57 | 1.998 |
| Mass of sand (g) | 662.92 | 664.58 | 661.04 | 666.39 | 663.11 | 2.000 |
| Estimated water content (%) | 0.42 | 0.42 | 0.42 | 0.42 | 0.42 | 0.000 |
| Unit weight (%) | 16.26 | 16.30 | 16.21 | 16.34 | 16.26 | 0.049 |
| Estimated maximum void ratio, $e_{max}$ | 0.60 | 0.60 | 0.60 | 0.59 | 0.60 | 0.005 |
| **ESTIMATION OF THE MAXIMUN VOID RATIO ($e_{min}$)** | | | | | | |
| Determination No. | T-1 | T-2 | T-3 | T-4 | T-5 | STDEV |
| Mass of container (g) | 309.33 | 309.35 | 309.36 | 309.33 | 309.35 | 0.013 |
| Container + soil (g) | 807.32 | 806.70 | 808.92 | 807.61 | 809.64 | 1.208 |
| Mass of soil (g) | 497.99 | 497.35 | 499.56 | 498.28 | 500.29 | 1.201 |
| Volume of the container (cc) | 300.00 | 300.00 | 300.00 | 300.00 | 300.00 | 0.000 |
| Diameter of the container (mm) | 80.00 | 80.00 | 80.00 | 80.00 | 80.00 | 0.000 |
| Initial height (from top), (mm) | 33.50 | 33.75 | 34.25 | 34.25 | 34.00 | 0.326 |
| Final height (from top), (mm) | 40.00 | 40.50 | 40.50 | 40.25 | 40.00 | 0.250 |
| Final Volume, (cc) | 267.33 | 266.07 | 268.58 | 269.84 | 269.84 | 1.638 |
| Estimated water content, (%) | 0.43 | 0.43 | 0.43 | 0.43 | 0.43 | 0.000 |
| Unit Weight, (%) | 18.27 | 18.34 | 18.25 | 18.11 | 18.19 | 0.085 |
| Estimated minimum void ratio, $e_{min}$ | 0.42 | 0.42 | 0.43 | 0.44 | 0.43 | 0.007 |

## 5.4 Modified Proctor Compaction Test and Soil Modulus Curve

General standards on compaction control required backfill for MSE walls, or reinforced soils for slopes, to be compacted at 95 % of the maximum dry unit weight, corresponding to the standard proctor compactive effort, or 90 % of the maximum dry unit weight, corresponding to the modified proctor compactive effort. The maximum dry unit weight obtained from compaction tests are also commonly used for transportation department to control placement of coarse and fine grained soils (Bareither, 2006).

Considering that, the modified compaction proctor was conducted on the clean sand in accordance with the designation ASTM D 1557-07 (Standard Method for Laboratory Compaction Characteristics of Soil Using Modified Effort -56,000 ft-lbf/ft$^3$). The test was performed on the soil particles passing sieve #4, following method C of the cited designation. The procedure followed to conduct the test is explained in section 4.10. Figure 24 shows the modified compaction curve for the clean sand.

It is clear from figure 24 that the compaction level of the clean sand do not experiment considerable changes as lubrication takes place. The nearly asymptotic behavior of the curve, as water content increases, is not surprising for granular material like the clean sand (SP). The reason is the lack of fine content present in the soil that prevents the retention of water. In fact the maximum dry density of this sand can be achieved at relatively low water content (around 2.0%). At this point, the curve shows a

slightly peak that can be interpreted as the point at which the maximum dry density is achieved. For the clean sand, the maximum dry density is estimated as $\gamma_{max}$= 18.7 kN/m$^3$ with an optimum water content of $w$ = 2.3%.

Another phenomenon was observed during testing. As water content increases, bleeding occurs through the gap between the mold and the plate base of the proctor mold. This reduces the water content and increases the unit weight by allowing the soil particles to replace the void spaces.

It can be seem from figure 24 that the total unit weight of the sand is increasing with the water content but the dry unit weight of the sand decreases.

Normally sands saturate a low water contents, specially those sands with a low fine content. In this case, the clean sand reaches the saturation line at a water content of approximately 10.5%.

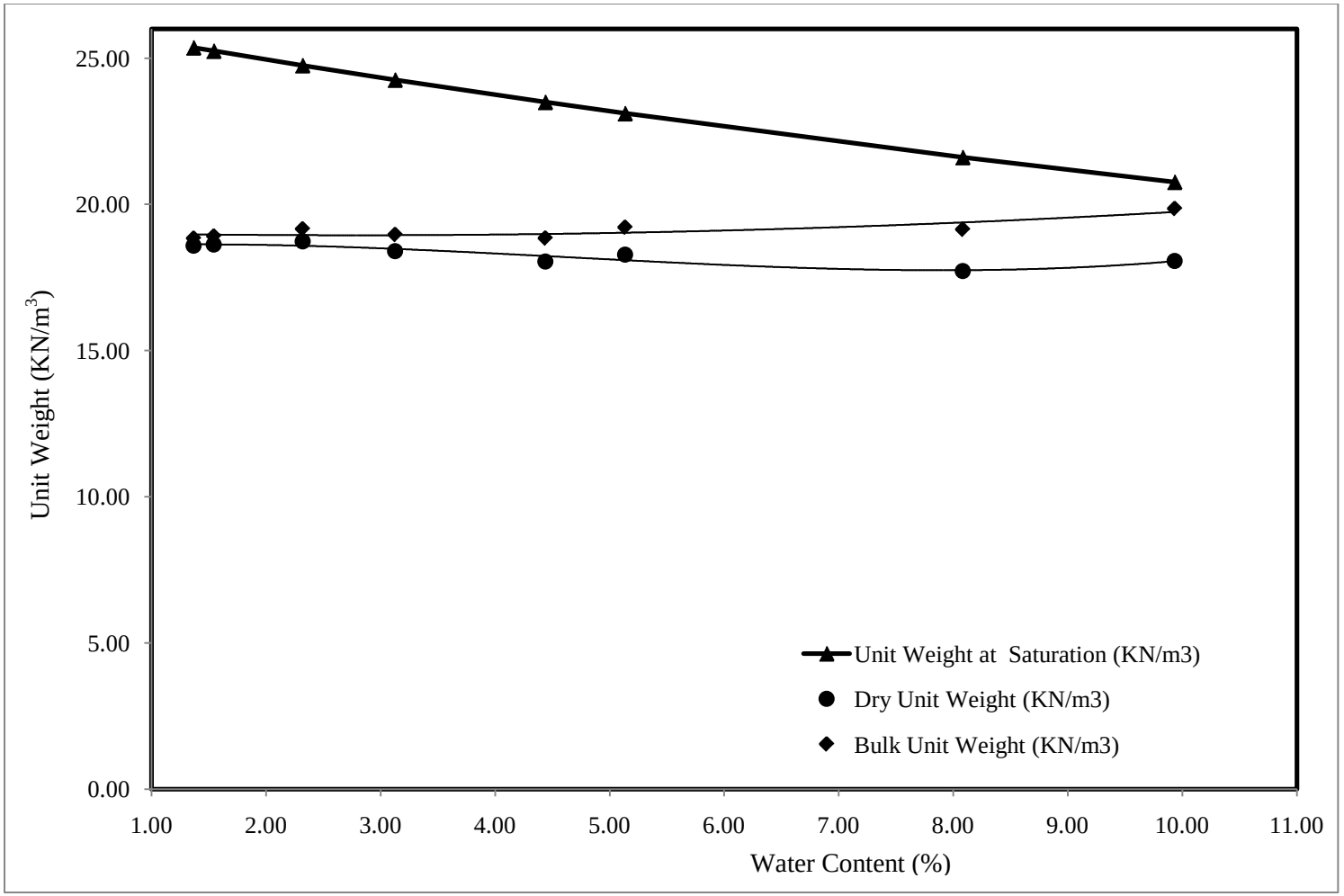


Figure 24. Modified Compaction Curve for the Clean Sand

## 5.5 Comparison between the Dry Unit Weight and the Laboratory Soil Modulus

A soil modulus versus water content curve was developed for the clean sand. The soil modulus was determined using the Briaud Compaction Device or BCD following the procedure describe in section 4.9.

Section 3.6 explains that the soil modulus is affected by different soil and loading parameters. Considering that, it seems more reasonable to control compaction on the basis of modulus rather than dry density. As it is specified for the dry unit weight, the control of compaction at the field can also be established under a target value of the maximum modulus obtained from the modulus versus water content curve. Briaud et al. (2009) establishes that a target value of 75% of $E_{max}$ may be reasonable since the modulus vary more with the water content than the dry density; however, he concluded that establishing such a target value will require more engineering judgment

It is clear from figure 25 that the soil modulus is a more susceptible parameter to the water content than the dry unit weight. Also, there is not an apparent relationship between the dry unit weight and the soil modulus in a particular soil. The maximum soil modulus is usually achieved at a lower water content value than the water content corresponding to the maximum dry unit weight. The clean sand achieves its maximum dry unit weight (18.7 $kN/m^3$) at a water content of approximately 2.3% while the maximum modulus (37 MPa) is achieved at a water content of 1.5%. The reason of this phenomenon, as explained in section 3.6, is the suction generated at low water contents.

Comparing the soil modulus curve of the clean sand and the road base presented in section 7.4, the variation of the soil modulus of the clean sand is smoother than the road base (figure 25). The low fine content present in the clean sand provide more stiffness to the aggregate under lubrication and load application.

## 5.6 Angle of Repose

The angle of repose of a granular material represents the steepest stable slope for very loosely packed sand; therefore, the angle of repose represents the angle of internal friction of the granular material at its loosest state (Holtz & Kovacs 1981). The angle of repose of the clean sand was determined by carefully pouring a pile of dry clean sand, from a single point, on a table. The sand formed a conical shape and the angle of repose was calculated from the horizontal plane. Figure 26 shows the conical shape formed by the dry clean sand. The repose angle was measured at four different locations, having an average repose angle of $33.7^{o}$ with the maximum value of $34.12^{o}$ and a minimum value of $33.12^{o}$. A field repose angle test was intended to perform but the pile of sand was wet producing suction between particles preventing the determination of an accurate repose angle.

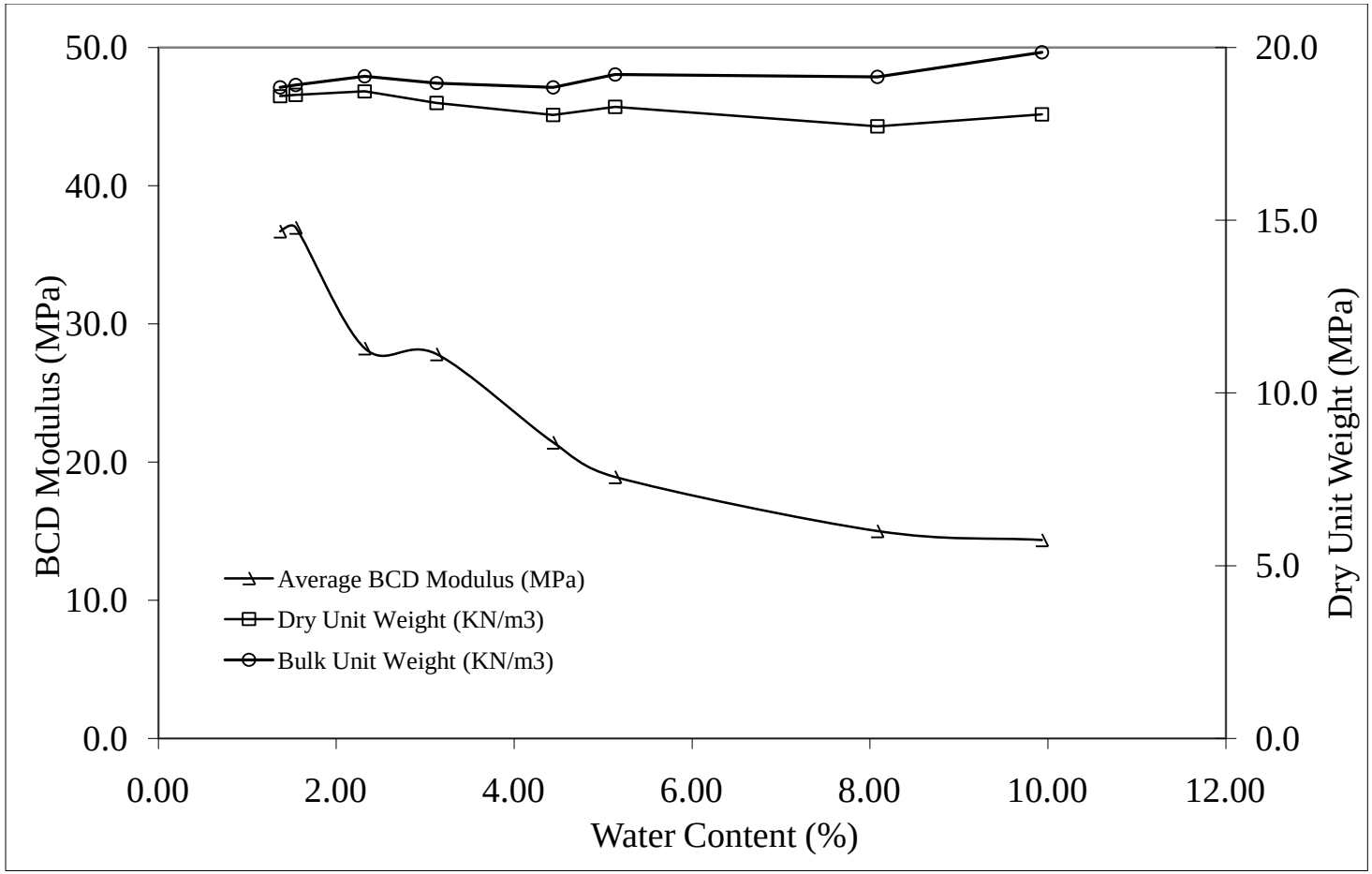


Figure 25. BCD Modulus and Unit Weight versus Water Content Curve for the Clean Sand

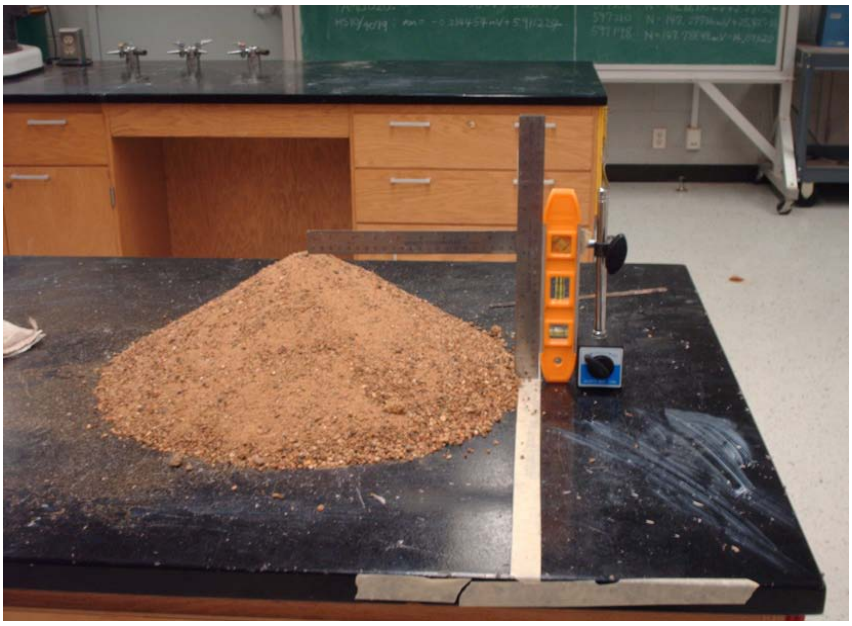

Figure 26. Experiment Set up for Determination of the Angle of Repose of the Clean Sand

5.7 Direct Shear Test (DST)

A set of Direct Shear Tests (DST) were conducted on the clean sand following the procedure describe in section 4.7. As explained in that section, the tests were performed on a circular shear box of 62-mm diameter containing a soil specimen of 27-mm height. The tests reproduce the entire range of states at which the sand can be subjected to in the field (loose, dense, and compacted states at 2%, 4% and 6% of water content).

Several set of normal stresses were applied to the soil sample, with a minimum normal stress of 20 kPa and a maximum compressive stress 315 kPa. The lower stresses

(less than 90 kPa) were chosen in accordance to the stresses generated in a profile of a 5-m backfill of the clean sand having an average unit weight of 18 $kN/m^3$.

The clean sand tested on the direct shear tests were sieved passed a No. 4 (4.75 mm). In the case of the loose state, the sand was air-dry and pour on the shear box in a way that the sand specimen could achieved a void ratio close to the loosest state, e=0.60 (following the criterion describe in section 4.7). The same procedure was conducted to achieve the densest state, but in that case, the specimen was hand-vibrated in three layers in order to increase the compactness of the soil particles. For the case of the compacted state, the soil sample was compacted in three lifts of equal thickness by tamping the top of each lift with the direct shear cap. The number of tamps per layer was adjusted to achieve an approximately density of 90% to 95% of the maximum dry density of the modified proctor compaction curve.

All tests were conducted using a constant rate of displacement of 0.5 mm/min. The horizontal and vertical displacements were recorded using two linear strain conversion transducers (LSCT), and the shear force was recorded using a force transducer. Both transducers were appropriately calibrated, showing a high degree of linearity ($R^2 \approx 1.0$). The data was recorded using a personal computer equipped with 4Channelgeotech.vi data acquisition card and LabView8.2 software. The computer program 4Channelgeotech.vi was written by Mike Limber.

Failure was defined as the peak shear stress for all sands exhibiting a peak stress (dense and compacted state). For the cases of the loose states that only exhibited an

ultimate strength, and failure was define as the ultimate stress corresponding to the initial horizontal tangent to the shear-stress displacement curve. The Mohr Coulomb failure envelopes were obtained by linear least-square regression with a non-negative intercept. The failure envelopes present a high degree of linearity, with a coefficient of determination ranging from $R^2$=0.9941 to $R^2$ = 1.00. In the loose and the dense cases, the coefficient intercept was small except for the stresses corresponding to above 150 kPa. The reason of having an increase on the intersection with higher confining pressure obeys to nonlinear relationship of the Mohr Coulomb enveloped (see section 3.5).

Results of the Direct Shear Test conducted on the clean sand are presented on tables 5 through 7. The maximum friction angle obtained for the loose case accounts for 36.66 degrees. This frictional resistance was determined using very low confining pressure; the minimum friction angle obtained from the results was 34.82 degrees, obtained when high confining stresses were applied. This behavior goes in accordance with the concept explained in section 3.6, where the friction angle of granular materials decreases with increasing confining pressure.

The literature normally account for friction angle, in the loosest state, to be around 30 to 34 degrees. In general, these values are documented under high confining pressure, which lead to a lower friction angle (section 3.6).

The physical properties of the clean sand indicated that a friction angle (in the loose state) of around 35 degrees is a reasonable recommended value for the clean sand. Properties such as its angularity, gradation, particle size, low normal stress application,

and low fine content also support this value. In addition, if a comparison between the friction angle from the DST and the repose angle obtained at the laboratory is made, it can be seemed that those values can be comparable with some degree of confidence. Normally, it is expected that the DS will overestimate the frictional resistance by around 2 degrees since the real failure plane is not necessarily horizontal, and overstresses are generated along the horizontal plane. Appendix A presents a complete description of the DST conducted to the clean sand.

From the results of the Direct Shear Tests (DST) conducted in the dense state of the clean sand, it is clear that an average frictional resistance of 40 degrees is a reasonable recommendation. This value can be used for design purposes when a compaction level of at least 90% of the maximum dry unit weight, from the modified proctor compaction test, has been achieved.

Table 5. Direct Shear Test Results for the Clean Sand in the Loose State

| Test Number | Applied Normal Stress (kPa) | Approx. Dry Unit Weight ($kN/m^3$) | Approx. Wet Unit Weight ($kN/m^3$) | Estimated Void Ratio | Shear Stress at Failure (kPa) | Water Content (%) | Friction Angle (Degrees) | Intersection (kPa) |
|---|---|---|---|---|---|---|---|---|
| 1 | 27.972 | 16.14 | 16.20 | 0.617 | 27.50 | 0.37 | 36.13 | 6.42 |
| | 54.188 | 16.13 | 16.19 | 0.618 | 45.00 | 0.36 | | |
| | 106.499 | 16.18 | 16.22 | 0.615 | 84.50 | 0.23 | | |
| 2 | 27.829 | 16.19 | 16.22 | 0.615 | 26.30 | 0.21 | 36.11 | 5.74 |
| | 53.907 | 16.11 | 16.15 | 0.622 | 44.66 | 0.23 | | |
| | 106.002 | 16.13 | 16.17 | 0.620 | 83.19 | 0.26 | | |
| 3 | 21.314 | 16.12 | 16.18 | 0.619 | 20.68 | 0.37 | 36.66 | 4.11 |
| | 40.918 | 16.12 | 16.18 | 0.619 | 33.60 | 0.40 | | |
| | 93.008 | 16.19 | 16.23 | 0.614 | 73.60 | 0.28 | | |
| 4 | 21.415 | 16.17 | 16.21 | 0.616 | 21.17 | 0.23 | 36.01 | 5.53 |
| | 41.101 | 16.17 | 16.22 | 0.615 | 35.30 | 0.28 | | |
| | 93.482 | 16.21 | 16.25 | 0.612 | 73.50 | 0.26 | | |
| 5 | 153.302 | 16.17 | 16.21 | 0.616 | 133.00 | 0.25 | 35.39 | 24.22 |
| | 206.369 | 16.08 | 16.12 | 0.625 | 171.00 | 0.24 | | |
| | 263.110 | 16.10 | 16.23 | 0.614 | 211.00 | 0.23 | | |
| 6 | 159.378 | 16.19 | 16.22 | 0.615 | 134.13 | 0.17 | 34.82 | 24.26 |
| | 257.857 | 16.20 | 16.24 | 0.613 | 202.14 | 0.22 | | |
| | 316.868 | 16.11 | 16.16 | 0.621 | 242.71 | 0.28 | | |

Table 6. Direct Shear Test Results for the Clean Sand in the Dense State

| Test Number | Applied Normal Stress (kPa) | Approx. Dry Unit Weight ($kN/m^3$) | Approx. Wet Unit Weight ($kN/m^3$) | Estimated Void Ratio | Shear Stress at Failure (kPa) | Water Content (%) | Friction Angle (Degrees) | Intersection (kPa) |
|---|---|---|---|---|---|---|---|---|
| 1 | 27.735 | 17.56 | 17.62 | 0.486 | 35.200 | 0.33 | 42.76 | 9.45 |
| | 53.769 | 17.51 | 17.55 | 0.496 | 59.000 | 0.21 | | |
| | 92.976 | 17.59 | 17.63 | 0.489 | 95.500 | 0.24 | | |

Table 7. Direct Shear Test Results for the Clean Sand in the Wet-Compacted State in the Field

| Test Number | Applied Normal Stress (kPa) | Approx. Dry Unit Weight (kN/m3) | Approx. Wet Unit Weight (kN/m3) | Estimated Void Ratio | Shear Stress at Failure (kPa) | Water Content (%) | Friction Angle (Degrees) | Intersection (kPa) |
|---|---|---|---|---|---|---|---|---|
| 1 | 33.810 | 17.50 | 18.25 | 0.445 | 33.800 | 2.43 | 39.87 | 6.72 |
| | 66.267 | 17.70 | 18.07 | 0.450 | 64.200 | 2.11 | | |
| | 104.947 | 17.78 | 1826 | 0.434 | 93.400 | 2.70 | | |
| 2 | 33.804 | 17.75 | 18.47 | 0.418 | 40.00 | 4.05 | 39.76 | 10.29 |
| | 65.983 | 17.53 | 18.25 | 0.435 | 62.30 | 4.09 | | |
| | 105.055 | 17.57 | 18.31 | 0.431 | 99.00 | 4.20 | | |
| 3 | 33.914 | 17.43 | 18.61 | 0.407 | 42.80 | 6.78 | 40.37 | 14.55 |
| | 131.059 | 17.50 | 18.70 | 0.401 | 127.70 | 6.83 | | |
| | 180.193 | 17.39 | 18.54 | 0.413 | 166.60 | 6.59 | | |

## 5.8 Estimation of the Dilatation Angle of the Clean Sand from the DST

Figures 27 through 36 show the stress-deformation curves and the deformation envelopes ($\Delta y$ vs $\Delta x$) of the clean sand for the loose state and the dense state. From these results, the dilation angle ($\psi$) of the clean sand was estimated as the instantaneous angle of motion of the particles' movements, following the concept presented in section 3.7 (the dilation angle corresponds to the slope of the curve $\Delta y$ vs $\Delta x$ at failure).

In the case of the loose states (figures 27 through 32), there is not significant interlocking to be overcome and the shear strength increases gradually to an ultimate value without a prior peak. It is accompanied for a decrease in volume (negative dilation angle, $\psi$) at low strain; however, at high strain values, dilation takes place indicating that the volume is increasing (positive dilation). The reason obeys to the application of very low confining pressures. Under these conditions, and considering the angularity of the clean sand, there was not considerable normal stress to overcome allowing the soil particle to move upward without too much effort.

The dense and the compacted states of the clean sand have a considerable degree of interlocking between particles that have to be overcome (in addition to the frictional resistance at the point of contact). Therefore, the clean sand shows a peak stress at relatively low strain and thereafter, as interlocking is overcome, shows a decrease in shear stress (figures 33 to 36). The decrease in the interlocking of the soil particle for the clean sand produces an increase in volume of the specimen during shearing (positive dilation angle).

Table 8 presents the results of the tangent angle of dilation and the secant angle of dilation for the loose, dense and compacted states condition of the clean sand. The tangent angle of dilation was computed as the slope of the tangent of the deformation enveloped ($\Delta y$ vs $\Delta x$) at the point of failure (indicated in figures 27 to 36); the secant angle of dilation was calculated as the slope of the deformation curve from zero strain.

Theoretically, dilation angle is negative for loose sand and positive for dense sands. However, this behavior cannot be seen from the results of the Direct Shear Test conducted to the clean sand since the values are in its majority positives. In addition, the DST results indicate that the angle of dilation does not take a representative value in the case of loose sands at high strains. As explained before, interlocking friction does not increases considerable for loose sand as the soil particles can find more space to be rearranged along the failure surface. However, in the case of dense sands, it is considerable high (up to 12 degrees).

The conclusion section of this thesis presents some recommended values for the angle of dilation ($\psi$) and frictional resistance ($\varphi$) for the clean sand. These values are based on the results of the direct shear tests (DST) and the numerical simulations conducted to the clean sand and they have been divided by considering low-strain condition and large-strain condition problems.

Table 8. Estimation of the Dilation Angle of the Clean Sand for the Loose and the Dense State

| Test Number | State Condition | Applied Normal Stress (kPa) | Shear Stress at Failure (kPa) | Tangent Dilation Angle (Degrees) | Secant Dilation [2]Angle (Degrees) |
|---|---|---|---|---|---|
| 1 | Loose | 21.314 | 20.68 | 4.6 | 3.27 |
| | | 40.918 | 33.60 | 3.4 | 1.15 |
| | | 93.008 | 73.60 | 2.12 | -1.5 |
| 2 | Loose | 21.415 | 21.17 | 4.76 | 2.5 |
| | | 41.101 | 35.30 | 4.45 | 0.61 |
| | | 93.482 | 73.50 | 1.8 | -0.85 |
| 3 | Loose | 27.972 | 27.70 | 7.25 | 2.96 |
| | | 54.188 | 45.00 | 3.57 | 1.0 |
| | | 106.499 | 84.50 | 3.4 | -1.03 |
| 4 | Loose | 27.829 | 26.30 | 5.7 | 3.0 |
| | | 53.907 | 44.66 | 3.52 | 1.39 |
| | | 106.002 | 83.19 | 3.43 | -0.60 |
| 5 | Loose | 153.302 | 133.00 | 5.50 | -0.4 |
| | | 206.369 | 171.00 | 3.60 | -1.02 |
| | | 263.110 | 211.00 | 3.70 | -0.50 |
| 6 | Loose | 159.378 | 134.13 | 3.15 | -0.70 |
| | | 257.857 | 202.14 | 2.00 | -1.00 |
| | | 316.868 | 242.71 | 1.15 | -1.70 |
| 7 | Dense | 27.735 | 35.200 | 10.95 | 2.77 |
| | | 53.769 | 59.000 | 10.46 | 4.00 |
| | | 92.976 | 95.500 | 7.99 | 4.45 |
| 8 | Compacted at w=2% | 33.59 | 33.19 | 8.0 | 5.30 |
| | | 65.89 | 63.59 | 7.80 | 6.00 |
| | | 104.72 | 92.39 | 8.10 | 4.80 |
| 9 | Compacted at w=4% | 33.58 | 39.39 | 12.5 | 8.10 |
| | | 65.76 | 61.69 | 12.0 | 6.80 |
| | | 104.83 | 97.39 | 11.90 | 5.20 |
| 10 | Compacted at w=6% | 33.69 | 41.89 | 1.53 | 13.6 |
| | | 130.83 | 127.09 | 2.00 | 9.46 |
| | | 179.79 | 165.39 | 6.90 | 7.59 |

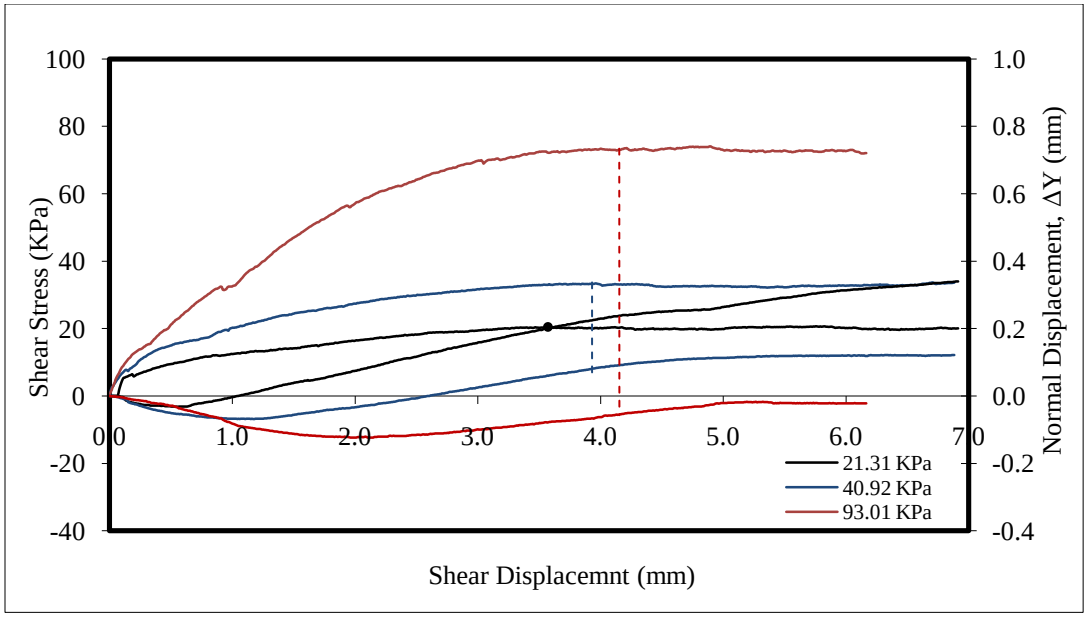


Figure 27. Shear Stress and Normal Displacement vs. Shear Displacement for the Clean Sand (Loose State-Test 1)

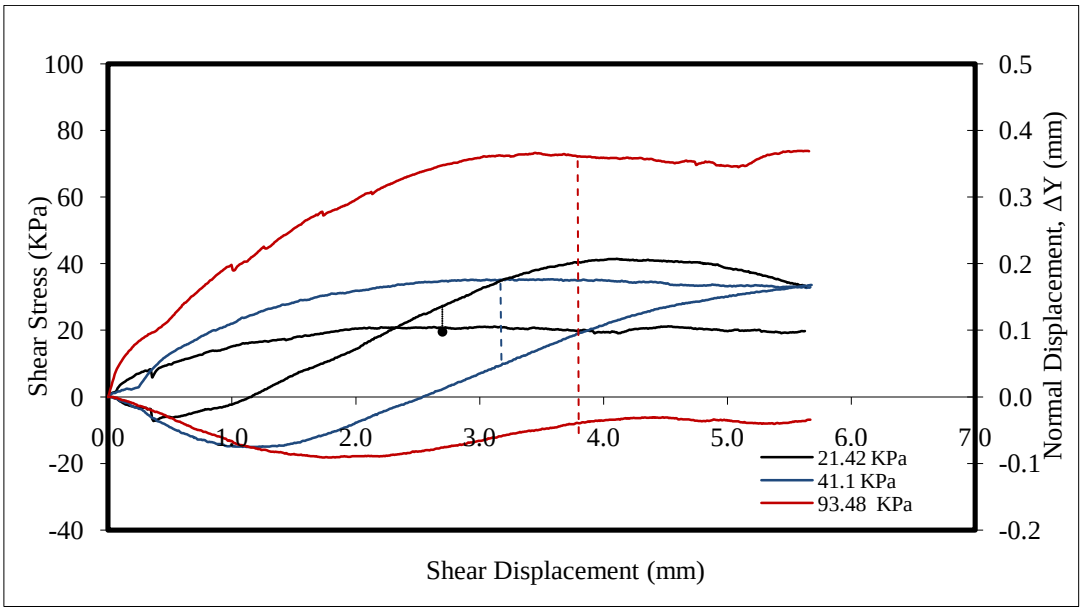


Figure 28. Shear Stress and Normal Displacement vs. Shear Displacement for the Clean Sand (Loose State-Test 2)

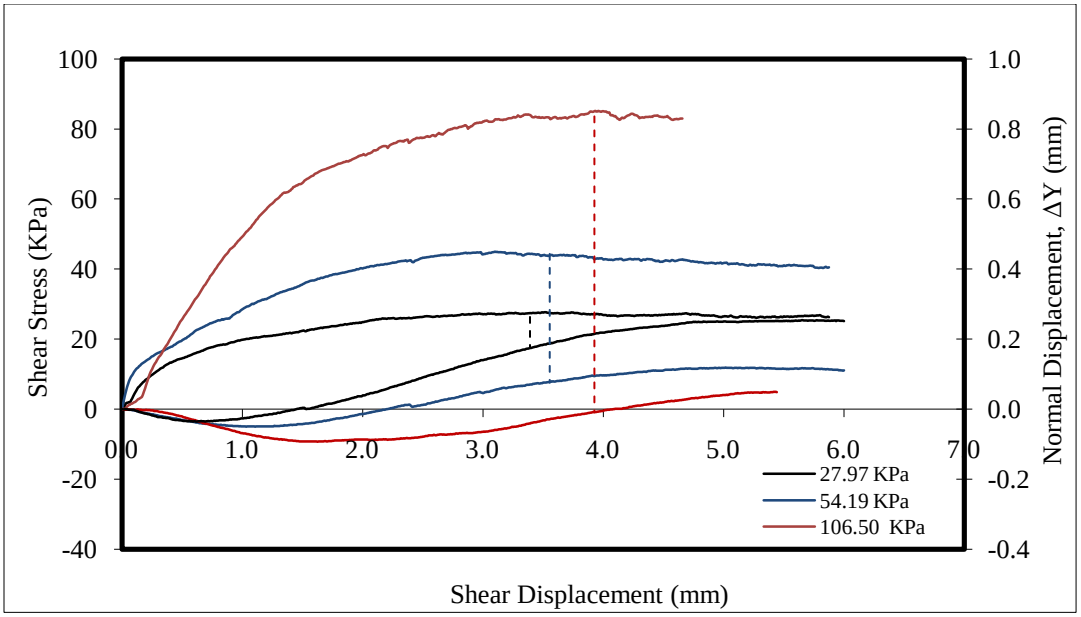


Figure 29. Shear Stress and Normal Displacement vs. Shear Displacement for the Clean Sand (Loose State-Test 3)

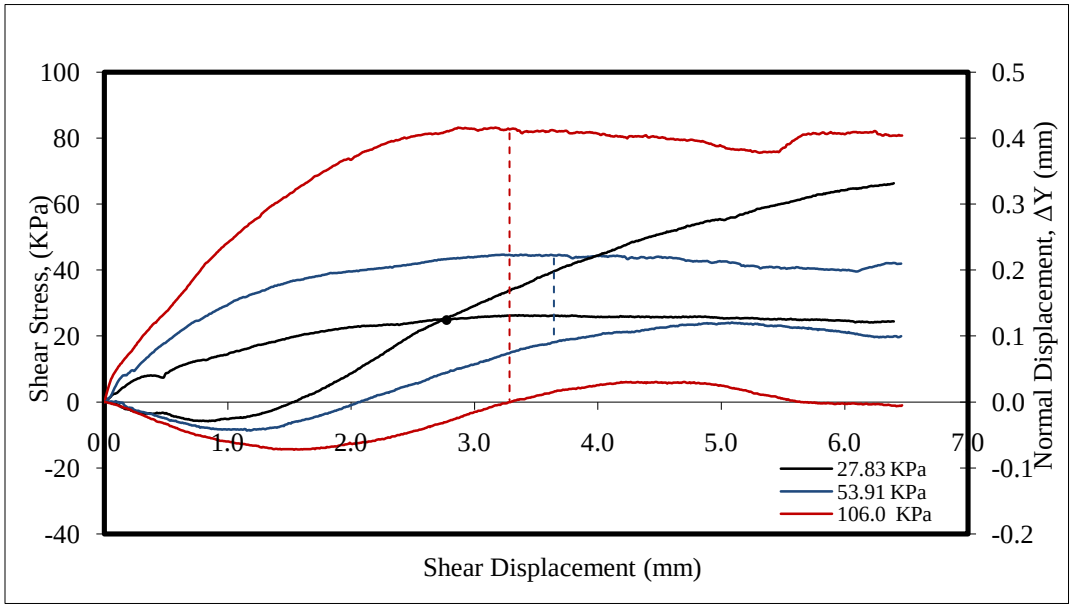


Figure 30. Shear Stress and Normal Displacement vs. Shear Displacement for the Clean Sand (Loose State-Test 4)

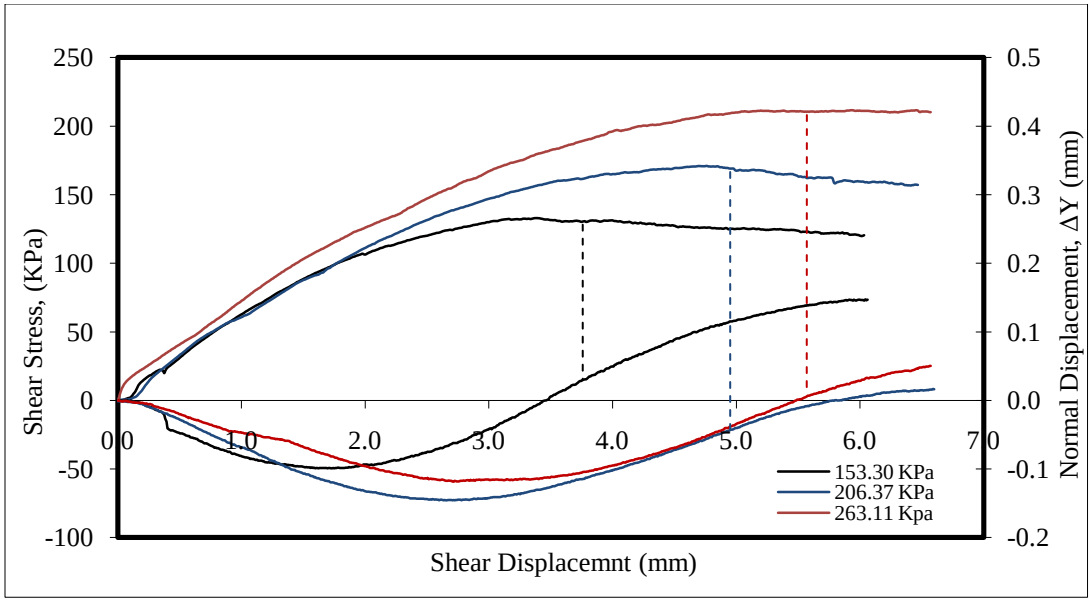


Figure 31. Shear Stress and Normal Displacement vs. Shear Displacement for the Clean Sand (Loose State-Test 5)

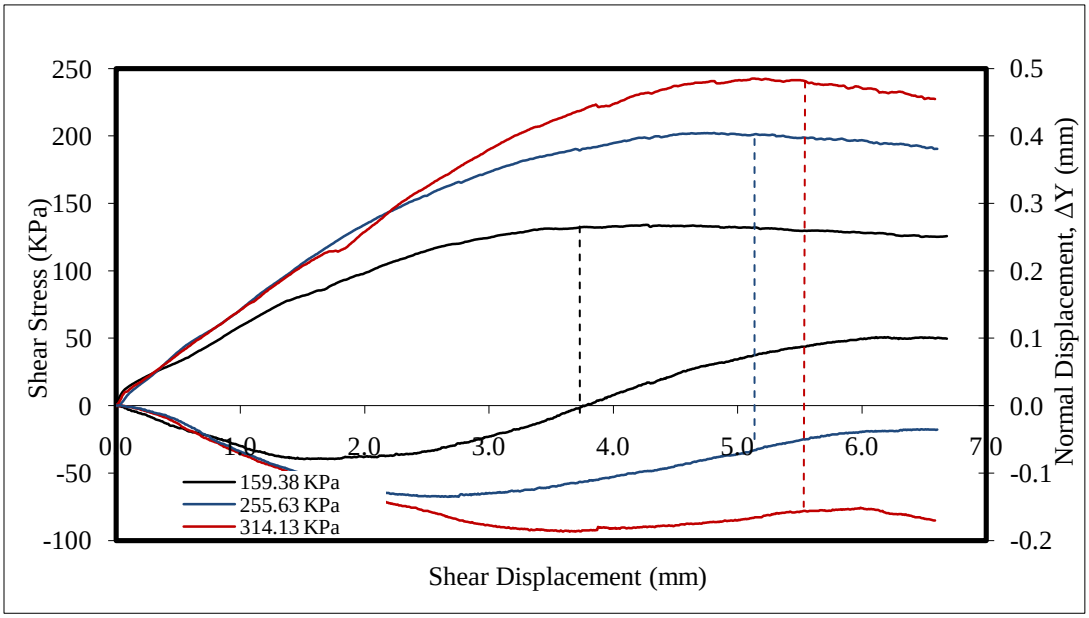


Figure 32. Shear Stress and Normal Displacement vs. Shear Displacement for the Clean Sand (Loose State-Test 6)

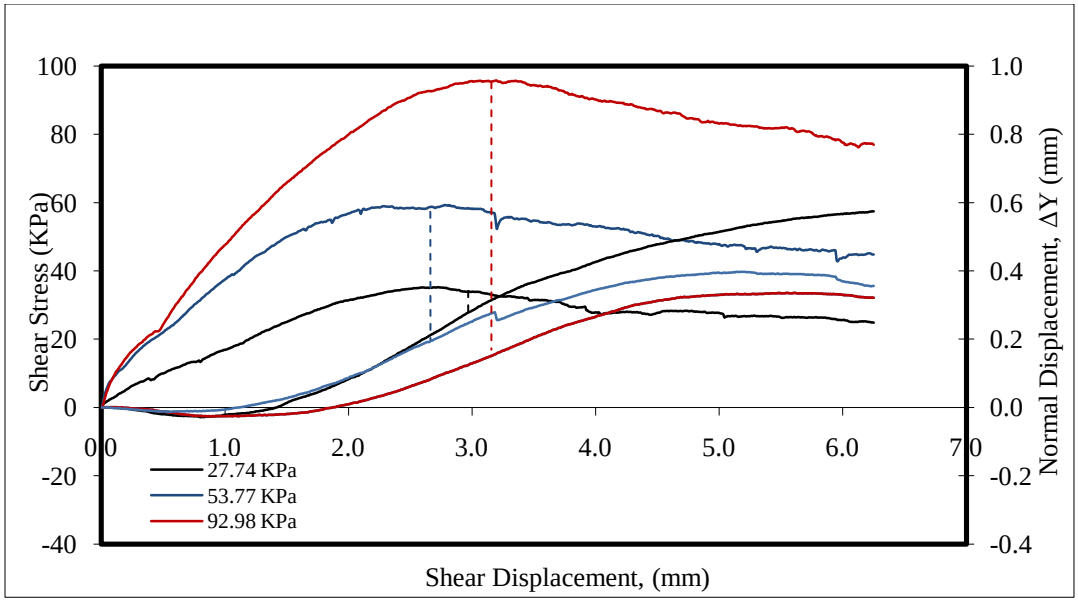


Figure 33. Shear Stress and Normal Displacement vs. Shear Displacement for the Clean Sand (Dense State)

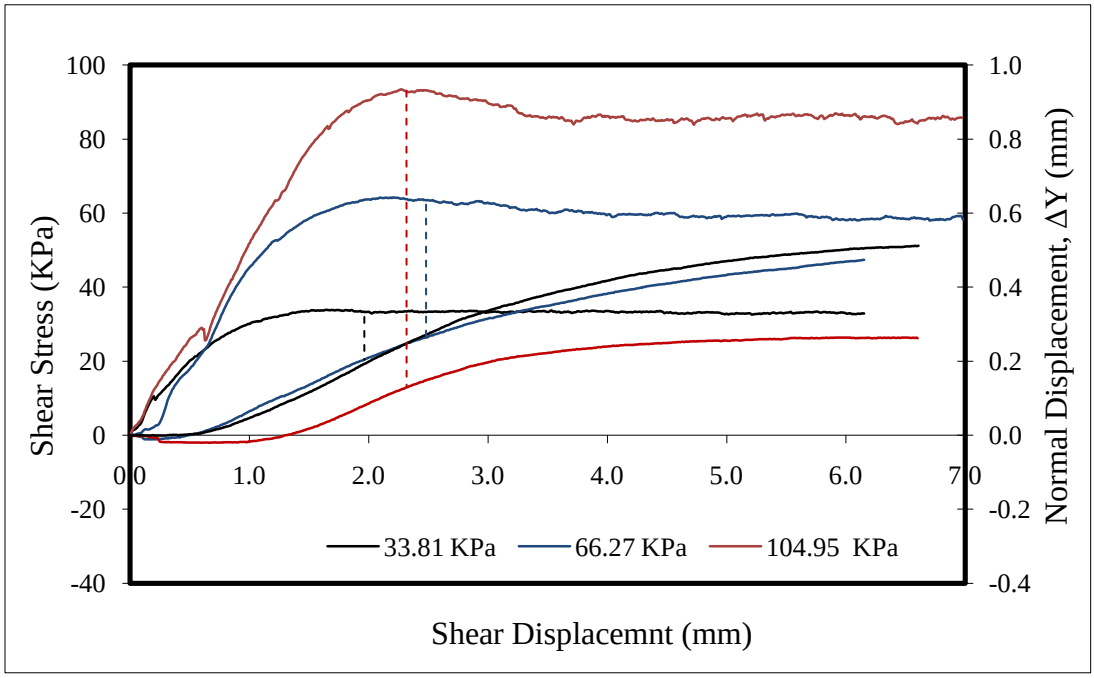


Figure 34. Shear Stress and Normal Displacement vs. Shear Displacement for the Clean Sand (Compacted at *w*=2%)

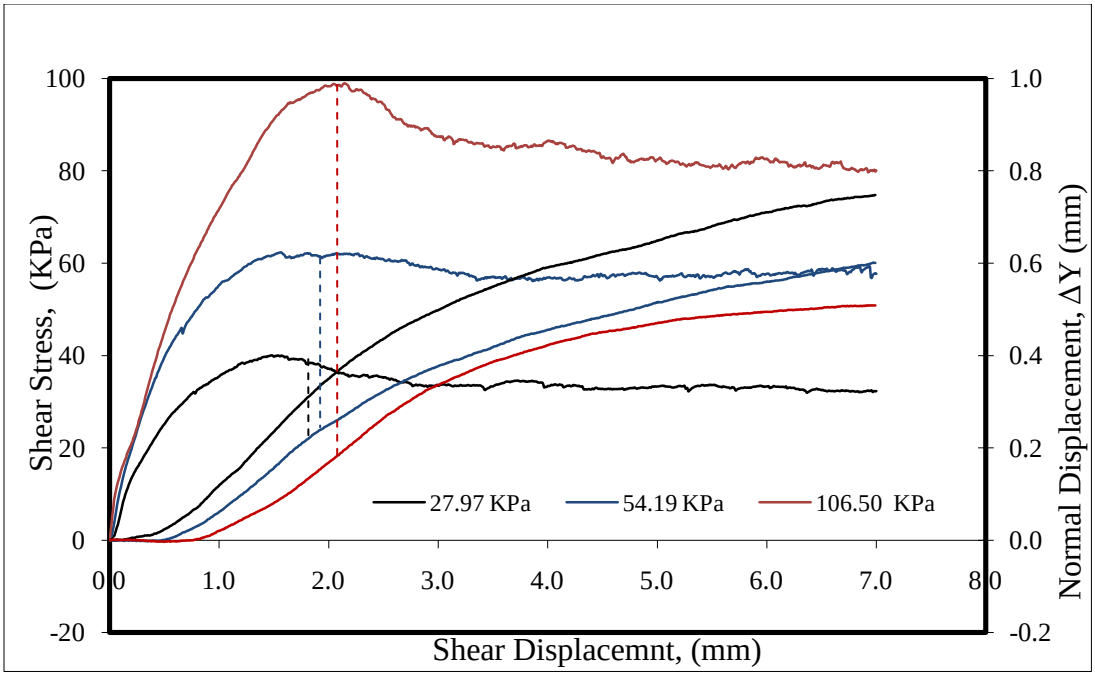


Figure 35. Shear Stress and Normal Displacement vs. Shear Displacement for the Clean Sand (Compacted at *w*=4%)

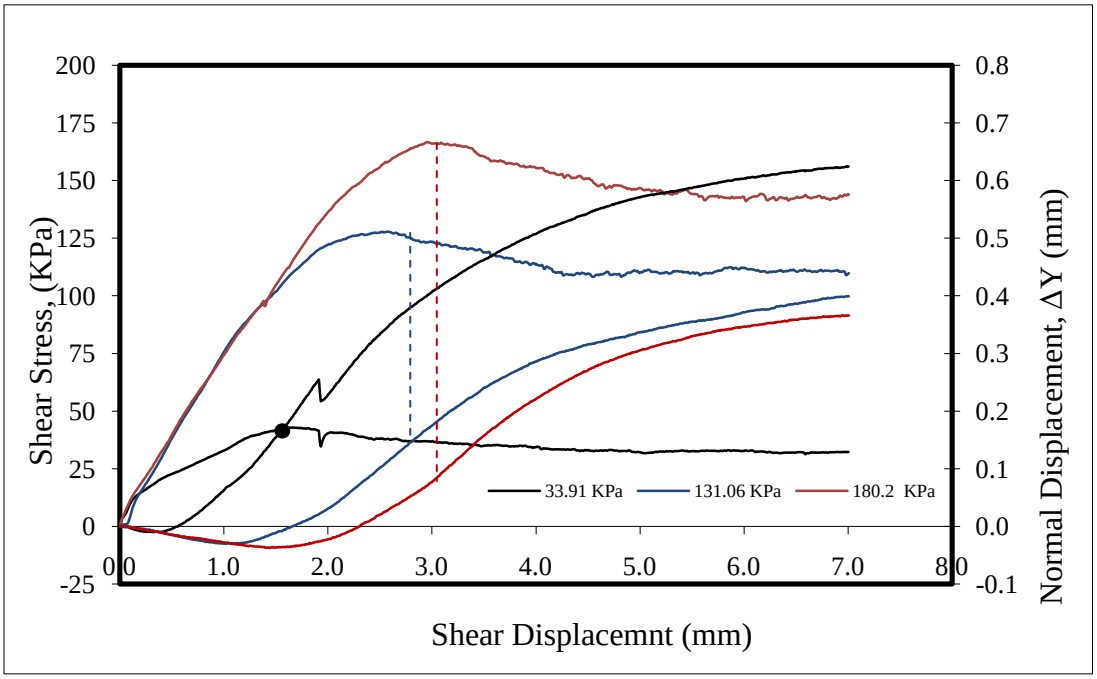


Figure 36. Shear Stress and Normal Displacement vs. Shear Displacement for the Clean Sand (Compacted at *w*=6%)

## 5.9 Triaxial Compression Test (TC)

As indicated in section 4.8, a Triaxial Compression Tests (TC) was conducted on the clean sand in a mold of 8.5 in by 6 in diameter. Two specimens were tested at a confining pressure of 7 psi and 12 psi (48.12 and 82.76 kPa) at a rate of 0.15 in/min (3.81 mm/min). The procedure for the sample preparation is indicated in section 4.8. The specimens were tested using a mold covered by a rubber membrane of unknown correction factor. Mohr Coulomb Envelopes were drawn for each test as shown in figure 37. For the clean sand, the friction angle was 35.14 degrees with an interception of 7.28 kPa.

Although the TC performed on the test did not follow the requirement of the American Society for Testing and Materials, the values of the friction angle determined by this test represents an estimation of the frictional resistance of the material and not its real value. However, the real frictional resistance of the material should not be far-off from the estimated value since the friction angles of the TC and the friction from the DST are comparables.

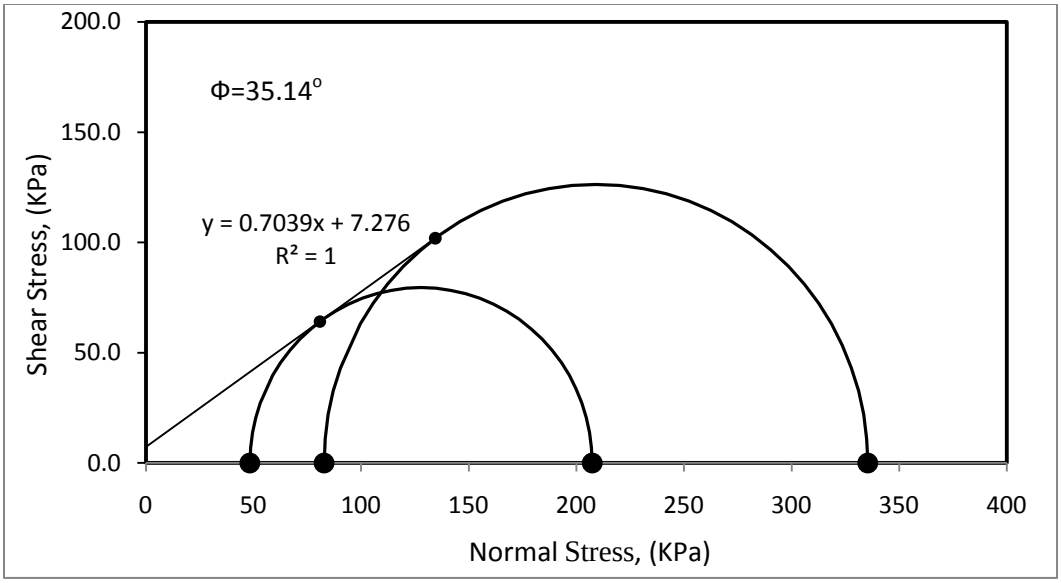


Figure 37. Mohr Coulomb Enveloped for the Clean Sand from the TC

# 6. TESTS RESULTS FOR THE SILTY SAND

The silty sand was also included in the testing schedule as a way of finding a local source of raw materials that can be used for full scale tests at the facility research area of Riverside Campus. The source of this sand is located at the pendulum area of Riverside Campus at about 10 ft below the ground surface The tests conducted to the silty consisted of wet sieve analysis (ASTM D2217-85 -Standard Practice for Wet Preparation of Soil Samples for Particle-Size Analysis and Determination of Soil Constants), Hydrometer Analysis (ASTM D 422 – Standard Method for Particle Size Analysis of Soils), Atterberg Limits (ASTM D4318-00 (Standard Tests Methods for Liquid Limit, Plastic Limit, and Plasticity Index of Soils), and Direct Shear Test (ASTM D 3080 – Standard Method for Direct Shear Test Under Consolidated Drained Condition). The results of the tests are shown on the following section:

## 6.1 Index Properties

A total of three particles sizes analysis and three hydrometer analyses were conducted to the silty sand in accordance with the designation ASTM D 2217 and ASTM D 422 respectively. The hydrometer analysis was performed in order to reproduce the entire particle size distribution of the sand and to discard the possibility of having clay particles present in the sample, which will greatly affect the behavior of the soil under wet conditions. The gradation curve shows that no clay particles (particles smaller than 2 microns) are present in the soil sample. The soil is composed of about

50% silts (particles bigger than 2 microns and smaller than 75 microns) and 50% sand particles (particles size bigger that 75 microns and smaller than 4.75 mm).

The sand presents a coefficient of uniformity ($C_u$) of 4.25 and a coefficient of curvature ($C_c$) of 1.09. The sand meets the requirement of the coefficient of curvature ($1.0<C_c<3.0$), for a good graded sand, imposed by the Unified Soil Classification System (USCS); however, it does not meet the requirement of $C_u>6.0$ for a well graded sand. Therefore, the sand was classified as poor-graded-silty sand SP-SM. Information about the Index Properties and soil constants of the silty- sand are presented on table 9 and figure 38.

Due to the high fine content presents on the sand, Atterberg Limits were conducted on the sample in the soil fraction passing sieve #40. The sand presents a liquid limit of 21.14 % (average of two tests). However, the soil specimen did not show plasticity; therefore, the soil can be classified as a non-plastic soil.

Table 9. Select Index Properties for the Silty Sand

| Sample | $D_{10}$[1] | $D_{30}$[2] | $D_{50}$[3] | $D_{60}$[4] | Perc. Fines | $C_c$[5] | $C_u$[6] | $w_L$ | $w_P$ | $w_{PI}$ | Perc. Gravel | USCS[5] |
|---|---|---|---|---|---|---|---|---|---|---|---|---|
| Silty Sand | 0.020 | 0.043 | 0.075 | 0.085 | ≈50 | 1.09 | 4.25 | 21.14 | N.P. | N.P. | ≈1 | SP-ML |

[1]$D_{10}$= particle diameter at 10% finer; [2]$D_{30}$= particle diameter at 30% finer; [3]$D_{50}$=particle diameter at 50% finer; [4]$D_{60}$= particle diameter at 60% finer; $C_c$ = coefficient of curvature; $C_u$= coefficient of uniformity; USCS[7]= Unified Soil Classification System.

Note: the index properties presented on table 1 represents the average of three tests for the soil constant and two tests for Atterberg Limits.

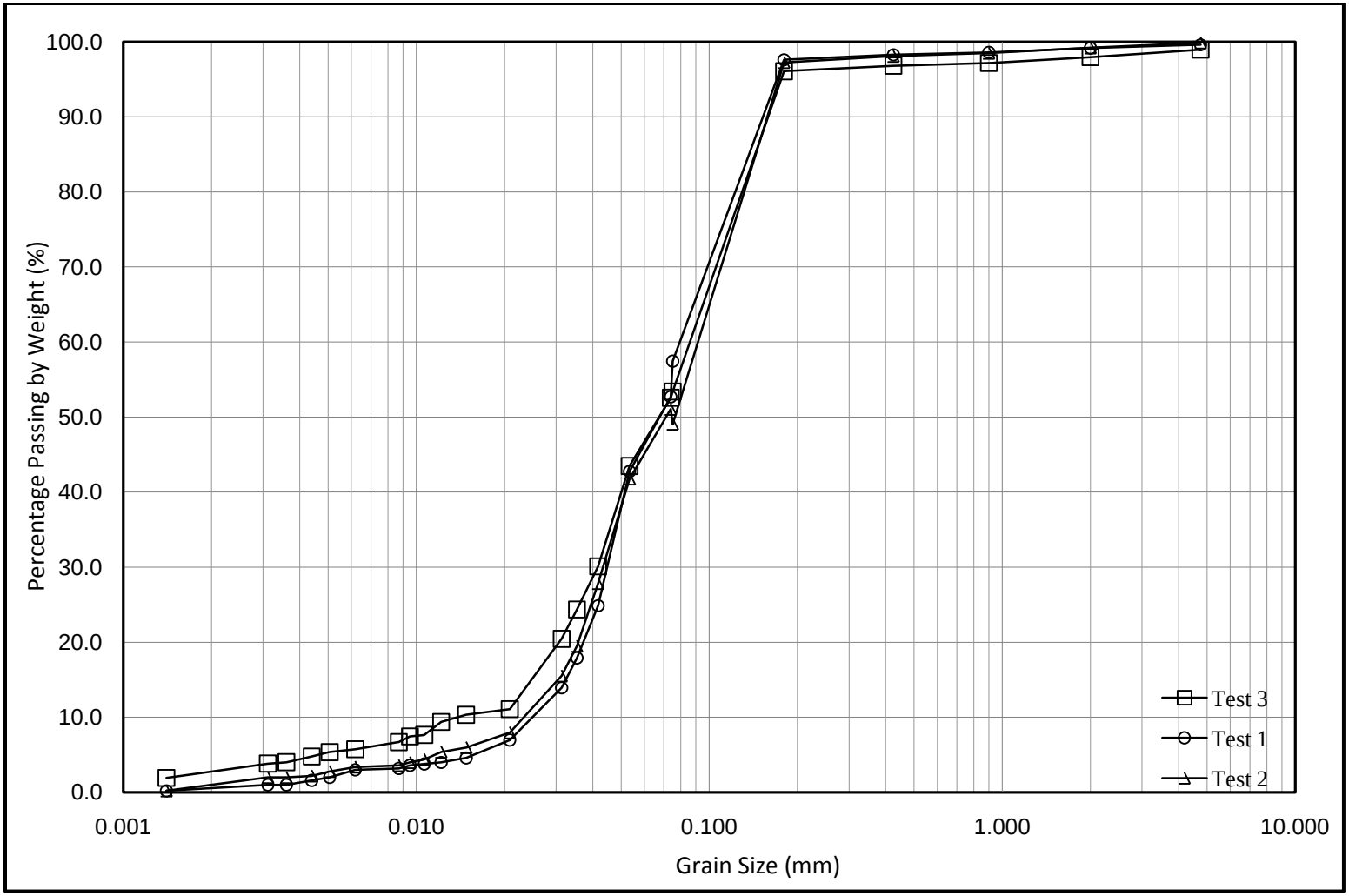


Figure 38. Particle Size Distribution Curve for the Silty Sand

## 6.2 Direct Shear Test (DST)

Three Direct Shear Test (DST) were conducted on the silty sand in accordance with the designation ASTM D 3080 (Standard Method for Direct Shear Test under Consolidated Drained Condition). The first two tests were performed at a constant rate of 0.5 mm/min with confining pressure of 21 kPa, 41 kPa, and 94 kPa or the first test and 21 kPa, 54 kPa, and 107 kPa for the second test. The third test was done at confining pressure of 20 kPa, 54 kPa, and 106 kPa with a shearing rate of 0.005 mm/min.

The silty sand also presents a high frictional resistance due to its physical properties such as angularity and particles size distribution that provides a good packing to the soil specimen. However, comparing the behavior of the clean sand and the silty sand under shearing, it can be drawn from the result of the direct shear tests that the silty sand present larger contraction behavior than the clean sand. One reason of this contractive behavior is the high fine content of the silty sand; this will allow particles to rearrange in a better way than soil samples containing larger particles.

In addition, the shearing resistance of the silty sand did not show shear-rate dependant since the two rates at which the silty sand was tested had comparable results. There is only a slight increase in the contraction at a lower rate that can be due to particle arrangement.

From the results of the DST presented in figures 39 to 47 and in tables 10 to 12, a recommended critical frictional resistance of 35.0 degrees is established. As explained before, the frictional resistance of the silty sand obeys to its mineralogy, angularity, and

the fact that particles arrangement takes place in a better way for fine sands rather than for granular sands.

Table 10. Results of the Direct Shear Test for the Silty Sand (Test 1)

| Point No. | σ (kPa) | τ (kPa) | Sample Height (mm) | Water Content, (%) |
|---|---|---|---|---|
| 1 | 21.463 | 18.39 | 27.0 | 0.89 |
| 2 | 41.398 | 33.39 | 27.0 | 0.94 |
| 3 | 94.349 | 70.00 | 27.0 | 0.96 |

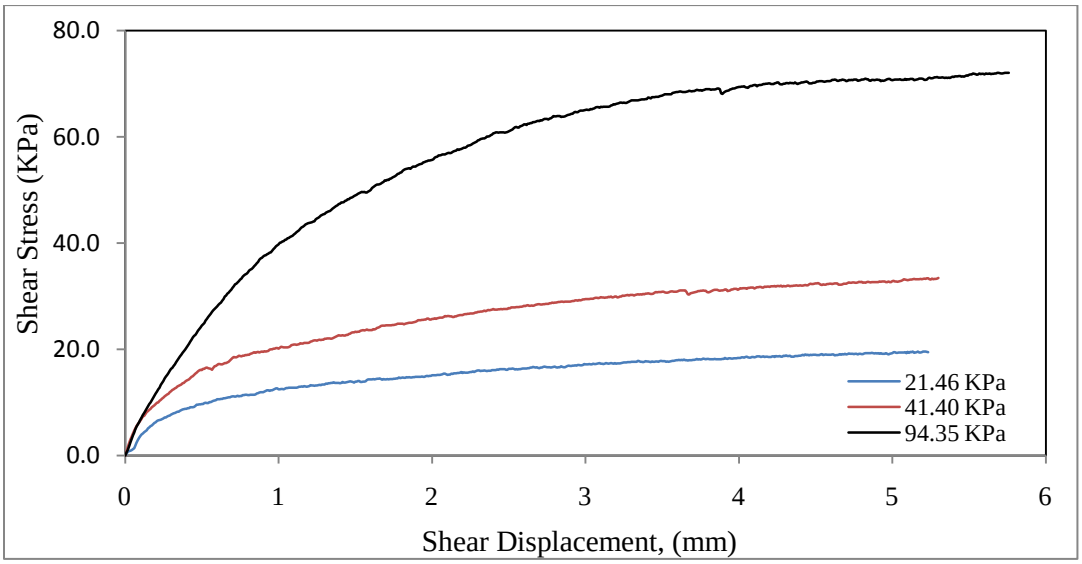


Figure 39. Shear Stress- Deformation Enveloped for the Silty Sand (Test 1)

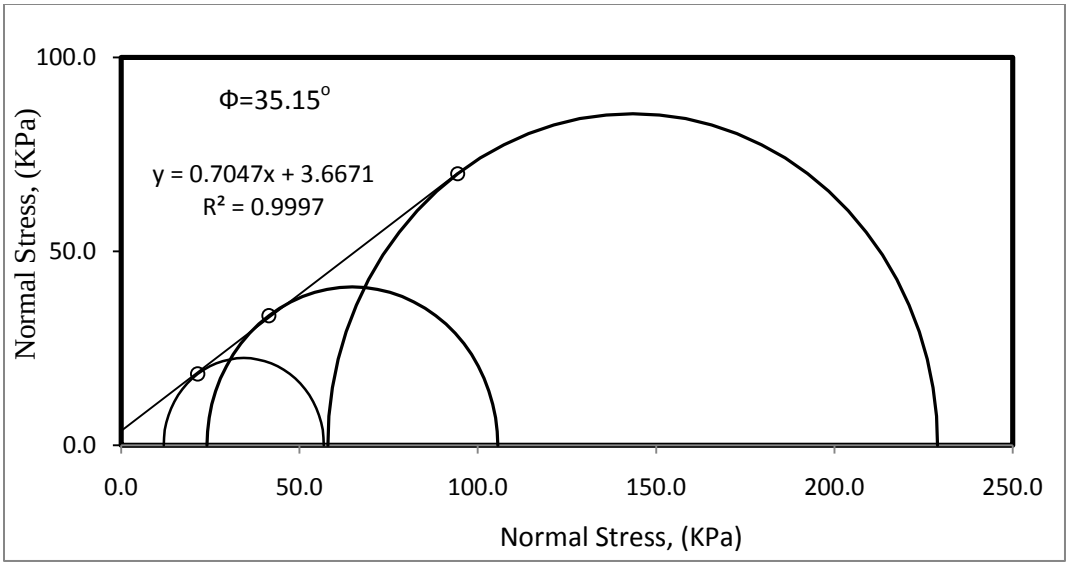


Figure 40. Mohr Coulomb Enveloped for the Silty Sand (Test1)

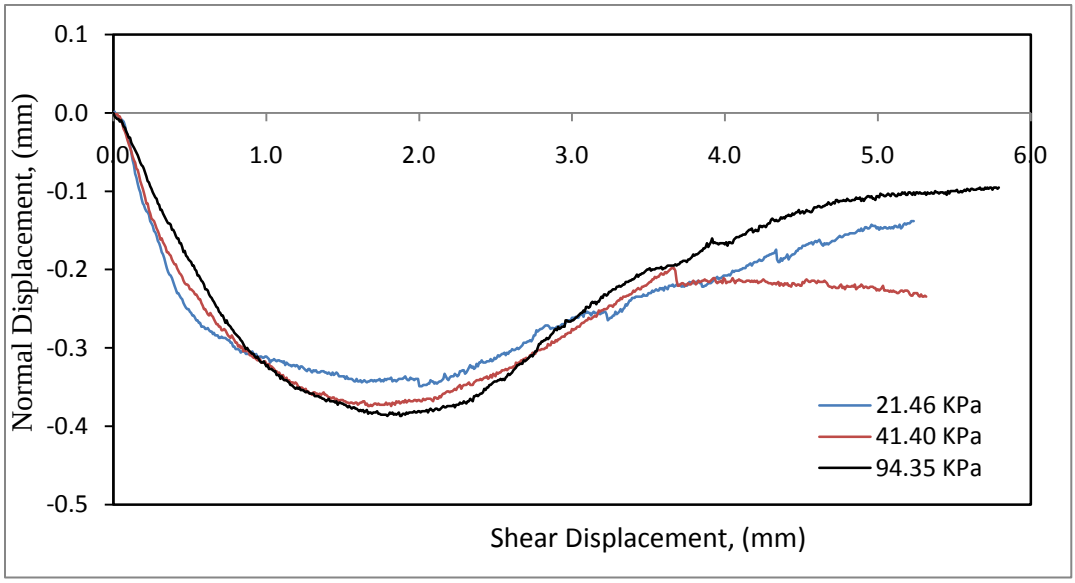


Figure 41. Dilation Enveloped for the Silty Sand (Test 1)

Table 11. Results of the Direct Shear Test for the Silty Sand (Test 2)

| Point No. | σ (kPa) | τ (kPa) | Sample Height (mm) | Water Content, (%) |
|---|---|---|---|---|
| 1 | 21.890 | 18.0 | 27.0 | 0.76 |
| 2 | 54.715 | 44.0 | 27.0 | 0.84 |
| 3 | 107.659 | 78.4 | 27.0 | 0.80 |

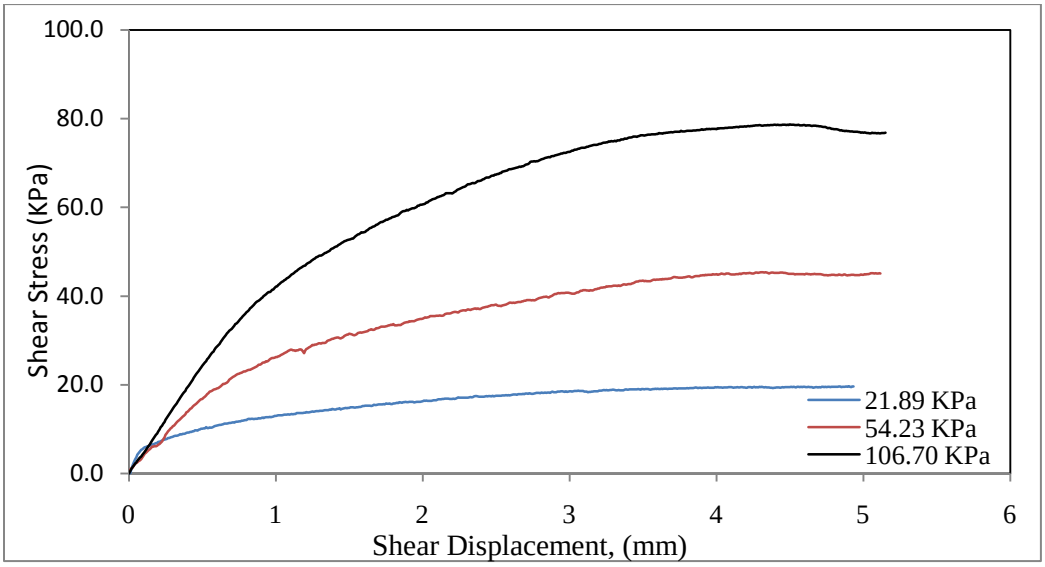


Figure 42. Shear Stress-Deformation Enveloped for the Silty Sand (Test 2)

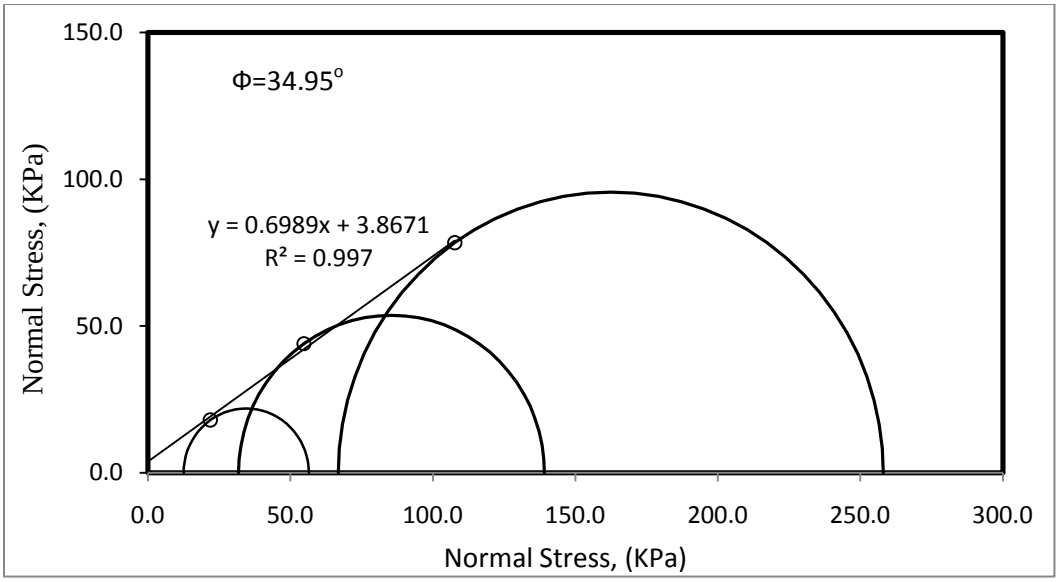


Figure 43. Mohr Coulomb Enveloped for the Silty Sand (Test2)

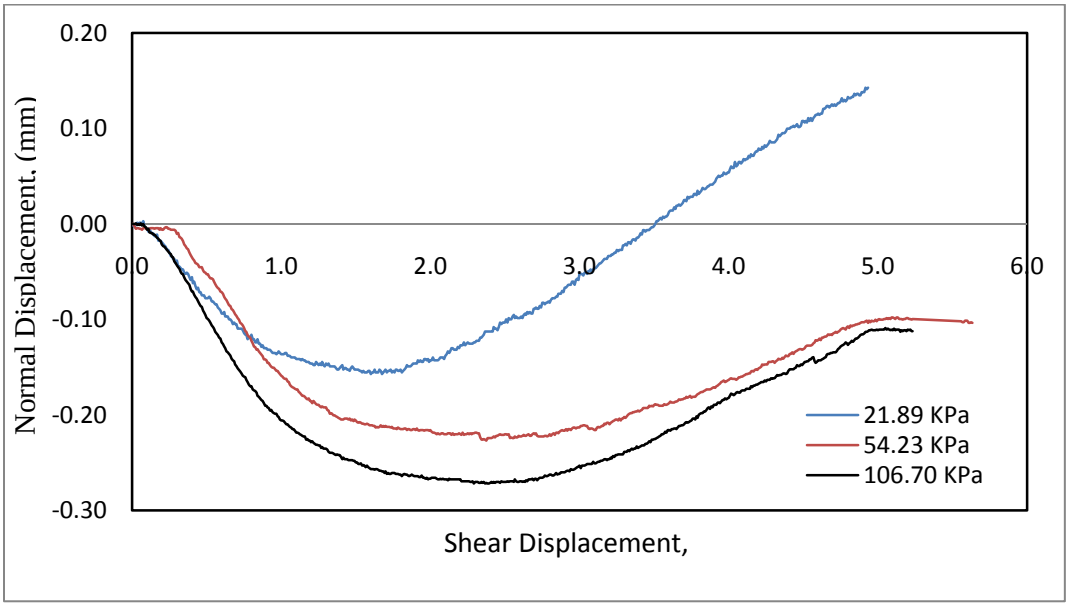


Figure 44. Dilation Enveloped for the Silty Sand (Test 2)

Table 12. Results of the Direct Shear Test for the Silty Sand (Test 3)

| Point No. | σ (kPa) | τ (kPa) | Sample Height (mm) | Water Content, (%) |
|---|---|---|---|---|
| 1 | 28.280 | 24.00 | 27.0 | 0.88 |
| 2 | 53.558 | 41.00 | 27.0 | 0.91 |
| 3 | 104.023 | 77.50 | 27.0 | 0.93 |

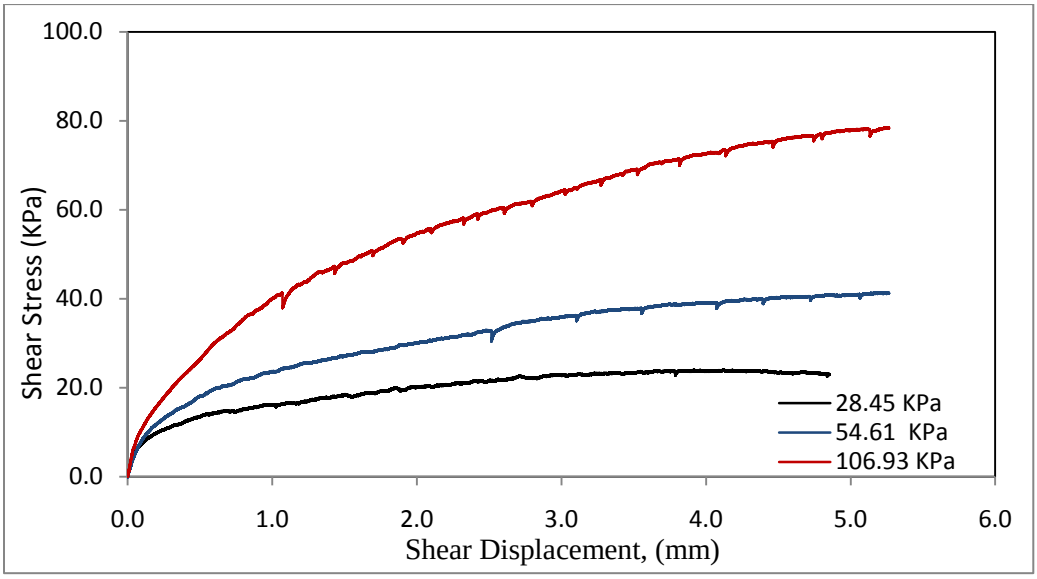


Figure 45. Shear Stress-Deformation Enveloped for the Silty Sand (Test 3)

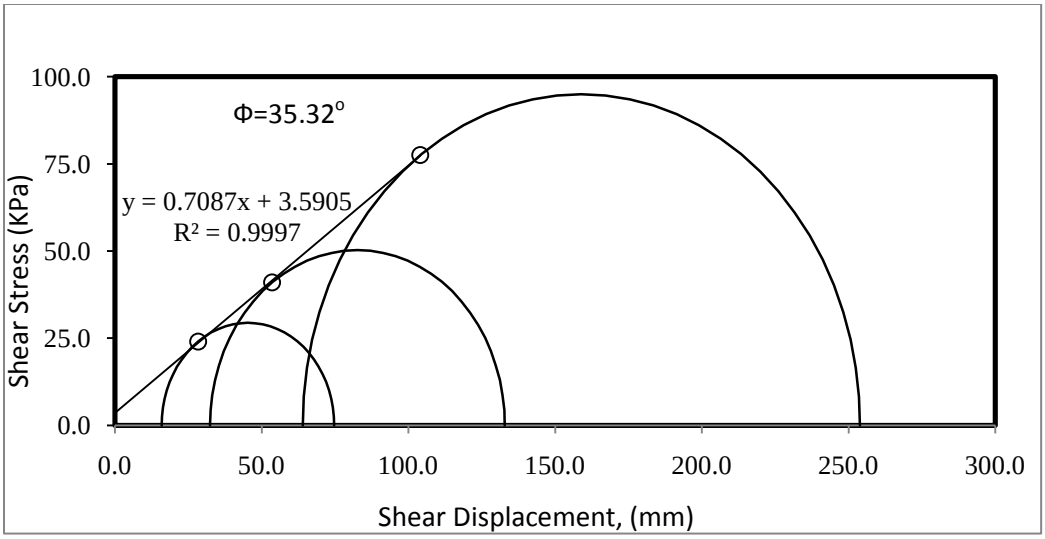


Figure 46. Mohr Coulomb Enveloped for the Silty Sand (Test 3)

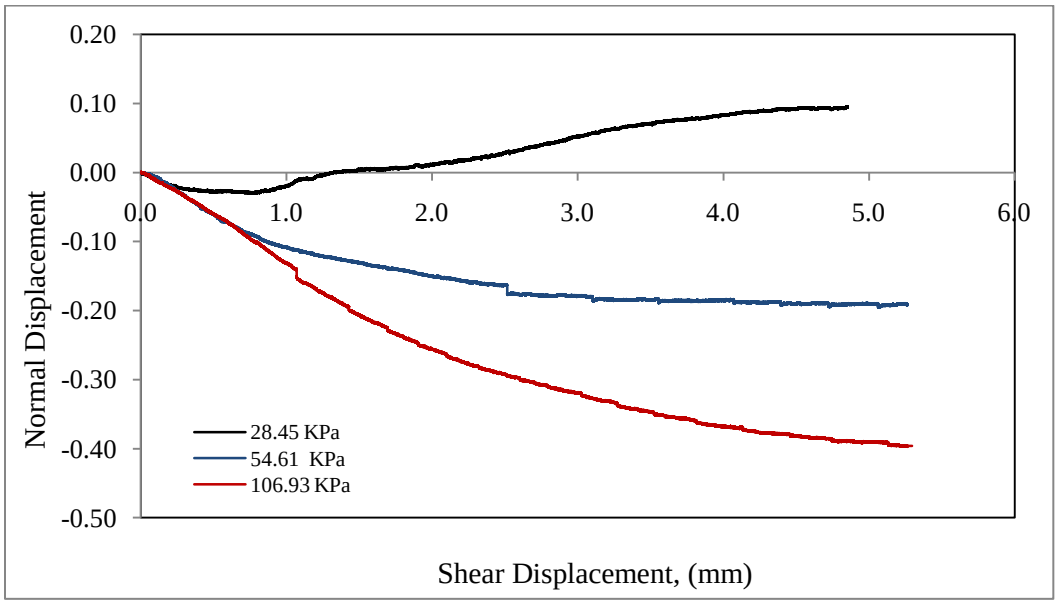


Figure 47. Dilation Enveloped for the Silty Sand (Test 3)

## 6.3 Estimation of the Angle of Dilation for the Silty Sand

The tangent angle of dilation and the secant angle of dilation were also computed for the silty sand using the results of the Direct Shear Test (DST). As well as in the case of the clean sand, the tangent angle of dilation represents the instantaneous angle of motion of the particles at failure. It can be concluded that the dilatancy effect gets minimize as the loose sand is approaching the critical state. One of the reasons of this is because at this state, the sand is sheared without experiencing any change in volume.

Table 13 shows the results of the dilation angle of the silty sand. It is clear that the sand experiment higher compression as normal stresses goes higher. This can be seemed from the secant angle of dilation, which increases as confinement stresses increases. However, this pattern is not clear from the tangent angle of dilation.

Recalling the recommendation given for the clean sand in reference to the dilation angle, it is also proposed the use of the secant dilation angle, determined from the vertical displacement vs. relative horizontal displacement curve, as the angle of dilation for the silty sand. Therefore, for low strain condition problems, it is recommended the use of -10.0 degrees for the dilation angle. In the case of large-strain condition problems, the recommended secant dilation angle of the silty sand is -3.0. As it was stated, these values are recommended based on the results of the laboratory Direct Shear Tests (DST).

Table 13. Estimation of the Dilation Angle of the Silty Sand in the Loose State

| Test Number | State Condition | Applied Normal Stress (kPa) | Shear Stress at Failure (kPa) | Tangent [1]Dilation Angle (Degrees) | Secant Dilation Angle (Degrees) |
|---|---|---|---|---|---|
| 1 | Loose | 21.463 | 18.39 | 2.48 | -1.90 |
| | | 41.398 | 33.39 | 2.29 | -2.30 |
| | | 94.349 | 70.00 | -1.10 | -2.90 |
| 2 | Loose | 21.890 | 18.0 | 6.40 | 1.20 |
| | | 54.715 | 44.0 | 4.70 | -2.00 |
| | | 107.659 | 78.4 | 4.40 | -2.26 |
| 3 | Loose | 28.280 | 24.00 | 0.70 | 1.15 |
| | | 53.558 | 41.00 | -0.80 | -2.50 |
| | | 104.023 | 77.50 | -1.50 | -4.80 |

# 7. TESTS RESULTS FOR THE ROAD BASE

As well as the clean sand, the road base also represents an aggregate with suitable mechanical properties for backfill. Therefore, it is very important to document the mechanical properties of this material in order to have a better estimation of the behavior of the structures under impact load. Considering that, a set of field and laboratory test were conducted on the road base and the results are presented in the following sections.

The material used for the different tests were obtained from the facility research area of Riverside Campus. The road base can be also found in local market as a material called Super-Flex.

## 7.1 Field Test Results for the Road Base (Density, Soil Modulus and Water Content)

The field tests conducted to the road base consisted on determination of in-situ density using the Sand Cone Method (ASTM D 1557-07), in-situ water content, and the BCD soil modulus. The tests were conducted on two of the Mechanically Stabilized Earth Wall (MSEW) constructed at the facility research area of Riverside Campus.

The results of the field tests are presented in table 14. The first two points were performed on the MSE wall that consisted of a backfill of 10 feet of compacted clean

sand and 3 feet of compacted road base at the top. The density, the water content, and the BCD Modulus were determined at a distance of approximately 1/3 of the edge of the wall (point 1 and 2 in table 14). The last test (point 4) was conducted on small MSE wall that consisted of a backfill of approximately 10 feet of compacted crashed rock and 3 feet of road base at the top. This test was conducted at the center of the wall.

The backfill of the first MSE wall presented a soil Modulus of 60.19 MPa (point 1) and 56.93 MPa (point 2) with a field water content of 4.12% and 4.38% respectively. These values correspond to the same field area and they can be comparables in term of modulus and water content. They also agree with the result of the BCD Modulus vs. Water Content curve presented in section 7.3, (Soil Modulus decreases with increasing water content). The second wall was about 18 months older; this is a good reason to have a larger soil modulus since the road base is mainly composed of limestone which present cementitious material that increases the stiffness (bonding) as a function of time.

## 7.2 Index Properties

Particles size analysis was conducted on the road base by performing a wet sieve analysis in accordance with the designation ASTM D 2217-85 (Standard Practice for Wet Preparation of Soil Samples for Particle-Size Analysis and Determination of Soil Constants).

Table 14. Results of the Field Tests Conducted to the Road Base

| IN PLACE DENSITY DETERMINATION- SAND CONE METHOD | | | |
|---|---|---|---|
| Project Name: MSE Wall Project | | Tested By: Deeyvid SAEZ | |
| Soil Type: Road Base | | Date: 07/22/2009 | |
| Test site: Riverside Campus | | Section: Area 3 | |
| **CALIBRATION OF THE SAND (STANDARD MATERIAL)** | | | |
| Weight of the mould (g) | 4591.66 | 4591.53 | 4591.48 |
| Weight of the mould + sand (g) | 6062.30 | 6060.87 | 6058.59 |
| Weight of material (g) | 1470.64 | 1469.34 | 1467.11 |
| Volume of the mould, ($m^3$) | 0.0009408211 | 0.0009408211 | 0.000940821 |
| Density of the material ($kg/m^3$) | 1.563 | 1.562 | 1.559 |
| Average density of the material ($kN/m^3$) | 1.561 | | |
| Average unit weight of the material ($kN/m^3$) | 15.318 | | |
| **CALIBRATION OF THE CONE** | | | |
| Initial weight of the cone +sand (g) | 6974.15 | 6090.67 | 6085.18 |
| Final weight of the cone + sand (g) | 5326.79 | 4428.28 | 4436.08 |
| Weight of the sand retained in the cone (g) | 1647.36 | 1662.39 | 1649.1 |
| Average weight of the sand retained in the cone (g) | 1652.95 | | |
| **VOLUME OF THE HOLE** | | | |
| | Point 1 | Point 2 | Point 4 |
| Initial weight of the cone + sand (g) | 6973.66 | 6800 | 6400 |
| Final weight of the cone + sand (g) | 3780 | 4000 | 3580 |
| Weight of the sand release (g) | 3193.66 | 2800 | 2820 |
| Weight of sand release in the hole (g) | 1540.71 | 1147.05 | 1167.05 |
| Volume of the hole ($m^3$) | 0.000986728 | 0.000734613 | 0.00074742 |
| **WATER CONTENT DETERMINATION** | | | |
| Weight of the bowl (g) | 276.80 | 296.90 | 138.90 |
| Weight of the wet soil + bowl (g) | 2664.00 | 2063.20 | 2000.90 |
| Weight of the dry soil + bowl (g) | 2558.70 | 1976.70 | 1937.40 |
| Weight of water (g) | 105.30 | 86.50 | 63.50 |
| Water Content (%) | **4.12** | **4.38** | **3.28** |
| **UNIT WEIGHT DETERMINATION** | | | |
| Weight of plastic bag (g) | 11.5 | 13.39 | 11.4 |
| Weight of wet soil + plastic bag (g) | 2420.9 | 1782.5 | 1875.9 |
| Weight of wet soil (g) | 2409.4 | 1769.11 | 1864.5 |
| Unit weight of the soil ($kN/m^3$) | 23.95 | 23.62 | 24.47 |
| Dry Unit Weight of the soil ($kN/m^3$) | 23.01 | 22.63 | 23.70 |
| BCD Modulus (MPa) | **60.18** | **56.93** | **84.28** |

A hydrometer analysis of the fraction passing sieve # 200 was also conducted to the base following the ASTM D 422 (Standard Method for Particle Size Analysis of Soils). The purpose of this test was to reproduce the complete particle size distribution of the road base (including those particles finer than 0.075 microns) as well as to determine the particle diameter corresponding to ten percent passing by weight, ($D_{10}$). The sample was classified as silty gravels with sand and sand mixtures (GM), according to the Unified Soil Classification System (USCS).

Atterberg limits were performed on the fraction of the soil passing sieve #40, in accordance with the designation ASTM D 4318-00 (Standard Tests Methods for Liquid Limit, Plastic Limit, and Plasticity Index of Soils). The finer particles of the road base showed some degree of plasticity with a liquid limit of 17.7% and a plastic limit of 14.40%, leading to a plasticity index of 3.2%. Although this aggregate is classified as a low plastic material, this plasticity index (3.2%), as well as its high fine content, is sufficient to weaken the soil under the presence of water. This behavior can be interpreted from the modulus versus water content curve that shows the variation of the soil modulus of the road base as lubrication occurs.

Index properties of the road base are summarized on table 15 and figure 48. The results presented in table 15 indicates that the road base meet the requirement of coefficient of uniformity for a well-graded soil ($Cu > 4.0$); however, the coefficient of

curvature is slightly above the limit ($1.0 < Cc < 3.0$). Nevertheless, the road base shows a good particles size distribution allowing a good packing during the compaction process.

As indicated before, the road base was classified as a GM (Silty Gravel according to SUCS); that means that the soil sample present a low plasticity (PI=3.30) with a very low percentage of clay particles. However, it is clear from the Soil Modulus vs. Water Content curve that the silts present in the sample has significant potential to absorb water and to reduce greatly the stiffness of the material. Therefore, it is recommended the control compaction of this material under the basis of dry unit weight rather than soil modulus.

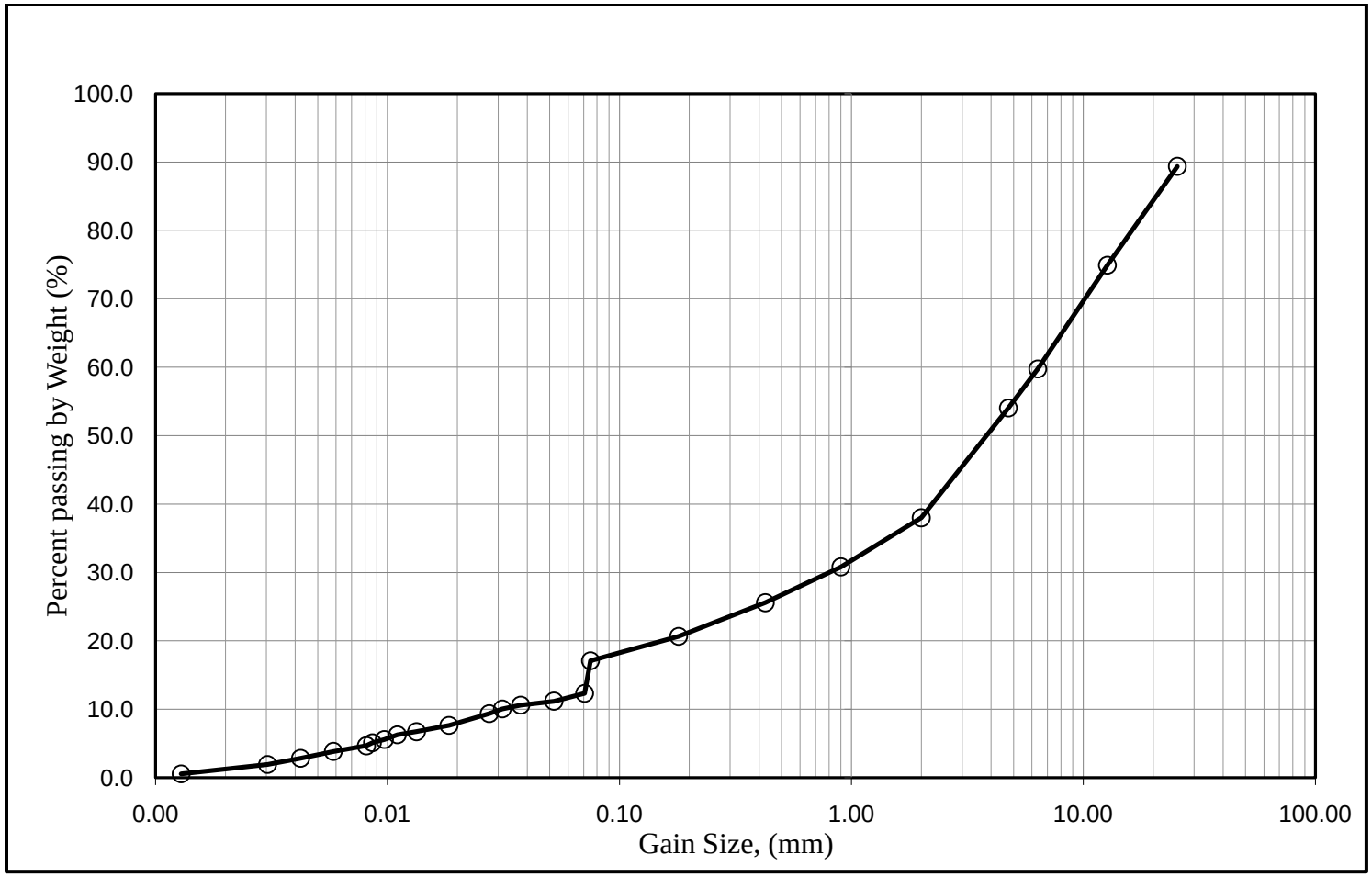


Figure 48. Particle Size Distribution Curve for the Road Base

Table 15. Select Index Properties of the Road Base

| Sample | $D_{10}$[1] | $D_{30}$[2] | $D_{50}$[3] | $D_{60}$[4] | Perc. Fines | $C_c$[5] | $C_u$[6] | $w_L$ | $w_P$ | $w_{PI}$ | Perc. Gravel | Perc. Sand | USCS[5] |
|---|---|---|---|---|---|---|---|---|---|---|---|---|---|
| Road Base | 0.03 | 0.8 | 4.0 | 6.5 | 17.1 | 3.28 | 216.67 | 17.7 | 14.39 | 3.31 | 45.97 | 36.93 | GM |

[1]$D_{10}$= particle diameter at 10% finer; [2]$D_{30}$= particle diameter at 30% finer; [3]$D_{50}$=particle diameter at 50% finer; [4]$D_{60}$= particle diameter at 60% finer; $C_c$ = coefficient of curvature; $C_u$= coefficient of uniformity; USCS[7]= Unified Soil Classification System.

## 7.3 Modified Proctor Compaction Test

The modified compaction test was conducted on the road base following the criterion establishes by the designation ASTM D 1557-07 (Standard Method for Laboratory Compaction Characteristics of Soil Using Modified Effort -56,000 ft-lbf/ft$^3$). The test was conducted on the soil particles passing sieve #3/4, in reference to the method C of the cited standard.

Figure 49 shows the result of the Modifies Proctor Compaction Test on the road base. According to the results of the tests, the maximum dry density of the aggregate corresponds to 21.5 kN/m$^3$, and it can be achieved at an optimum water content of 6.6%. Water contents beyond the optimum value leads to a decrease in the dry density due to the high fine content present in the soil. In addition, it can also lead to segregation or migration of the fine portion.

## 7.4 Comparison between the Dry Unit Weight of the Soil and the Soil Modulus

As well as the case of the clean sand, Figure 50 shows that the soil modulus of the road base is a more susceptible parameter to the water content than the dry unit weight. The maximum soil modulus is achieved at a water content of 5.5% while the maximum dry unit weight is achieved at a water content of 6.6%.

However, a difference from the clean sand, the soil modulus of the road base drops very quickly as the water content increases. The reason of this behavior obeys to the high fine content (around 17%) of the road base, which makes its soil modulus more

vulnerable to the water content than the clean sand. This concept is very important to take into account while taken decision on the selection of a material. For example, if the road base has to be chosen for a particular project (for an embankment, backfill or roadway), controlling compaction under the basis of maximum dry unit weight seems to be preferable. The reason is that the suction generated at low water content will increase the stiffness, which gets destroys as soon as the soil gets wet. On the other hand, if the clean sand is chosen, controlling compaction under the basis of soil modulus appears to be a better decision. The dry unit weight of the clean sand does not vary considerable under different water condition; therefore, the sand can reach its maximum dry density but still have a low modulus.

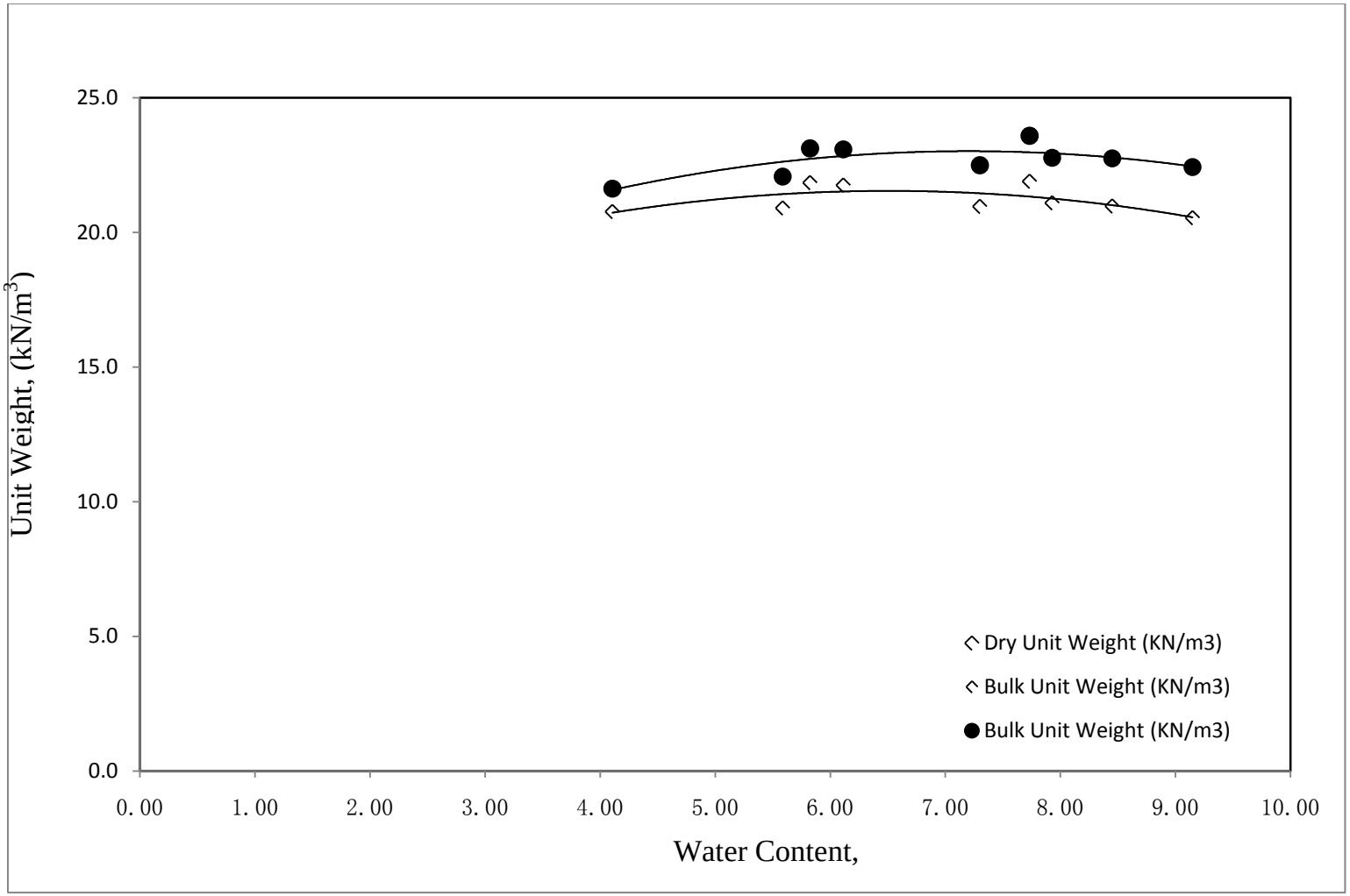


Figure 49. Modified Proctor Compaction Test for the Road Base

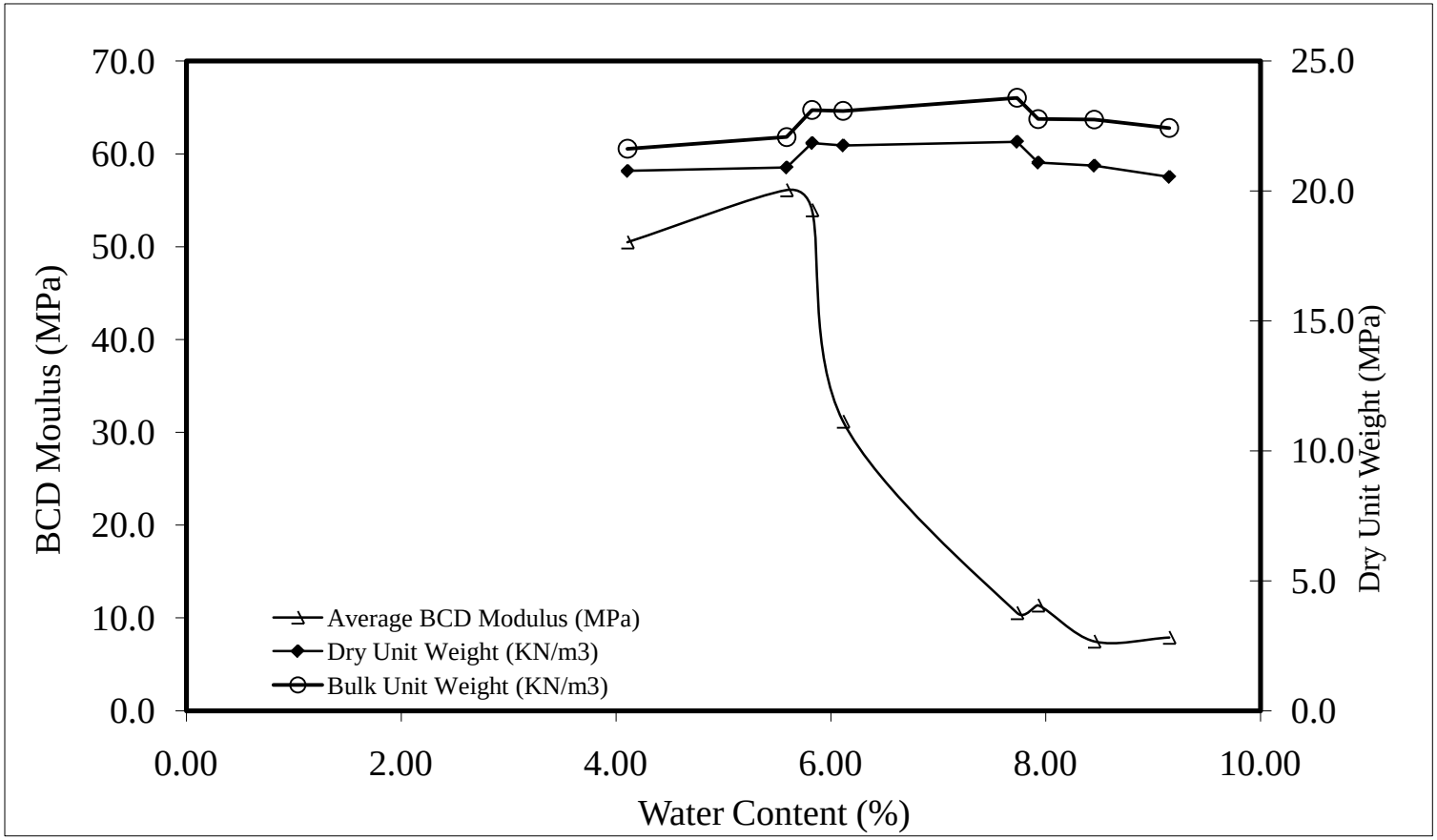


Figure 50. Modified Proctor Compaction Curve and BCD Modulus for the Road Base

## 7.5 Triaxial Compression Test (TC)

Triaxial Compression Tests (TC) was conducted on the road base on a large triaxial cell (figure 18). The tests were conducted on a mold of 8.5-inches height and 6 inches diameter with a maximum particle size of 25 mm. These conditions do not follow the requirement of the American Standard Testing of Materials (ASTM) that required a ratio of height- diameter of 2:1. Also, the standard requires that the maximum particle size of one tenth of the diameter, which correspond to 15.24 mm for the road base.

The specimens for the TC were prepared in a cylindrical mold of 8.75 inches height and 6 inches diameter. The soil was air-dried and compaction was achieved using the modified proctor test with 7 layers and 56 blows per layer. The number of layers was adjusted accordingly in order to achieve a maximum dry unit weight of approximately 90% to 95 % of the maximum dry unit weight obtained from the modified compaction curve (figure 50). The final dry unit weight and water content for the two specimen tested at the TC were 21.64 kN/m$^3$ ($w$ = 6.6%) and 21.95 kN/m$^3$ ($w$ = 6.7%) respectively.

The specimens were tested using a mold covered by a rubber membrane of unknown correction factor. The two specimens were tested at confining pressure of 7 psi and 10 psi (48.28 and 68.97 kPa). The Mohr Coulomb Envelopes was drawn for the tests, resulting on a friction angle of approximately 45$^o$ with cohesion value of 83 kPa.

Because the test performed did not follow the requirement of the American Society of Civil Engineering, the values of the friction angle represent an estimation of the frictional resistance of the material and not its real value. However, the real frictional resistance of the material should not be far-off from the estimated value since the results of the TC and DST conducted on the clean sand shown comparable results.

One of the reasons that the road base account for a high friction angle ($\Phi$=45), as shown in figure 51, is that the material used for the test specimen did not met the particle size requirement. The decision of using particles of sizes bigger than 15 mm obeys to the fact that the particles broken under the application of the compaction energy with the modified proctor hammer. No particles sizes beyond 15 mm were found after the test.

In addition, the road base contains limestone which is a sedimentary rock compose of mineral such as calcite ($CaCO_3$). Once this material is in place, chemical reaction between the calcium carbonate, water and carbon dioxide starts leading to the formation of cementitious material that increases greatly its strength.

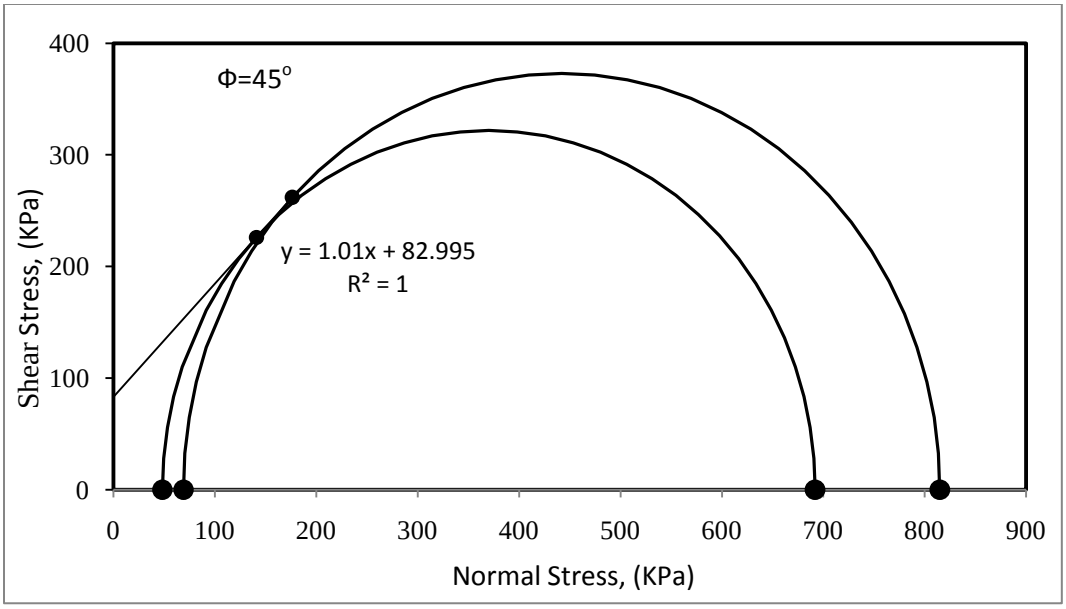


Figure 51. Mohr Coulomb Enveloped for the Road Base from the TC

# 8. PROPOSED TEST FOR THE CRUSHED ROCK.

It was stated in previous section that the crushed rock was used for the backfill of one of the MSE wall tested at Riverside Campus. The material comes from Georgetown, Texas from a company called Texas Crushed Stone. This aggregate account for particles sizes that goes beyond the application of any laboratory tests in a geotechnical lab. The inconvenient of having such larger particles prevented the determination of the mechanical properties of this aggregate, especially, the frictional resistance which represents the most important parameter on the design of a backfill of a structure.

Considering how important the determination of the angle of friction for computer modeling is, it was decided to propose a recommendation to conduct a Full-Scale Direct Shear Test that will allow a close computation of this parameter, as well as its dilatancy effects. The proposal is explained in the following section.

## 8.1 Proposal for a Full-Scale Direct Shear Test for Large Aggregates

The Full-Scale Direct Shear Test will allow the computation of the friction angle of large aggregates that cannot be tested in standard lab equipment. In addition, the test will provide more reasonable results since it will reproduce the behavior of a large mass of soil that can be a better representation of real conditions. Figure 52 through figure 54 is a schematic representation of the side view of a Full-Scale Direct Shear Test (FS-DST) that is being proposed in this report to test aggregates such as the road base and the crashed rock.

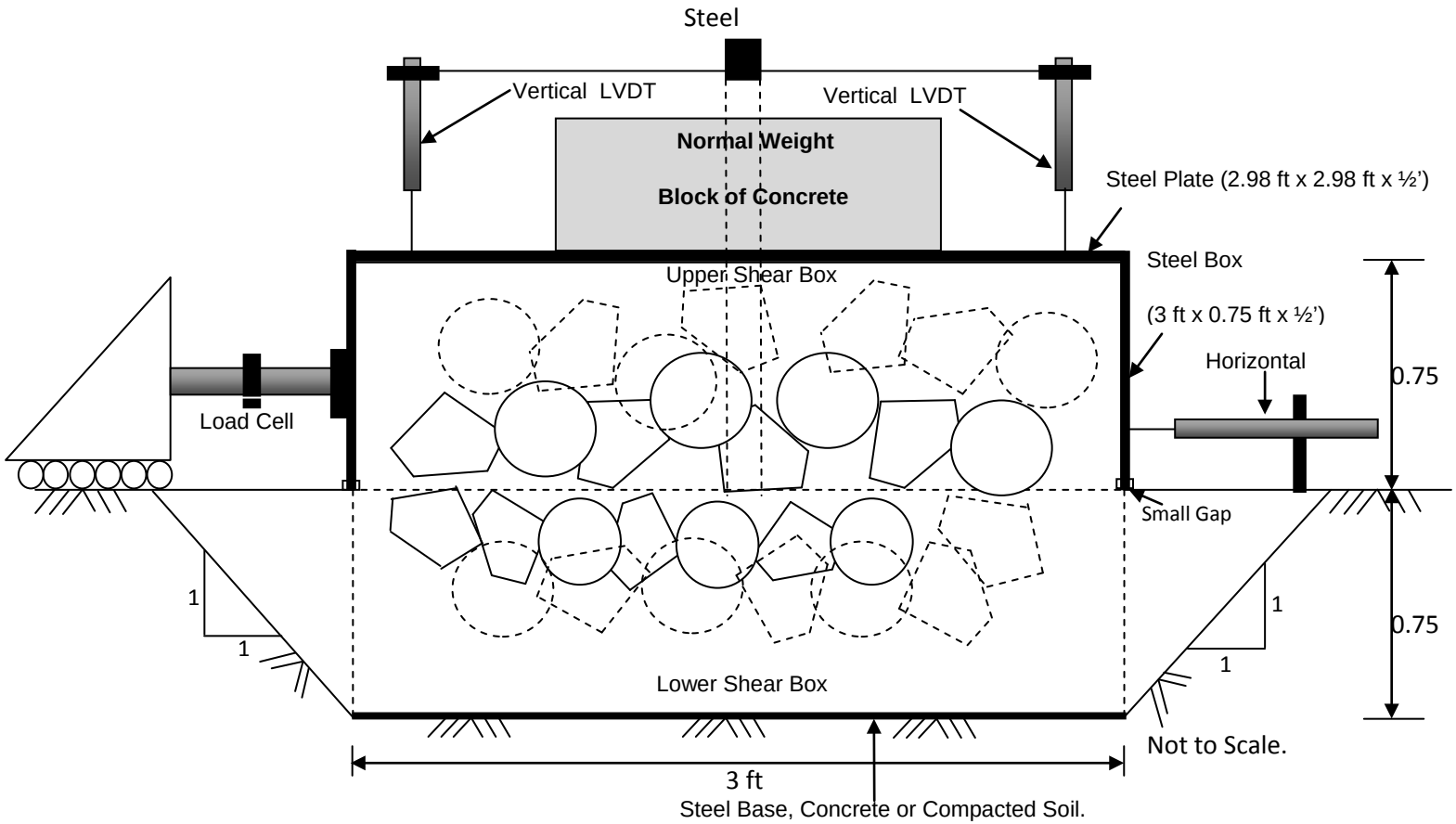


Figure 52. Schematic Representation of the Lateral View of the Propose Full-Scale Direct Shear Test (FS-DST)

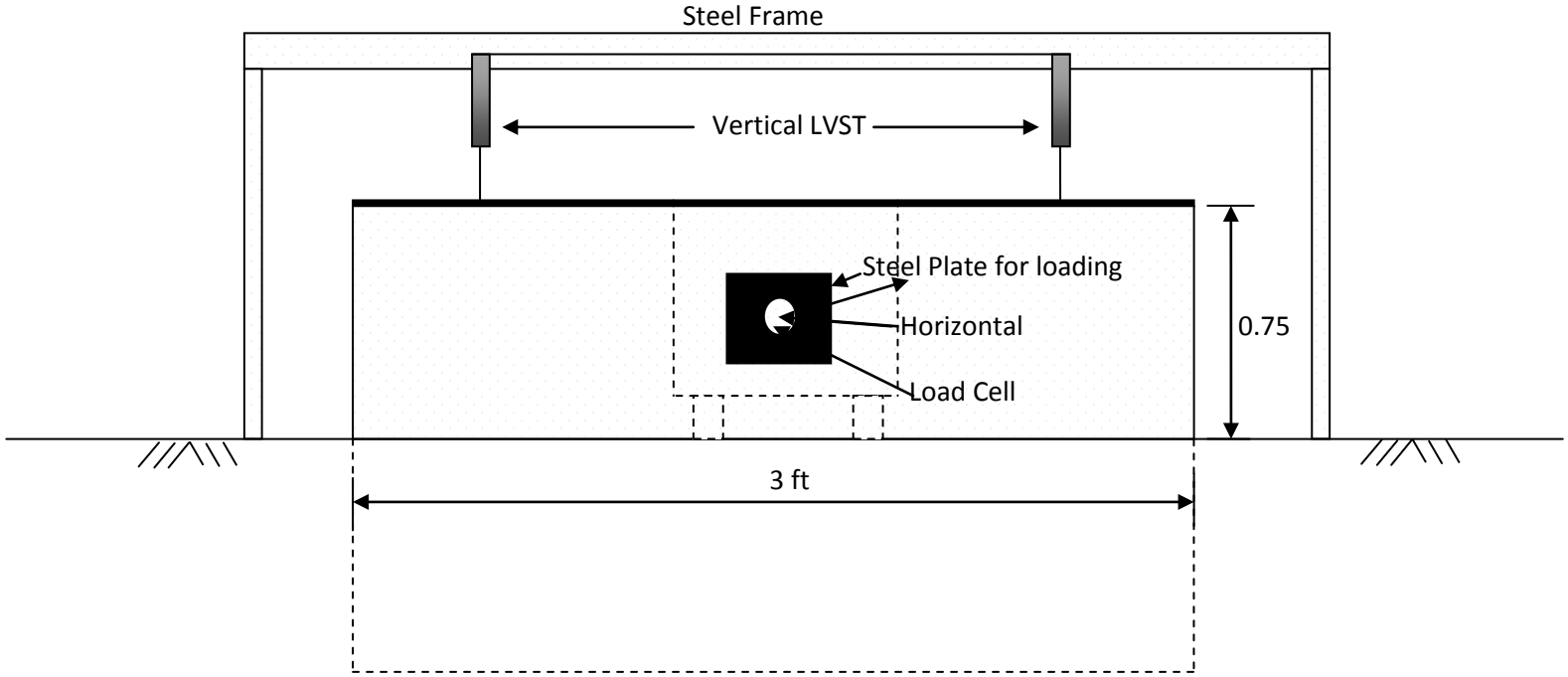


Figure 53. Schematic Representation of the Front View of the Propose Full-Scale Direct Shear Test (FS-DST)

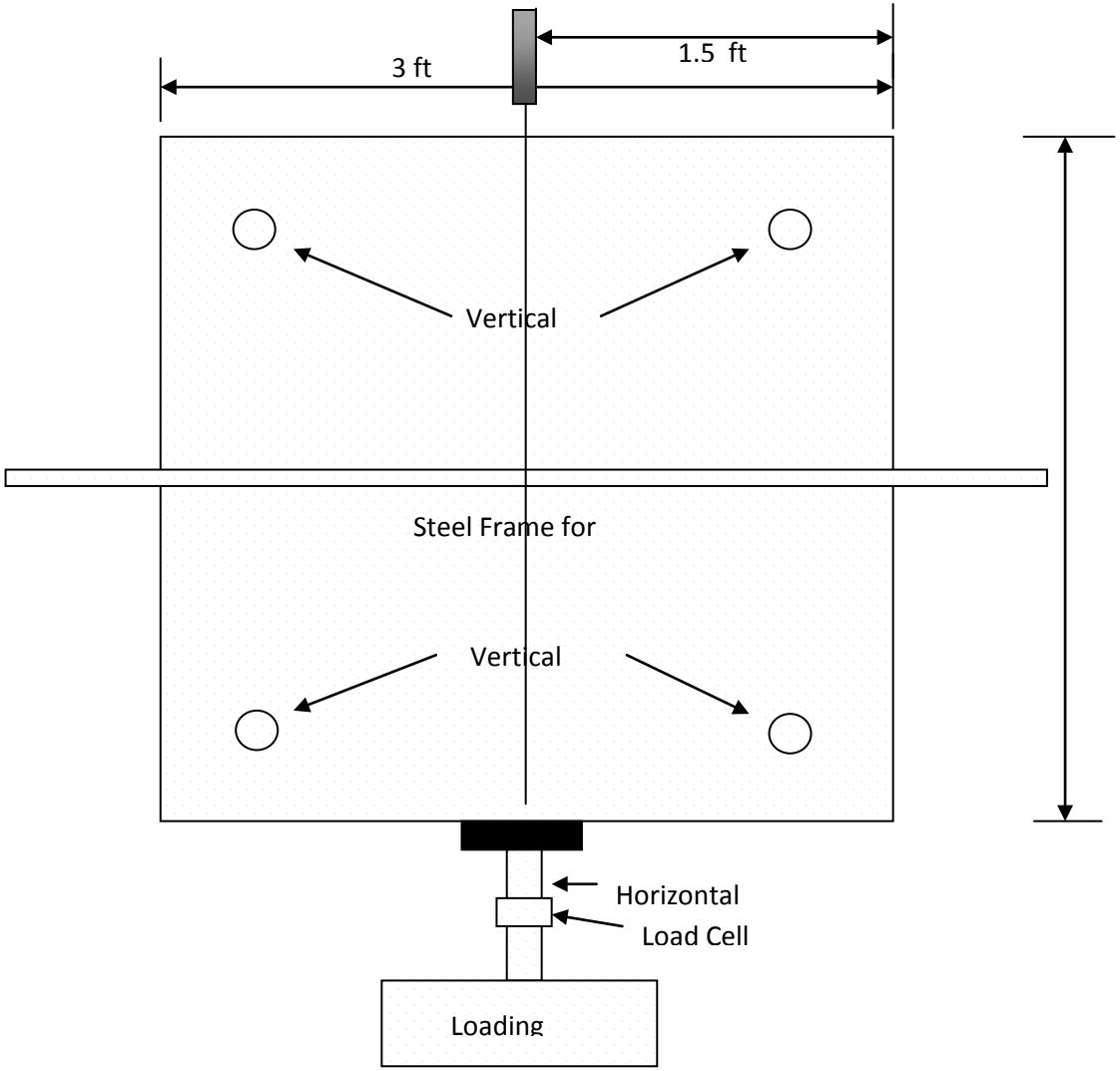


Figure 54. Schematic Representation of the Plan View of the Propose Full-Scale Direct Shear Test (FS-DST)

The propose FS-DST box is 36 inches square, contains 18 inches height, and should be constructed of stainless steel in order to avoid corrosion for further tests. About 17.7 $ft^3$ of material are needed to fill the entire box considering the requirement of compaction level established for a backfill. The sketch of the FS-DST has been designed to follow the requirement established by the designation ASTM D 3080 (Standard Method for Direct Shear Test Under Consolidated Drain Conditions). The propose dimensions will allow to test aggregate of a maximum particle size of 3.0 inches (ratio of $W/D_{max} > 10$). In addition, the ratio of height to maximum particle size ($H/D_{max}$) also meets the criterion of $H \geq 6D_{max,}$ as well as the ratio of with to height (W/H) that should be at least 2.0.

For practical purposes, the lower box can be inserted in the ground surface with a recommended steel plate at the bottom (or a stiff material to avoid settlement of the local material) in order to reduce errors in the computation of the vertical displacement. The shear displacement of the box can be controlled using a stepper motor that drives the upper box over the ground surface. A load cell mounted between the arm and the frame can be used to measure the shear force. The normal force can be applied by adding blocks of concrete of known weight and dimensions. The normal weight should be applied uniformly over the upper steel plate in order to avoid the presence of any parasite moment.

The measurement of the vertical and horizontal displacement can be done using a digital displacement or a linear strain conversion transducer (LVCT). Because of the large size of the shear box, a total of four displacement transducers are recommended. The transducers should be located at each corner of the shear box at about 8 inches from the edges. It is expected that the opposite site at the load application will dilate while the other side will contract. Depending on the loading device used for the test, it is recommended to check the frictional resistance of the system by following the procedure describes in section 4.7.2.

Based on the results of Bareither et al. (2008a), it is expected to have a reduction of the frictional resistance of the crashed rock (and in the case of the clean sand if tested) tested in a full scale DST, in reference realistic values since the effect of particle size has been minimized.

# 9. NUMERICAL SIMULATION OF THE DIRECT SHEAR TESTS FOR THE CLEAN SAND

The Laboratory-Direct Shear Test (DST) conducted on the clean sand was simulated using finite element method (FEM). A parametric study was carried out in order to determine the sensitivity of each soil-input parameter in the soil model. The FEM gives the advantage of providing any response of interest and allows changes in the values of the parameters, which would have otherwise proven to be expensive or impossible to implement in the experimental setup. The FEM is used to assess and study the effects of the friction angle and the dilation angle under a given normal stress condition.

The main goal of the numerical analysis is to correlate the results of the stress-strain deformation curve and the vertical displacement curve obtained from the Laboratory Direct Shear Test (DST) with a Finite Element Model using the soil-failure criterion of the Extended Drucker-Prager Model (Mat. Model_193). This simulation allows a better estimation of the frictional resistance and the dilation angle of the clean sand subjected to different confining pressures.

## 9.1 The Finite Element Model

In this study, the commercial finite element program LS-DYNA was used for the analysis. The Finite Elements Model considered in this study was generated by HyperMesh and it was developed by Seok-You Lim, a PhD student of Geotechnical Engineering from the Zachry Department of Civil Engineering. The mesh is shown in

figures 55 through 58 and they match the dimensions of the experiment of the Laboratory Direct Shear Test (DST). The material properties were obtained by a combination of laboratory testing and manufacturer specifications. The material properties used were as follows:

(1) DST-BOX (steel) :-Modulus of Elasticity (E) = 210 GPa, $\rho$=7850 kg/m$^3$, $\upsilon$=0.29

(2) Soil Material:-Modulus of Elasticity (E) = 0.008 GPa, $\rho$=1700 kg/m$^3$ and $\rho$=1800 kg/m$^3$ in some cases, $\upsilon$=0.35.

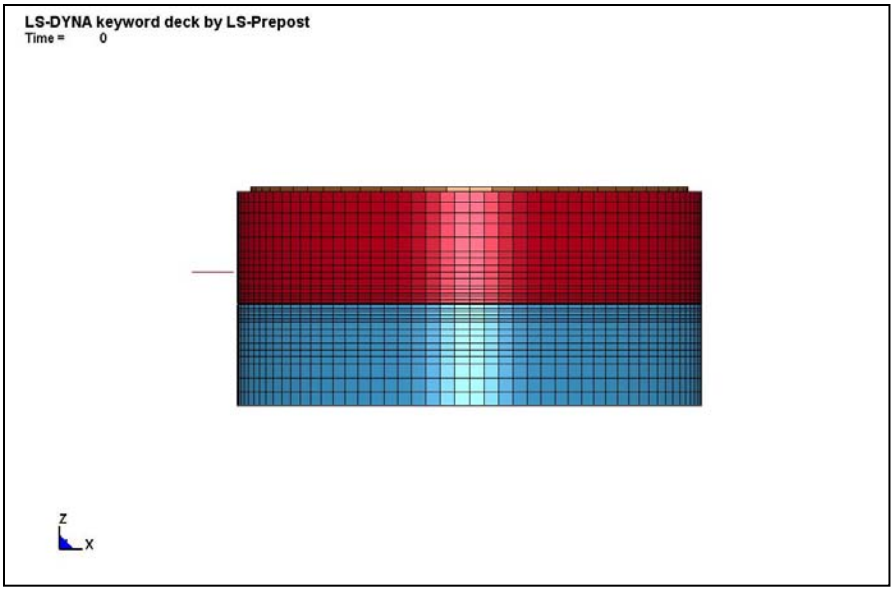


Figure 55. FEMs for the Laboratory Direct Shear Test – Front View of the DST-BOX

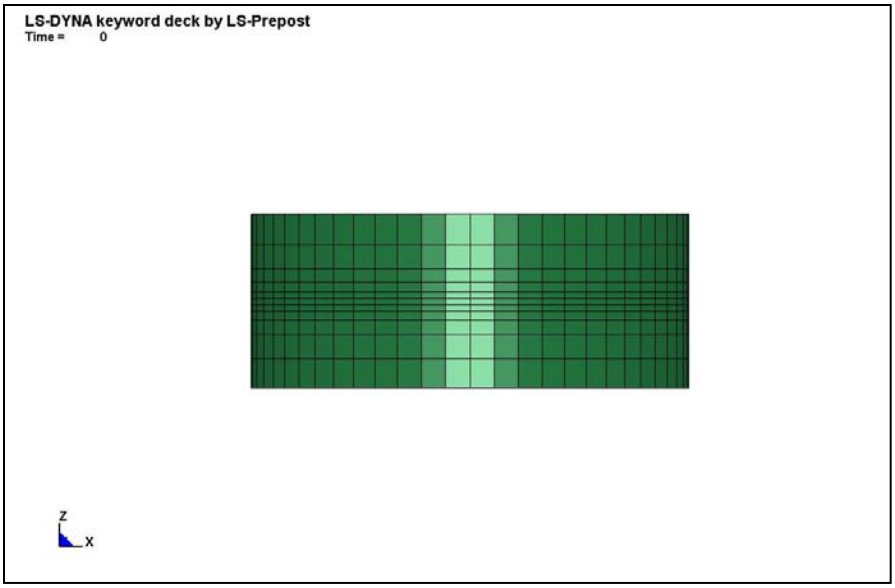


Figure 56. FEMs for the Laboratory Direct Shear Test – Front View of the Soil Mass

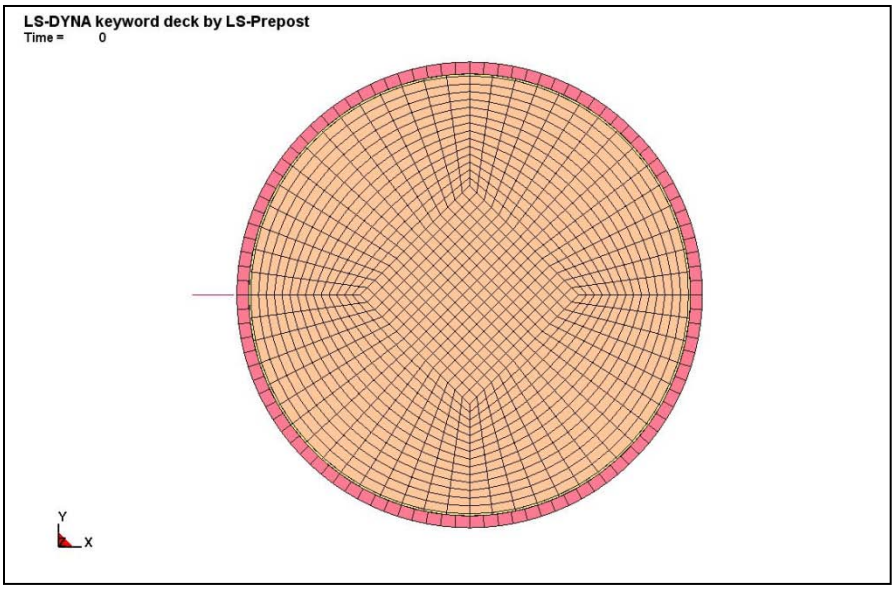


Figure 57. FEMs for the Laboratory Direct Shear Test – Plan View of the Weight.

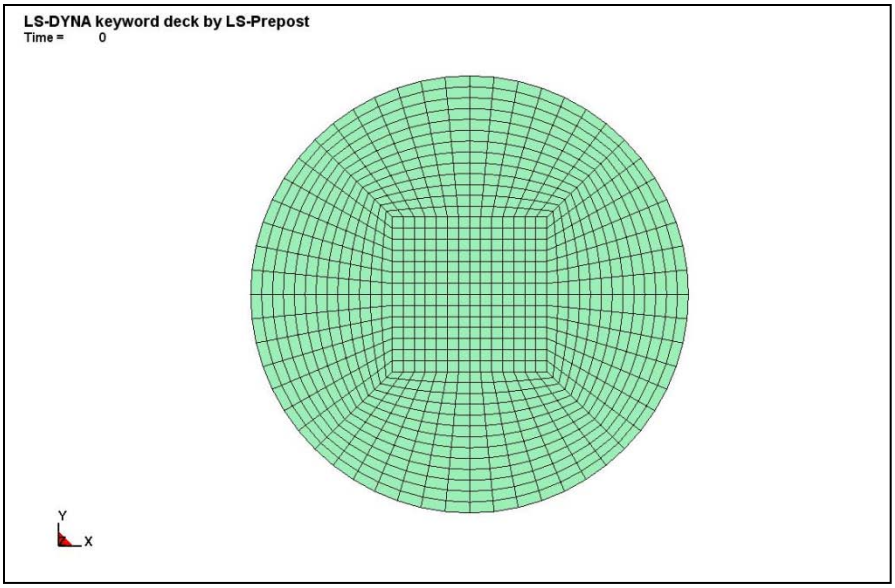


Figure 58. FEMs for the Laboratory Direct Shear Test – Plan View of the Soil

## 9.2 Description of the DST-MODEL

The DST-MODEL used in the numerical simulation reproduces the direct shear box used in the laboratory tests. The model includes an upper and lower case, a material representing the soil mass, a steel plate at the bottom to constrain the mass of soil in place, and a upper steel plate use to apply the normal stresses to the soil mass. The analysis was done under displacement control at a rate of 0.5 mm/min. This rate corresponds to the same shearing rate used in the Laboratory Direct Shear Tests. A description of each component of the model and its input parameters is given as follows (LS-DYNA Keyword User's Manual version 970 (2007); LS-DYNA Theoretical Manual version 940 (1998)) :

a) Bottom Plate of the DST-MODEL: a bottom rigid plate inside of the DST-BOX was developed in order to hold the soil as it happens to be at the laboratory DST test. This plate was constrained in all direction in order to fix the bottom part of the DST. The plate was analyzed as a rigid material using the Material Rigid Model (Mat_20) from LS-DYNA. The parts made from this material are considered to belong to a rigid body. The most important parameter used to analyze this material was the mass density ($\rho$=7850 kg/m$^3$), the Modulus of Elasticity (E=210 GPa) and the Poisson's Ratio ($\upsilon$=0.29). Figure 59 shows the material bottom plate of the DST-BOX.

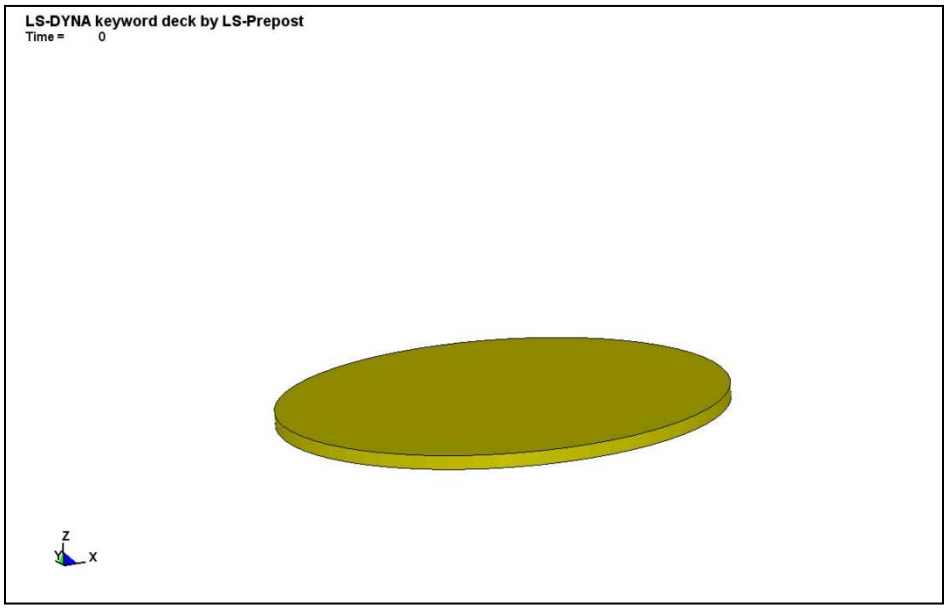


Figure 59. Material Used to Represent the Bottom Steel Plate of the DST-MODEL

b) Upper Case of the DST-MODEL: it corresponds to a steel disc of 63 mm diameter that represents the upper-half part of the DST-BOX MODEL. The material is analyzed as an isotropic elastic material model by using the Material Elastic Model (Mat_01) from LS-DYNA. The most important parameters used to analyze this material was the Modulus of Elasticity (E=210 GPa), the Poisson's Ratio ($\upsilon$=0.29) and the mass density ($\rho$=7850 kg/m$^3$). Figure 60 shows a sketch of this component of the DST-BOX MODEL.

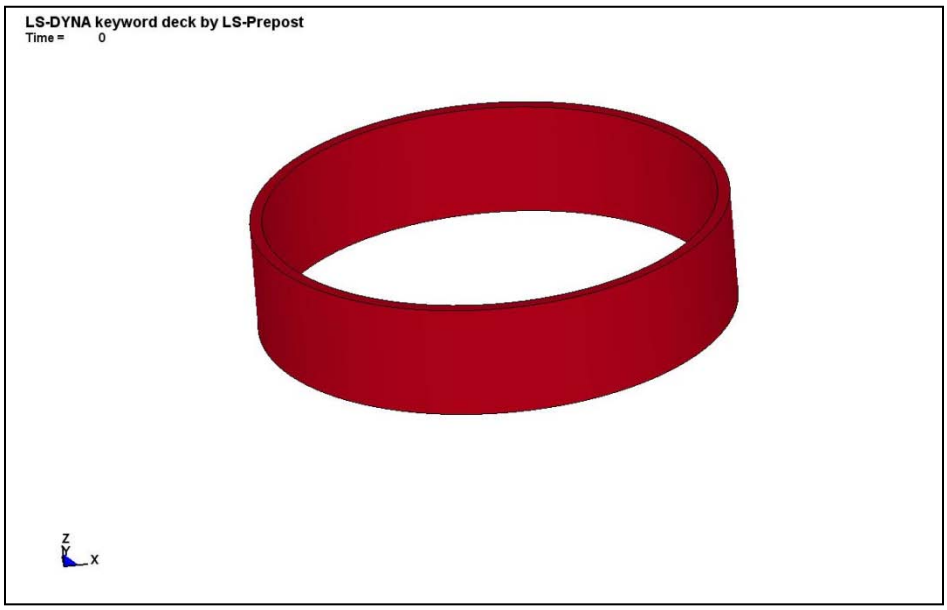


Figure 60. Material Used to Represent the Upper Half Part of the DST-MODEL

c) Bottom Case of the DST-BOX: it corresponds to a disc of 63 mm diameter that represents the bottom part of the DST-MODEL. This component of the DST-BOX corresponds to a rigid body material and it was analyzed using the Material

Rigid Model (Mat_20). As well as the bottom plate, the bottom case was also constrained in the “x” “y”, and “z” directions. The most important parameter used to analyze this material was the mass density ($\rho$=7850 kg/m$^3$), the Modulus of Elasticity (E=210 GPa) and the Poisson’s Ratio ($\upsilon$=0.29). Figure 61 shows the bottom case of the DST-BOX.

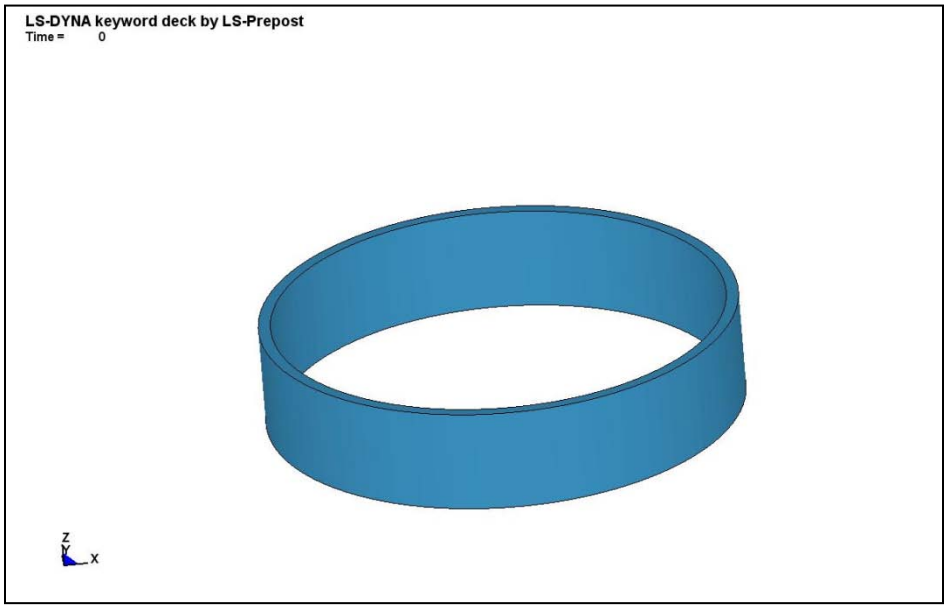


Figure 61. Material Used to Represent the Bottom Half Part of the DST-MODEL

d) The Soil Mass: the material used to represent the soil mass of the FE model has the dimensions of the laboratory soil specimen used to conduct the laboratory direct shear test (62 mm diameters and 27 mm height) an it is presented in figure 62. The soil was initially analyzed using the Modified Drucker-Prager Model (Mat_193) and the Jointed Rock Model (Mat_198) with zero joints for this last

model. When analyzing a soil mass using the Jointed Rock Model with a number of zero joints, the model becomes in the Modified Drucker-Prager Model. For this reason, the material analyzed in this section uses a yield surface criterion that corresponds to the Modified Drucker-Prager Model (Mat_193) since it enables the shape of the surface to be distorted into more realistic definition for soils. The most important inputs parameter used for this materials are presented in table 16.

Table 16: Main Input Parameters of the Drucker-Prager Model Used to Analyze the Idealized Soil Material of the DST-MODEL

| Variable | ρ | G | υ | K | φ | c | ψ |
|---|---|---|---|---|---|---|---|
| Value | 1.7E-9 | 2.96295 | 0.35 | 1.0 | 0.610865 | 0.002 | -0.0524 |

Note: ρ= mass density in tons/mm$^3$; G=Elastic Shear Modulus in MPa; υ=Poisson's ratio; R=failure surface shape parameter; φ= angle of friction (in radians); c= cohesion value, and; ψ=dilation angle (in radians).

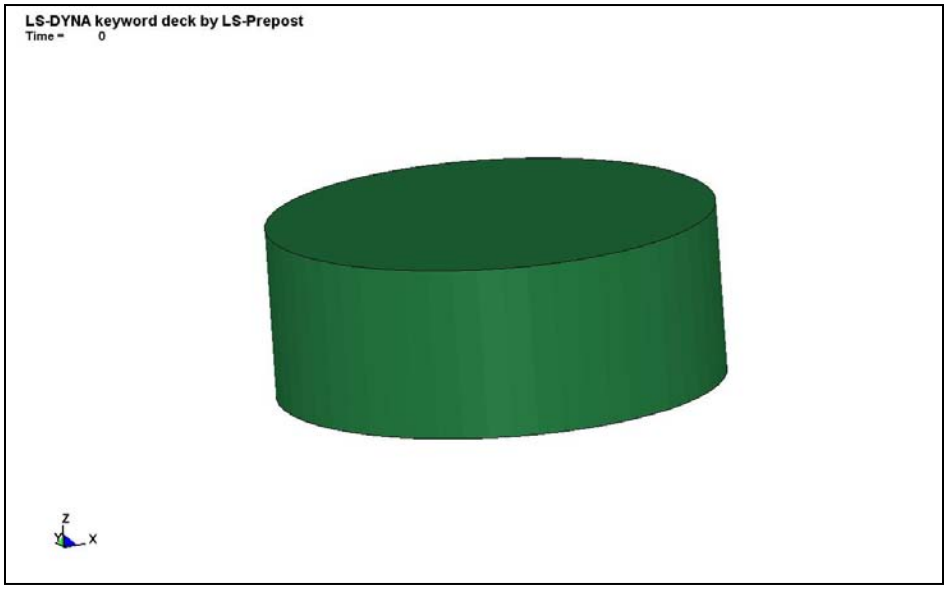


Figure 62. Material Used to Represent the Soil Mass of the DST-MODEL

From the conduction of the numerical simulation, it was founded that the cohesion value, the angle of internal friction (φ), and the dilation angle (ψ) are the most susceptible parameters in the results of the soil model.

e) The Weight Plate of the DST-MODEL: This material is analyzed as a rigid material plate that is used to reproduce the applied normal effective stress in the soil sample. As well as the bottom plate and the bottom case of the DST-MODEL, the material used to analyze this section was also the Material Rigid Model (Mat_20). The most important parameters used to analyze this material was the Modulus of Elasticity (E=210 GPa), the Poisson's Ratio (υ=0.29), and the mass density (ρ=7850 kg/m$^3$). This last input changed in accordance to the desired normal stress applied to the soil material. Figure 63 shows the weight plate of the DST-BOX MODEL.

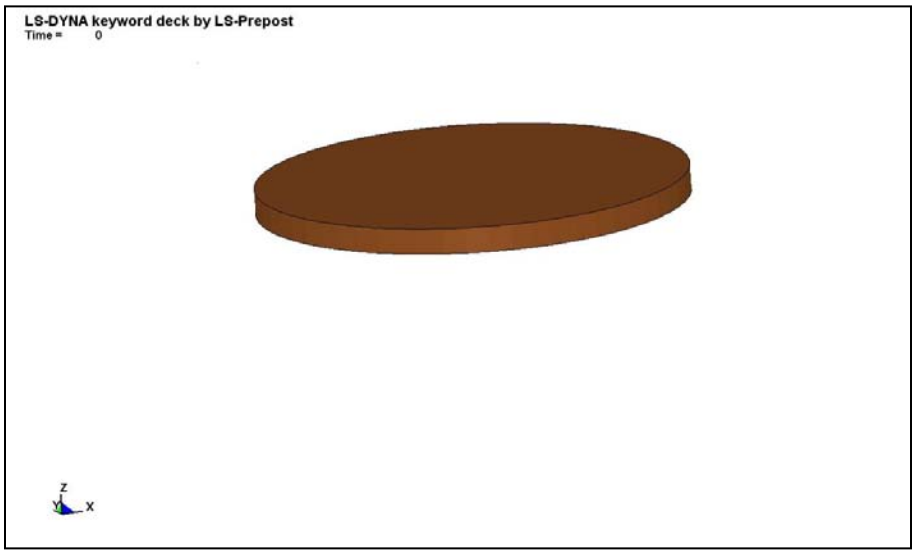


Figure 63. Material Used to Represent the Weight Plate of the DST-MODEL

The main function of the weight plate is to reproduce the normal stress that is applied to the soil sample during the laboratory test. The gravity load is appropriately applied to the soil material before shearing starts throughout an initialization process. Several normal stresses conditions were considered during the simulation (28.0 kPa, 54.0 kPa; 106.0 kPa; 153.0 kPa; 206.0 kPa; and 253.0 kPa). The changes in normal stresses were considered by changing the mass density of the plate.

f) The Beam: the beam element of the DST-BOX MODEL was analyzed as an isotropic elastic material using the Mat-Elastic Model (Mat_01). The beam is composed of three elements with the same element properties. The function of the beam is to apply the force and to pull the upper case of the DST- BOX MODEL at a constant rate of 0.5 mm/min. Figure 64 presents the representation of the beam element in the DST-BOX.

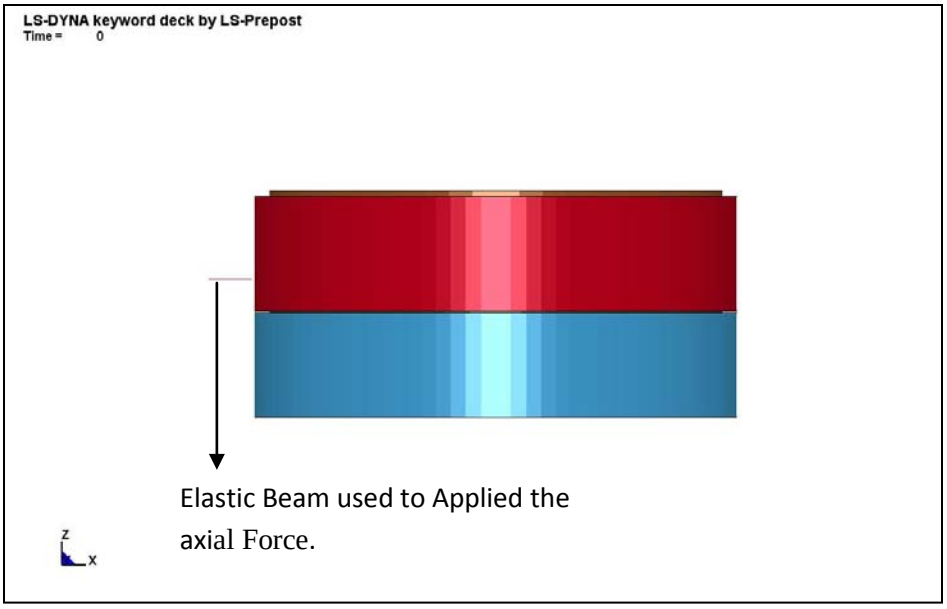


Figure 64. Material Used to Represent the Beam of the DST-MODEL

9.3 Description of the Drucker-Prager Model used to analyze the Soil Material

Problems of soil mechanics related to impact loads in laterally-loaded piles are normally treated as a plasticity problem. In the conduction of the numerical simulation, the soil is replaced by an idealized material which behaves elastically up to some state of stresses at which slip or yielding occurs (Drucker & Prager 1951). In this case, the idealized material representing the soil mass was analyzed using the Modified Drucker-Prager Model. As described by its failure criterion, the shear stress required for simple slip of the soil depends upon the cohesion (c), the normal stresses applied to the soil sample, the deviatory stresses, and the angle of internal friction. A difference from other cemented soils (i.e. clayey soils) that present true cohesion due to its structure and

cementitious properties, the cohesion intercept of the clean sand used in these simulations depended on the results of the laboratory tests. It was seen, from the results of the DST, that even a very low water content is capable of generating suction which can be translate as an apparent cohesion of the material.

The Model used to analyze the idealized material, representing the clean sand, corresponds to the Jointed Rock Model with zero joint (Designation Mat_198 in LS_DYNA). By adding zero joints as an input, the model becomes in a modified version of the Drucker-Prager Model (Designation Mat_193 in LS-DYNA). The selection of this model obeys to its ability to model frictional materials, which are typically granular soils as it is the case of the tested clean sand.

For granular materials, the Drucker-Prager Model is often used as a failure surface, in the sense that the materials can exhibit unlimited flow when the stresses reach the yield surface. Plastic flow can be seen from the results of the numerical simulation when the angle of dilation was given as a negative input. In those cases, when the material reaches the yield surface, it may behave as a perfectly plastic material. On the other hand, the model also provides a hardening behavior. In these cases, plastic flow causes the yield surface to change its size uniformly with respect to all stress directions leading to an increase of the strength resistance of the soil. This behavior can also be seen in the results presented from the numerical simulations when the dilation angle was given as a positive input value.

In the Drucker-Prager Model (modified version), the incremental plastic strain vector of this model is a negative component, meaning that the volume dilate at failure. However, in experimental tests, that is not a general case since contraction occurs for normally consolidated soils and loose sands. Considering that, the model is not suitable for these conditions since the normality rule may not be valid leading to instability, according to the Drucker's requirements (Desai & Siriwardane 1984).

### 9.3.1 Yield Function and Stress-Strain Relation

The central element in plasticity theory is the yield surface function. This is a relationship among the stress components at which insipient yielding occurs (Murff 2008). A difference from other materials, for soils is necessary to make some assumptions regarding the yield point due to its complex behavior under loading conditions. For example, in most of the cases it is considered that soils behave as an elastic material up to the yield point; however, this assumption is not always true (Murff 2008).

The inelastic behavior of geomaterial whose yield is governed by the Drucker-Prager yield condition can be written as:

$$F(J_1, J_2^{'}) = J_2^{'} - \alpha J_1 + K = 0 \tag{14}$$

Where: $J_1$= is the first invariant of the stress tensor and it is related to pressure (mean stress); $J_2$= is the second invariant of the deviatoric stress tensor and it is related to shear; α= is a material parameter related to the friction angle, and; $K$= material

parameter related to cohesion and the friction angle. The formulation of the components of the Drucker-Prager yield surface criterion is described as followed:

$$J_1 = \sigma_{11} + \sigma_{22} + \sigma_{33} \tag{15}$$

$$J_2^{'} = \frac{1}{2}\left(s_{11}^2 + s_{22}^2 + s_{33}^2\right) + \sigma_{23}^2 + \sigma_{31}^2 + \sigma_{12}^2 \tag{16}$$

$$S_{ij} = \sigma_{ij} - P\delta_{ij} \tag{17}$$

Where; $\sigma_{11}$, $\sigma_{22}$, $\sigma_{33}$= normal stresses in the *x*, *y* and *z* direction; $s_{11}$= $s_{22}$= $s_{33}$= deviatoric stresses in the *x*, *y*, and *z* direction; P=mean stress; $\sigma_{23}$, $\sigma_{31}$, $\sigma_{12}$=shear stresses in each plane; c=cohesion intercep, and φ= angle of internal friction. The formulation of α and k depends on whether the yield surface is written from a triaxial compression, extension or in plane strain condition (Shewer 2010).

The Drucker-Prager yield surface criterion is shown in figures 65 and 66 in a principal stress-space-plane. The conceptual frame of any material model in LS-DYNA is basically based on the yield criterion established by the model and the constitutive algorithm to update the stresses when yielding occurs. It is noticed, from figure 65, that three conditions can happen when analyzing the soil material model. These conditions are (Schwer 2010):

a) If $F_{(J_1, J_2')} < 0$, the material behaves as an elastic material. The stresses states will be located inside the yield surface and no volume change is recorded;
b) If $F_{(J_1, J_2')} = 0$, the stress level will be located over the yield surface (yielding),

c) If $F_{(J1, J2')} > 0$, the stress state is not permitted. In this case, the trial stresses are returned to the yield surface by plasticity algorithm.

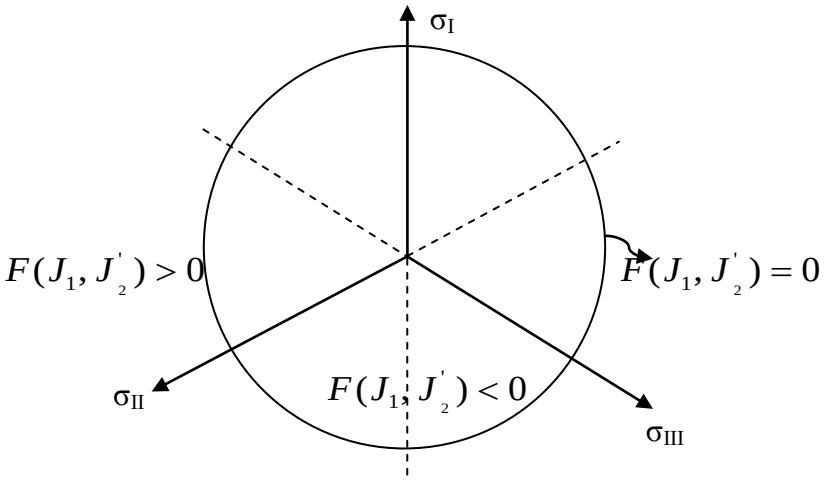


Figure 65. Drucker–Prager Surface Failure Criterion in a Principal Stress Plane (Modified After Murff 2008)

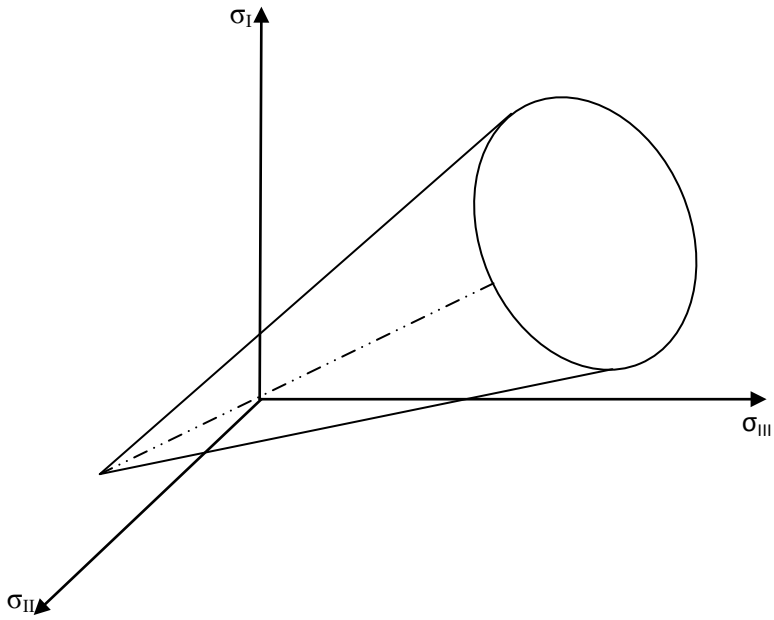


Figure 66. The Drucker–Prager Surface Failure Criterion in a Principal Stress-Space (Modified from Abaqus User's and Theory Manual version 2007)

In the case of the numerical simulation of the Direct Shear Test, it is noticeable that yielding occurs after certain level of stresses. Therefore, they end up in the third case, described above, in which incipient yielding occurs and the stress state is located outside the yield surface. As explained before, the stress state is returned to the yield surface by the plasticity algorithm and given to the potential function (G).

In a general sense, the plastic analysis of the material model starts by computing the trail stresses using the constitutive law and assuming a constant strain increment. Once those stresses are computed, the invariant of the deviator-stress tensor are determined as well as the location of all the yield points (*F*). These stresses can be computed by elasticity using the following equation (Schwer 2010):

$$\sigma_{ij}^{trials} = \sigma_{ij}^{n} + \Delta\sigma_{ij} = \sigma_{ij}^{n} + C_{ijkl}\Delta\varepsilon_{ij} \tag{18}$$

Where: $\sigma^{trial}$= corresponds to the principal stresses computed by assuming elastic strain increments; $C_{ijkl}$=Elasticity Tensor which is a function of Lame Modulus and Shear Modulus, and; $\Delta\varepsilon$=corresponds to the strain increment.

Once the trial stresses and the invariants are computed, they are given as an input to the yield function. If the new trial-state of stress is located outside of the yield surface ($F_{(J1,\ J2')} > 0$), this implies that the assumption that the strain increment was elastic is incorrect. Then, the strain tensor is broken into two components: an elastic component and a plastic component (Schwer 2010).

$$\Delta\varepsilon_{ij} = \Delta\varepsilon_{ij}^{e} + \Delta\varepsilon_{p}^{p} \tag{19}$$

Where: $\Delta\varepsilon^e$= is the elastic component of the strain tensor, and; $\Delta\varepsilon^p$= is the plastic component of the strain tensor.

The updated stresses are computed by using the following equation:

$$\sigma_{ij}^{n+1} = \sigma_{ij}^{n} + \Delta\sigma_{ij} = \sigma_{ij}^{n} + C_{ijkl}\Delta\varepsilon_{ij}^{e} = \sigma_{ij}^{n} + C_{ijkl}\left(\Delta\varepsilon_{ij} - \Delta\varepsilon^{p}{}_{ij}\right) \quad (20)$$

As state before, the yield function of any elasto-plastic model is used to identify the material behavior. Beyond yielding, the material starts experimenting plastic strains which are normal to the yield surface, if there is an associate flow rule, or they are no longer normal to the yield surface, if there is a non-associate flow rule. In the case of the associate flow rule, the yield function and the plastic potential function are the same. However, in the case of the non-associated flow rule, the plastic strain is now normal to the potential function and it is also function of the dilation angle and the stress invariants.

A non-associated flow rule tends to be more realistic for the case of geomaterial, like soils, since the associated flow rule tends to overpredict the amount of volumetric plastic strain (Hibbit et al. 2007). The non-normality condition, of a non-associated flow rule, can be represented by a constant ($\lambda$) that provides the magnitude of the plastic deformation times the gradient of the plastic potential function. This last provides the direction of the plastic deformation vector. The equation can be expressed as:

$$\Delta\varepsilon^{p}_{ij} = \lambda\frac{\partial G}{\partial\sigma_{ij}} \quad (21)$$

Where: λ= is the magnitude of the plastic strain, and; $\frac{\partial G}{\partial \sigma_{ij}}$ = is the gradient of the plastic potential function which provides the direction of the plastic deformation.

The value of λ is also called the consistency parameter. It is determined by demanding that that the stresses must remain in the yield surface during inelastic loading (Fossum &Brannon 2004). The plastic potential has the same shape as the yield function but with different parameters α and k, which now are also function of the dilation angle of the material.

From the above equation, the only unknown variable is the constant λ, which is computed from the combination of the non-associated flow rule, the computation of the trial stresses and the consistency condition. Therefore, the magnitude (λ) of the plastic flow, can be determined as follow:

$$\lambda = \frac{\left(\frac{\partial G}{\partial \sigma_{ij}}\right) C_{ijkl} \Delta \varepsilon_{ij}}{\left(\frac{\partial G}{\partial \sigma_{ij}}\right) C_{ijkl} \left(\frac{\partial G}{\partial \sigma_{ij}}\right)} \tag{22}$$

## 9.4 Results of the Numerical Simulation of the Direct Shear Test Conducted to the Clean Sand

Numerical simulations of the Direct Shear Test (DST) were conducted to the clean sand in order to correlate the results of the laboratory DST test. This will allow having a better estimation of the internal angle of friction (φ) and the dilation angle (ψ) of this material computed from the DST. The DST-BOX and the soil mass used in the

FE model matches the dimensions of the laboratory test. The tests were conducted at a shear velocity of 0.05 mm/min as it is required in the Designation ASTM D-3080 (Standard Method for Direct Shear Test under Consolidated Drained Condition).

Different soil conditions were analyzed in a parametric study carries out during the numerical simulation. The input values of this study are based on the results of the laboratory Direct Shear Test (DST). Normally, a friction angle (φ) varying from 33 to 36 degrees and a dilation angle (ψ) varying from -4.0 to +3.0 degrees were used in the simulations for the case of the loose sand. For the case of the dense, the input friction angle was 41 and 42 degrees and the dilation angle was between 3 and 5 degrees. In addition to the friction angle (φ) and the dilation angle (ψ), a cohesion interception (c) of 2.0 kPa, 5.0 kPa, 7.0 and 10.0 kPa was also given as an input to the soil model in order to simulate the effect that suction has over granular materials when low water content is present in the soil mass. The Elastic Young Modulus (E) used in the simulations corresponds to 50% of the Soil Modulus determined in the laboratory Test using the Briaud Compaction Device (BCD).

The failure criterion of the results obtained from the numerical simulation is based on a modified version of the Drucker-Prager Model (Mat_193). The maximum shear stress, from the Shear Stress (SS) vs. Relative Horizontal Displacement (RHD) curve, was computed and it is given in tables 17 to 19 as the maximum Shear Strength of the idealized soil material. However, since the Modified Drucker-Prager model allows an increased in shear stress as hardening occurs, failure shear strength of the soil mass is

also defined from the SS vs. RHD curve. The criterion for the failure shear stress is based on the analysis of the inflexion points of the SS vs. RHD curve. In the cases of perfectly plastic behavior after yielding, both stresses, the maximum shear stress and the failure shear stress, have the same value.

The results of the parametric study of the FE analysis conducted on the clean sand are presented in tables 17 to 19. These tables include the soil input parameters as well as the shear strength results from the simulated Shear Stress (SS) vs. Relative Horizontal Displacement (RHD) curves presented in figures 67 through 98.

Table 17. Results of the FEM Model Conducted on the Direct Shear Test (DST-Loose Case 1)

| Test Number | Applied Normal Stress (kPa) | Approx. Dry Unit Weight ($kN/m^3$) | [(1)]Elastic Young Modulus (MPa) | Cohesion (KPa) | Max. Shear Stress (kPa) | Failure Shear Stress (kPa) | Friction Angle (Degrees) | Dilation Angle (Degrees) |
|---|---|---|---|---|---|---|---|---|
| 1 | 106.0 | 17.66 | 8.0 | 2.0 | 54.0 | 54.0 | 36.0 | -4.0 |
| 2 | 106.0 | 17.66 | 8.0 | 2.0 | 57.0 | 57.0 | 36.0 | -3.0 |
| 3 | 106.0 | 17.66 | 8.0 | 2.0 | 60.0 | 58.0 | 36.0 | -2.0 |
| 4 | 106.0 | 17.66 | 8.0 | 2.0 | 68.0 | 58.0 | 36.0 | -1.0 |
| 5 | 106.0 | 17.66 | 8.0 | 2.0 | 78.0 | 58.0 | 36.0 | 0.0 |
| 6 | 106.0 | 17.66 | 8.0 | 2.0 | 86.0 | 58.0 | 36.0 | 1.0 |
| 7 | 106.0 | 17.66 | 8.0 | 2.0 | 93.0 | 58.0 | 36.0 | 2.0 |

(1) The Elastic Young Modulus was taken as one half of the Briaud Compaction Device Modulus ($E_{BCD}$) - $E=1/2E_{BCD}$

Table 18. Results of the FEM Model Conducted on the Direct Shear Test (DST-Lose Case 2)

| Test Number | Applied Normal Stress (kPa) | Approx. Dry Unit Weight ($kN/m^3$) | [(1)] Elastic Young Modulus (MPa) | Cohesion (kPa) | Max. Shear Stress (kPa) | Failure Shear Stress (kPa) | Friction Angle (Degrees) | Dilation Angle (Degrees) |
|---|---|---|---|---|---|---|---|---|
| 1 | 54.0 | 16.68 | 8.0 | 5.0 | 37.0 | 37.0 | 35.0 | -2.0 |
| 2 | 54.0 | 16.68 | 8.0 | 5.0 | 42.0 | 37.0 | 35.0 | -1.0 |
| 1 | 54.0 | 16.68 | 8.0 | 5.0 | 51.0 | 38.0 | 35.0 | 1.0 |
| 2 | 54.0 | 16.68 | 8.0 | 5.0 | 54.0 | 38.0 | 35.0 | 2.0 |
| 3 | 54.0 | 16.68 | 8.0 | 5.0 | 57.0 | 38.0 | 35.0 | 3.0 |
| 4 | 28.0 | 16.68 | 8.0 | 5.0 | 25.0 | 24.0 | 35.0 | -2.0 |
| 5 | 28.0 | 16.68 | 8.0 | 5.0 | 27.0 | 24.0 | 35.0 | -1.0 |
| 6 | 28.0 | 16.68 | 8.0 | 5.0 | 31.0 | 24.0 | 35.0 | 2.0 |
| 7 | 28.0 | 16.68 | 8.0 | 5.0 | 32.0 | 24.0 | 35.0 | 3.0 |

(1) The Elastic Young Modulus was taken as one half of the Briaud Compaction Device Modulus ($E_{BCD}$) - $E=1/2E_{BCD}$

Table 19. Results of the FEM Model Conducted on the Direct Shear Test (DST- Loose Case 3)

| Test Number | Applied Normal Stress (kPa) | Approx. Dry Unit Weight ($kN/m^3$) | [(1)]Elastic Young Modulus (MPa) | Cohesion (kPa) | Max. Shear Stress (kPa) | Failure Shear Stress (kPa) | Friction Angle (Degrees) | Dilation Angle (Degrees) |
|---|---|---|---|---|---|---|---|---|
| 1 | 153.0 | 16.68 | 8.0 | 7.0 | 83.0 | 83.0 | 34.0 | -2.0 |
| 2 | 153.0 | 16.68 | 8.0 | 7.0 | 116.0 | 110.0 | 34.0 | -1.0 |
| 3 | 153.0 | 16.68 | 8.0 | 7.0 | 116.0 | 90.0 | 34.0 | 2.0 |
| 4 | 153.0 | 16.68 | 8.0 | 10.0 | 119.0 | 94.0 | 34.0 | 2.0 |
| 5 | 153.0 | 16.68 | 8.0 | 7.0 | 127.0 | 98.0 | 34.0 | 3.0 |
| 6 | 153.0 | 16.68 | 8.0 | 7.0 | 128.0 | 108.0 | 34.0 | 4.0 |
| 7 | 206.0 | 16.68 | 8.0 | 7.0 | 152.0 | 128.0 | 34.0 | 3.0 |
| 8 | 206.0 | 16.68 | 8.0 | 7.0 | 158.0 | 130.0 | 34.0 | 4.0 |
| 9 | 263.0 | 16.68 | 8.0 | 7.0 | 181.0 | 154.0 | 34.0 | 3.0 |
| 10 | 263.0 | 16.68 | 8.0 | 7.0 | 201 | 160.0 | 34.0 | 4.0 |

(1) The Elastic Young Modulus was taken as one half of the Briaud Compaction Device Modulus ($E_{BCD}$) - $E=1/2E_{BCD}$.

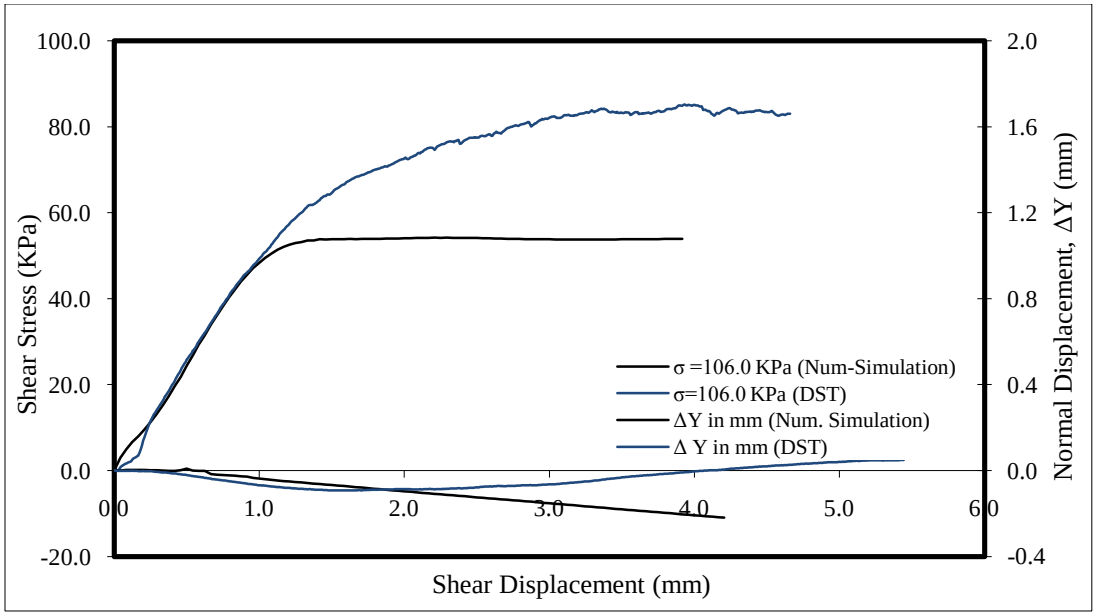


Figure 67. Results of the Numerical Simulation of the DST (E=8 MPa; ρ=18 kg/m$^3$; c= 2.0 kPa; ψ=-4.0 degrees; φ=36.0 degrees; σ= 106 kPa)

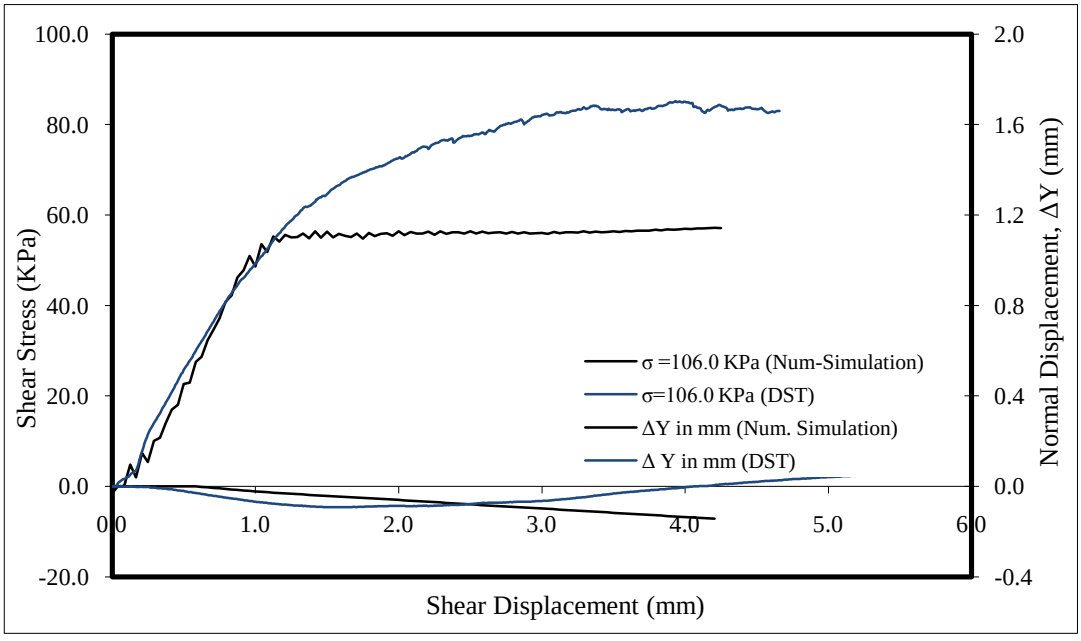


Figure 68. Results of the Numerical Simulation of the DST (E=8 MPa; ρ=18 kg/m$^3$; c= 2.0 kPa; ψ= -3.0 degrees; φ= 36.0 degrees; σ= 106 kPa)

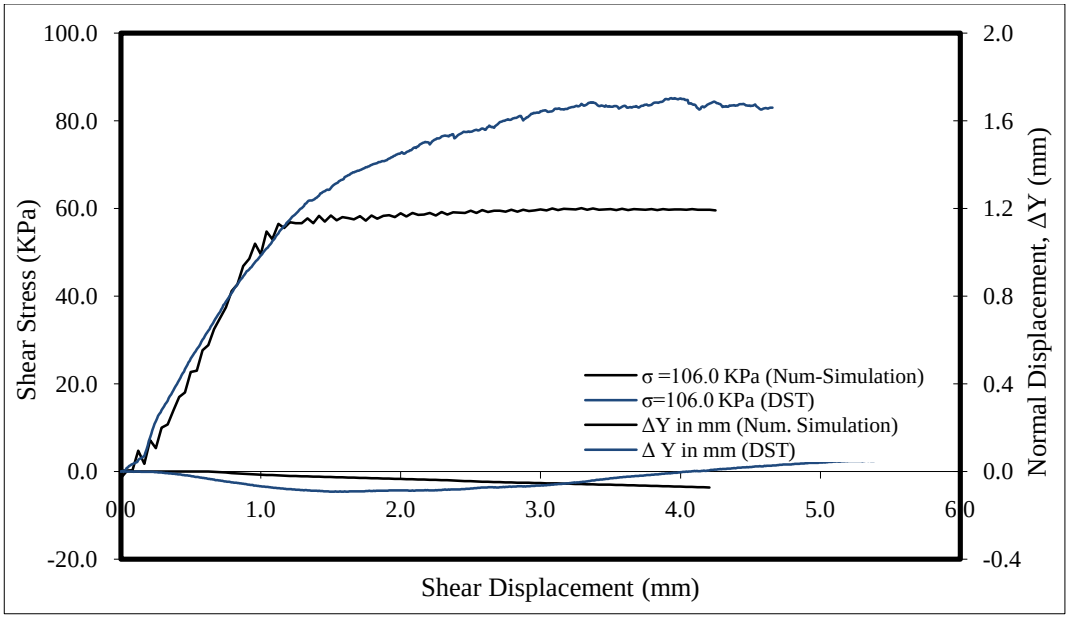


Figure 69. Results of the Numerical Simulation of the DST (E=8 MPa; ρ=1 8 kg/m$^3$; c= 2.0 kPa; ψ= -2.0 degrees; φ= 36.0 degrees; σ= 106 kPa)

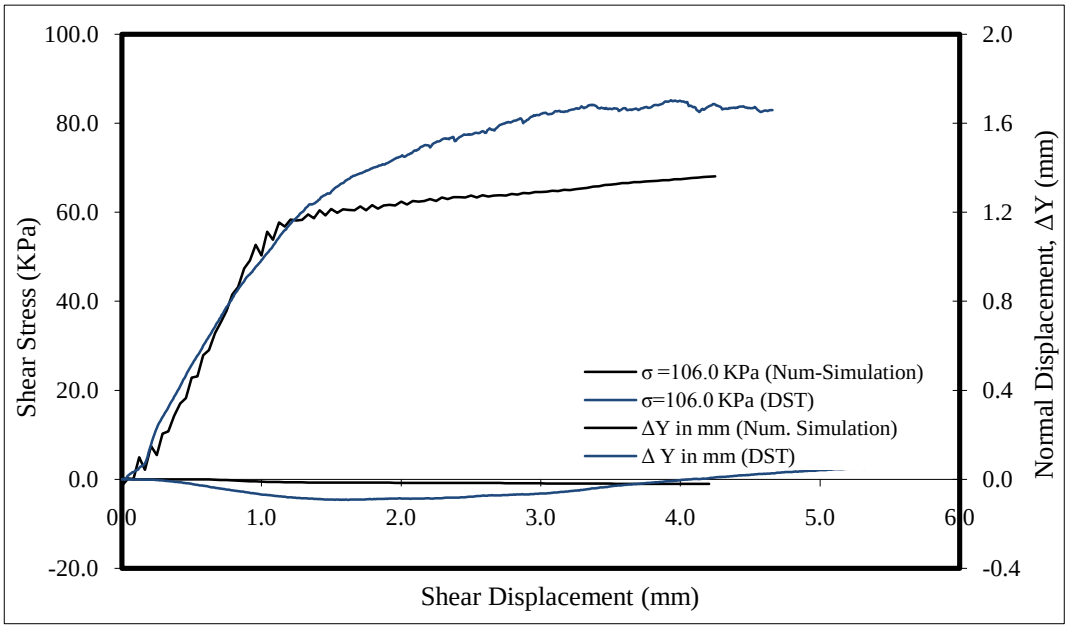


Figure 70. Results of the Numerical Simulation of the DST (E=8 MPa; ρ=18 kg/m$^3$; c= 2.0 kPa; ψ= -1.0 degrees; φ= 36.0 degrees; σ= 106 kPa )

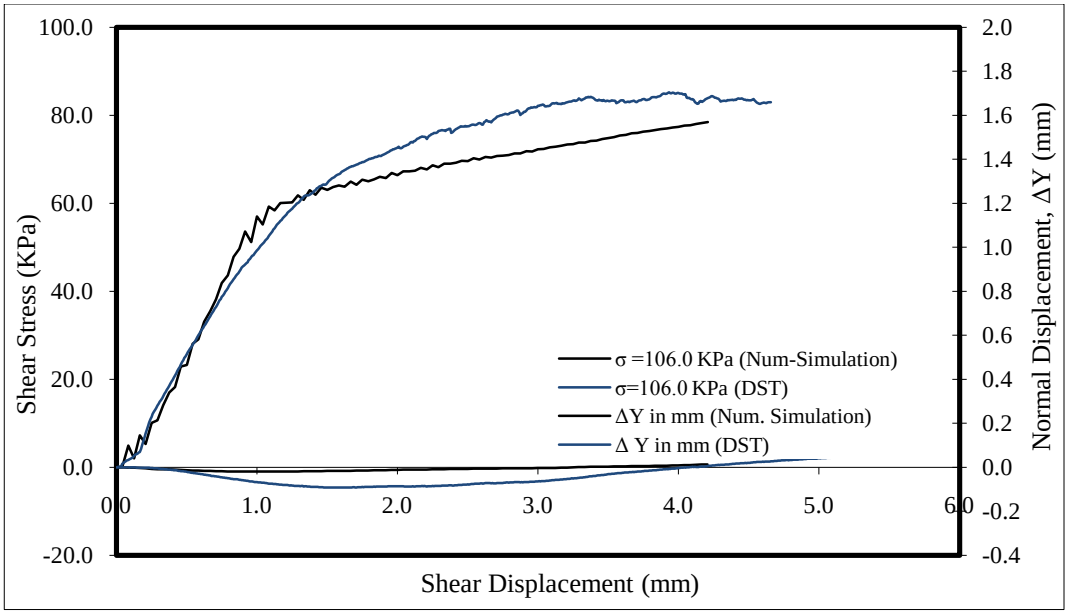


Figure 71. Results of the Numerical Simulation of the DST (E=8 MPa; ρ=18 kg/m$^3$; c= 2.0 kPa; ψ= 0 degrees; φ= 36.0 degrees; σ= 106 kPa)

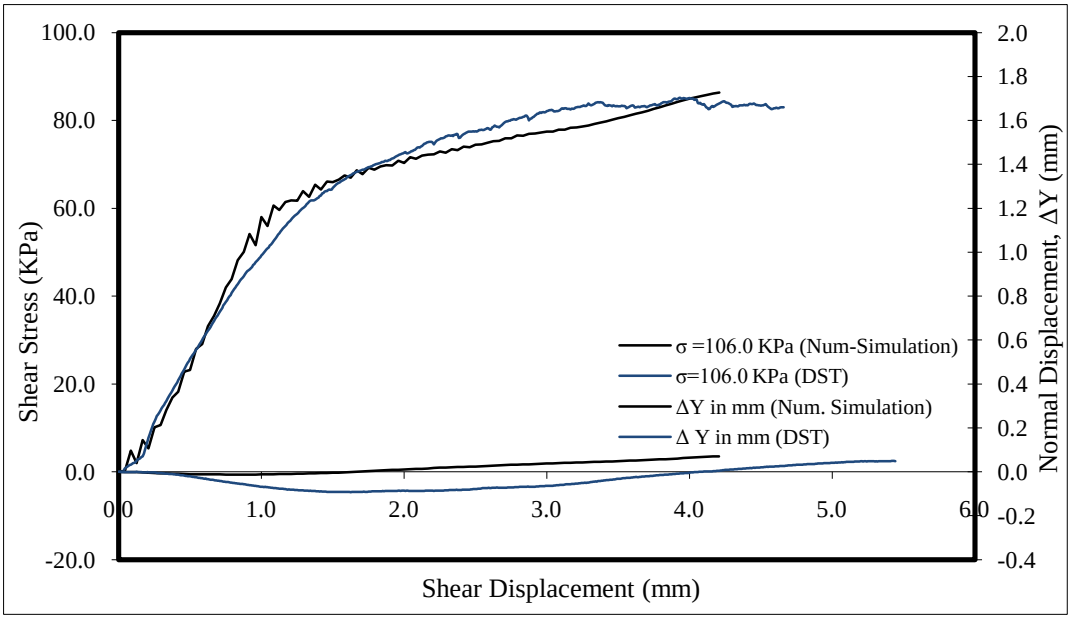


Figure 72. Results of the Numerical Simulation of the DST (E=8 MPa; ρ=18 kg/m$^3$; c= 2.0 kPa; ψ= 1.0 degrees; φ= 36.0 degrees; σ= 106 kPa )

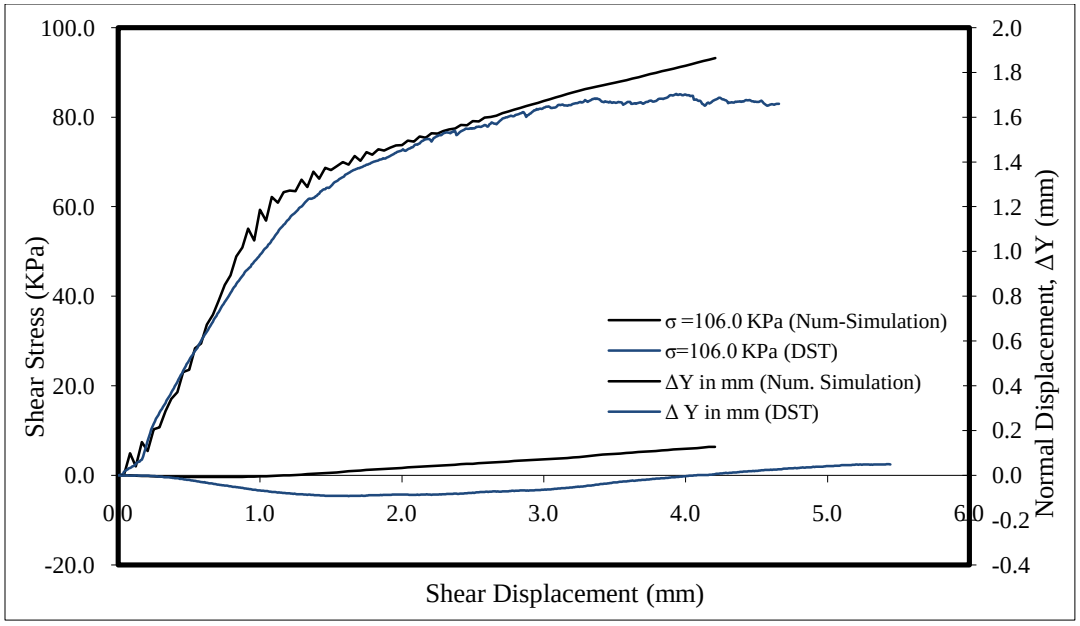


Figure 73. Results of the Numerical Simulation of the DST (E=8 MPa; ρ=18 kg/m$^3$; c= 2.0 kPa; ψ= 2.0 degrees; φ= 36.0 degrees; σ= 106 kPa)

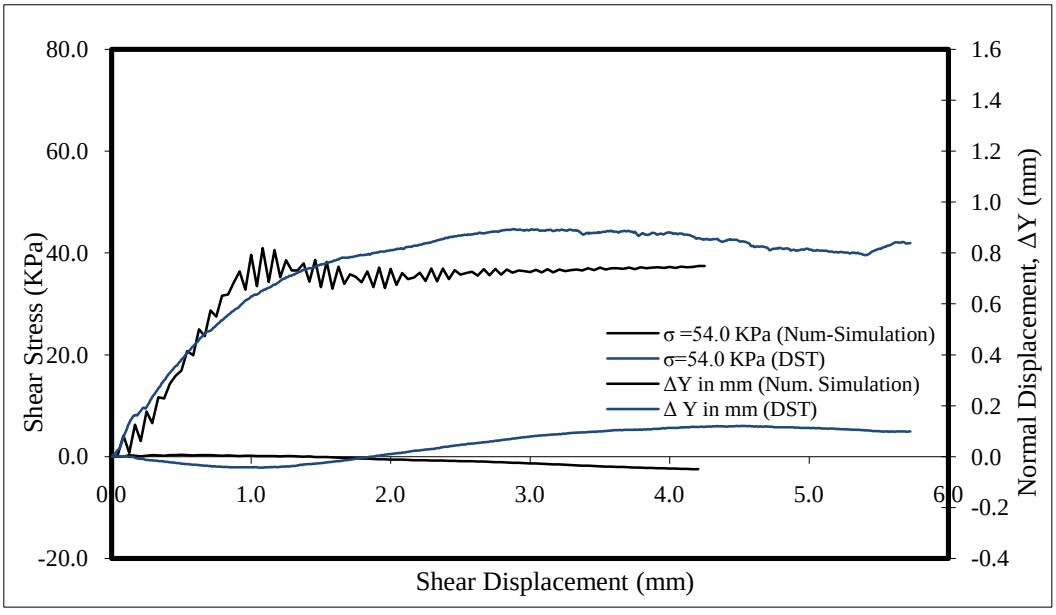


Figure 74. Results of the Numerical Simulation of the DST (E=8 MPa; ρ=17 kg/m$^3$; c= 5.0 kPa; ψ= -2.0 degrees; φ= 35.0 degrees; σ= 54.0 kPa)

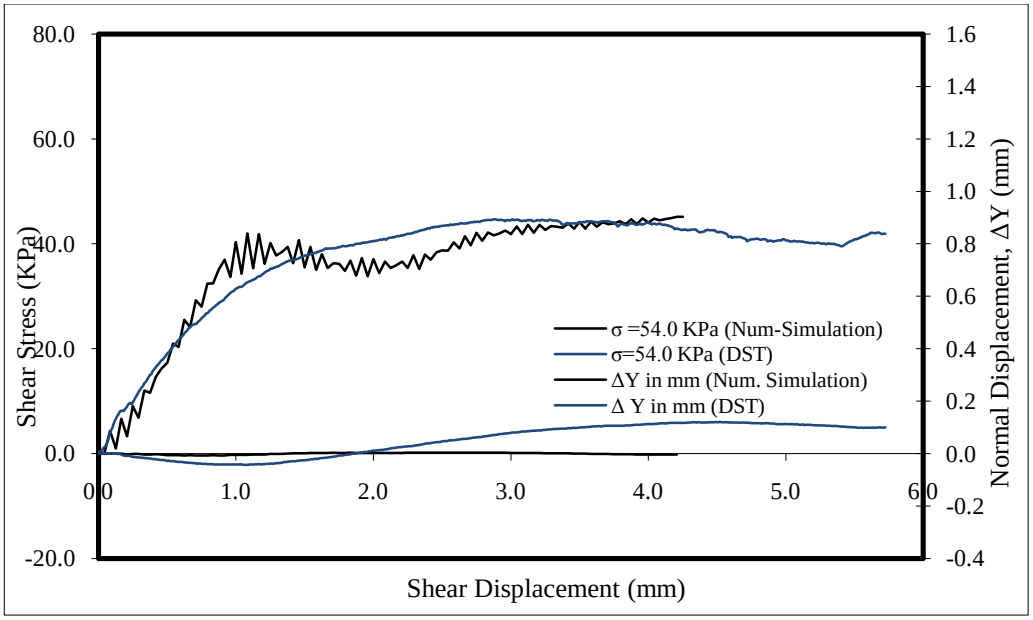


Figure 75. Results of the Numerical Simulation of the DST (E=8 MPa; ρ=17 kg/m$^3$; c= 5.0 kPa; ψ= -1.0 degrees; φ= 35.0 degrees; σ= 54.0 kPa)

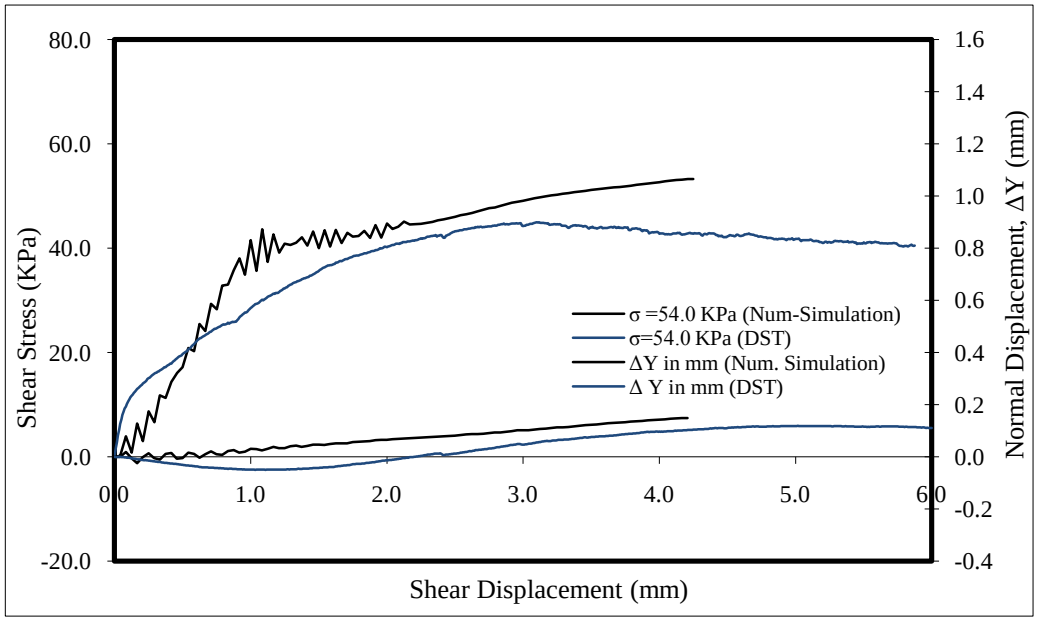


Figure 76. Results of the Numerical Simulation of the DST (E=8 MPa; ρ=17 kg/m$^3$; c= 5.0 kPa; ψ= 1.0 degrees; φ= 35.0 degrees; σ=54.0 kPa)

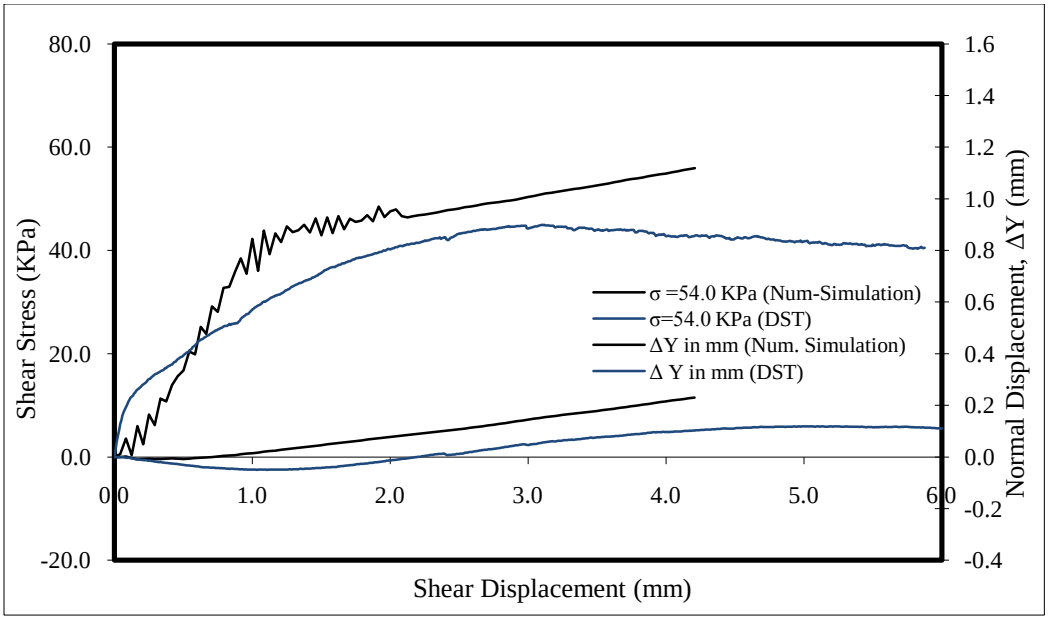


Figure 77. Results of the Numerical Simulation of the DST (E=8 MPa; ρ=17 kg/m$^3$; c= 5.0 kPa; ψ= 2.0 degrees; φ= 35.0 degrees; σ=54.0 kPa)

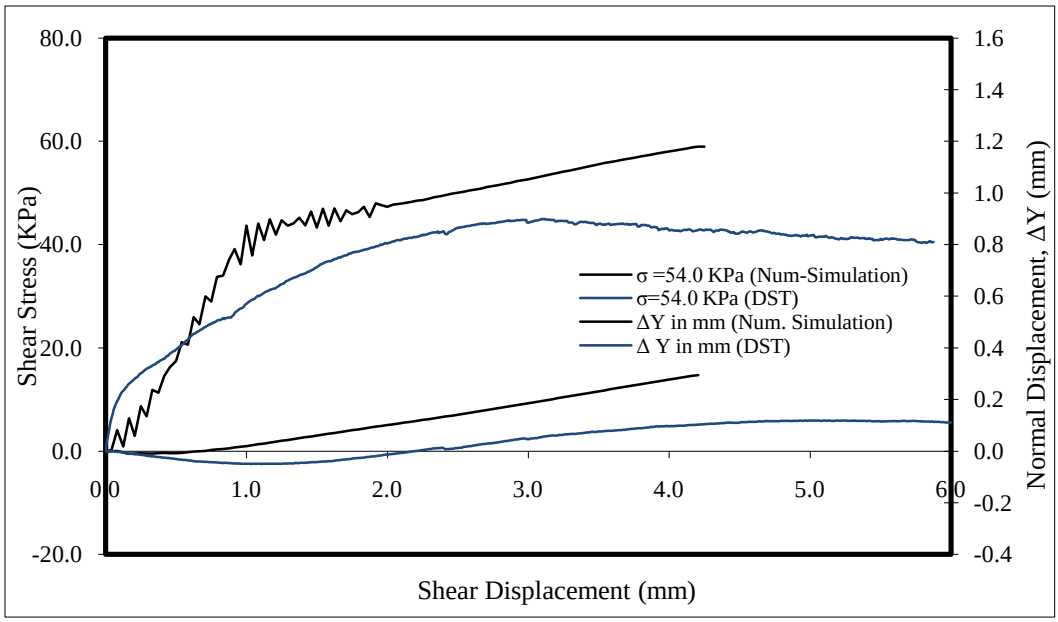


Figure 78. Results of the Numerical Simulation of the DST (E=8 MPa; ρ=17 kg/m$^3$; c= 5.0 kPa; ψ= 3.0 degrees; φ= 35.0 degrees; σ=54.0 kPa)

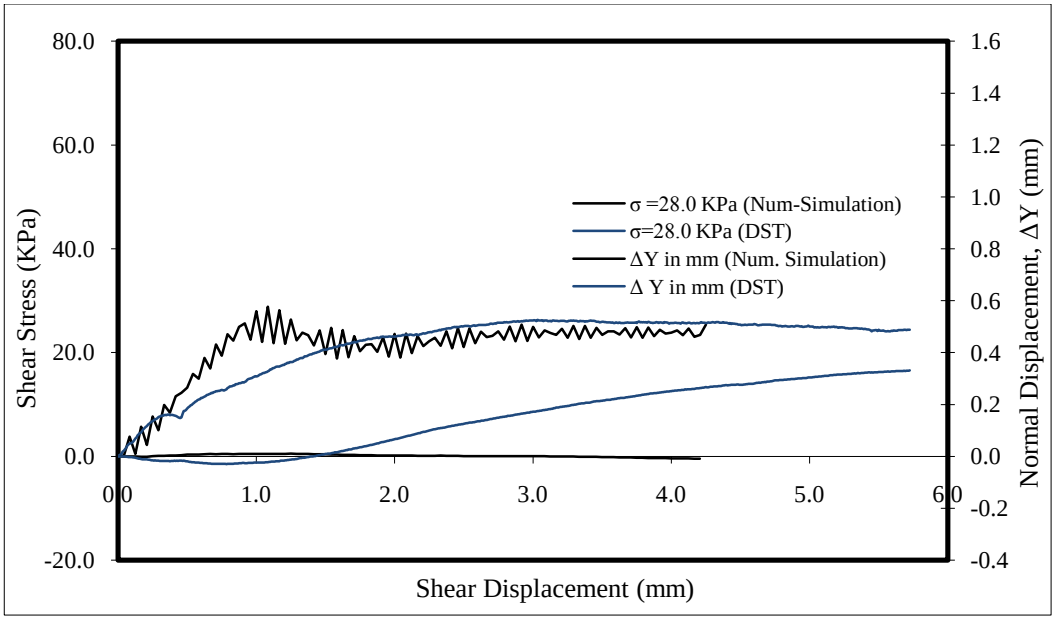


Figure 79. Results of the Numerical Simulation of the DST (E=8 MPa; ρ=17 kg/m$^3$; c= 5.0 kPa; ψ= -2.0 degrees; φ= 35.0 degrees; σ=28.0 kPa)

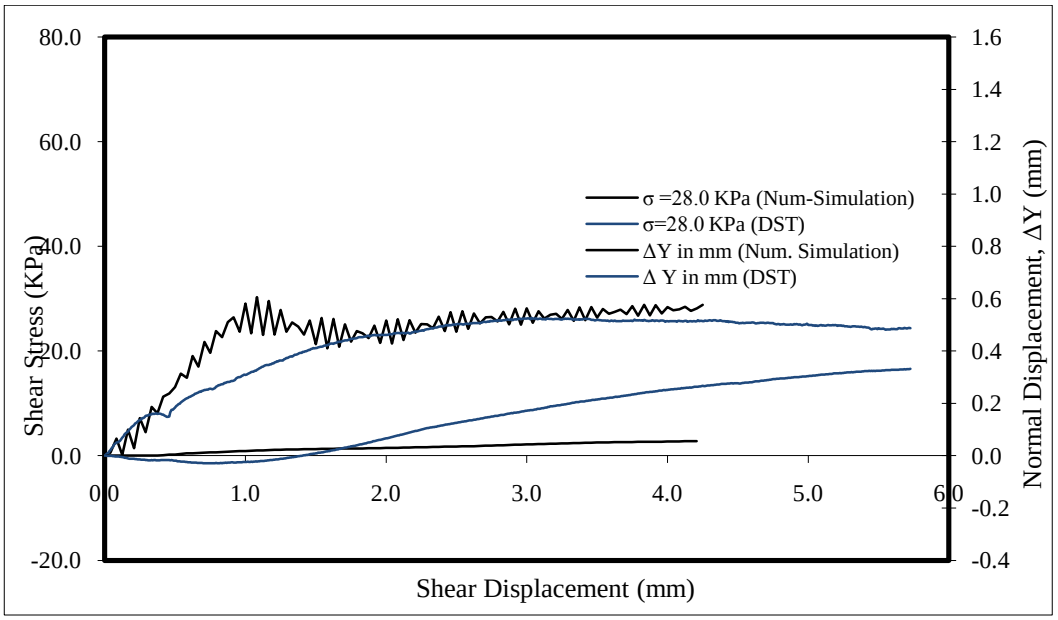


Figure 80. Results of the Numerical Simulation of the DST (E=8 MPa; ρ=17 kg/m$^3$; c= 5.0 kPa; ψ= -1.0 degrees; φ= 35.0 degrees; σ=28.0 kPa)

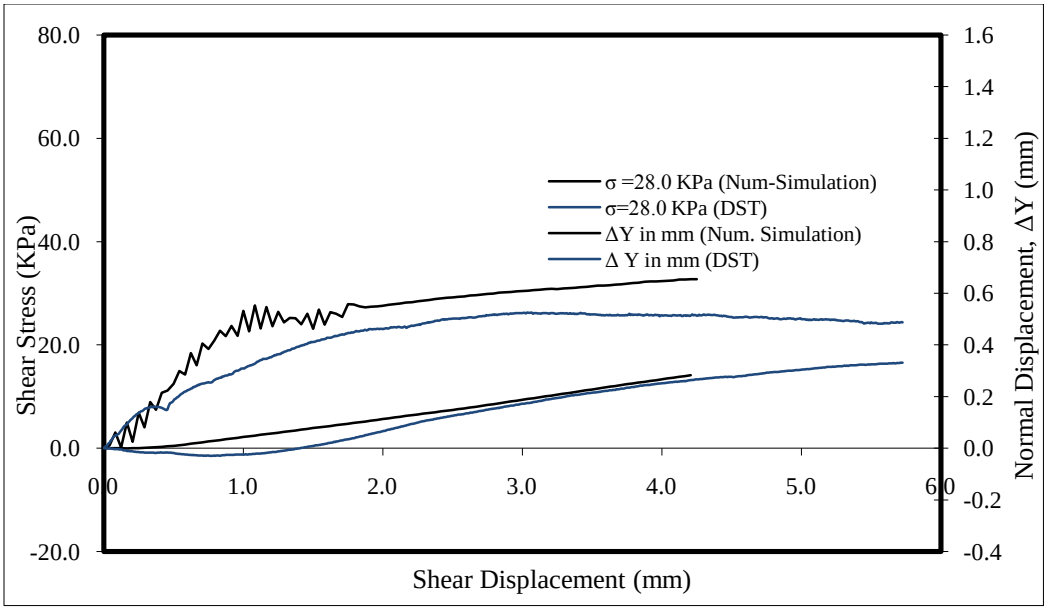


Figure 81. Results of the Numerical Simulation of the DST (E=8 MPa; ρ=17 kg/m$^3$; c= 5.0 kPa; ψ= 2.0 degrees; φ= 35.0 degrees; σ=28.0 kPa)

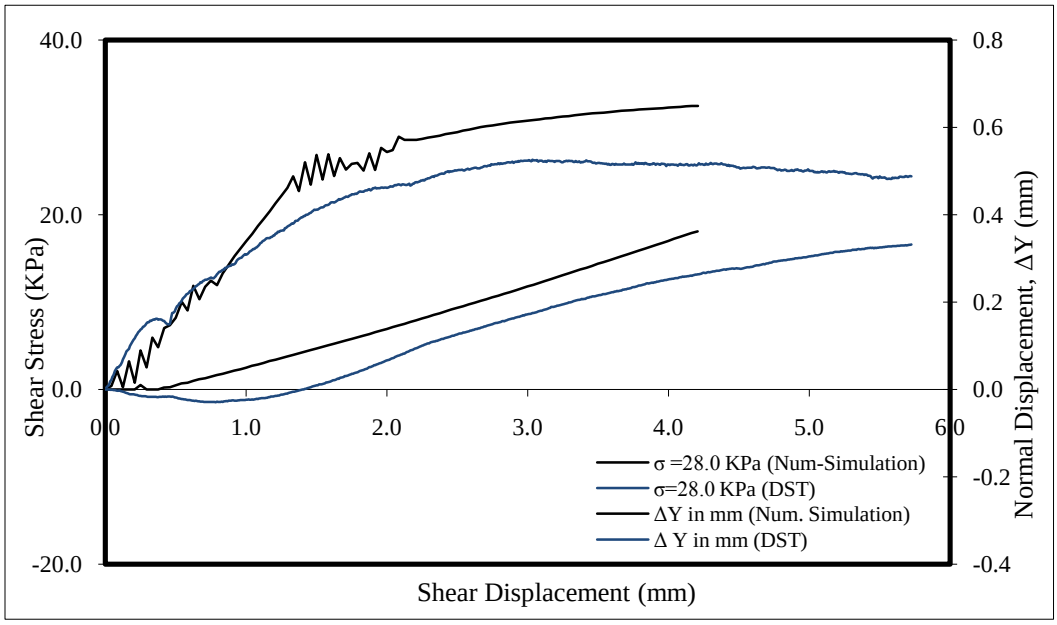


Figure 82. Results of the Numerical Simulation of the DST (E=8 MPa; ρ=17 kg/m$^3$; c= 5.0 kPa; ψ= 3.0 degrees; φ= 35.0 degrees; σ=28.0 kPa)

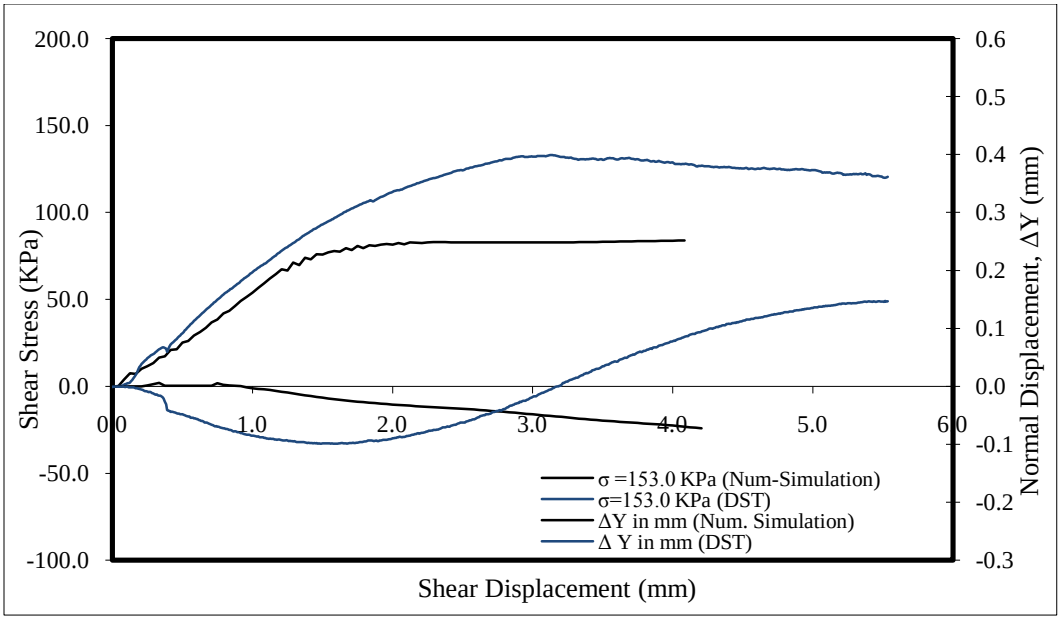


Figure 83. Results of the Numerical Simulation of the DST (E=8 MPa; ρ=17 kg/m$^3$; c= 7.0 kPa; ψ= -2.0 degrees; φ= 34.0 degrees; σ=153.0 kPa)

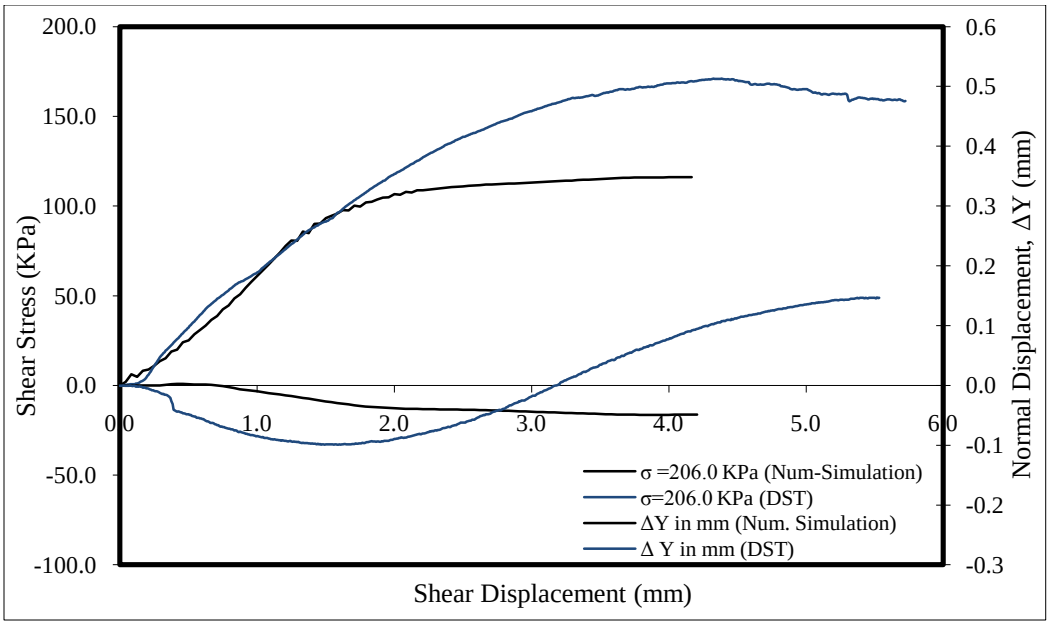


Figure 84. Results of the Numerical Simulation of the DST (E=8 MPa; ρ=17 kg/m$^3$; c= 7.0 kPa; ψ= -1.0 degrees; φ= 34.0 degrees; σ=153.0 kPa)

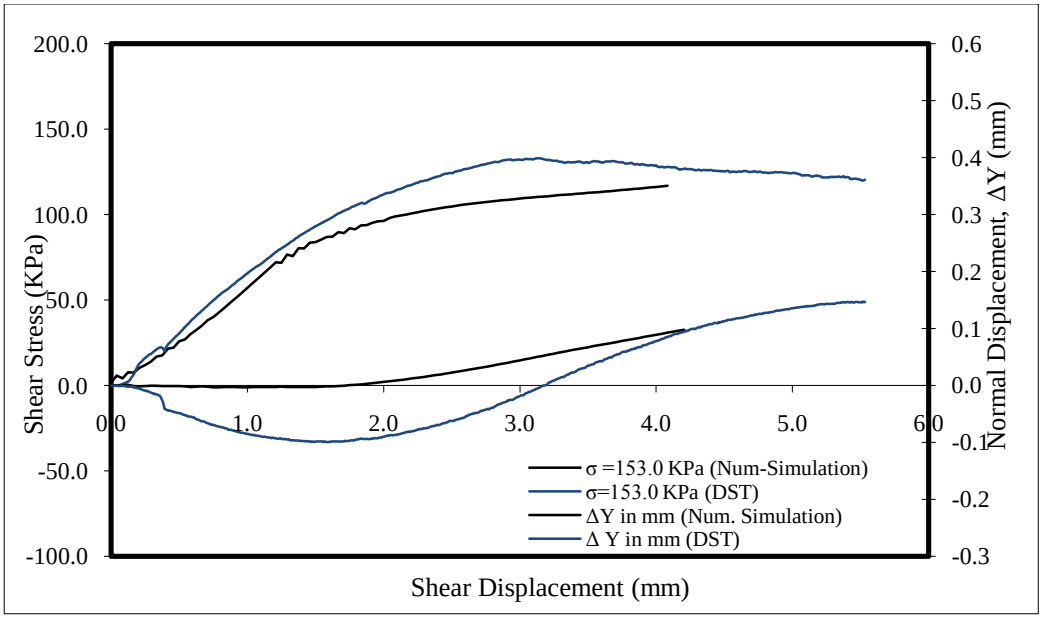


Figure 85. Results of the Numerical Simulation of the DST (E=8 MPa; ρ=17 kg/m$^3$; c= 7.0 kPa; ψ= 2.0 degrees; φ= 34.0 degrees; σ=153.0 kPa)

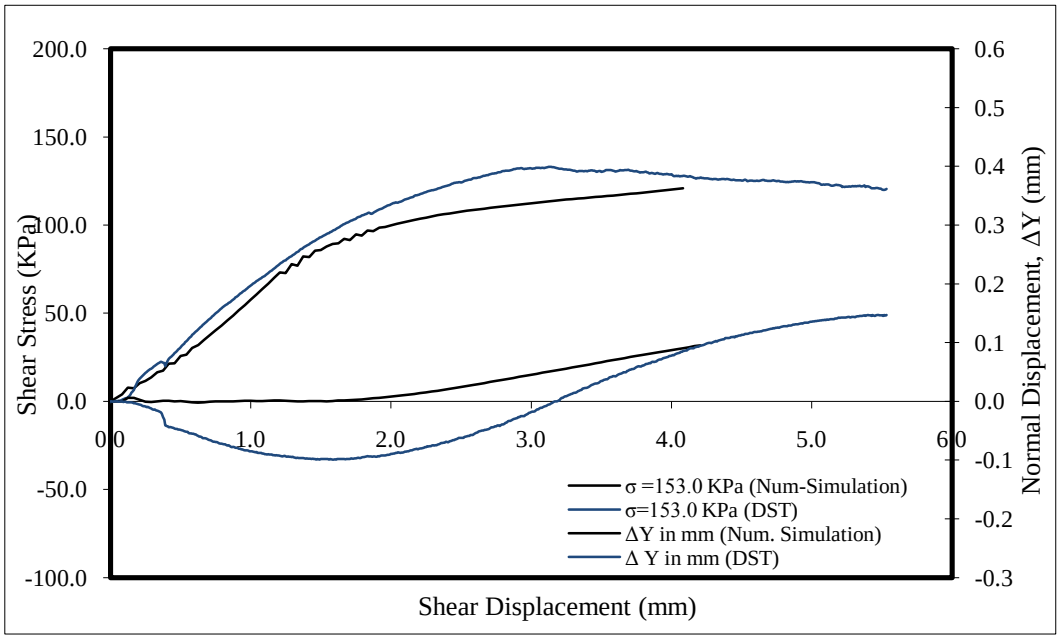


Figure 86. Results of the Numerical Simulation of the DST (E=8 MPa; ρ=17 kg/m$^3$; c= 10.0 kPa; ψ= 2.0 degrees; φ= 34.0 degrees; σ=153.0 kPa)

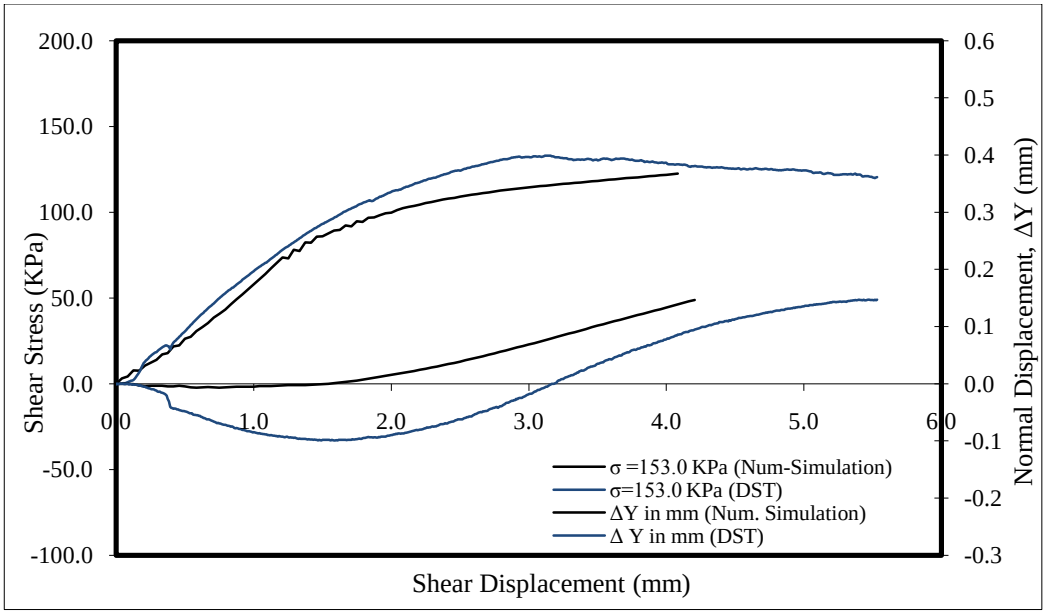


Figure 87. Results of the Numerical Simulation of the DST (E=8 MPa; ρ=17 kg/m$^3$; c= 7.0 kPa; ψ= 3.0 degrees; φ= 34.0 degrees; σ=153.0 kPa)

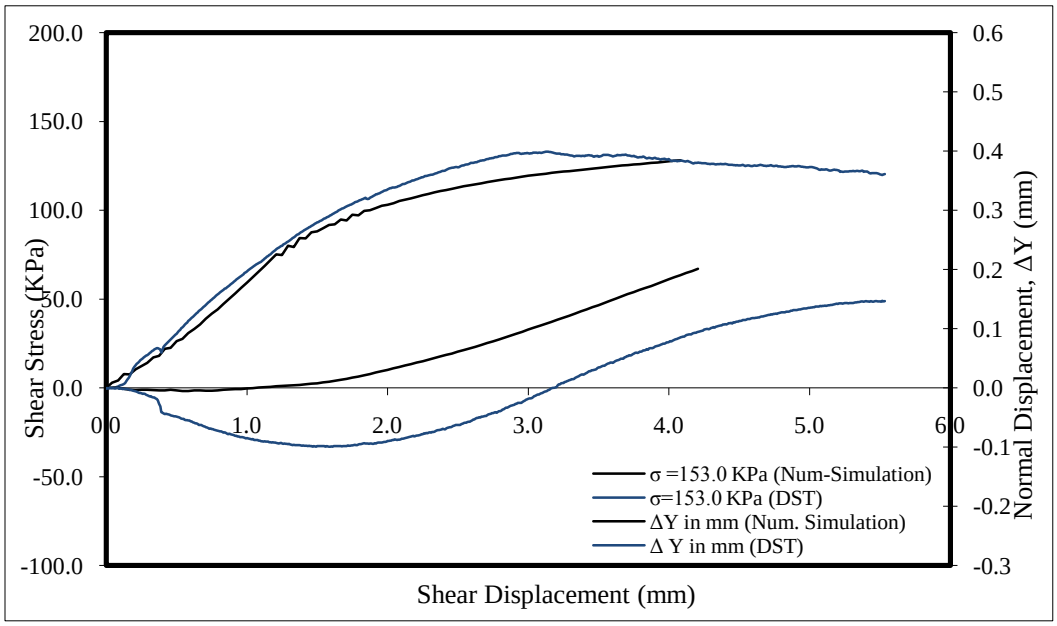


Figure 88. Results of the Numerical Simulation of the DST (E=8 MPa; ρ=17 kg/m$^3$; c= 7.0 kPa; ψ= 4.0 degrees; φ= 34.0 degrees; σ=153.0 kPa)

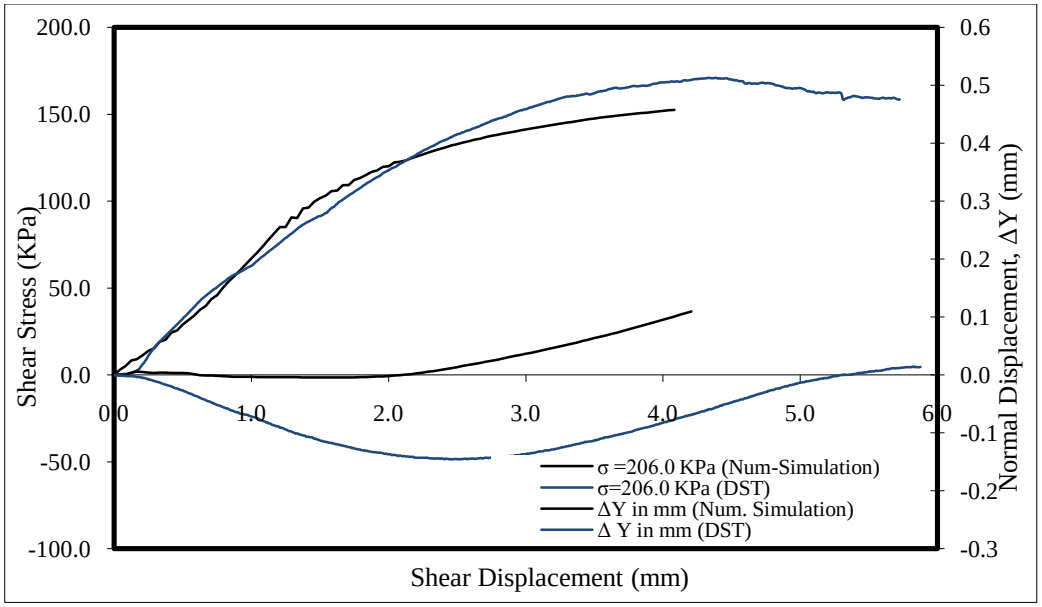


Figure 89. Results of the Numerical Simulation of the DST (E=8 MPa; ρ=17 kg/m$^3$; c= 7.0 kPa; ψ= 3.0 degrees; φ= 34.0 degrees; σ=206.0 kPa)

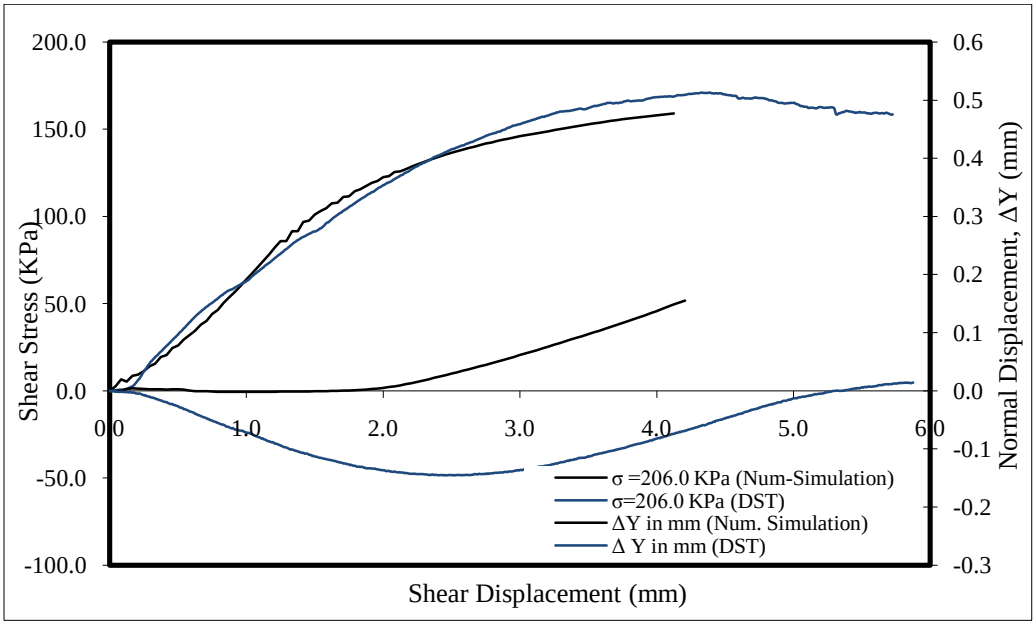


Figure 90 Results of the Numerical Simulation of the DST (E=8 MPa; ρ=17 kg/m$^3$; c= 7.0 kPa; ψ= 4.0 degrees; φ= 34.0 degrees; σ=206.0 kPa)

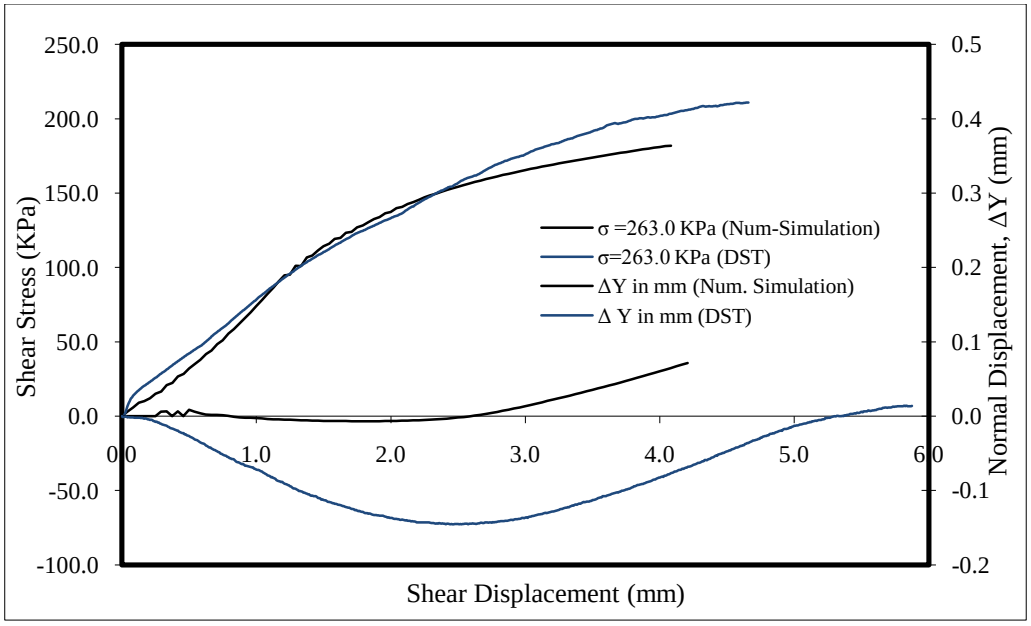


Figure 91. Results of the Numerical Simulation of the DST (E=8 MPa; ρ=17 kg/m$^3$; c= 7.0 kPa; ψ= 3.0 degrees; φ= 34.0 degrees; σ=263.0 kPa)

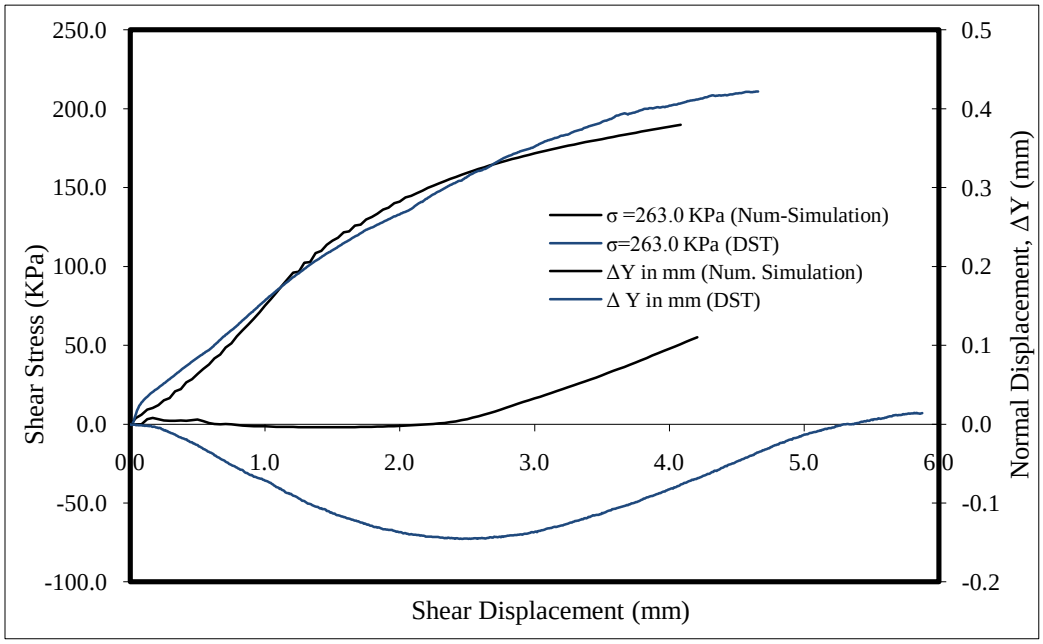


Figure 92. Results of the Numerical Simulation of the DST (E=8 MPa; ρ=17 kg/m$^3$; c=7.0 kPa; ψ= 4.0 degrees; φ= 34.0 degrees; σ=263.0 kPa)

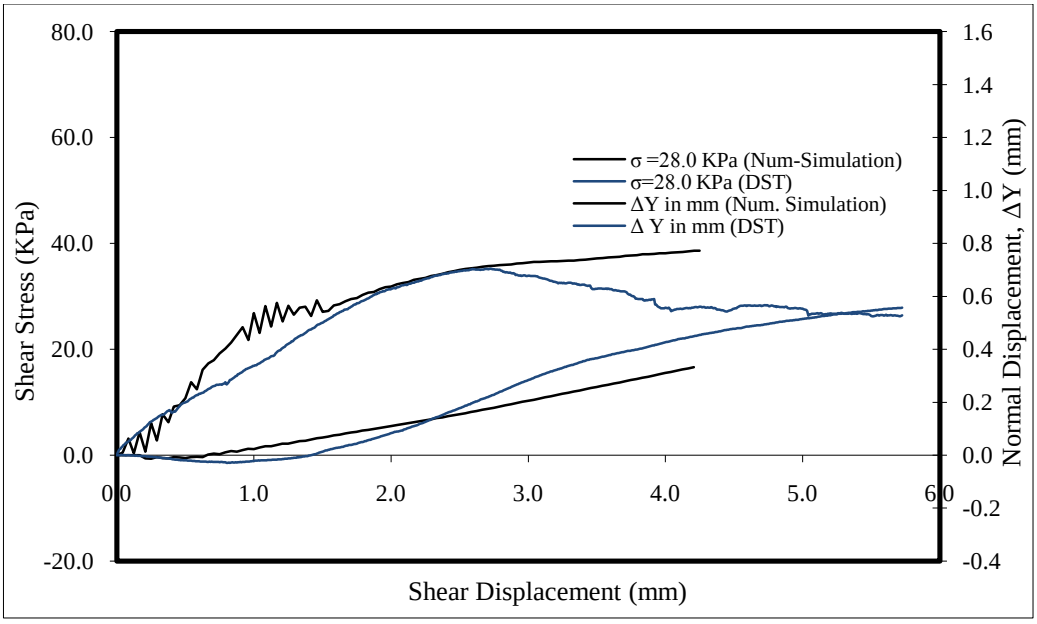


Figure 93. Results of the Numerical Simulation of the DST (E=8 MPa; ρ=18 kg/m$^3$; c=5.0 kPa; ψ= 3.0 degrees; φ= 42.0 degrees; σ=28.0 kPa)

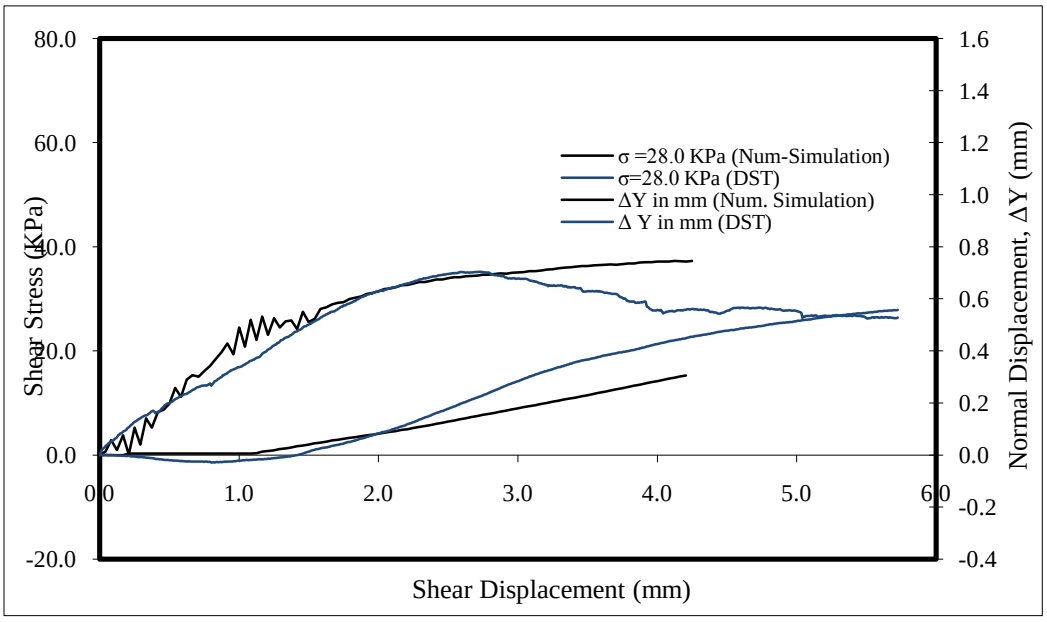


Figure 94. Results of the Numerical Simulation of the DST (E=8 MPa; ρ=18 kg/m$^3$; c=5.0 kPa; ψ= 3.0 degrees; φ= 41.0 degrees; σ=28.0 kPa)

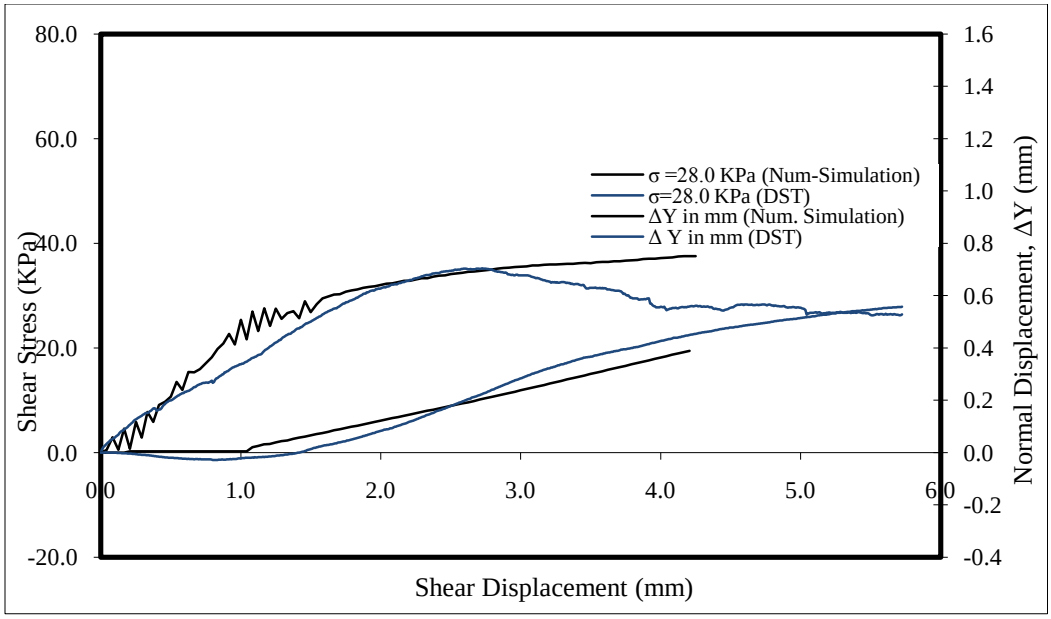


Figure 95. Results of the Numerical Simulation of the DST (E=8 MPa; ρ=18 kg/m$^3$; c=5.0 kPa; ψ= 4.0 degrees; φ= 40.0 degrees; σ=28.0 kPa)

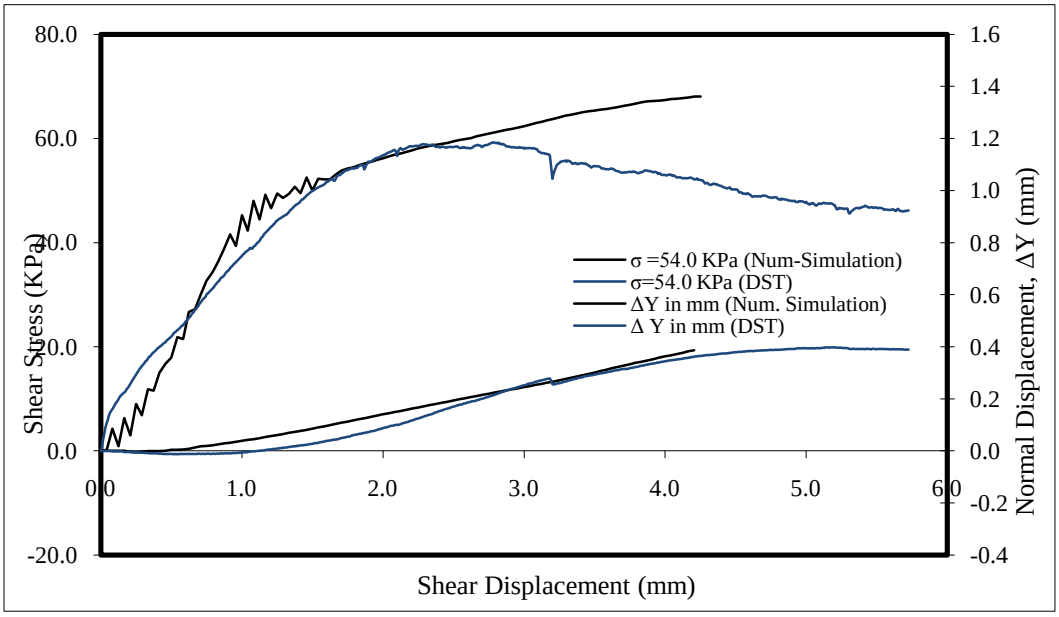


Figure 96. Results of the Numerical Simulation of the DST (E=8 MPa; ρ=18 kg/m$^3$; c=5.0 kPa; ψ= 4.0 degrees; φ= 42.0 degrees; σ=54.0 kPa)

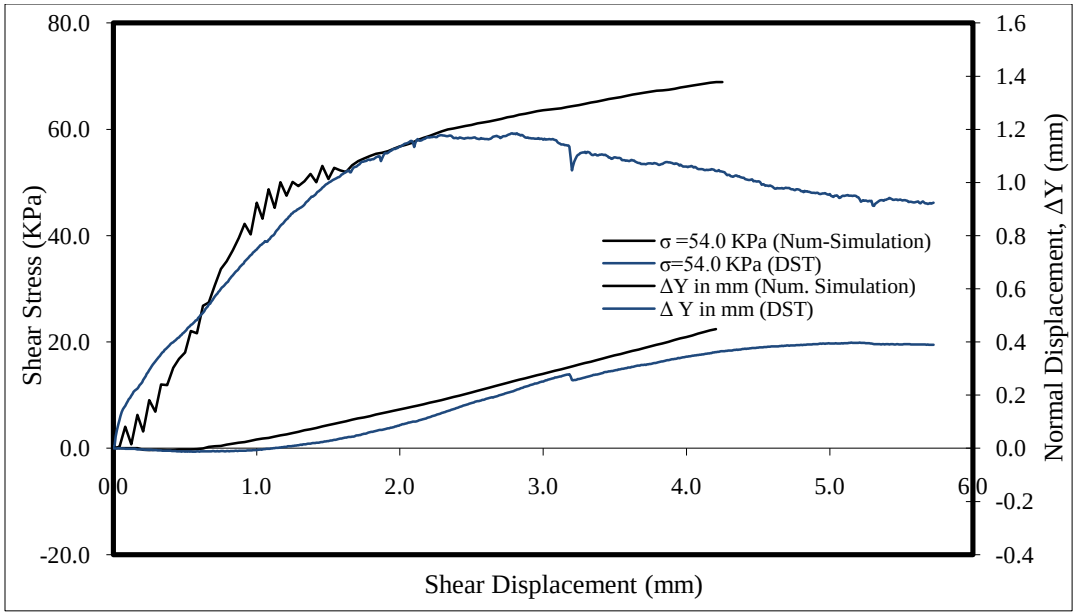


Figure 97. Results of the Numerical Simulation of the DST (E=8 MPa; ρ=18 kg/m$^3$; c=5.0 kPa; ψ= 5.0 degrees; φ= 42.0 degrees; σ=54.0 kPa)

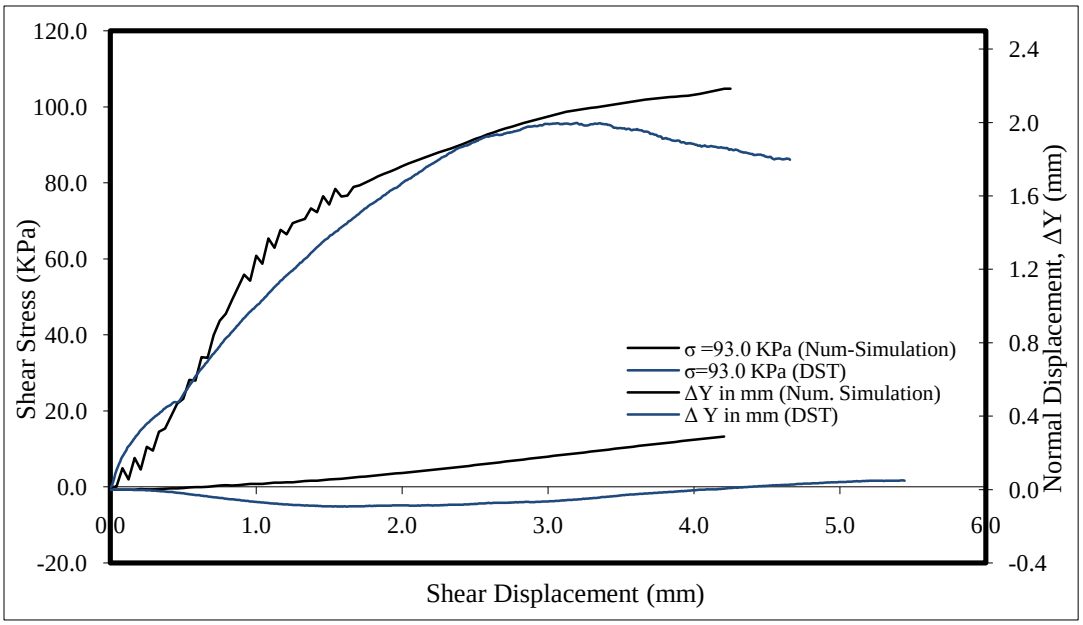


Figure 98. Results of the Numerical Simulation of the DST (E=8 MPa; ρ=18 kg/m$^3$; c=5.0 kPa; ψ= 4.0 degrees; φ= 42.0 degrees; σ=93.0 kPa).

Table 20. Comparison of the Results of the Friction Angle (φ) and the Dilation Angle (ψ) from the DST and the Numerical Simulation

| State Condition | Ave. Applied Normal Stress (kPa) | Direct Shear Test (DST) | | | | Numerical Simulation (FEM) | | |
|---|---|---|---|---|---|---|---|---|
| | | Tangent Dilation Angle, ψ (Degrees) | Secant Dilation [2]Angle, ψ (Degrees) | Angle Of Internal Friction (φ) | Cohesion Intercept, c (kPa) | Dilation Angle, ψ (Degrees) | Angle Of Internal Friction (φ) | Cohesion Intercept, c (kPa) |
| Loose | 28.0 | 7.25 | 2.96 | 36.66 | 6.42 | -1.0 | 36.0 | 2.0 |
| | 54.0 | 3.57 | 1.0 | | | -1.0 | 35.0 | 5.0 |
| | 106.0 | 3.4 | -1.03 | | | 1.0 | 36.0 | 2.0 |
| Loose | 28.0 | 5.7 | 3.0 | 36.01 | 5.53 | 2.0 | 35.0 | 5.0 |
| | 54.0 | 3.52 | 1.39 | | | 1.0 | 35.0 | 5.0 |
| | 106.0 | 3.43 | -0.60 | | | 2.0 | 36.0 | 2.0 |
| Loose | 154.0 | 5.50 | -0.4 | 35.39 | 24.22 | 4.0 | 34.0 | 7.0 |
| | 206.0 | 3.60 | -1.02 | | | 4.0 | 34.0 | 7.0 |
| | 263.110 | 3.70 | -0.50 | | | 4.0 | 34.0 | 7.0 |
| Loose | 160.0 | 3.15 | -0.70 | 34.82 | 24.26 | 3.0 | 34.0 | 7.0 |
| | 263.0 | 2.00 | -1.00 | | | 3.0 | 34.0 | 7.0 |
| Dense | 28.0 | 10.95 | 2.77 | 42.76 | 9.45 | 3.0 | 42.0 | 5.0 |
| | 54.0 | 10.46 | 4.00 | | | 5.0 | 42.0 | 5.0 |
| | 93.0 | 7.99 | 4.45 | | | 4.0 | 42.0 | 5.0 |

Table 20 presents the results of the parametric study conducted on the FEM model for the case of the loose-clean sand. The results of the frictional resistance, dilation angle, and cohesion intercep are compared with the laboratory values obtained from the DST. It can be seen that there is a general agreement on the results of the friction angle but not too much with the dilation angle.

The Modified Drucker-Prager Model allows the analysis of dilative and contractive behavior of granular materials. As explained before, the dilatancy effects are controlled by the angle of dilation ($\psi$) which is given as an input to the Soil Model. From the analysis of the results of the parametric study, two important aspects of the behavior of the clean sand can be withdrawn:

a) When the model is analyzed as a contractive material, the SS vs. RHD behave almost plastically once it reaches the yield point. Additional deformation occurs to the sample without an increase in the shear stress. This can be seen from the SS vs. RHD curves in which a negative dilation angle was used as an input to the program. However, softening can also occurs upon large negative value of angle of dilation; however, it is quite difficult to control.
b) When the model is analyzed as a dilative material, the Modified Drucker-Prager Model allows an increase in strength beyond the yield point. The material start to dilate after the yield surface has been reached and the strength of the material continued increasing as shearing occurs. The rate of increment, represented by the slope of the SS vs. RHD after yielding, will increase proportional to the dilation angle given to the model. As well as the contractive effect, this behavior can also be seen from the SS vs. RHD curves in which dilation angles are given as positives values.

Another important finding from the parametric study conducted in the FEM corresponds to the fact that the assumption made in section 4.8 is met. Recalling the fact

that the dilation angle can be computed from the results of the DST (by assuming that contraction or dilatancy occurs in a small band along the shearing zone,), this concept is validated by the results of the FEM since the result are comparables. Figure 99 shows the mesh of the soil material after shearing. It is noticed that the deformation of the material takes place in the shearing-band zone. The upper-half part of the material is deformed in the left side while the bottom-half part is deformed in the right side, as shown in figure 99. Beyond the shearing zone, the material behaves as a rigid block with zero shear deformation (concept of zero extension line).

Figures 100 through 104 show the stress contours in the horizontal direction ($x$), vertical direction ($z$) and the maximum shear stress. It is clear that the larger normal stresses are located in the upper-left part and in the lower-right part of the of the soil material. These results are in accordance with the deformed area of the soil elements. On the other hand, the largest shear stresses are located along the shearing band, having its maximum values at the center of the soil mass.

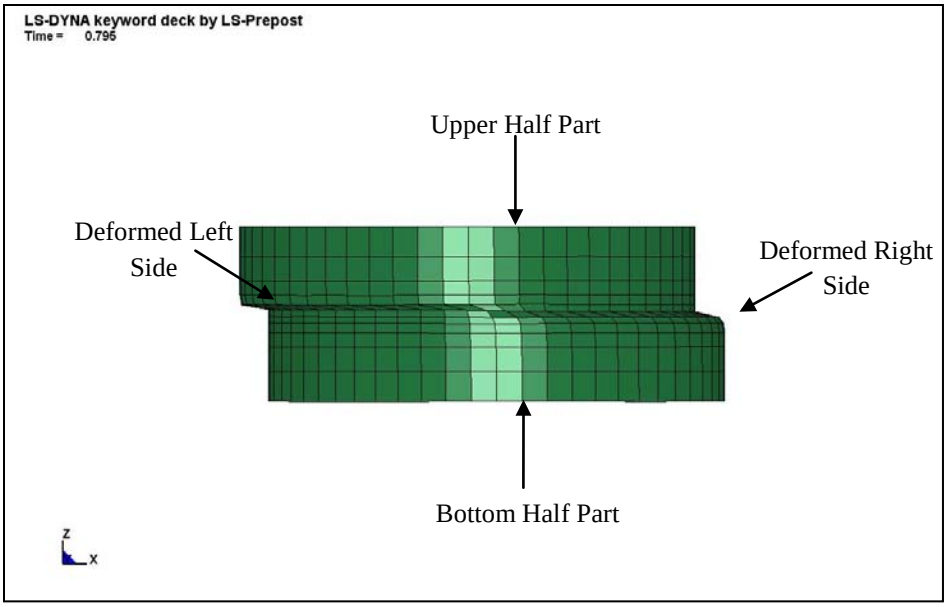


Figure 99. Deformed Mesh of the Idealized Soil Material after Shearing

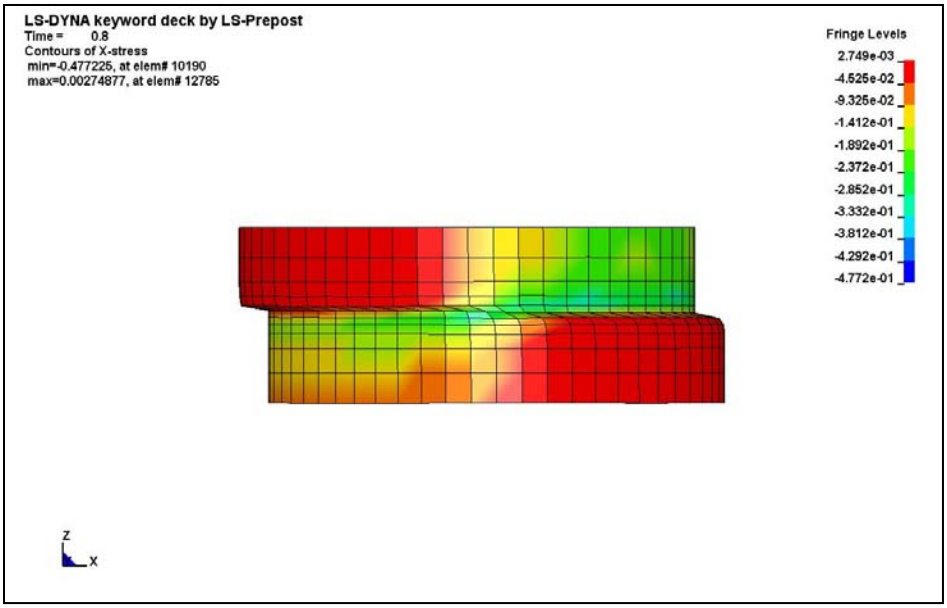


Figure 100. Stress Contours in the x-Direction of the Idealized Soil Material Model (Front-View)

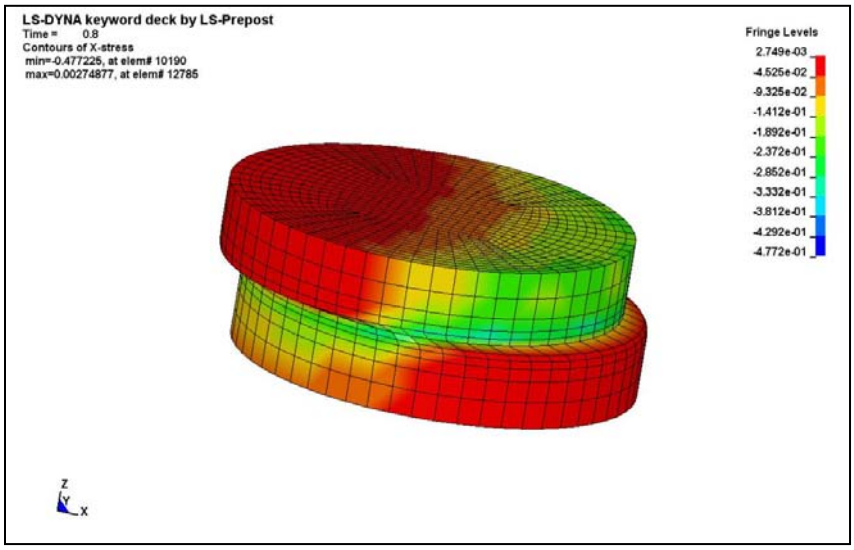


Figure 101. Stress Contours in the x-Direction of the Soil Material Model (3D-View)

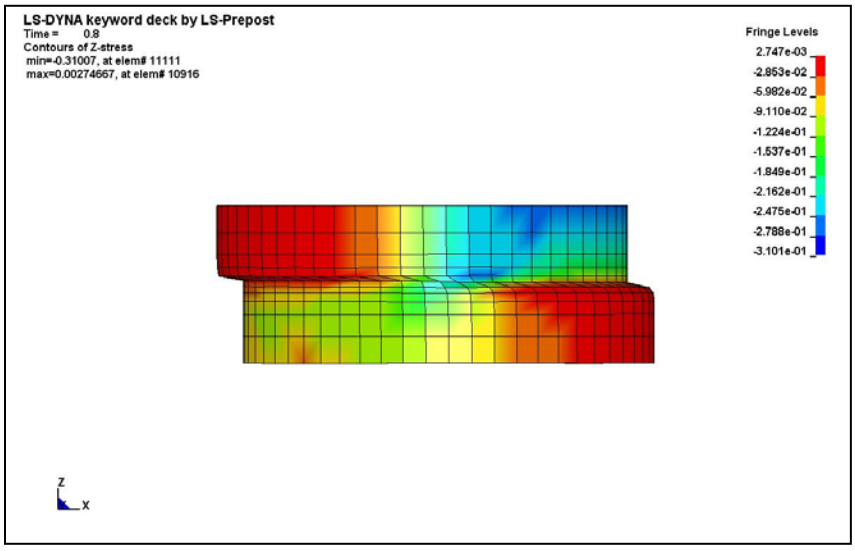


Figure 102. Stress Contours in the z-Direction of the Idealized Soil Material Model (Front-View)

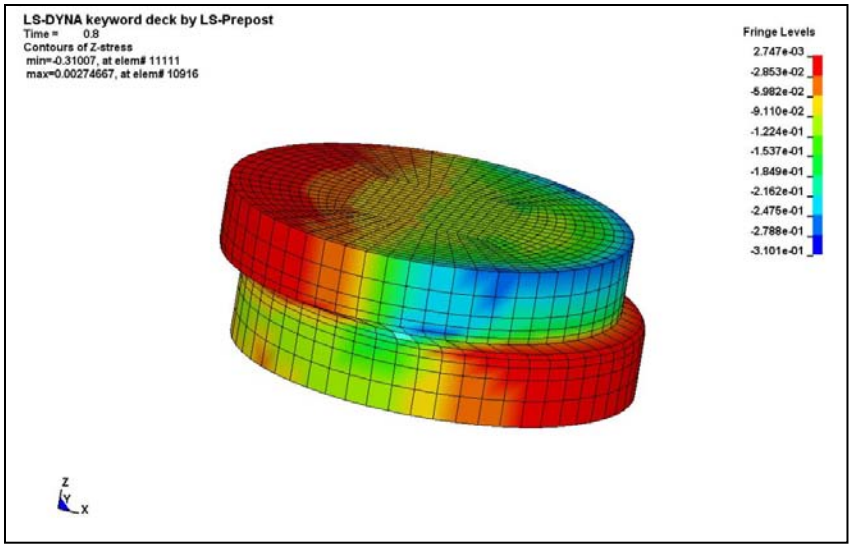


Figure 103. Stress Contours in the z-Direction of the Soil Material Model (3D-View)

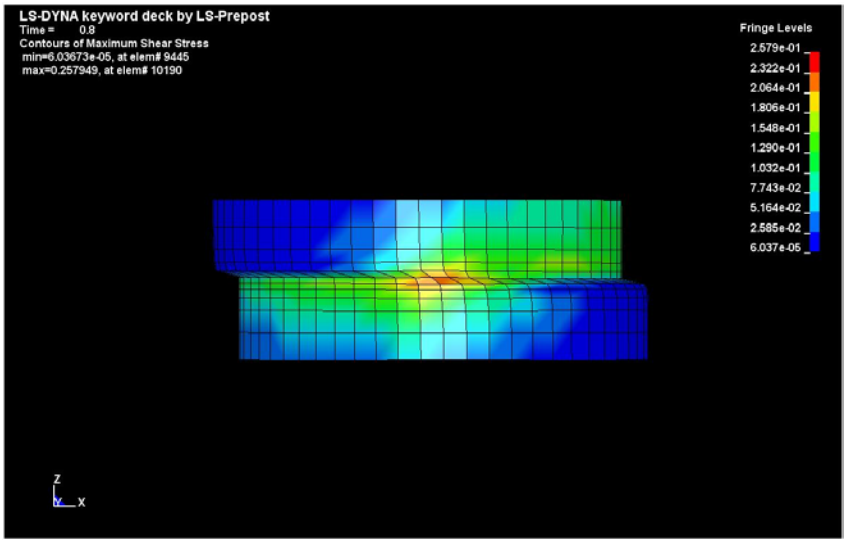


Figure 104. Maximum Shear Stress Contour of the Soil Material Model (Front-View)

# 11. CONCLUSIONS AND RECOMMENDATIONS

On the ground of the evaluations of the mechanical properties of the three soils tested, the conclusions and analysis of this study can be summarized as followed:

## 10.1 Finding for the Clean Sand

- Field tests, laboratory tests, and numerical simulations were conducted to the clean sand. The most important parameters determined from the laboratory tests and numerical simulation corresponds to the angle of internal friction (Φ) and the dilation angle of the material. It was found that the clean sand presents a very high frictional resistance even when it is tested in its loosest state.

- A simple procedure is described to compute the dilation angle of a material. Following the description presented by Bolton (1986), the contractive and dilative behavior of the material was computed by measuring the vertical displacement and the relative horizontal displacement from the Direct Shear Test (DST). Then, the angle of dilation was determined as either the ratio of $\Delta y$ to $\Delta x$ (secant angle of dilation) or the slope of the curve of $\Delta y$ vs. $\Delta x$ at the point of failure (tangent angle of dilation).

- The dilatancy effect of the clean sand was found to be significantly important depending on the strain condition it will be subjected to. In the case of the loose state, a low strain condition problem will be dominated by a negative dilation angle (contractive behavior); however, for large strain conditions problems, as well as a dense state, the behavior will be controlled by a positive dilation angle (dilation) depending on the confining pressure. This can be reflected in the recommendation tables for the clean sand.

- It is understandable that the clean sand presented a high shear resistance. The physical and mechanical properties determined by the other laboratory tests (grain size analysis, visual analysis, repose angle, etc.) support this computation. Therefore, recommendation of the friction angle and dilation angles are presented in tables 21 and 22. In addition, Figure 105 also present a empirical chart that correlate dilation angle with the shear strain. These recommendations are obtained from a combination of the result of the DST and the numerical simulation in LS-DYNA.

## 10.2 Finding for the Silty Sand

- A set of laboratory tests were carried out on the silty sand in order to determine its physical and mechanical properties. It was founded that the fine content on the sand was very high (about 50%) allowing compression to occur during the

application of normal stresses. The high fine content present in the sample also lead to a considerable liquid limit ($w_L$=21.14%) which can reduce the frictional resistance of the material under the presence of water.

- The high resistance of the silty sands obeys to its physical properties observed during the conduction of the laboratory tests including the DST. The average angle of frictional resistant estimated from the results of the DST was $\Phi=35^o$; however, the dilation angle, determined from the results of the vertical displacement vs. relative horizontal displacement plays an important role, leading to a lower mobilized frictional resistance. The results indicate that the contraction angle (secant dilation angle) can be close to -10.0 degrees under the application of confining pressure of 100 kPa under low strain condition. For the case of high strain condition problems the drop of frictional resistant of the silty sand can be considered to be -3.0.

Table 21. Recommended Values of the Angle of Internal Friction at the Critical State ($\varphi_{crit}$) and the Angle of Dilation ($\psi$) of the Clean Sand for Low Strain Conditions

| RECOMENDATION FOR CLEAN SAND IN A LOOSE STATE | | | | | RECOMENDATION FOR CLEAN SAND IN A DENSE STATE | | | |
|---|---|---|---|---|---|---|---|---|
| Stress Level (kPa) | [1]Critical Friction Angle in degrees ($\varphi$) | [2]Cohesion Intercept (kPa) | [1]Dilation Angle in degrees ($\psi$) | | Stress Level (kPa) | [1]Critical Friction Angle in degrees ($\varphi$) | [2]Cohesion Intercept (kPa) | [1] Dilation Angle in degrees ($\psi$) |
| 0-50 | 35.0 | 3.0 | -2.0 | | 0-50 | 35.0 | 4.0 | 7.0 |
| 50-100 | 35.0 | 3.0 | -3.0 | | 50-100 | 35.0 | 4.0 | 7.0 |
| 100-300 | 35.0 | 3.0 | -5.0 | | 100-300 | 35.0 | 4.0 | 5.0 |
| >300 | 35.0 | 3.0 | -6.0 | | >300 | 35.0 | 4.0 | 4.0 |

[1]The values of critical friction angle ($\varphi$) and dilation angle ($\psi$) recommended in these tables are based on the results of the secant dilation angle computed from the laboratory tests and the numerical simulation using a modified version of the Drucker-Prager Model.

[2]The values of cohesion intercept are input-recommended values for the Modified Drucker-Prager Model in LS-DYNA. If a hand computation, of any other analysis is being done using the above values, it is upon the designer's decision the use of the cohesion intercept.

Note: the recommended values of frictional resistance for the clean sand are based on considering a dry soil condition. As lubrication occurs, it is recommended to reduce the frictional resistance up to about 4.0 degrees. The reduction can be changed under engineering judgment of upon previous laboratory tests performed to the sample.

Table 22. Recommended Values of the Angle of Internal Friction at the Critical State ($\varphi_{crit}$) and the Angle of Dilation ($\psi$) of the Clean Sand for Large Strain Condition-Problems

| RECOMENDATION FOR CLEAN SAND IN A LOOSE STATE | | | | | RECOMENDATION FOR CLEAN SAND IN A DENSE STATE | | | |
|---|---|---|---|---|---|---|---|---|
| Stress Level (kPa) | [1]Critical Friction Angle in degrees ($\varphi$) | [2]Cohesion Intercept (kPa) | [1]Dilation Angle in degrees ($\psi$) | | Stress Level (kPa) | [1] Critical Friction Angle in degrees ($\varphi$) | [2]Cohesion Intercept (kPa) | [1] [3]Dilation Angle in degrees ($\psi$) |
| 0-50 | 35.0 | 3.0 | 2.0 | | 0-50 | 35.0 | 4.0 | 4.0 |
| 50-100 | 35.0 | 3.0 | 1.0 | | 50-100 | 35.0 | 4.0 | 3.0 |
| 100-300 | 35.0 | 3.0 | -1.0 | | 100-300 | 35.0 | 4.0 | 2.0 |
| >300 | 35.0 | 3.0 | -2.0 | | >300 | 35.0 | 4.0 | 1.0 |

[1]The values of critical friction angle ($\varphi$) and dilation angle ($\psi$) recommended in this tables are based on the results of the secant dilation angle computed from the laboratory tests and the numerical simulation using the Modified Drucker-Prager Model.

[2]The values of cohesion intercept are input-recommended values for the Modified Drucker-Prager Model in LS-DYNA. If a hand computation, of any other analysis is being done using the above values, it is upon the designer's decision the use of the cohesion intercept.

[3]The values of the dilation angle ($\psi$) are considered to be right after failure. If the sample reaches the critical state condition, then a dilation angle ($\psi$) is recommended.

Note: the recommended values of frictional resistance of the clean sand are based on considering a dry soil condition. As lubrication occurs, it is recommended to reduce the frictional resistance up to about 4.0 degrees. The reduction can be changed under engineering judgment of upon previous laboratory tests performed to the sample.

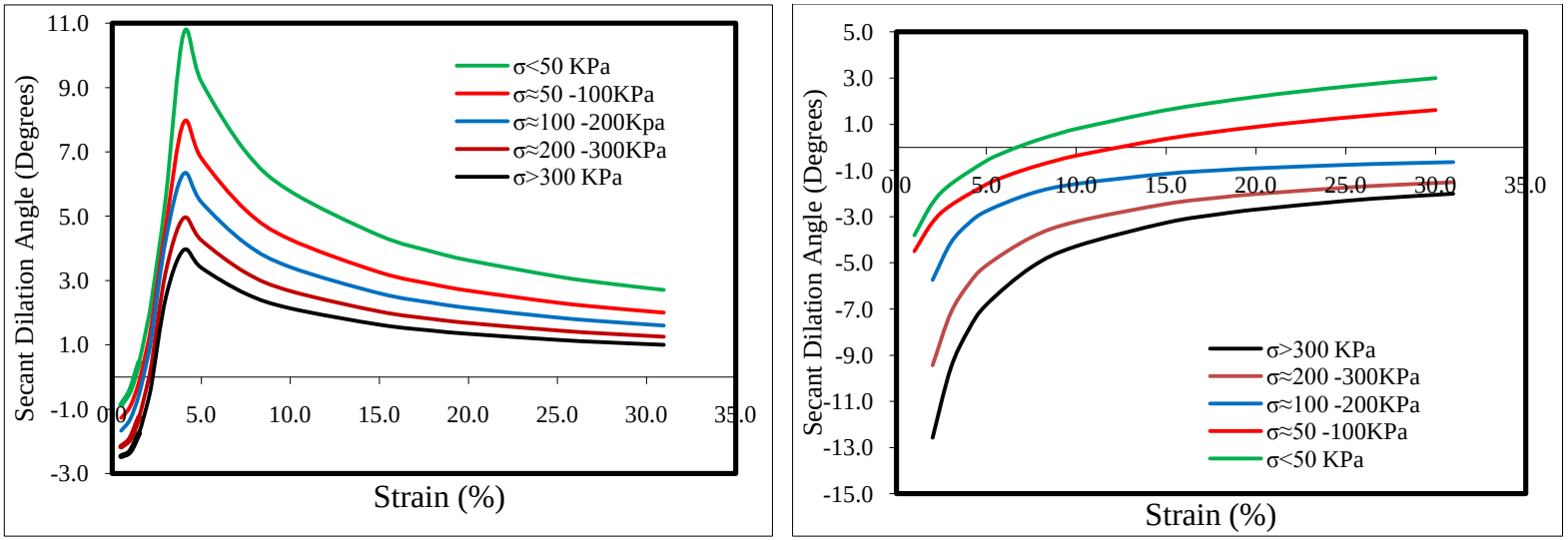


a) Clean Sand in a Dense State

b) Clean Sand in a Loose State

Figure 105. Empirical Charts for the Estimation of the Dilation Angle (ψ) of the Clean Sand based on the amount of Plastic Strain

Note: The above charts are based on the results of the tangent dilation angle of the laboratory Direct Shear Tests (DST) and the Numerical Simulation in LS-DYNA. It does not apply to a tangent dilation angle.

## 10.3 Finding for the Road Base

- Field and laboratory tests were performed on the road base. The grain size distribution of the road base prevented the application of the DST; therefore, the estimation of the frictional resistance of the material was computed by performing a confined triaxial compression test. The angle of internal friction was reported as $\Phi = 45^{o}$ with a cohesion of 83 kPa. Because the sample mold did not meet all the requirement dimension of the American Society for Testing and Materials, these values are reported as estimated values.

- A Soil Modulus versus Water Content Curve was developed using the Briaud Compaction Device, BCD. It was observed that the road base looses stiffness rapidly as the water content increases. The reason of this behavior obeys to high fine content present in the material, leading to a reduction of the suction and the cementitious properties of the material, which increases the soil modulus.

- It was also concluded that the road base has cementitious behavior. The material is composed of limestone (a sedimentary rock) whose bonding become stronger a function of t time. This phenomenon was observed on the field test (in-situ density and BCD Modulus) where the older placement of the material presented

a very high stiffness compare with the more recent placement.

## 10.4 Future Works

- Because of the costs and the importance of the full- scale tests conducted at the facility research area of Riverside Campus, it is strongly recommended the application of Full- Scale Direct Shear Test (FS-DST). The application of the FS-DST will allow testing aggregates which particles sizes prevent the computation of its mechanical properties using standard lab equipment. The Materials that should be included in these tests are the road base and the crashed rock. The clean sand can also be computed if time and budget allows.

# REFERENCES

*ABAQUS User's and Theory Manual version 6.7.* (2007). Hubbit, Karlson, and Sorensen, Pawtucketet, RI.

Bardet, J-P. (1997). *Experimental Soil Mechanic*, Prentice Hall, Upper Saddle River, N.J.

Bareither, C. (2006). "Shear strength of backfill sands in Wisconsin." MS thesis, Dept. of Geological Engineering, Univ. of Wisconsin-Madison, Madison, Wis.

Bareither, C., Edil, T., Bensen, C. & Mickelson, D. (2008a). "Comparison of shear strength of sand backfills in small-scale and large-scale direct shear test." *Can. Geotech. J.*, 45, 1224-1256.

Bareither, C., Edil, T., Bensen, C. & Mickelson, D. (2008b). "Geological and physical factors affecting the friction angle compacted sands." *J. Geotech. Geoenviron. Eng.*, 134(10), 1476-1489.

Bolton, M. (1986). "The strength and dilatancy of sands." *Geotech.*,36 (1), 65-78.

Briaud, J. L. (2002). "Introduction to soil moduli." *Geotech. News*, June 2001, BiTech Publishers, B.C., Canada.

Briaud, J.- L., Rhee, K, & Saez, D. (2009). "The BCD: A new instrument for compaction control." *NCHRP-IDEA Project 118,* National Research Council, Washington D.C.

Craig, R. F. (2004). *Craig's Soils Mechanics,* Chapman & Hall, New York.

Dass, B. (2006). *Principles of Geotechnical Engineering*, Thompson Learning, Toronto.

Desai, C.S. & Siriwardane, H.J. (1984). *Constitutive Laws for Engineering Materials: With Emphasis on Geologic Materials,* Prentice Hall, Englewood Cliffs, N.J.

Drucker, D. C. & Prager, W. (1951). "Soil mechanics and plastic analysis or limit design." <https://ceprofs.civil.tamu.edu/dmurff/CE651ClassNotes/Plasticity/DruckPragerPpr.pdf>

Fakhimi, A. & Hosseinpour, H. (2008). "The role of oversize particles on the shear strength and deformational behavior of rock pile material." *Proc., 42th US American Rock Mechanic Association, San Francisco,* CA. June29-July 2.

Fossum, A.F. & Brannon A.M. (2004). "The sandia geomodel: theory and user's guide.".*Prepared by the Sandia National Laboratories, Albuquerque, New Mexico, 87185 and Livermore, California 94550 for the United States Department of Energy under Contract DE-AC04-94AL85000.*

Holtz, R. & Kovacs, W. (1981). *An Introduction to Geotechnical Engineering,* Prentice Hall, Upper Saddle River, N.J.

Lings, M. & Dietz, M. (2004). "An improved direct shear apparatus." *Geotech.*, 54 (4), 245-256.

*LS-DYNA Theoretical Manual Version 940 (1998).* Livermore Software Technology Corporation, Livermore, CA.

*LS-DYNA Keyword User's Manual Version 970 (2007).* Livermore Software Technology Corporation, Livermore, CA.

Mitchell, J. & Soga, K. (2005). *Fundamental of Soil Behavior,* Wiley & Sons, Hoboken, N.J.

Murff, J. (2008). "CVEN-651: Geomechanics' class notes." *Texas A&M University*, College Station.

Rowe, P. (1962). "Stress-dilatancy relation for static equilibrium of assembly of particles in contact." *Royal Society-Proc. Serie,* 269(1339), 500, 527.

Schwer, L. (2010). "Computational constitutive models." Online *Conference on Modeling and Simulation with LS-DYNA*, February 11-12, 2010.

Wood, D. (1990). *Soil Behavior and Critical State Soil Mechanics*, Press Sindicate of the University of Cambridge, New York.

Wu, P., Matsushima, K. & Tatsuoka, F. (2008). "Effects of specimen size and some other factors on the shear strength and deformation of granular soils in direct shear test." *Geotech. Test. J.,* 31 (1), 1-20.

# APPENDIX A-RESULTS OF THE DIRECT SHEAR TEST FOR THE CLEAN SAND

## A.1 Small Scale Direct Shear Test for the Clean Sand (SS-DST)

### A.1.1 Introduction

The direct shear test (DST) using a pair of rigid shear boxes has been and is widely employed in Geotechnical Engineering practice and research to evaluate the shear strength as well as the shear stress, shear displacement and volume change relations of geomaterial (Wu et al. 2008).

Most of tests are conducted following the procedures describes in AASHTO T 236 (Standard Method of Test for Direct Shear Test of Soil Under Consolidated Drained Conditions) or ASTM D 3080 (Standard Method of Test for Direct Shear Test of Soil Under Consolidated Drained Conditions) in a small-scale direct shear box that is square (64-mm x 64-mm) or circular (62-mm diameter). The dimensional criterion establishes in AASHTO T 236 or ASTM D 3080 indicates that the maximum particle for the tests conducted in shear boxes of this size is approximately 5 mm. Therefore, when granular backfill material contain gravel (e.g. particles sizes greater than 4.8 mm), the gravel size particles must be scalped if testing is conducted on small scale direct shear test box.

The popularity of the Direct Shear Test (DST) for testing the frictional resistance of granular materials used as a backfill obeys to its relatively simple apparatus test operation. It also represents a general mode of failure and the interpretation of its results is relatively straightforward. However, it also account with the following drawbacks (Wu et al. 2008):

- Local strain in the shear zone cannot be accurately evaluated.
- The stress and strain condition in the shear zone becomes non-uniform.
- In the Direct Shear Test (DST) the friction angle is defined in term of the stresses at the horizontal plane, which no necessarily is the plane of maximum stresses. Therefore, it is not possible to evaluate the mobilized friction angle in the shear zone.

### A.1.2 Background

The specification ASTM D 3080 and AASHTO T 236 stipulate that square or circular boxes may be used to conduct the tests. Both test methods require that the with or diameter must be at least 50 mm and specimen thickness at least 13 mm while maintaining a minimum specimen with or diameter to thickness ratio of 2:1. Adjusting the shear box dimensions to meet the criterion in ASTM D 3080 and AASHTO T 236 is important to test the shear strength behavior of the material and not to the individual particles.

The influence of the specimen size and the scale factor of the Direct Shear Test (DST) have been studied by several researchers. Cerator & Lutenegger (2006) conducted Direct Shear Test (DST) using three different square shear boxes: 60 x 60 mm, 101.6 x 101.6 mm, and 304.8 x 304.8 mm with a ratio of width (W) to specimen thickness (W/H) of 0.44, 0.40, and 0.58 respectively. They reported a decrease on friction angle with increasing shear box dimensions. However, they also cited a work conducted by

Palmira and Milligan (1989) who performed DST in a small, medium, and large shear boxes finding that there were not significant differences on the resulting friction angles.

They concluded that for dense sand, the friction angle measured by the direct shear testing can depend on specimen size and recommend ratio of shear box width to maximum particle size of 50 or beyond in order to minimize the size effect of the friction angle of the sand.

A.2 Results of the Direct Shear Test Conducted of the Clean Sand (DST)

A total of 10 Direct Shear Tests (DST) were conducted on the clean sand. Six tests were performed on a loose state, 1 on the dense state, and three tests on the compacted state (using different water content). All the samples met the requirement of the ASTM D 3080 regarding the ratio of with/maximum particle size ($W/D_{max}>10.0$) and height/maximum particle size ($H/D_{max}>6.0$). The ratio of H/W was approximately 0.44, which did not met the requirement establish by the designation ASTM D 3080 of 0.50. However, it has been reported that this ratio will not affect the result of the frictional resistance when the ratio of the $W/D_{50}$ is between 50 and 300. In this case, the $D_{50}$ for the wash sand is 0.52, resulting in a ratio of $W/D_{50}$ of 121. Also, a DST was conducted using the required ratio of diameter to high of 0.5, resulting in no differences on the shear resistance of the clean sand.

Table A.1 to A.10 presents all the results of the DST conducted on the clean sand. Also Figures A.1 to A.30 shows the Stress – Deformation curve, the Mohr Coulomb Enveloped, and the Dilation Enveloped of the all the tests.

Table A.1: Direct Shear Test Result for the Clean Sand in the Loose State (Test 1).

| Point No. | σ (kPa) | τ (kPa) | Sample Height (mm) | Water Content, (%) |
|---|---|---|---|---|
| 1 | 21.415 | 21.17 | 27.00 | 0.23 |
| 2 | 41.101 | 35.30 | 27.00 | 0.28 |
| 3 | 93.482 | 73.50 | 27.00 | 0.26 |

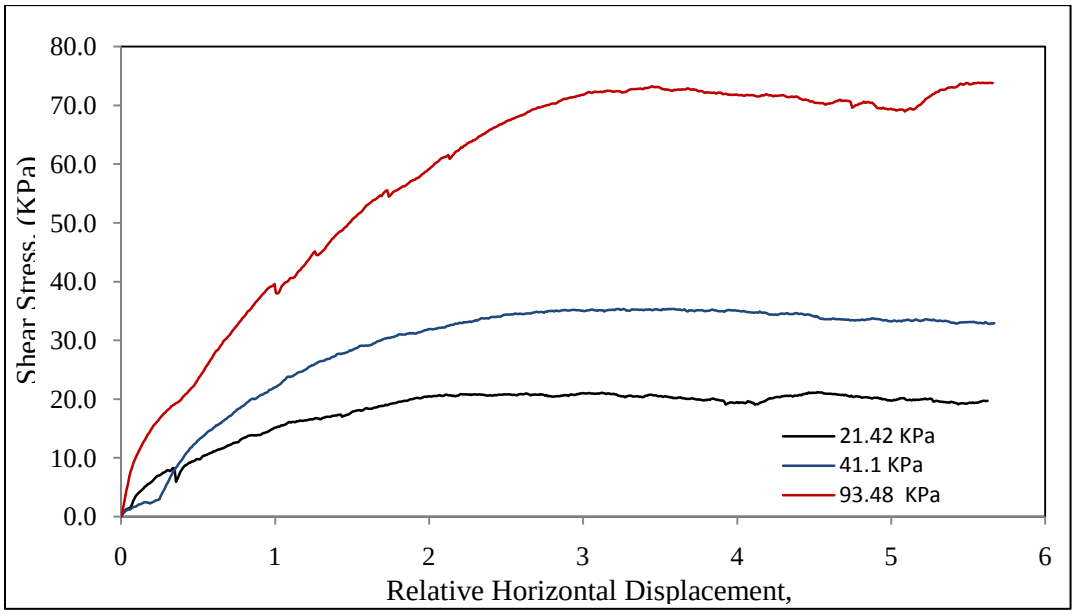


Figure A.1: Stress-Deformation Curve for the Loose-Clean Sand (Test 1).

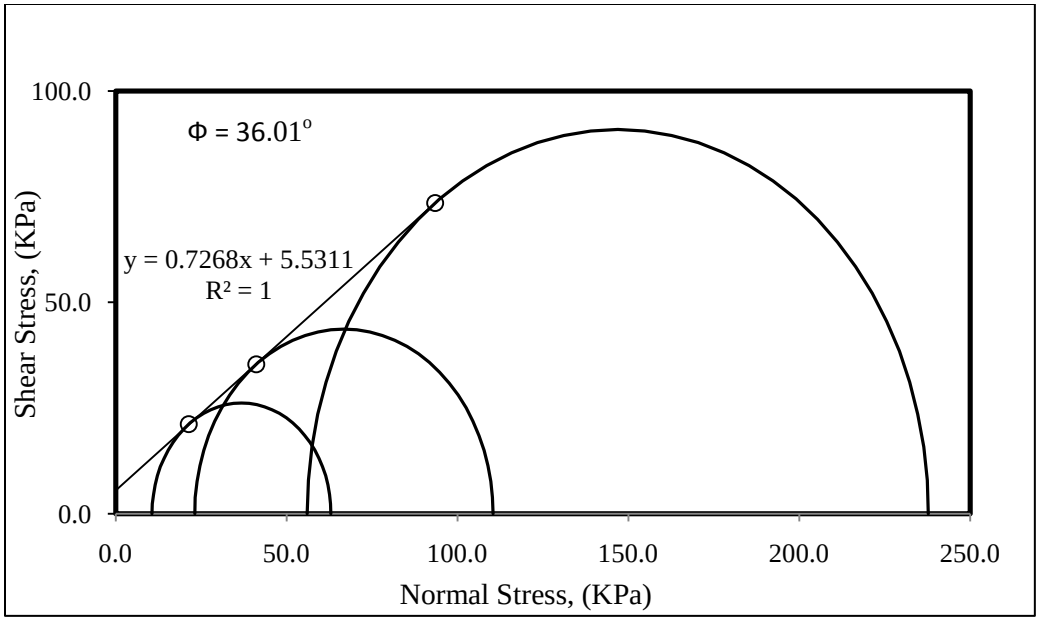


Figure A.2: Mohr Coulomb Enveloped for the Loose-Clean Sand (Test 1).

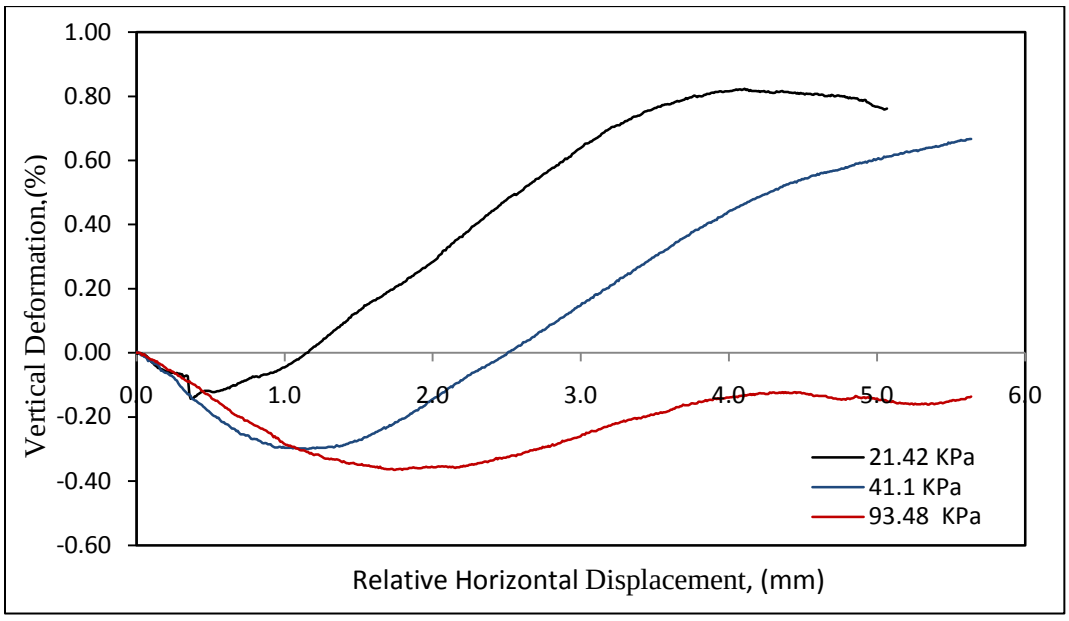


Figure A.3: Dilation Enveloped for the Loose-Clean Sand (Test 1).

Table A.2: Direct Shear Test Result for the Clean Sand in the Loose State (Test 2).

| Point No. | σ (kPa) | τ (kPa) | Sample Height (mm) | Water Content, (%) |
|---|---|---|---|---|
| 1 | 21.106 | 20.68 | 27.00 | 0.386 |
| 2 | 40.710 | 33.60 | 27.00 | 0.398 |
| 3 | 92.800 | 73.60 | 27.00 | 0.280 |

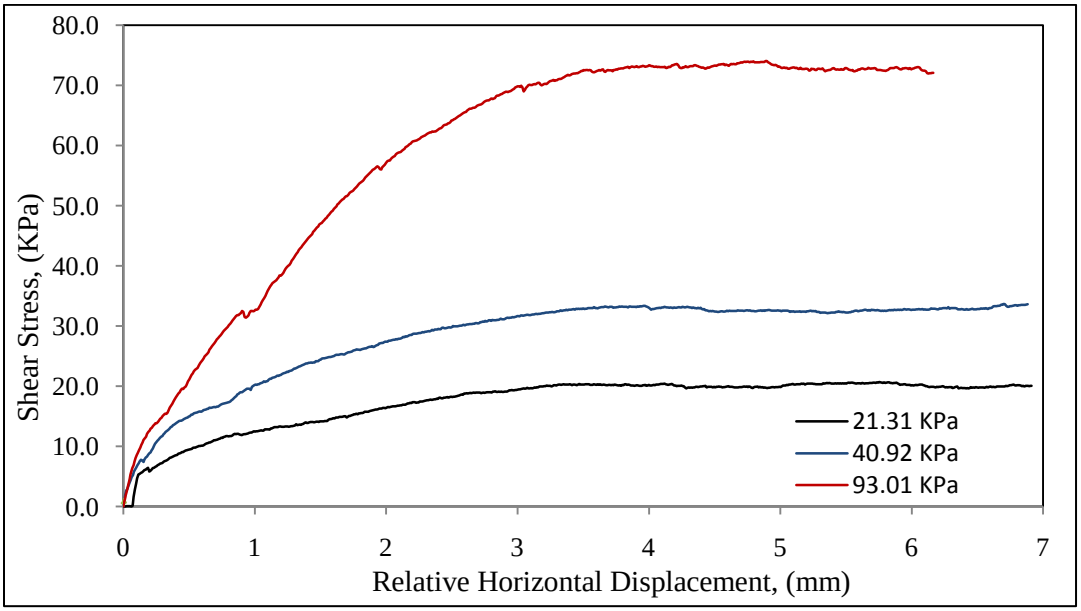


Figure A.4: Stress-Deformation Curve for the Loose-Clean Sand (Test 2).

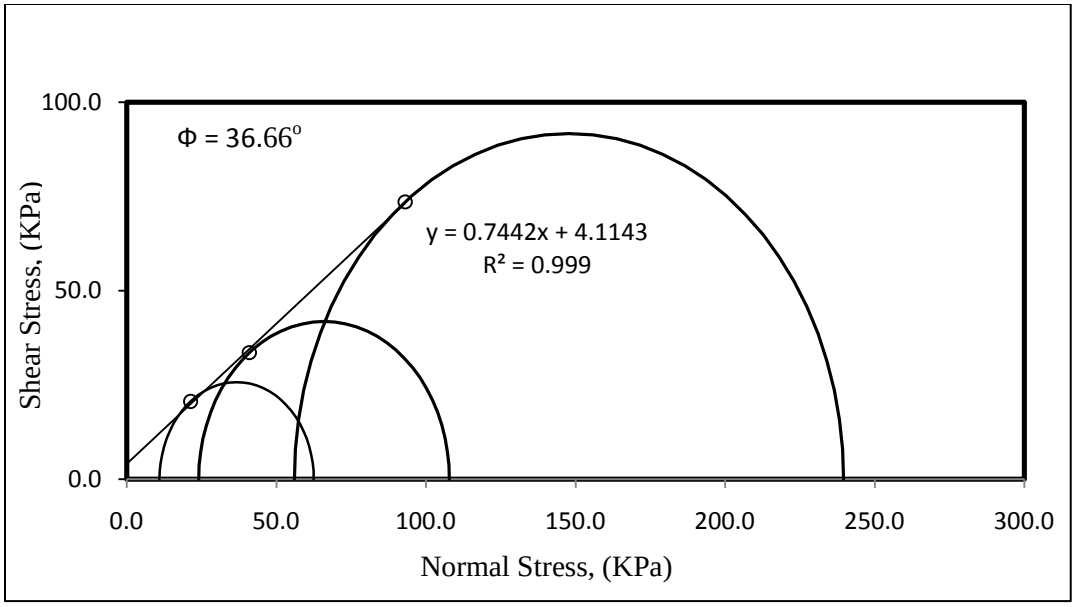


Figure A.5: Mohr Coulomb Enveloped for the Loose-Clean Sand (Test 2).

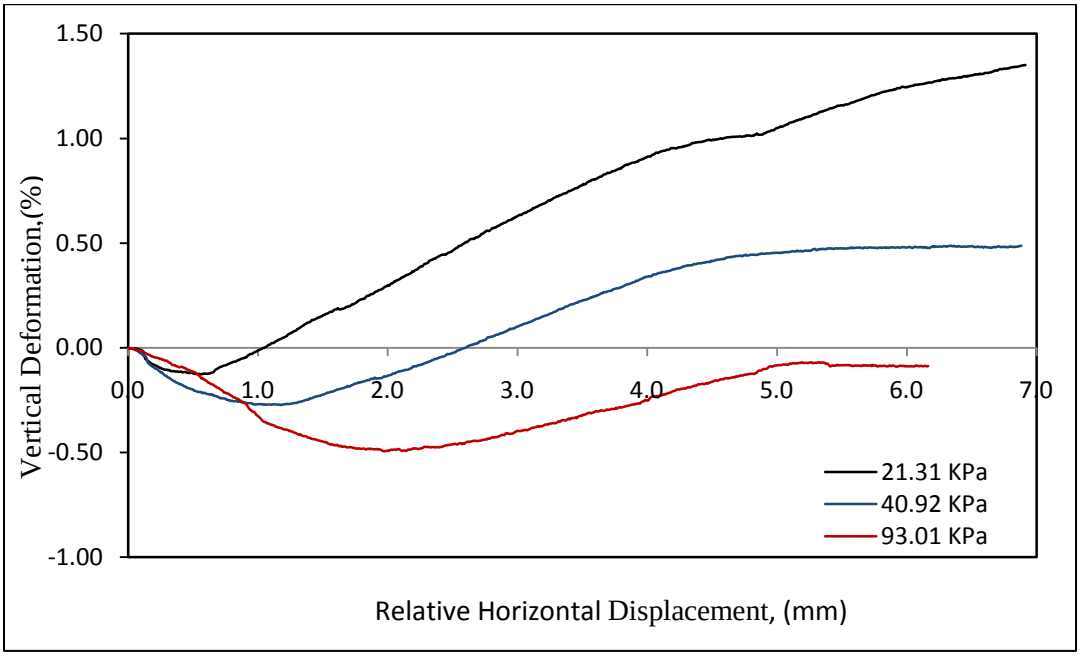


Figure A.6: Dilation Enveloped for the Loose-Clean Sand (Test 2).

Table A.3: Direct Shear Test Result for the Clean Sand in the Loose State (Test 3).

| Point No. | σ (kPa) | τ (kPa) | Sample Height (mm) | Water Content, (%) |
|---|---|---|---|---|
| 1 | 27.972 | 27.50 | 27.20 | 0.365 |
| 2 | 54.188 | 45.00 | 27.15 | 0.363 |
| 3 | 106.499 | 84.50 | 27.00 | 0.234 |

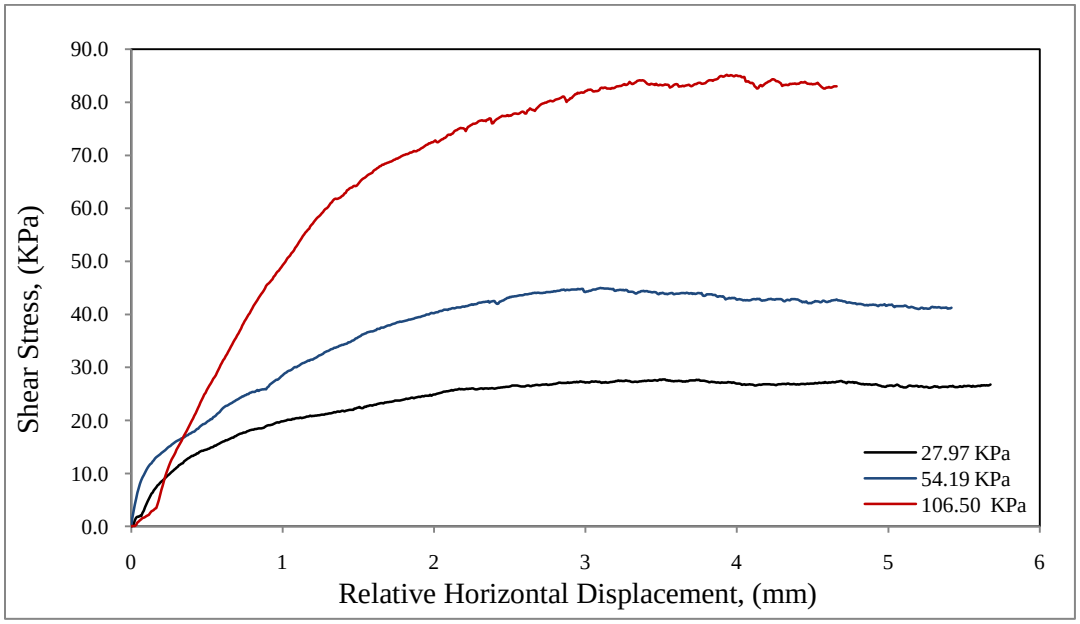


Figure A.7: Stress-Deformation Curve for the Loose-Clean Sand (Test 3).

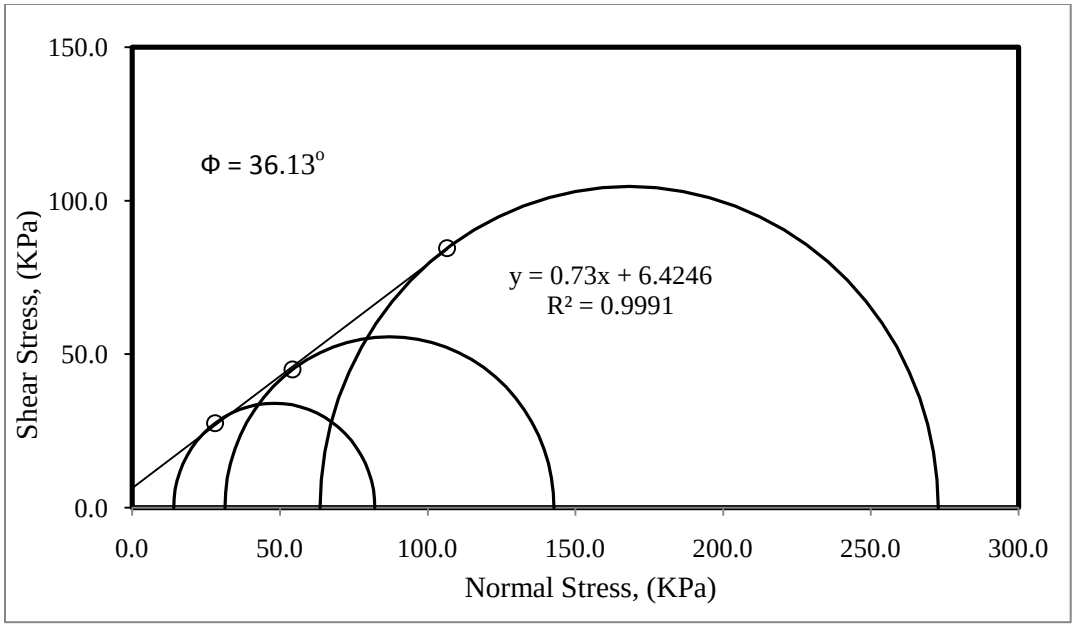


Figure A.8: Mohr Coulomb Enveloped for the Loose-Clean Sand (Test 3).

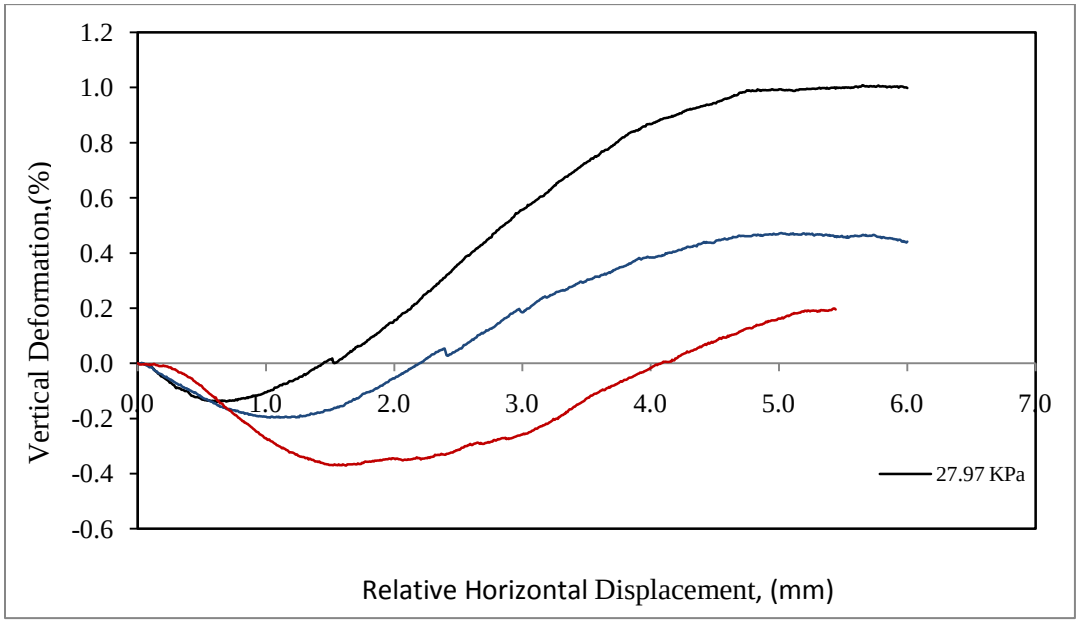


Figure A.9: Mohr Coulomb Enveloped for the Loose-Clean Sand (Test 3).

Table A.4: Direct Shear Test Result for the Clean Sand in the Loose State (Test 4).

| Point No. | σ (kPa) | τ (kPa) | Sample Height (mm) | Water Content, (%) |
|---|---|---|---|---|
| 1 | 27.829 | 26.30 | 27.00 | 0.21 |
| 2 | 53.907 | 44.66 | 27.00 | 0.23 |
| 3 | 106.002 | 83.19 | 27.00 | 0.26 |

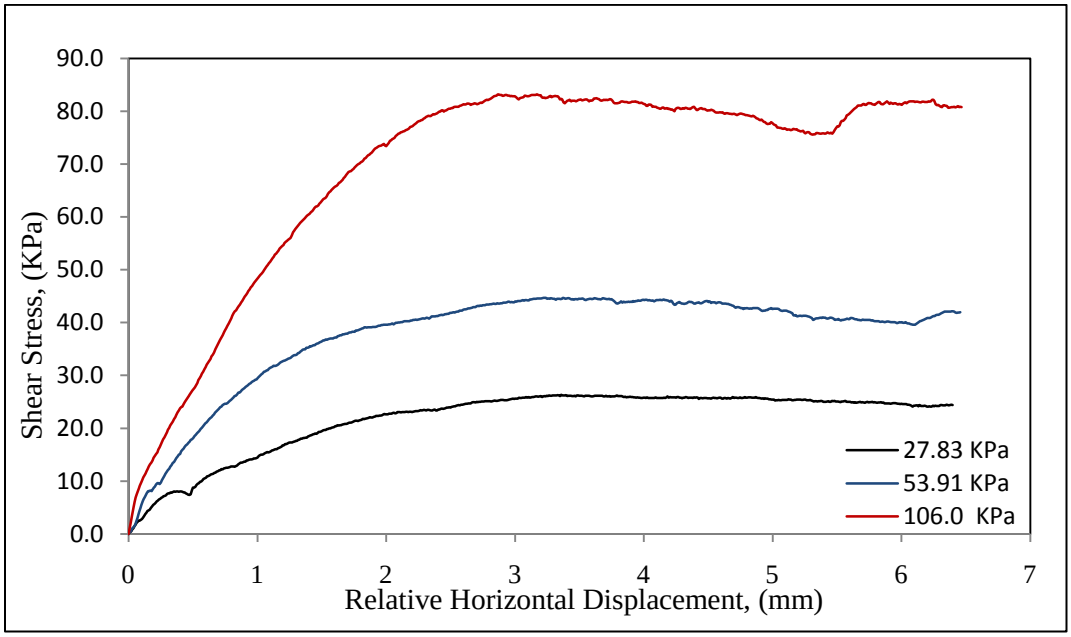


Figure A.10: Stress–Deformation Curve for the Loose-Clean Sand (Test 4).

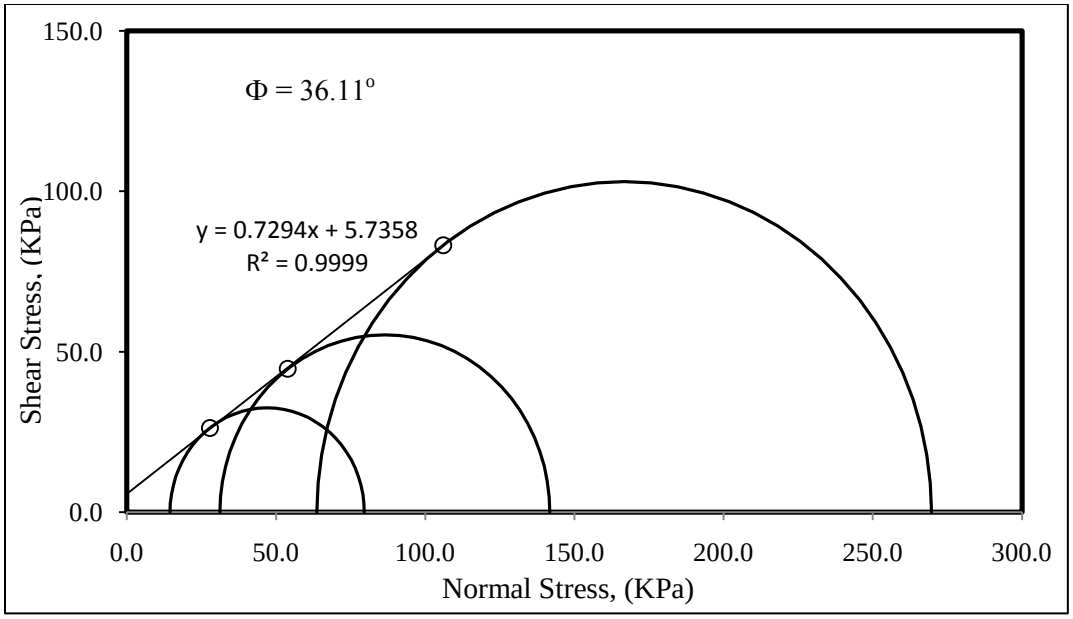


Figure A.11: Mohr Coulomb Enveloped for the Loose-Clean Sand (Test 4).

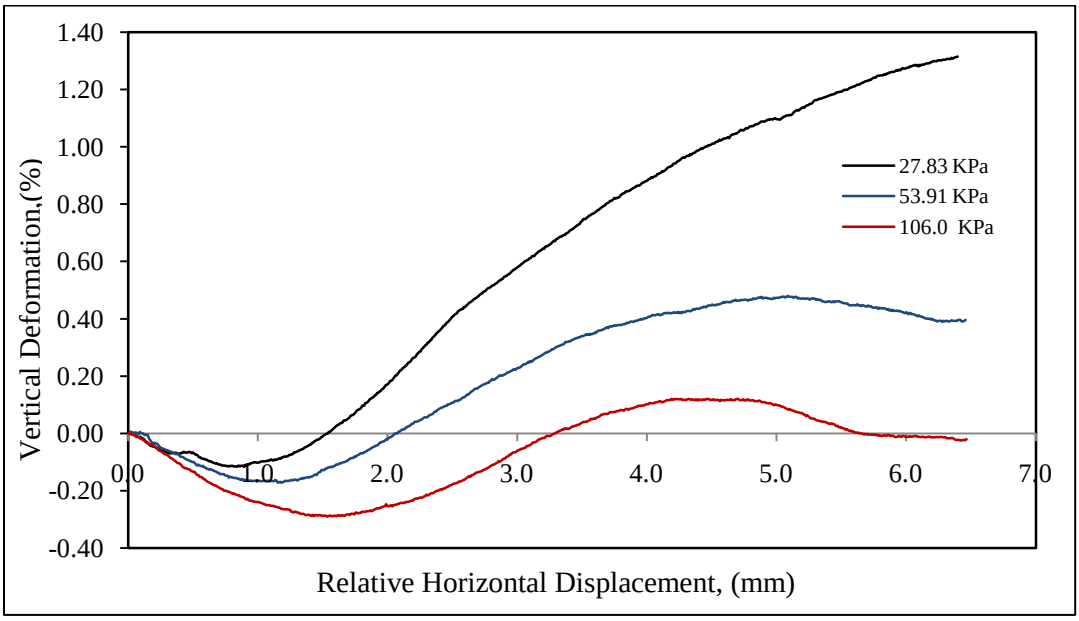


Figure A.12: Mohr Coulomb Enveloped of Loose-Clean Sand (Test 4).

Table A.5: Direct Shear Test Result for the Clean Sand in the Loose State (Test 5).

| Point No. | σ (kPa) | τ (kPa) | Sample Height (mm) | Water Content, (%) |
|---|---|---|---|---|
| 1 | 153.302 | 133.000 | 27.00 | 0.25 |
| 2 | 206.369 | 171.000 | 27.00 | 0.24 |
| 3 | 263.110 | 211.000 | 27.00 | 0.23 |

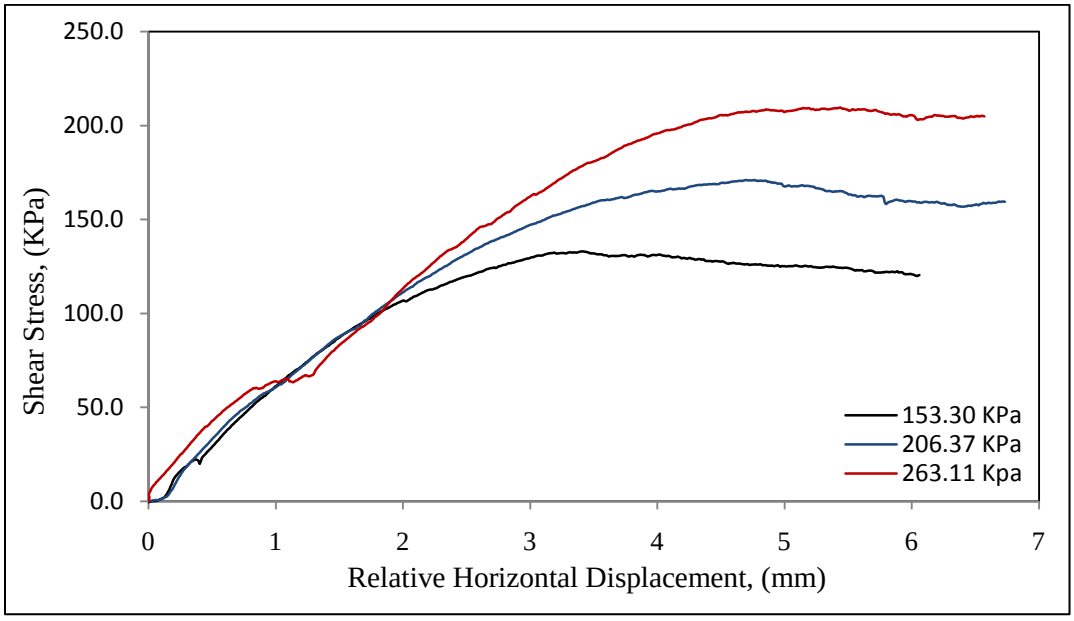


Figure A.13: Stress–Deformation Curve for the Loose-Clean Sand (Test 5).

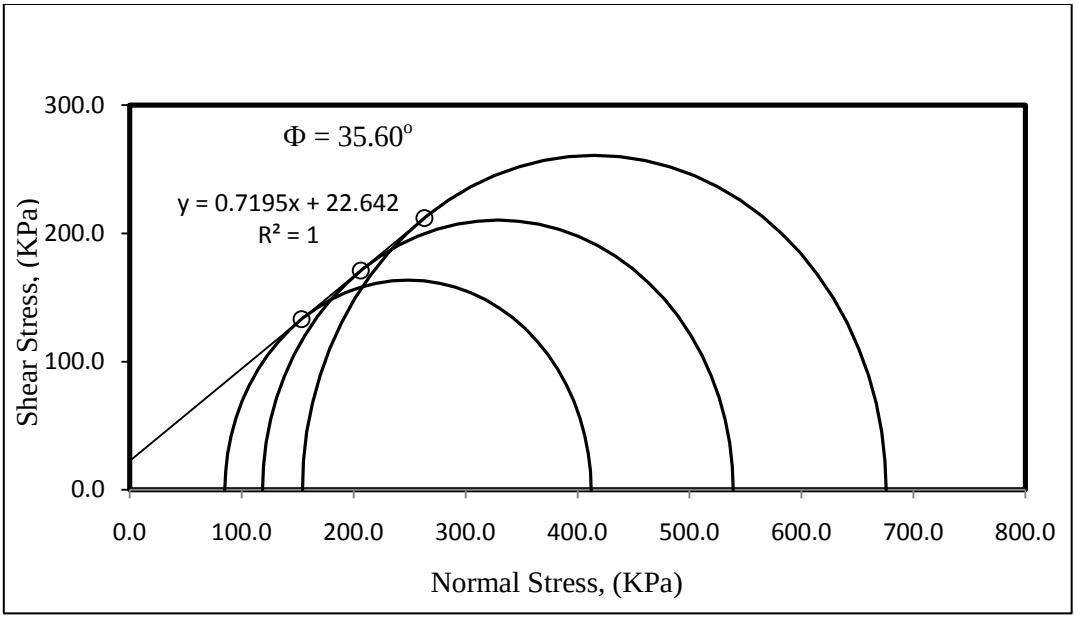


Figure A.14: Mohr Coulomb Enveloped for Loose-Clean Sand (Test 5).

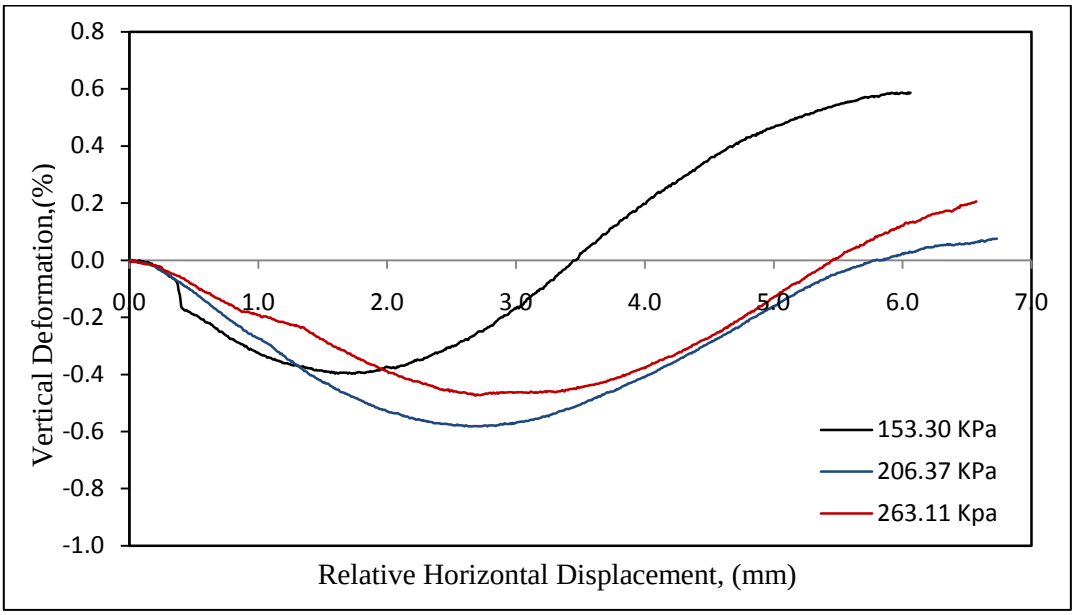


Figure A.15: Mohr Coulomb Enveloped for Loose-Clean Sand (Test 5).

Table A.6: Direct Shear Test Result for the Clean Sand in the Loose State (Test 6).

| Point No. | σ (kPa) | τ (kPa) | Sample Height (mm) | Water Content, (%) |
|---|---|---|---|---|
| 1 | 158.005 | 134.13 | 27.00 | 0.17 |
| 2 | 255.634 | 202.14 | 27.00 | 0.22 |
| 3 | 314.137 | 242.71 | 27.10 | 0.28 |

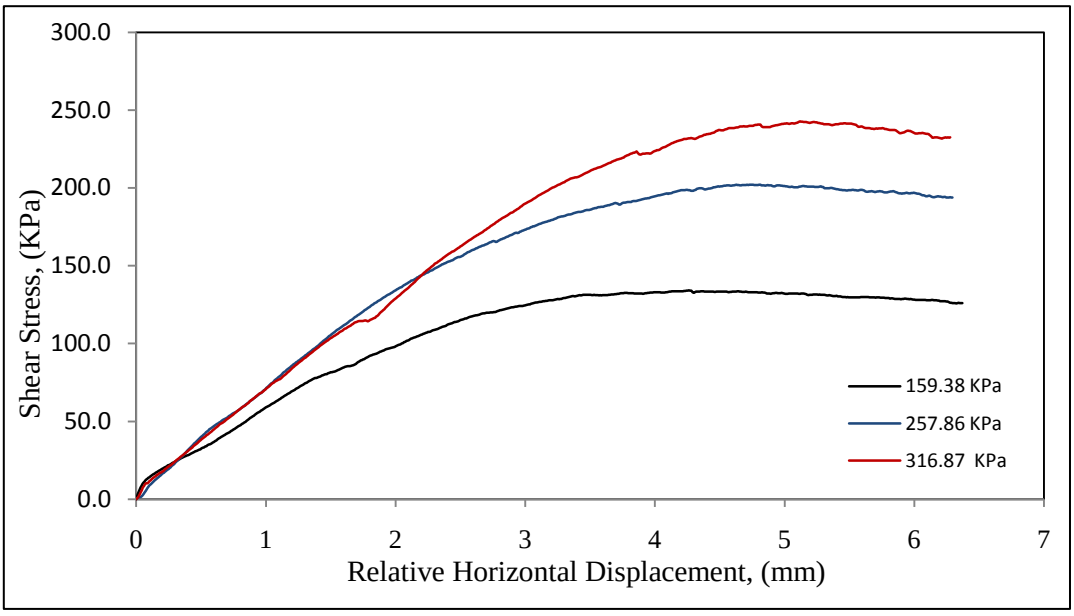


Figure A.16: Stress-Deformation Curve for Loose-Clean Sand (Test 6).

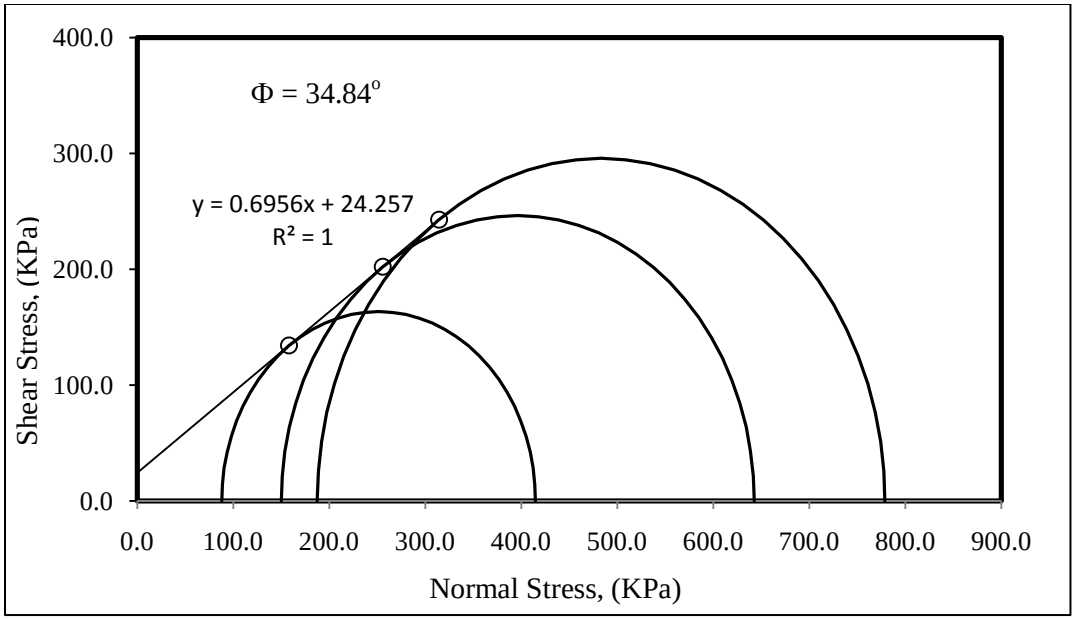


Figure A.17: Mohr Coulomb Enveloped for the Loose-Clean Sand (Test 6).

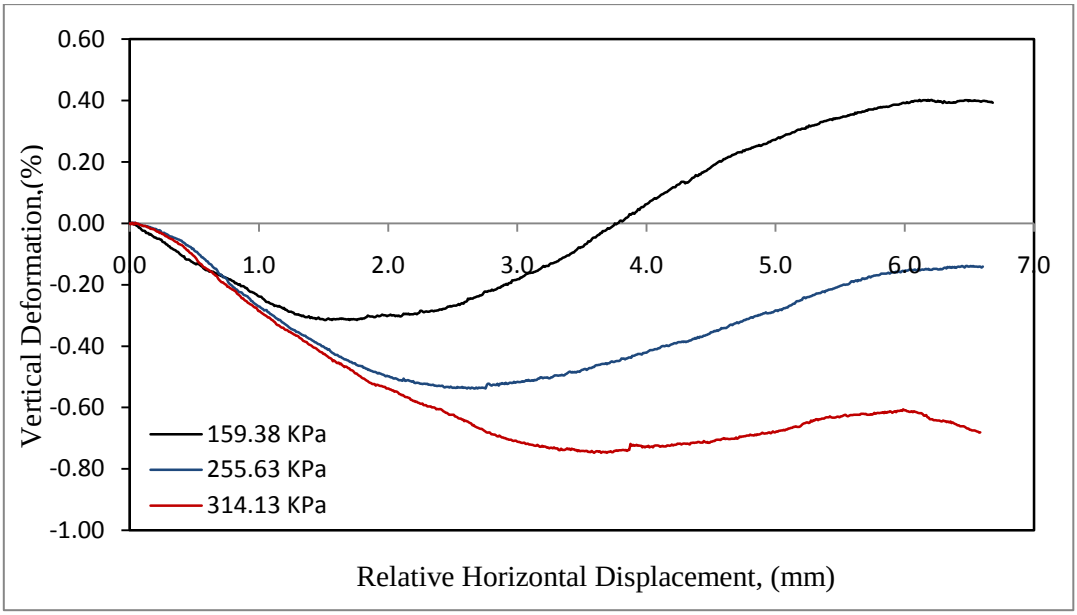


Figure A.18: Mohr Coulomb Enveloped for the Loose-Clean Sand (Test 6).

Table A.7: Direct Shear Test Result for the Clean Sand in the Dense State.

| Point No. | σ (kPa) | τ (kPa) | Sample Height (mm) | Water Content, (%) |
|---|---|---|---|---|
| 1 | 27.527 | 34.59 | 27.16 | 0.33 |
| 2 | 53.562 | 58.39 | 27.00 | 0.21 |
| 3 | 92.768 | 94.89 | 27.00 | 0.24 |

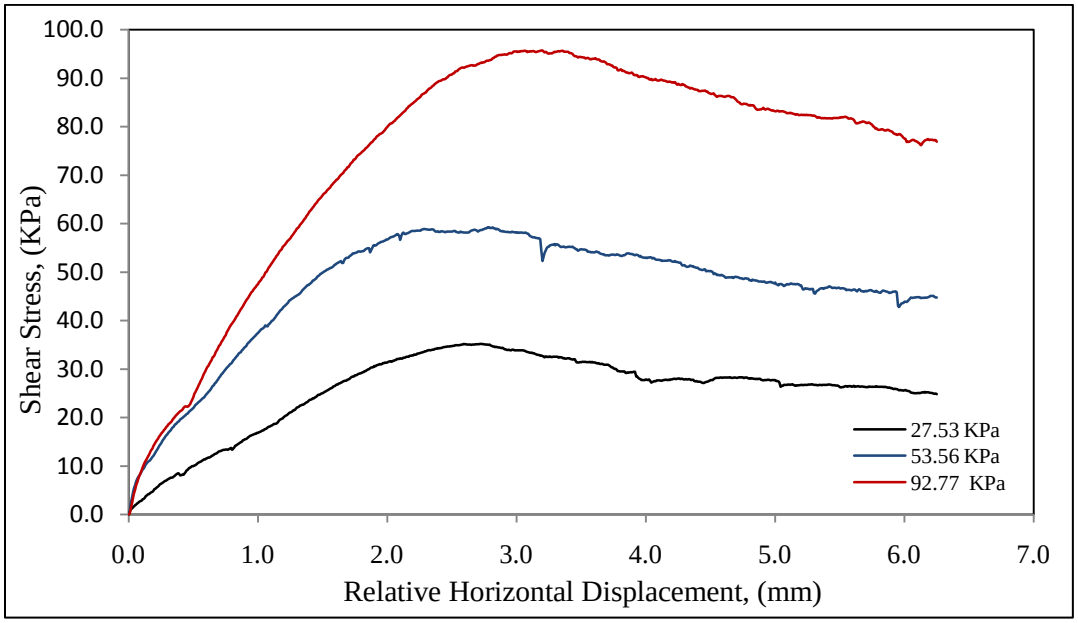


Figure A.19: Stress – Deformation Curve for Dense-Clean Sand.

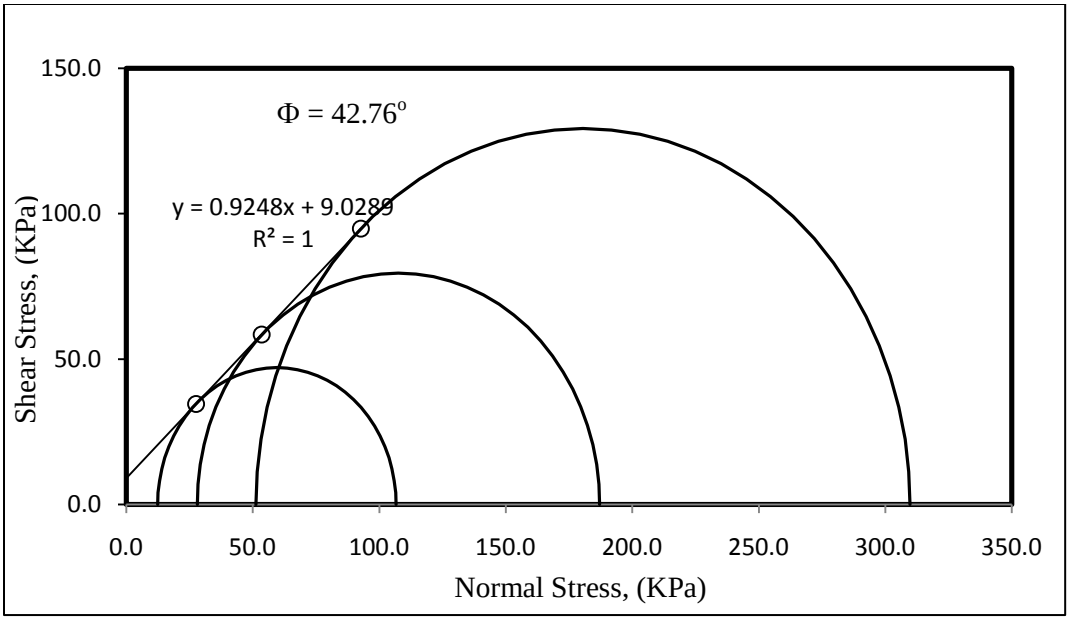


Figure A.20: Mohr Coulomb Enveloped of Dense-Clean Sand.

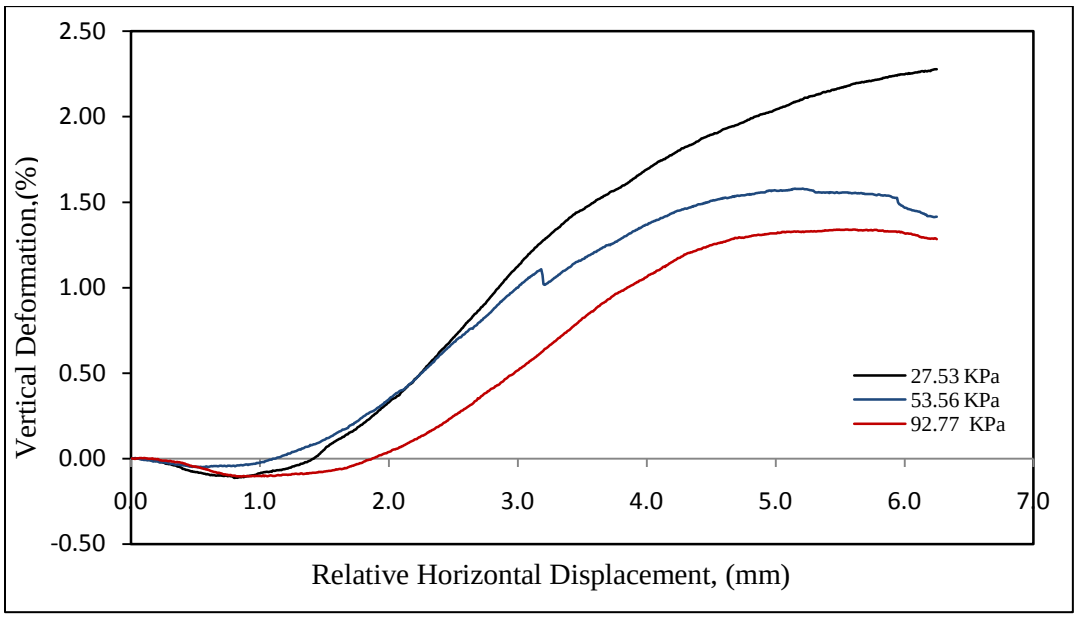


Figure A.21: Mohr Coulomb Enveloped of Dense-Clean Sand.

Table A.8: Direct Shear Test Result for the Compacted Clean Sand at *w*=2%.

| Point No. | σ (kPa) | τ (kPa) | Sample Height (mm) | Water Content, (%) |
|---|---|---|---|---|
| 1 | 33.586 | 33.19 | 27.0 | 2.43 |
| 2 | 65.890 | 63.59 | 27.0 | 2.10 |
| 3 | 104.722 | 92.39 | 27.0 | 2.70 |

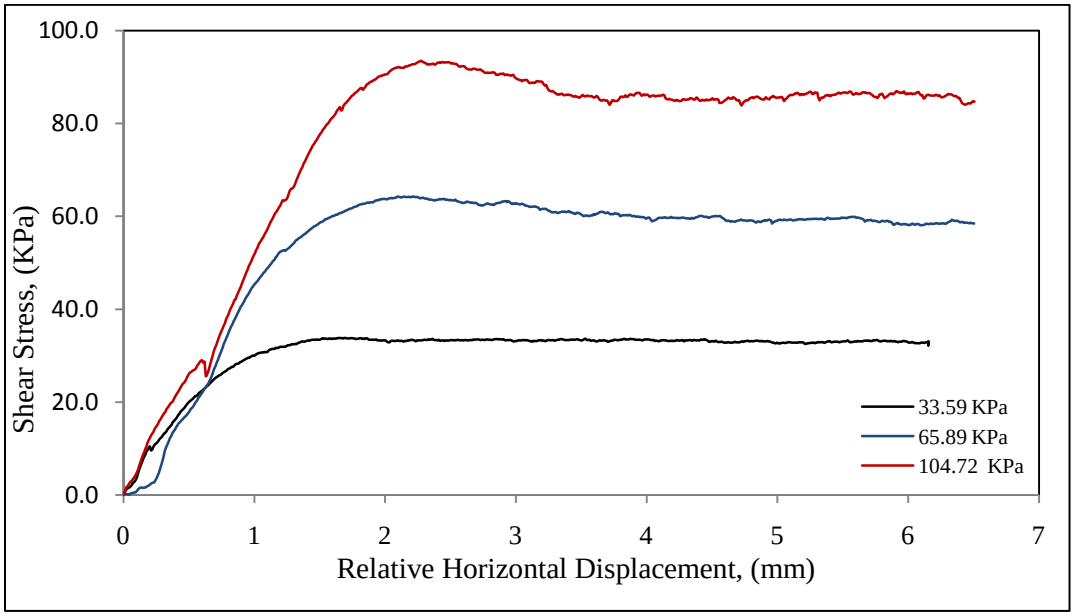


Figure A.22: Stress-Deformation Curve for the Compacted-Clean Sand at *w*=2%.

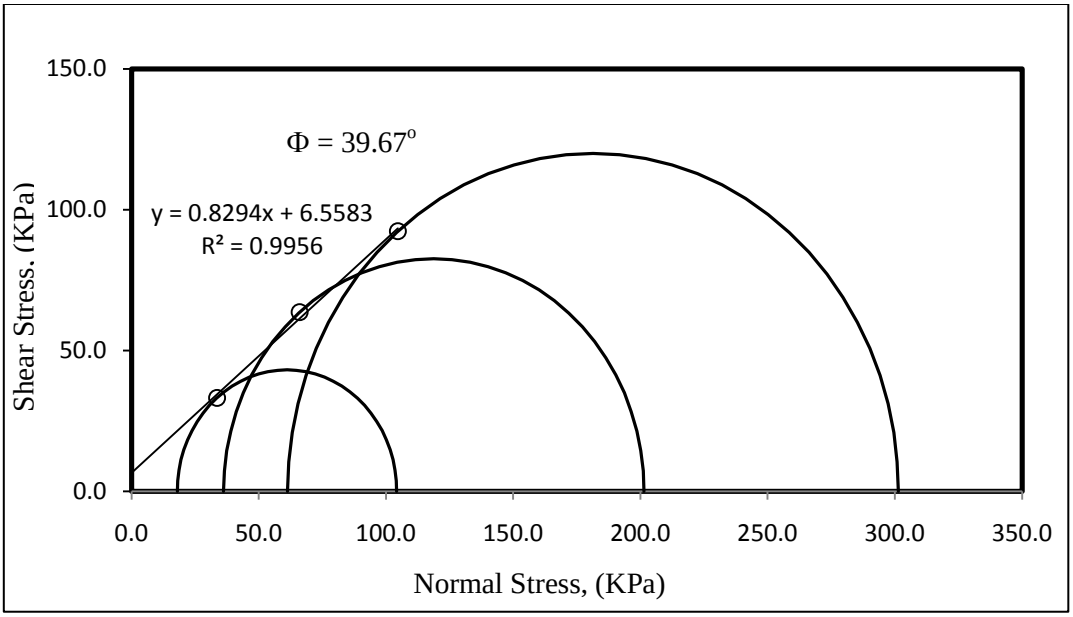


Figure A.23: Mohr Coulomb Enveloped for the Compacted-Clean Sand at *w*=2%.

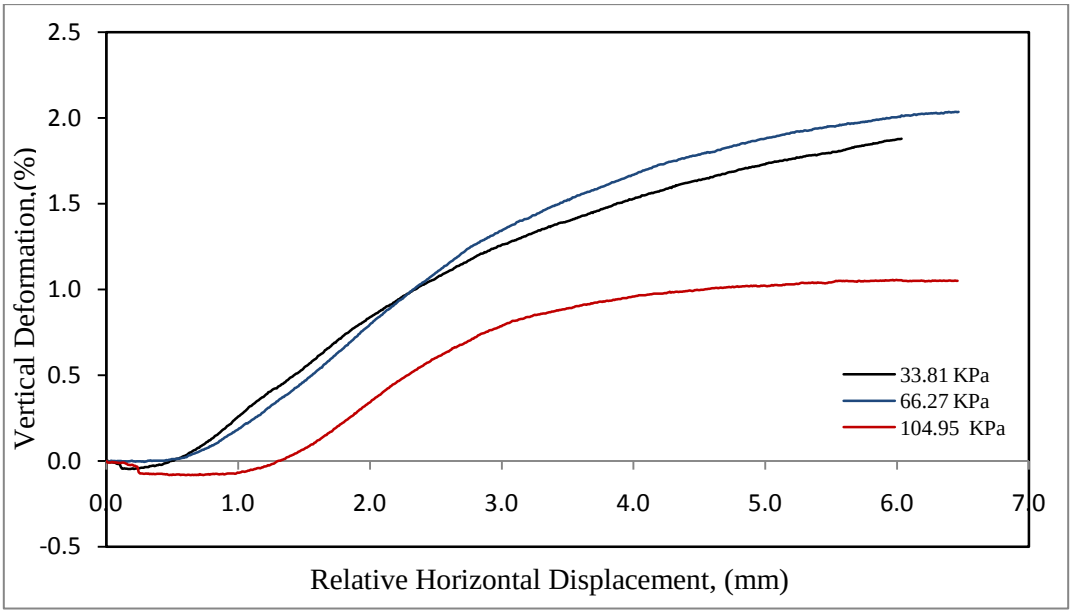


Figure A.24: Mohr Coulomb Enveloped for the Compacted-Clean Sand at *w*=2%.

Table A.9: Direct Shear Test Result for the Compacted Clean Sand *w* = 4%.

| Point No. | σ (kPa) | τ (kPa) | Sample Height (mm) | Water Content, (%) |
|---|---|---|---|---|
| 1 | 33.581 | 39.39 | 27.0 | 3.66 |
| 2 | 65.759 | 61.69 | 27.0 | 4.12 |
| 3 | 104.830 | 97.39 | 27.0 | 4.40 |

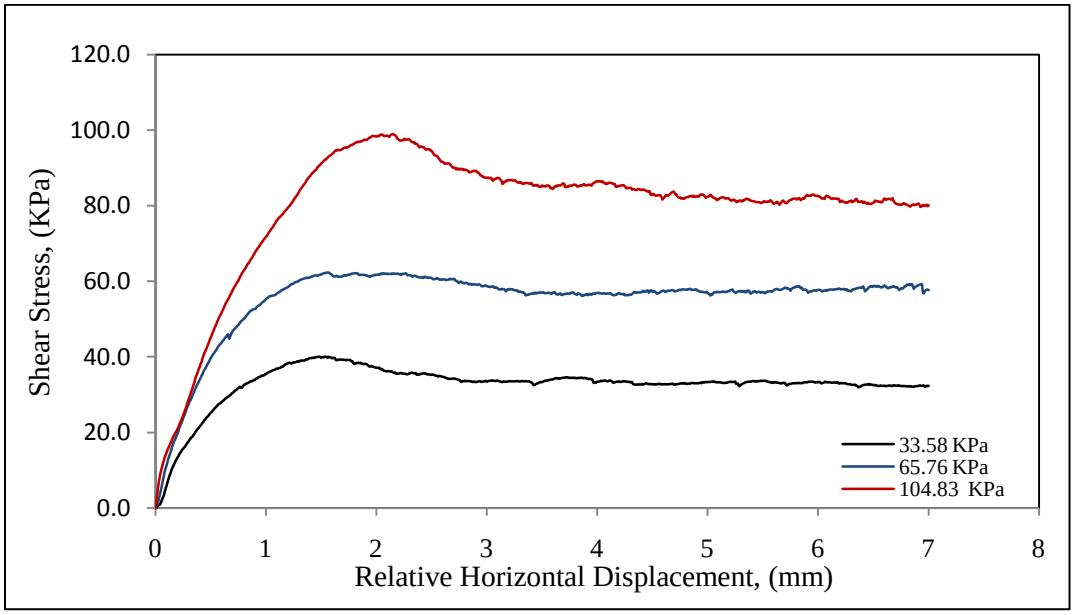


Figure A.25: Stress-Deformation Curve for the Compacted-Clean Sand at *w*=4%.

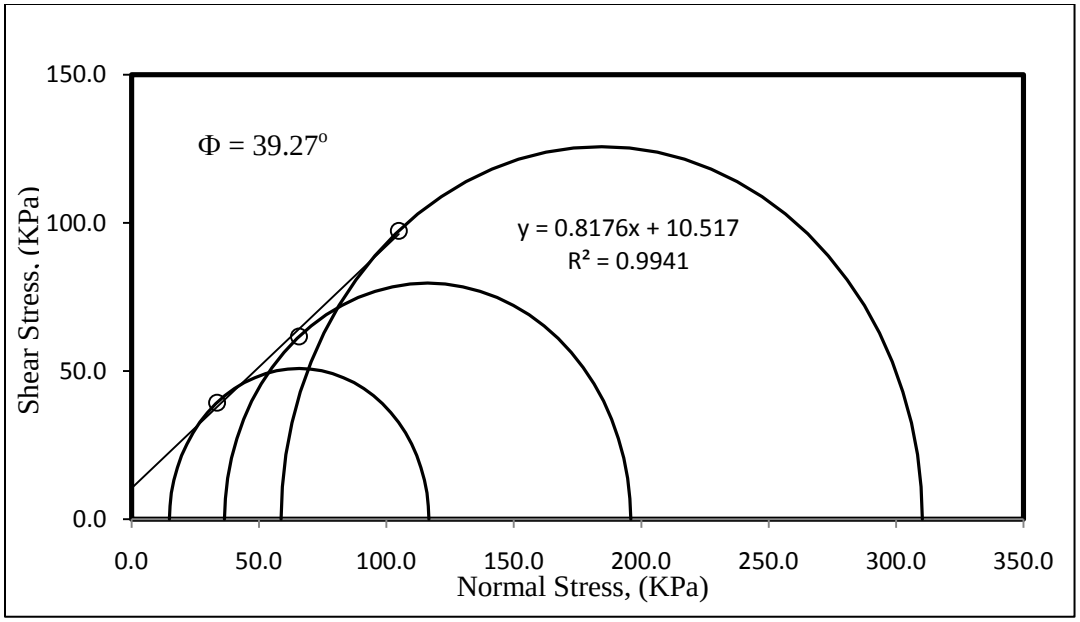


Figure A.26: Mohr Coulomb Enveloped for the Compacted-Clean Sand at w=4%

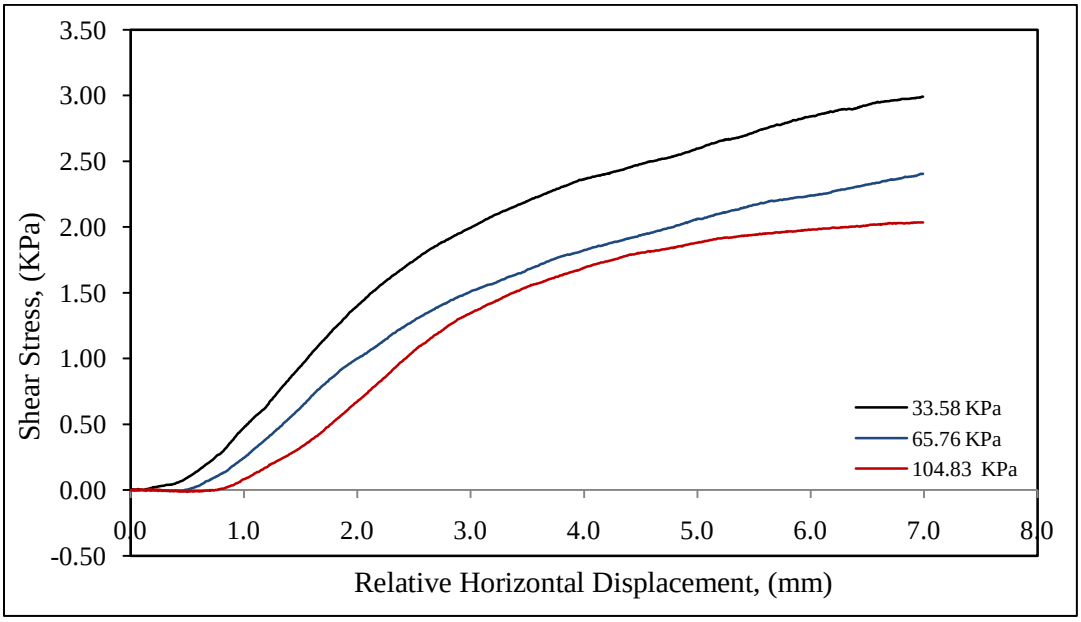


Figure A.27: Mohr Coulomb Enveloped for the Compacted-Clean Sand at w=6%

Table A.10: Direct Shear Test Result for the Compacted-Clean Sand at w=6%..

| Point No. | σ (kPa) | τ (kPa) | Sample Height (mm) | Water Content, (%) |
|---|---|---|---|---|
| 1 | 33.691 | 41.89 | 27.0 | 6.93 |
| 2 | 130.834 | 127.09 | 27.0 | 6.83 |
| 3 | 179.967 | 165.39 | 27.0 | 6.59 |

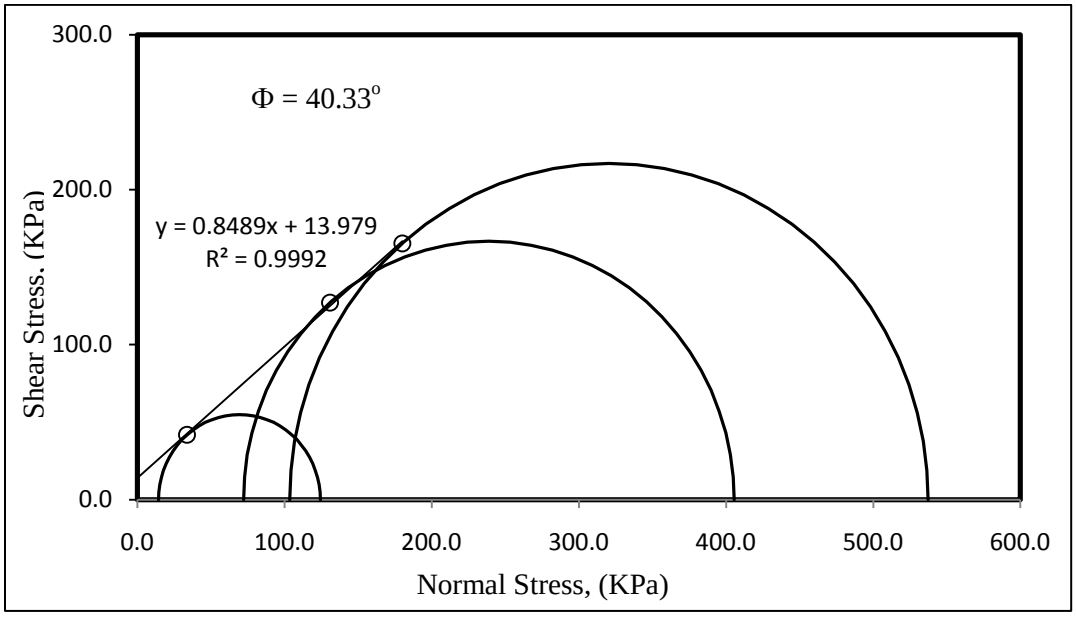


Figure A.28: Mohr Coulomb Enveloped for the Compacted-Clean Sand at *w*=6%.

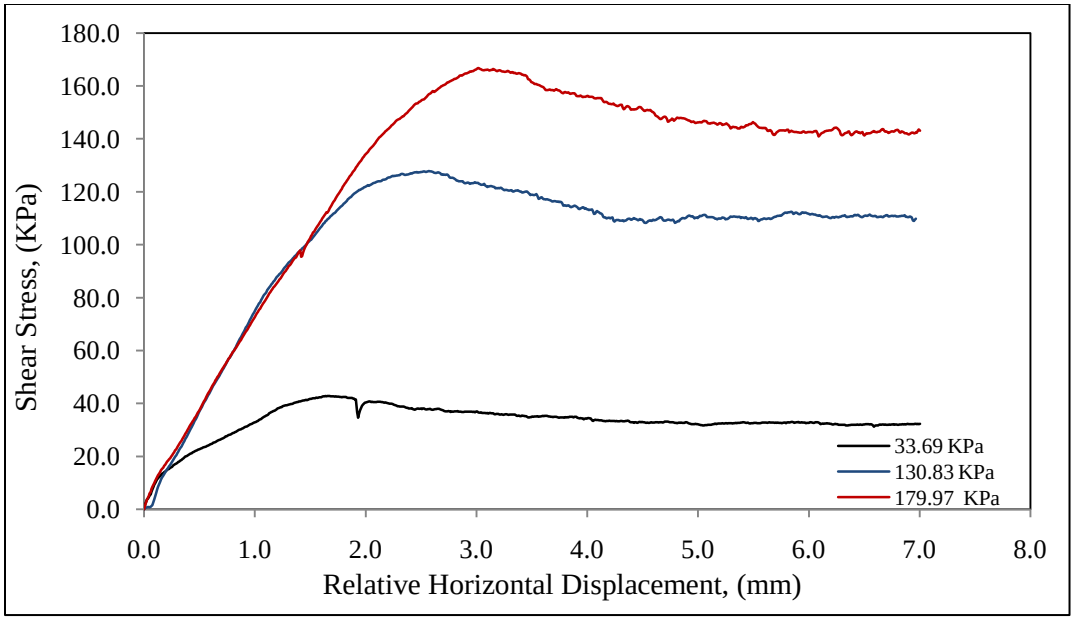


Figure A.29: Stress–Deformation Curve of Compacted-Clean Sand at *w*=6%

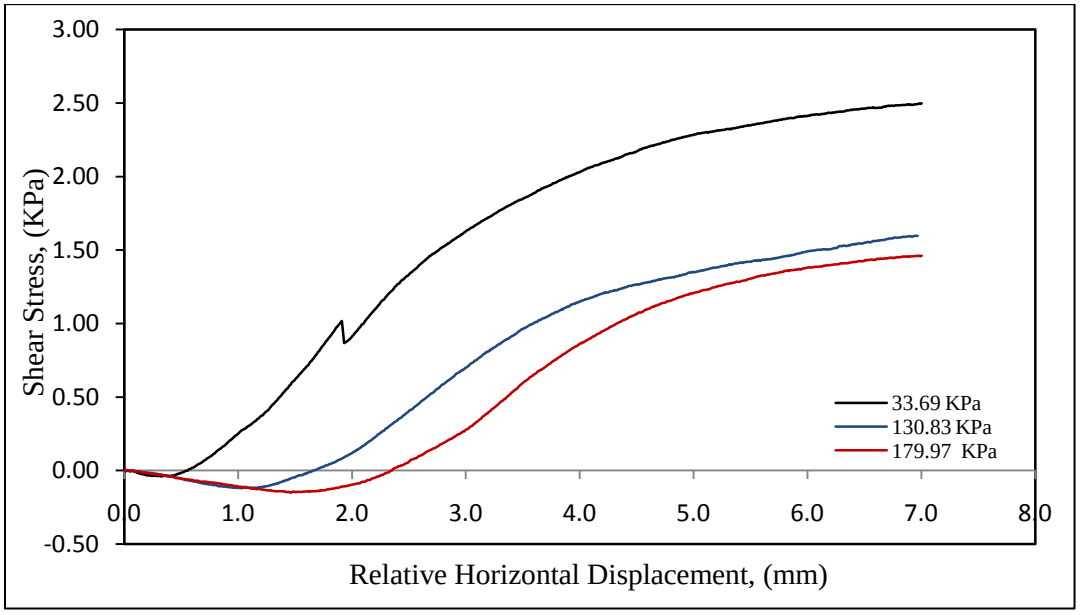


Figure A.30: Stress–Deformation Curve of Compacted-Clean Sand at *w*=6%.

# APPENDIX B- RESULTS OF THE MECHANICAL ANALYSIS CONDUCTED TO THE CLEAN SAND.

Tables B.1 to B.3 show the results of the three Mechanical Analysis conducted in the clean sand. The tests were performed in accordance to the designation ASTM D 2217-85 (Standard Practice for Wet Preparation of Soil Samples for Particle-Size Analysis and Determination of Soil Constants). The tests were conducted in the Geotechnical Graduate Lab. of the Zachry Department of Civil Engineering at Texas A&M University.

Table B.1: Results of the Mechanical Analysis #1 Conducted to the Clean Sand.

| Mechanical Analysis for Clean Sand- Result #1 | | | | | | | |
|---|---|---|---|---|---|---|---|
| Description of Sample: Clean Sand | | | | | Project: Pile Group Test | | |
| Unifies Soil Classification: SP (poor graded sand) | | | | | Location: Riverside Campus- Texas A&M University | | |
| | | | | | Date: 07/13/09 | | |
| | | | | | Tested by: Deeyvid O. Saez Barrios | | |
| Total weight of sample (g): | | | | 702.53 | | | |
| Total weight of fine particles (g): | | | | 18.18 | | | |
| Total weight of sand particles (g): | | | | 684.35 | | | |
| Sieve No. | Size (mm) | Weight of Sieve (g) | Weight of Sieve + Soil (g) | Weight of Soil Retained (g) | Percent. Retained by Weight (%) | Percent. Accum. by Weight (%) | Percentage Passing by Weight (%) |
| 3/8 " | 9.525 | 705.34 | 705.34 | 0.00 | 0.00 | 0.00 | 100.00 |
| 4 | 4.75 | 603.84 | 606.57 | 2.73 | 0.39 | 0.39 | 99.61 |
| 10 | 2.00 | 606.76 | 727.88 | 121.12 | 17.24 | 17.63 | 82.37 |
| 20 | 0.90 | 369.23 | 470.31 | 101.08 | 14.39 | 32.02 | 67.98 |
| 40 | 0.43 | 345.04 | 565.77 | 220.73 | 31.42 | 63.44 | 36.56 |
| 80 | 0.18 | 317.46 | 533.11 | 215.65 | 30.70 | 94.14 | 5.86 |
| 200 | 0.075 | 340.86 | 362.97 | 22.11 | 3.15 | 97.29 | 2.71 |
| Pan | | 377.41 | 378.30 | 19.07 | 2.71 | 100.00 | 0.00 |
| Total Weight of Soil (g) = | | | | 702.49 | 100.00 | | |
| Percentage Error (%) = | | | | 0.01 | < 2% O.K. | | |
| Total Percent of Particles Passing Sieve # 200 (%) = | | | | 2.71 | | | |

Table B.2: Results of the Mechanical Analysis #2 Conducted to the Clean Sand.

| Mechanical Analysis for Clean Sand- Result #2 | | | | | | | |
|---|---|---|---|---|---|---|---|
| Description of Sample: Clean Sand | | | | | Project: Pile Group Test | | |
| Unifies Soil Classification: SP (poor graded sand) | | | | | Location: Riverside Campus- Texas A&M University | | |
| | | | | | Date: 07/14/09 | | |
| | | | | | Tested by: Deeyvid O. Saez Barrios | | |
| Total weight of sample (g): | | | | 659.81 | | | |
| Total weight of fine particles (g): | | | | 21.2 | | | |
| Total weight of sand particles (g): | | | | 638.61 | | | |
| Sieve No. | Size (mm) | Weight of Sieve (g) | Weight of Sieve + Soil (g) | Weight of Soil Retained (g) | Percent. Retained by Weight (%) | Percent. Accum. by Weight (%) | Percentage Passing by Weight (%) |
| 3/8" | 9.53 | 705.34 | 705.34 | 0.00 | 0.00 | 0.00 | 100.00 |
| 4 | 4.75 | 603.84 | 610.68 | 6.84 | 1.04 | 1.04 | 98.96 |
| 10 | 2.00 | 606.71 | 735.36 | 128.65 | 19.49 | 20.53 | 79.47 |
| 20 | 0.90 | 368.93 | 468.37 | 99.44 | 15.06 | 35.59 | 64.41 |
| 40 | 0.43 | 344.96 | 561.90 | 216.94 | 32.86 | 68.45 | 31.55 |
| 80 | 0.18 | 317.44 | 483.32 | 165.88 | 25.13 | 93.58 | 6.42 |
| 200 | 0.075 | 340.85 | 361.48 | 20.63 | 3.13 | 96.71 | 3.29 |
| Pan | | 479.08 | 479.62 | 21.74 | 3.29 | 100.00 | 0.00 |
| Total Weight of Soil (g) = | | | | 660.12 | 100.00 | | |
| Percentage Error (%) = | | | | 0.05 | < 2% O.K. | | |

Table B.3: Results of the Mechanical Analysis #3 Conducted to the Clean Sand.

| Mechanical Analysis for Clean Sand- Result #3 | | | | | | | |
|---|---|---|---|---|---|---|---|
| Description of Sample: Clean Sand | | | | | Project: Pile Group Test | | |
| Unifies Soil Classification: SP (poor graded sand) | | | | | Location: Riverside Campus- Texas A&M University | | |
| | | | | | Date: 07/14/09 | | |
| | | | | | Tested by: Deeyvid O. Saez Barrios | | |
| Total weight of sample (g): | | | | 704.09 | | | |
| Total weight of fine particles (g): | | | | 24.61 | | | |
| Total weight of sand particles (g): | | | | 679.48 | | | |
| Sieve No. | Size (mm) | Weight of Sieve (g) | Weight of Sieve + Soil (g) | Weight of Soil Retained (g) | Percent. Retained by Weight (%) | Percent. Accum. by Weight (%) | Percentage Passing by Weight (%) |
| 3/8" | 9.53 | 700 | 700 | 0.00 | 0.00 | 0.00 | 100.00 |
| 4 | 4.75 | 603.81 | 608.56 | 4.75 | 0.67 | 0.67 | 99.33 |
| 10 | 2.00 | 606.76 | 728.92 | 122.16 | 17.34 | 18.01 | 81.99 |
| 20 | 0.90 | 369.09 | 471.90 | 102.81 | 14.59 | 32.61 | 67.39 |
| 40 | 0.43 | 345.02 | 560.43 | 215.41 | 30.58 | 63.18 | 36.82 |
| 80 | 0.18 | 317.47 | 528.14 | 210.67 | 29.90 | 93.09 | 6.91 |
| 200 | 0.075 | 340.83 | 364.21 | 23.38 | 3.32 | 96.41 | 3.59 |
| Pan | | 377.42 | 378.12 | 25.31 | 3.59 | 100.00 | 0.00 |
| | | | Total Weight of Soil (g) = | 704.49 | 100.00 | | |
| | | | Percentage Error (%) = | 0.06 | < 2% O.K. | | |
| | | | Total Percent of Particles Passing Sieve # 200 (%) = | 3.59 | | | |

# APPENDIX C- RESULTS OF THE TESTS CONDUCTED TO THE SILTY SAND.

Tables C.1 to C.3 show the results of the three Mechanical Analysis conducted in the silty sand. The tests were performed in accordance to the designation ASTM D 2217-85 (Standard Practice for Wet Preparation of Soil Samples for Particle-Size Analysis and Determination of Soil Constants).

Tables C.4 to C.6 present the results of the Hydrometer analysis conducted in the silty sand. The Hydrometer test were conducted following the criterion established by the designation ASTM D 422 (Standard Method for Particle Size Analysis of Soils)

Finally, tables C.7 and C.8 and figures C.1 and C.2 present all the information concerning the computation of the Liquid Limit ($w_L$) of the Silty Sand. The tests were conducted following the standard ASTM D 4318-00 (Standard Tests Methods for Liquid Limit, Plastic Limit, and Plasticity Index of Soils.

All these tests were conducted in the Geotechnical Graduate Lab. of the Zachry Department of Civil Engineering at Texas A&M University.

Table C.1: Results of the Mechanical Analysis #1 Conducted to the Silty Sand.

| Mechanical Analysis for Silty Sand - Result # 1 | | | | | | | |
|---|---|---|---|---|---|---|---|
| Sample No. : 2 | | | | | Project: Pile Group Test | | |
| Boring No.: hand augered hole | | | | | Location: Riverside Campus - Sand Site | | |
| Depth: 10 ft | | | | | Date: 06/17/09 | | |
| Description of sample: Very Silty Sand | | | | | Tested by: Deeyvid O. Saez Barrios | | |
| Total weight of sample (g): | | | | 507.04 | | | |
| Total weight of fine particles (g): | | | | 185.99 | | | |
| Total weight of sand particles (g): | | | | 321.05 | | | |
| Sieve No. | Size (mm) | Weight of Sieve (g) | Weight of Sieve + Soil (g) | Weight of Soil Retained (g) | Percent. Retained by Weight (%) | Percent. Accum. by Weight (%) | Percentage Passing by Weight (%) |
| 4 | 4.75 | 608.20 | 608.74 | 0.54 | 0.11 | 0.11 | 99.89 |
| 10 | 2.00 | 606.82 | 610.94 | 4.12 | 0.81 | 0.92 | 99.08 |
| 20 | 0.90 | 369.21 | 373.18 | 3.97 | 0.78 | 1.70 | 98.30 |
| 40 | 0.43 | 345.11 | 348.03 | 2.92 | 0.58 | 2.28 | 97.72 |
| 80 | 0.18 | 317.54 | 322.61 | 5.07 | 1.00 | 3.28 | 96.72 |
| 200 | 0.075 | 340.90 | 580.47 | 239.57 | 47.24 | 50.52 | 49.48 |
| Pan | | 479.20 | 544.16 | 250.95 | 49.48 | 100.00 | 0.00 |
| Total Weight of Soil (g) = | | | | 507.14 | 100.00 | | |
| Percentage Error (%) = | | | | 0.02 | < 2% O.K. | | |
| Total Percent of Particles Passing Sieve # 200 (%) = | | | | 49.48 | | | |

Table C.2: Results of the Mechanical Analysis #2 Conducted to the Silty Sand.

| Mechanical Analysis for Silty Sand – Result # 2 | | | | | | | |
|---|---|---|---|---|---|---|---|
| Sample No. : 2 | | | | | Project: Pile Group Test | | |
| Boring No.: hand augered hole | | | | | Location: Riverside Campus - Sand Site | | |
| Depth: 10 ft | | | | | Date: 06/17/09 | | |
| Description of sample: Very Silty Sand | | | | | Tested by: Deeyvid O. Saez Barrios | | |
| Total weight of sample (g): | | | | 558.12 | | | |
| Total weight of fine particles (g): | | | | 194.54 | | | |
| Total weight of sand particles (g): | | | | 363.58 | | | |
| Sieve No. | Size (mm) | Weight of Sieve (g) | Weight of Sieve + Soil (g) | Weight of Soil Retained (g) | Percent. Retained by Weight (%) | Percent. Accum. by Weight (%) | Percentage Passing by Weight (%) |
| 4 | 4.75 | 608.12 | 621.15 | 13.03 | 2.33 | 2.33 | 97.67 |
| 10 | 2.00 | 606.77 | 610.70 | 3.93 | 0.70 | 3.04 | 96.96 |
| 20 | 0.90 | 368.99 | 372.97 | 3.98 | 0.71 | 3.75 | 96.25 |
| 40 | 0.43 | 345.04 | 347.11 | 2.07 | 0.37 | 4.12 | 95.88 |
| 80 | 0.18 | 317.47 | 323.30 | 5.83 | 1.04 | 5.17 | 94.83 |
| 200 | 0.075 | 340.88 | 596.64 | 255.76 | 45.81 | 50.98 | 49.02 |
| Pan | | 479.24 | 558.40 | 273.70 | 49.02 | 100.00 | 0.00 |
| Total Weight of Soil (g) = | | | | 558.30 | 100.00 | | |
| Percentage Error (%) = | | | | 0.03 | < 2% O.K. | | |
| Total Percent of Particles Passing Sieve # 200 (%) = | | | | 49.02 | | | |

Table C.3: Results of the Mechanical Analysis #3 Conducted to the Silty Sand.

| Mechanical Analysis for Silty Sand - Result #3 | | | | | | | |
|---|---|---|---|---|---|---|---|
| Sample No. : 2 | | | | | Project: Pile Group Test | | |
| Boring No.: hand augered hole | | | | | Location: Riverside Campus - Sand Site | | |
| Depth: 10 ft | | | | | Date: 06/17/09 | | |
| Description of sample: Silt | | | | | Tested by: Deeyvid O. Saez Barrios | | |
| Total weight of sample (g): | | | | 537.04 | | | |
| Total weight of fine particles (g): | | | | 208.57 | | | |
| Total weight of sand particles (g): | | | | 328.47 | | | |
| Sieve No. | Size (mm) | Weight of Sieve (g) | Weight of Sieve + Soil (g) | Weight of Soil Retained (g) | Percent. Retained by Weight (%) | Percent. Accum. by Weight (%) | Percentage Passing by Weight (%) |
| 4 | 4.75 | 608.14 | 620.55 | 12.41 | 2.31 | 2.31 | 97.69 |
| 10 | 2.00 | 606.74 | 611.16 | 4.42 | 0.82 | 3.13 | 96.87 |
| 20 | 0.90 | 368.96 | 372.55 | 3.59 | 0.67 | 3.80 | 96.20 |
| 40 | 0.43 | 344.99 | 347.19 | 2.20 | 0.41 | 4.21 | 95.79 |
| 80 | 0.18 | 317.48 | 321.74 | 4.26 | 0.79 | 5.00 | 95.00 |
| 200 | 0.075 | 340.88 | 578.01 | 237.13 | 44.12 | 49.12 | 50.88 |
| Pan | | 479.20 | 544.06 | 273.43 | 50.88 | 100.00 | 0.00 |
| Total Weight of Soil (g) = | | | | 537.44 | 100.00 | | |
| Percentage Error (%) = | | | | 0.07 | < 2% O.K. | | |
| Total Percent of Particles Passing Sieve # 200 (%) = | | | | 50.88 | | | |

Table C.4: Results of the Hydrometer Analysis conducted to the Silty Sand.

| Hydrometer Analysis No. 1 – Silty Sand | | | | | | | | | | |
|---|---|---|---|---|---|---|---|---|---|---|
| Date: | 6/11/2009 | Tested: | 06/20/2009 - 06/21/2009 | Boring: | hand augured hole | Tested By: | | | | |
| Sample No.: | 2 | Project: | Pile Group Test | Depth: | 10 ft | Deeyvid Saez Barrios | | | | |
| Hygroscopic Water Content | | | | | | | | | | |
| 1) Cup No. : | | 1 | | 2) Mass of cup (g): | | 22.85 | | | | |
| 3) Mass cup + soil (air dry) (g): | | 39.41 | | 4) Mass cup + soil (oven dry) (g): | | 39.08 | | | | |
| 5) Mass of water (g): | | 0.33 | | 6) Mass of soil (oven dry) (g): | | 16.23 | | | | |
| 7) Mass of soil (air dry) (g): | | 16.56 | | 8) Hygroscope. water content (%): | | 2.03 | | | | |
| 9) Hygroscope. correction factor: | | 0.980 | | | | | | | | |
| Hydrometer Analysis | | | | | | | | | | |
| Hydrometer Type: | | 151 H | | Specific Gravity: | | 2.67 | | | | |
| Hydrometer Reading in the Control Solution: | | 1.0025 | | Calculate mass of oven dry soil: | | 78.41 | | | | |
| Mass of air dry soil: | | 80 | | Starting Time: | | 13:30:00 | | | | |

| Date | Time | Elapsed Time (min) | Actual Hydrometer Reading (Rh) | Composite Correction | Hydrometer Reading Correction (Rh) | Temperature (Degrees C) | Effective Hydrometer Depth (L) | K from table | Diameter of Particle, D (mm) | Percent finer in suspension (%) |
|---|---|---|---|---|---|---|---|---|---|---|
| 6/20/2009 | 13:30:04 | 0.07 | 1.0370 | 0.0025 | 1.0345 | 23.8 | 6.50 | 0.01285 | 0.12688 | 63.07 |
| 6/20/2009 | 13:30:15 | 0.25 | 1.0320 | 0.0025 | 1.0295 | 23.8 | 7.80 | 0.01285 | 0.07178 | 53.06 |
| 6/20/2009 | 13:30:30 | 0.50 | 1.0270 | 0.0025 | 1.0245 | 23.8 | 9.20 | 0.01285 | 0.05512 | 43.05 |
| 6/20/2009 | 13:31:00 | 1.00 | 1.0180 | 0.0025 | 1.0155 | 23.8 | 11.50 | 0.01285 | 0.04358 | 25.03 |
| 6/20/2009 | 13:31:30 | 1.50 | 1.0145 | 0.0025 | 1.0120 | 23.8 | 12.45 | 0.01285 | 0.03702 | 18.02 |
| 6/20/2009 | 13:32:00 | 2.00 | 1.0125 | 0.0025 | 1.0100 | 23.8 | 13.00 | 0.01285 | 0.03276 | 14.01 |
| 6/20/2009 | 13:35:00 | 5.00 | 1.0090 | 0.0025 | 1.0065 | 23.8 | 13.90 | 0.01285 | 0.02143 | 7.01 |
| 6/20/2009 | 13:40:00 | 10.00 | 1.0078 | 0.0025 | 1.0053 | 23.8 | 14.24 | 0.01285 | 0.01533 | 4.60 |
| 6/20/2009 | 13:45:00 | 15.00 | 1.0075 | 0.0025 | 1.0050 | 23.8 | 14.30 | 0.01285 | 0.01255 | 4.00 |
| 6/20/2009 | 13:50:00 | 20.00 | 1.0074 | 0.0025 | 1.0049 | 23.7 | 14.32 | 0.012865 | 0.01089 | 3.80 |
| 6/20/2009 | 13:55:00 | 25.00 | 1.0073 | 0.0025 | 1.0048 | 23.8 | 14.34 | 0.01285 | 0.00973 | 3.60 |
| 6/20/2009 | 14:00:00 | 30.00 | 1.0071 | 0.0025 | 1.0046 | 23.8 | 14.38 | 0.01285 | 0.00890 | 3.20 |
| 6/20/2009 | 14:30:00 | 60.00 | 1.0070 | 0.0025 | 1.0045 | 23.9 | 14.40 | 0.012835 | 0.00629 | 3.00 |
| 6/20/2009 | 15:00:00 | 90.00 | 1.0065 | 0.0025 | 1.0040 | 24.1 | 14.55 | 0.012805 | 0.00515 | 2.00 |
| 6/20/2009 | 15:30:00 | 120.0 | 1.0063 | 0.0025 | 1.0038 | 24.1 | 14.61 | 0.012805 | 0.00447 | 1.60 |
| 6/20/2009 | 16:30:00 | 180.0 | 1.0060 | 0.0025 | 1.0035 | 24.3 | 14.70 | 0.012775 | 0.00365 | 1.00 |
| 6/20/2009 | 17:30:00 | 240.0 | 1.0060 | 0.0025 | 1.0035 | 24.5 | 14.70 | 0.012745 | 0.00315 | 1.00 |
| 6/21/2009 | 8:30:00 | 1140. | 1.0056 | 0.0025 | 1.0031 | 24.0 | 14.85 | 0.01282 | 0.00146 | 0.20 |

Table C.5: Results of the Hydrometer Analysis #2 Conducted to the Silty Sand.

| Hydrometer Analysis No. 2- Silty Sand | | | | | | | | | | |
|---|---|---|---|---|---|---|---|---|---|---|
| Date: | 6/11/2009 | Tested: | 06/21/2009 - 06/22/2009 | Boring: | hand augured hole | Tested By: | | | | |
| Sample No.: | 2 | Project: | Pile Group Test | Depth: | 10 ft | Deeyvid Saez Barrios | | | | |
| Hygroscopic Water Content | | | | | | | | | | |
| 1) Cup No. : | | 1 | | 2) Mass of cup (g): | | 22.8 | | | | |
| 3) Mass cup + soil (air dry) (g): | | 41.24 | | 4) Mass cup + soil (oven dry) (g): | | 41.04 | | | | |
| 5) Mass of water (g): | | 0.2 | | 6) Mass of soil (oven dry) (g): | | 18.24 | | | | |
| 7) Mass of soil (air dry) (g): | | 18.44 | | 8) Hygrosc. water content (%): | | 1.10 | | | | |
| 9) Hygrosc. correction factor: | | 0.989 | | | | | | | | |
| Hydrometer Analysis | | | | | | | | | | |
| Hydrometer Type: | | 151 H | | Specific Gravity: | | 2.67 | | | | |
| Hydrometer Reading in the Control Solution: | | 1.003 | | Calculate mass of oven dry soil: | | 79.13 | | | | |
| Mass of air dry soil: | | 80 | | Starting Time: | | 13:40:00 | | | | |
| Date | Time | Elapsed Time (min) | Actual Hydrometer Reading (Rh) | Composite Correction | Hydrometer Reading Correction (Rh) | Temperature (Degrees C) | Effective Hydrometer Depth (L) | K from table | Diameter of Particle, D (mm) | Percent finer in suspension (%) |
| 6/21/2009 | 13:40:04 | 0.07 | 1.0370 | 0.0030 | 1.0340 | 23.5 | 6.50 | 0.012895 | 0.12733 | 62.07 |
| 6/21/2009 | 13:40:15 | 0.25 | 1.0315 | 0.0030 | 1.0285 | 23.5 | 8.10 | 0.012895 | 0.07340 | 51.05 |
| 6/21/2009 | 13:40:30 | 0.50 | 1.0270 | 0.0030 | 1.0240 | 23.5 | 9.20 | 0.012895 | 0.05531 | 42.04 |
| 6/21/2009 | 13:41:00 | 1.00 | 1.0200 | 0.0030 | 1.0170 | 23.5 | 11.80 | 0.012895 | 0.04430 | 28.03 |
| 6/21/2009 | 13:41:30 | 1.50 | 1.0158 | 0.0030 | 1.0128 | 23.5 | 12.14 | 0.012895 | 0.03668 | 19.62 |
| 6/21/2009 | 13:42:00 | 2.00 | 1.0138 | 0.0030 | 1.0108 | 23.5 | 12.66 | 0.012895 | 0.03244 | 15.62 |
| 6/21/2009 | 13:45:00 | 5.00 | 1.0100 | 0.0030 | 1.0070 | 23.5 | 13.70 | 0.012895 | 0.02135 | 8.01 |
| 6/21/2009 | 13:50:00 | 10.00 | 1.0090 | 0.0030 | 1.0060 | 23.5 | 13.90 | 0.012895 | 0.01520 | 6.01 |
| 6/21/2009 | 13:55:00 | 15.00 | 1.0087 | 0.0030 | 1.0057 | 23.5 | 13.99 | 0.012895 | 0.01245 | 5.41 |
| 6/21/2009 | 14:00:00 | 20.00 | 1.0082 | 0.0030 | 1.0052 | 23.5 | 14.14 | 0.012895 | 0.01084 | 4.40 |
| 6/21/2009 | 14:05:00 | 25.00 | 1.0080 | 0.0030 | 1.0050 | 23.5 | 14.20 | 0.012895 | 0.00972 | 4.00 |
| 6/21/2009 | 14:10:00 | 30.00 | 1.0078 | 0.0030 | 1.0048 | 23.7 | 14.24 | 0.012865 | 0.00886 | 3.60 |
| 6/21/2009 | 14:40:00 | 60.00 | 1.0077 | 0.0030 | 1.0047 | 23.7 | 14.26 | 0.012865 | 0.00627 | 3.40 |
| 6/21/2009 | 15:10:00 | 90.00 | 1.0074 | 0.0030 | 1.0044 | 23.9 | 14.32 | 0.012835 | 0.00512 | 2.80 |
| 6/21/2009 | 15:40:00 | 120.00 | 1.0071 | 0.0030 | 1.0041 | 24.0 | 14.38 | 0.01282 | 0.00444 | 2.20 |
| 6/21/2009 | 16:40:00 | 180.00 | 1.0070 | 0.0030 | 1.0040 | 24.2 | 14.40 | 0.01279 | 0.00362 | 2.00 |
| 6/21/2009 | 17:40:00 | 240.00 | 1.0070 | 0.0030 | 1.0040 | 24.2 | 14.40 | 0.01279 | 0.00313 | 2.00 |
| 6/22/2009 | 9:40:00 | 1200.00 | 1.0061 | 0.0030 | 1.0031 | 23.9 | 14.67 | 0.012835 | 0.00142 | 0.20 |

Table C.6: Results of the Hydrometer Analysis #2 Conducted to the Silty Sand.

| Hydrometer Analysis No.3 | | | | | | | | | | |
|---|---|---|---|---|---|---|---|---|---|---|
| Date: | 6/11/2009 | | Tested: | 06/23/2009 - 06/24/2009 | | Boring: | hand augered hole | | Tested By: | |
| Sample No.: | 2 | | Project: | Pile Group Test | | Depth: | 10 ft | | Deeyvid Saez Barrios | |
| Hygroscopic Water Content | | | | | | | | | | |
| 1) Cup No. : | | | 1 | | | 2) Mass of cup (g): | | | 22.83 | |
| 3) Mass cup + soil (air dry) (g): | | | 39.9 | | | 4) Mass cup + soil (oven dry) (g): | | | 39.62 | |
| 5) Mass of water (g): | | | 0.28 | | | 6) Mass of soil (oven dry) (g): | | | 16.79 | |
| 7) Mass of soil (air dry) (g): | | | 17.07 | | | 8) Hygrosc. water content (%): | | | 1.67 | |
| 9) Hygrosc. correction factor: | | | 0.984 | | | | | | | |
| Hydrometer Analysis | | | | | | | | | | |
| Hydrometer Type: | | | 151 H | | | Specific Gravity: | | | 2.67 | |
| Hydrometer Reading in the Control Solution: | | | 1.003 | | | Calculate mass of oven dry soil: | | | 82.43 | |
| Mass of air dry soil: | | | 83.8 | | | Starting Time: | | | | |
| Date | Time | Elapsed Time (min) | Actual Hydrometer Reading (Rh) | Composite Correction | Hydrometer Reading Correction (Rh) | Temperature (Degrees C) | Effective Hydrometer Depth (L) | K from table | Diameter of Particle, D (mm) | Percent finer in suspension (%) |
| 6/23/2009 | 13:40:04 | 0.07 | 1.0380 | 0.0030 | 1.0350 | 23.8 | 6.20 | 0.012850 | 0.12392 | 61.16 |
| 6/23/2009 | 13:40:15 | 0.25 | 1.0335 | 0.0030 | 1.0305 | 23.8 | 8.25 | 0.012850 | 0.07382 | 52.56 |
| 6/23/2009 | 13:40:30 | 0.50 | 1.0288 | 0.0030 | 1.0258 | 23.8 | 8.66 | 0.012850 | 0.05348 | 43.48 |
| 6/23/2009 | 13:41:00 | 1.00 | 1.0218 | 0.0030 | 1.0188 | 23.8 | 10.54 | 0.012850 | 0.04172 | 30.10 |
| 6/23/2009 | 13:41:30 | 1.50 | 1.0188 | 0.0030 | 1.0158 | 23.8 | 11.34 | 0.012850 | 0.03533 | 24.37 |
| 6/23/2009 | 13:42:00 | 2.00 | 1.0167 | 0.0030 | 1.0137 | 23.8 | 11.89 | 0.012850 | 0.03133 | 20.45 |
| 6/23/2009 | 13:45:00 | 5.00 | 1.0118 | 0.0030 | 1.0088 | 23.8 | 13.16 | 0.012850 | 0.02085 | 11.09 |
| 6/23/2009 | 13:50:00 | 10.00 | 1.0114 | 0.0030 | 1.0084 | 23.8 | 13.28 | 0.012850 | 0.01481 | 10.32 |
| 6/23/2009 | 13:55:00 | 15.00 | 1.0109 | 0.0030 | 1.0079 | 23.8 | 13.43 | 0.012850 | 0.01216 | 9.37 |
| 6/23/2009 | 14:00:00 | 20.00 | 1.0100 | 0.0030 | 1.0070 | 23.7 | 13.70 | 0.012865 | 0.01065 | 7.65 |
| 6/23/2009 | 14:05:00 | 25.00 | 1.0099 | 0.0030 | 1.0069 | 23.8 | 13.72 | 0.012850 | 0.00952 | 7.45 |
| 6/23/2009 | 14:10:00 | 30.00 | 1.0095 | 0.0030 | 1.0065 | 23.8 | 13.80 | 0.012850 | 0.00872 | 6.69 |
| 6/23/2009 | 14:40:00 | 60.00 | 1.0090 | 0.0030 | 1.0060 | 23.7 | 13.90 | 0.012865 | 0.00619 | 5.73 |
| 6/23/2009 | 15:10:00 | 90.00 | 1.0088 | 0.0030 | 1.0058 | 23.8 | 13.96 | 0.012850 | 0.00506 | 5.35 |
| 6/23/2009 | 15:40:00 | 120.00 | 1.0085 | 0.0030 | 1.0055 | 23.8 | 14.05 | 0.012850 | 0.00440 | 4.78 |
| 6/23/2009 | 16:40:00 | 180.00 | 1.0081 | 0.0030 | 1.0051 | 23.9 | 14.17 | 0.012835 | 0.00360 | 4.01 |
| 6/23/2009 | 17:40:00 | 240.00 | 1.0080 | 0.0030 | 1.0050 | 24.1 | 14.20 | 0.012805 | 0.00311 | 3.82 |
| 6/24/2009 | 9:40:00 | 1200.00 | 1.0070 | 0.0030 | 1.0040 | 24.0 | 14.40 | 0.012820 | 0.00140 | 1.91 |

Table C.7: Results of the Liquid Limit #1 Conducted to the Silty Sand.

| Atterberg Limits for Sandy Silty Soil (Sample 2) | | | |
|---|---|---|---|
| Sample No.: 2 | | Location: Riverside Campus - Texas A&M University | |
| Boring No.: hang augered hole | | | |
| Depth: 10 ft | | Tested by: Deeyvid Oscar Saez Barrios | |
| Description of sample: very silty sand | | | |
| Date: 06/23/2009 | | | |
| Can No. | 1 | 2 | 3 |
| Mass of Can (g) | 1.01 | 1.03 | 1.01 |
| Mass of wet soil + can (g) | 12.92 | 13.75 | 13.51 |
| Mass of dry soil + can (g) | 10.74 | 11.48 | 11.32 |
| Mass of water (g) | 2.18 | 2.27 | 2.19 |
| Mass of dry soil (g) | 9.73 | 10.45 | 10.31 |
| Water content, (%) | 22.40 | 21.72 | 21.24 |
| Number of drops | 15 | 20 | 25 |
| Note: Plastic limit could not be determined because of the lack of plasticity of the sample. | | | |

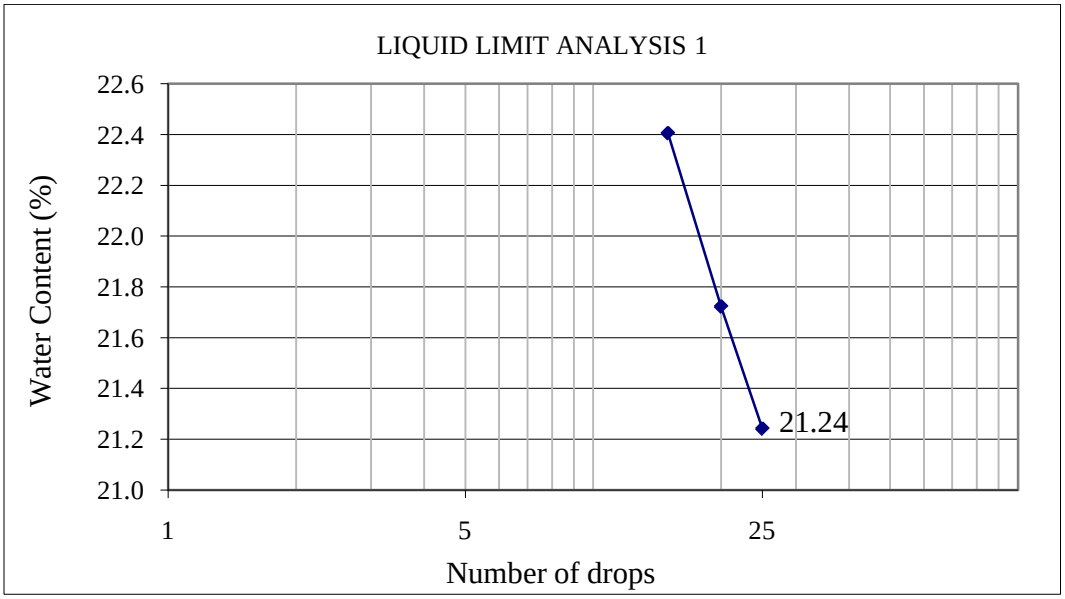


Figure C.1: Water Content (%) vs. Number of Drops for computation of the Liquid Limit of the Silty Sand (Test #1).

Table C.8: Results of the Liquid Limit #1 Conducted to the Silty Sand.

| Atterberg Limits for the Silty Sand | | | |
|---|---|---|---|
| Sample No.: 2 | | Location: Riverside Campus - Texas A&M University | |
| Boring No.: hang augered hole | | | |
| Depth: 10 ft | | Tested by: Deeyvid Oscar Saez Barrios | |
| Description of sample: very silty sand | | | |
| Date: 06/23/2009 | | | |
| Can No. | 5 | 6 | 7 |
| Mass of Can (g) | 0.99 | 0.99 | 0.98 |
| Mass of wet soil + can (g) | 16.57 | 14.99 | 18.11 |
| Mass of dry soil + can (g) | 13.96 | 12.5 | 15.16 |
| Mass of water (g) | 2.61 | 2.49 | 2.95 |
| Mass of dry soil (g) | 12.97 | 11.51 | 14.18 |
| Water content, (%) | 20.12 | 21.63 | 20.80 |
| Number of drops | 35 | 21 | 28 |
| Note: Plastic limit could not be determined because of the lack of plasticity of the sample. | | | |

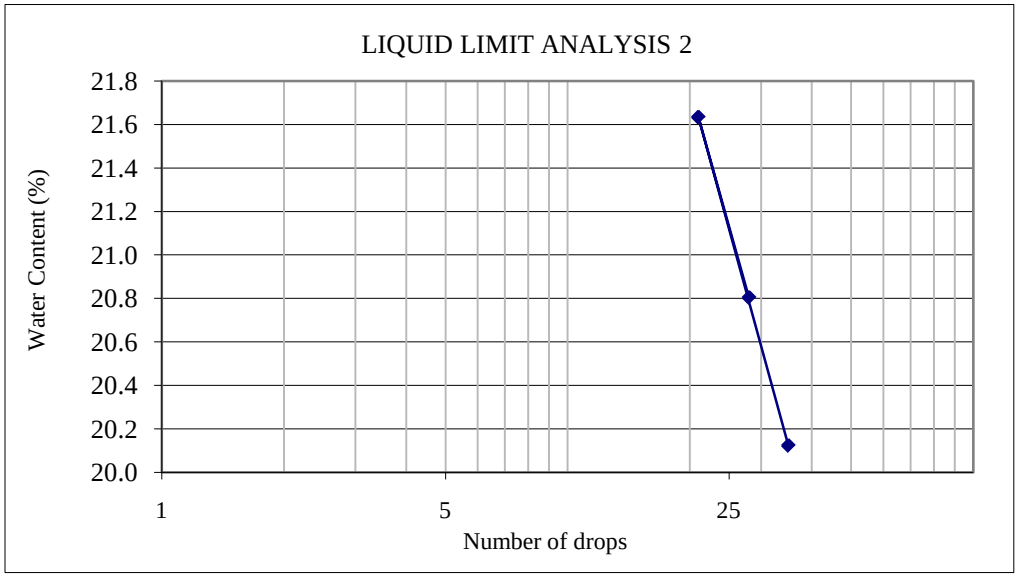


Figure C.2: Water Content (%) vs. Number of Drops for computation of the Liquid Limit of the Silty Sand (Test #2).

# APPENDIX D- RESULTS OF THE TESTS CONDUCTED TO THE ROAD BASE.

Table C.1 shows the results of the Mechanical Analysis conducted to the Road Base. The test was performed in accordance to the designation ASTM D 2217-85 (Standard Practice for Wet Preparation of Soil Samples for Particle-Size Analysis and Determination of Soil Constants). In addition, Table D.2 presents the results of the Hydrometer analysis conducted in the Road Base. The Hydrometer test was conducted following the criterion established by the designation ASTM D 422 (Standard Method for Particle Size Analysis of Soils).

Tables D.3 and D.4 show the results of the Modified Proctor Compaction Test and the Soil Modulus Determination using the Briaud Compaction Device (BCD). The Modified Proctor Compaction Test was performed in accordance to the designation ASTM D 1557-07 (Standard Method for Laboratory Compaction Characteristics of Soil Using Modified Effort -56,000 ft-lbf/ft$^3$) and the BCD Modulus Test was conducted following the procedure presented in section 4.9 for the laboratory test.

Finally, Table D.4 and Figure D.1 have the information regarding the computation of the Liquid Limit ($w_L$) of the Road Base. The tests were conducted following the standard ASTM D 4318-00 (Standard Tests Methods for Liquid Limit, Plastic Limit, and Plasticity Index of Soils).

All these tests were conducted in the Geotechnical Graduate Lab. of the Zachry Department of Civil Engineering at Texas A&M University.

Table D.1: Results of the Mechanical Analysis Conducted to the Road Base.

| Mechanical Analysis for Road Base | | | | | | | |
|---|---|---|---|---|---|---|---|
| Description of Sample: Road Base | | | | | Project: Pile Group Test | | |
| Unifies Soil Classification: SP | | | | | Location: Riverside Campus- Texas A&M University | | |
| | | | | | Date: 08/11/09 | | |
| | | | | | Tested by: Deeyvid O. Saez Barrios | | |
| Total weight of sample (g): | | | | 4313.06 | | | |
| Sieve No. | Size (mm) | Weight of Sieve (g) | Weight of Sieve + Soil (g) | Weight of Soil Retained (g) | Percent. Retained by Weight (%) | Percent. Accum. by Weight (%) | Percentage Passing by Weight (%) |
| Gravel Portion | | | | | | | |
| 1" | 25.4 | 801.92 | 1261.47 | 459.55 | 10.64 | 10.64 | 89.36 |
| 1/2" | 12.7 | 781.83 | 1405.99 | 624.16 | 14.46 | 25.10 | 74.90 |
| 1/4" | 6.35 | 515.82 | 1170.05 | 654.23 | 15.15 | 40.25 | 59.75 |
| 4 | 4.75 | 513.16 | 759.89 | 246.73 | 5.71 | 45.97 | 54.03 |
| 10 | 2.00 | 488.45 | 1180.62 | 692.17 | 16.03 | 62.00 | 38.00 |
| Pan | | 377.34 | 2018.01 | 1640.67 | 38.00 | 100.00 | 0.00 |
| | | | Total Weight of Soil (g) = | 4317.51 | 100.00 | | |
| | | | Percentage Error (%) = | 0.10 | < 2% O.K. | | |
| Wet Sieve Analysis with a Soil Portion of 500 g Passing Sieve #10 | | | | | | | |
| Total weight of sample (g): | | | | 504.95 | | | |
| Water content (%): | | | | 2.8 | | | |
| Total dry weight of the sample (g): | | | | 491.20 | | | |
| Total weight of soil retained in sieve #200 (g): | | | | 277.69 | | | |
| Total weight of fine particles (g): | | | | 213.5 | | | |
| Sieve No. | Size (mm) | Weight of Sieve (g) | Weight of Sieve + Soil (g) | Weight of Soil Retained (g) | Percent. Retained by Weight (%) | Percent. Accum. by Weight (%) | Percentage Passing by Weight (%) |
| 20 | 0.90 | 369.17 | 461.85 | 92.68 | 18.91 | 18.91 | 81.09 |
| 40 | 0.43 | 345.29 | 412.77 | 67.48 | 13.77 | 32.68 | 67.32 |
| 80 | 0.18 | 317.76 | 381.02 | 63.26 | 12.91 | 45.59 | 54.41 |
| 200 | 0.075 | 341.07 | 387.22 | 46.15 | 9.42 | 55.01 | 44.99 |
| Pan | | 479.13 | 486.13 | 220.51 | 44.99 | 100.00 | 0.00 |
| | | | Total Weight of Soil (g) = | 490.08 | 259.75 | | |
| | | | Percentage Error (%) = | 0.23 | < 2% O.K. | | |
| | | | Total Percent Passing Sieve # 200 (%) = | 44.99 | | | |

Table D.2: Results of the Hydrometer Analysis Conducted to the Road Base.

| Hydrometer Analysis for Road Base | | | | | | | | | | |
|---|---|---|---|---|---|---|---|---|---|---|
| Date: | 8/12/2009 | | Tested: | 06/12/2009 - 06/14/2009 | | Boring: | 3 | | Tested By: | |
| Sample No.: | Road Base | | Project | Pile Group Test | | Depth: | surface | | | |
| Hygroscopic Water Content | | | | | | | | | | |
| 1) Cup No. : | | | | 1 | | 2) Mass of cup (g): | | | 0.96 | |
| 3) Mass cup + soil (air dry) (g): | | | | 5.44 | | 4) Mass cup + soil (oven dry) (g): | | | 5.36 | |
| 5) Mass of water (g): | | | | 0.08 | | 6) Mass of soil (oven dry) (g): | | | 4.4 | |
| 7) Mass of soil (air dry) (g): | | | | 4.48 | | 8) Hygrosc. water content (%): | | | 1.82 | |
| 9) Hygrosc. correction factor: | | | | 0.982 | | | | | | |
| **Hydrometer Analysis** | | | | | | | | | | |
| Hydrometer Type: | | | | 151 H | | Specific Gravity: | | | 2.7 | |
| Hydrometer Reading in the Control Solution: | | | | 1.0028 | | Calculate mass of oven dry soil: | | | 59.09 | |
| Mass of air dry soil: | | | | 60.16 | | Starting Time: | | | 11:00:00 | |
| **Date** | **Time** | **Elapsed Time (min)** | **Actual Hydrometer Reading (Rh)** | **Composite Correction** | **Hydrometer Reading Correction (Rh)** | **Temperature (Degrees C)** | **Effective Hydrometer Depth (L)** | **K from table** | **Diameter of Particle, D (mm)** | **Percent finer in suspension (%)** |
| 8/13/2009 | 11:00:00 | 0.07 | 1.0350 | 0.0028 | 1.0322 | 25.5 | 7.00 | 0.01279 | 0.13106 | 77.22 |
| 8/13/2009 | 11:00:15 | 0.25 | 1.0328 | 0.0028 | 1.0300 | 25.5 | 7.64 | 0.01279 | 0.07070 | 71.27 |
| 8/13/2009 | 11:00:30 | 0.50 | 1.0303 | 0.0028 | 1.0275 | 25.5 | 8.31 | 0.01279 | 0.05214 | 64.66 |
| 8/13/2009 | 11:01:00 | 1.00 | 1.0290 | 0.0028 | 1.0262 | 25.5 | 8.60 | 0.01279 | 0.03751 | 61.36 |
| 8/13/2009 | 11:01:30 | 1.50 | 1.0278 | 0.0028 | 1.0250 | 25.5 | 8.96 | 0.01279 | 0.03126 | 58.05 |
| 8/13/2009 | 11:02:00 | 2.00 | 1.0263 | 0.0028 | 1.0235 | 25.5 | 9.20 | 0.01279 | 0.02743 | 54.08 |
| 8/13/2009 | 11:05:00 | 5.00 | 1.0225 | 0.0028 | 1.0197 | 25.5 | 10.35 | 0.01279 | 0.01840 | 44.17 |
| 8/13/2009 | 11:10:00 | 10.00 | 1.0205 | 0.0028 | 1.0177 | 25.5 | 10.85 | 0.01279 | 0.01332 | 38.88 |
| 8/13/2009 | 11:15:00 | 15.00 | 1.0195 | 0.0028 | 1.0167 | 25.5 | 11.15 | 0.01279 | 0.01103 | 36.23 |
| 8/13/2009 | 11:20:00 | 20.00 | 1.0180 | 0.0028 | 1.0152 | 25.6 | 11.50 | 0.012776 | 0.00969 | 32.27 |
| 8/13/2009 | 11:26:00 | 26.00 | 1.0170 | 0.0028 | 1.0142 | 25.7 | 11.80 | 0.012762 | 0.00860 | 29.62 |
| 8/13/2009 | 11:34:00 | 30.00 | 1.0160 | 0.0028 | 1.0132 | 25.7 | 12.10 | 0.012762 | 0.00810 | 26.98 |
| 8/13/2009 | 12:00:00 | 60.00 | 1.0142 | 0.0028 | 1.0114 | 25.7 | 12.54 | 0.012762 | 0.00583 | 22.22 |
| 8/13/2009 | 1:00:00 | 120.00 | 1.0120 | 0.0028 | 1.0092 | 25.7 | 13.10 | 0.012762 | 0.00422 | 16.40 |
| 8/13/2009 | 3:00:00 | 240.00 | 1.0100 | 0.0028 | 1.0072 | 26.0 | 13.70 | 0.01272 | 0.00304 | 11.11 |
| 8/14/2009 | 11:00:00 | 1440.00 | 1.0070 | 0.0028 | 1.0042 | 24.8 | 14.40 | 0.01289 | 0.00129 | 3.17 |

Table D.3: Results of the Modified Compaction Test and the Stiffness Curve Conducted to the Road Base.

| COMPACTION CURVE FOR SANDY SOIL | | | | | | | | |
|---|---|---|---|---|---|---|---|---|
| Sample No.: 3 | | Location: Riverside Campus - Texas A&M University | | | | | | |
| Description of sample: Road Base | | Tested by: Deeyvid Saez | | | | | | |
| Date: 07/23/2009 | | Volume of the Modified Proctor Mould ($m^3$) | | | | | 0.0021029 | |
| MOISTURE CONTENT DETERMINATION | | | | | | | | |
| Determination No. | 1 | 2 | 3 | 4 | 5 | 6 | 7 | 8 |
| Container No. | P-1 | P-2 | P-3 | P-8 | P-5 | P-9 | P-6 | P-7 |
| Mass of container (g) | 27.15 | 23.39 | 24.1 | 21.54 | 31.21 | 22.59 | 31.9 | 31.19 |
| Container + wet Soil (g) | 261.65 | 195.75 | 179.81 | 124.12 | 157.3 | 133.26 | 209.64 | 236.27 |
| Container + dry Soil (g) | 252.4 | 186.63 | 171.24 | 118.21 | 148.25 | 125.13 | 195.79 | 219.08 |
| Mass of water (g) | 9.25 | 9.12 | 8.57 | 5.91 | 9.05 | 8.13 | 13.85 | 17.19 |
| Mass of Dry Soil (g) | 225.25 | 163.24 | 147.14 | 96.67 | 117.04 | 102.54 | 163.89 | 187.89 |
| Water Content (%) | 4.11 | 5.59 | 5.82 | 6.11 | 7.73 | 7.93 | 8.45 | 9.15 |
| DRY DENSITY DETERMINATION | | | | | | | | |
| Mass of Mould (kg) | 3.02877 | 3.02937 | 3.03213 | 3.03084 | 3.02884 | 3.02826 | 3.02943 | 3.03085 |
| Compacted Soil + Mould (kg) | 7.66475 | 7.76133 | 7.98782 | 7.979 | 8.08523 | 7.90892 | 7.90634 | 7.83797 |
| Mass of Compacted Soil (kg) | 4.63598 | 4.73196 | 4.95569 | 4.94816 | 5.056388 | 4.88066 | 4.87691 | 4.80712 |
| Wet Density ($kg/m^3$) | 2.20 | 2.25 | 2.36 | 2.35 | 2.40 | 2.32 | 2.32 | 2.29 |
| Dry Density ($kg/m^3$) | 2.12 | 2.13 | 2.23 | 2.22 | 2.23 | 2.15 | 2.14 | 2.09 |
| Bulk Unit Weight ($kN/m^3$) | 21.63 | 22.07 | 23.12 | 23.08 | 23.59 | 22.77 | 22.75 | 22.43 |
| Dry Unit Weight ($kN/m^3$) | 20.77 | 20.91 | 21.85 | 21.75 | 21.90 | 21.10 | 20.98 | 20.55 |
| Average BCD Modulus (MPa) | 50.49 | 56.11 | 53.95 | 31.17 | 10.54 | 11.36 | 7.47 | 7.89 |

Table D.4: Results of the Liquid Limit Conducted to the Road Base.

| Atterberg Limits for Road Base | | | |
|---|---|---|---|
| Description of sample: road base soil | | Location: Riverside Campus - Texas A&M University | |
| Unified Soil Classification: | | | |
| Date: 08/12/2009 | | Tested by: Deeyvid Saez Barrios | |
| | | | |
| Can No. | 1 | 2 | 3 |
| Mass of Can (g) | 0.97 | 1.03 | 0.96 |
| Mass of wet soil + can (g) | 17.66 | 15.4 | 14.76 |
| Mass of dry soil + can (g) | 15.1 | 13.22 | 12.72 |
| Mass of water (g) | 2.56 | 2.18 | 2.04 |
| Mass of dry soil (g) | 14.13 | 12.19 | 11.76 |
| Water content, (%) | 18.12 | 17.88 | 17.35 |
| Number of drops | 17 | 21 | 35 |
| Liquid Limit (%) = 17.70 | | | |

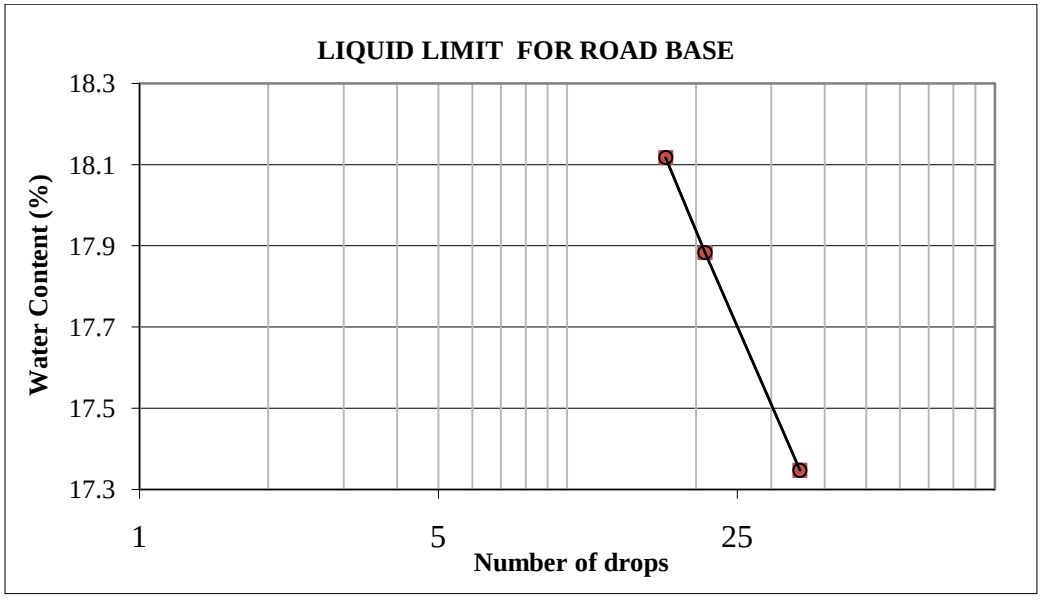


Figure D.1: Water Content (%) vs. Number of Drops for Computation of the Liquid Limit of the Road Base.

# VITA

Name: Deeyvid Oscar Saez Barrios

Address: Texas A&M University, Zachry Department of Civil Engineering, College Station, TX, 77843.

E-mail: dsaez01@neo.tamu.edu

Education: B.En. Civil Engineering, Technological University of Panama, Panama, April 2005.

M.S. Civil Engineering, Texas A&M University, College Station, TX-77840, U.S.A., May 2010